Samuel Adelabu · Abel Ramoelo ·
Adeyemi Olusola ·
Efosa Adagbasa *Editors*

Remote Sensing of African Mountains

Geospatial Tools Toward Sustainability

Springer

Remote Sensing of African Mountains

Samuel Adelabu • Abel Ramoelo
Adeyemi Olusola • Efosa Adagbasa
Editors

Remote Sensing of African Mountains

Geospatial Tools Toward Sustainability

Springer

Editors
Samuel Adelabu
Department of Geography
University of the Free State
Bloemfontein, South Africa

Adeyemi Olusola
Department of Geography
University of the Free State
Bloemfontein, South Africa

Abel Ramoelo
Department of Geography, Geoinformatics and Meteorology
University of Pretoria
Pretoria, South Africa

Efosa Adagbasa
Department of Geography
University of the Free State
Phuthaditjhaba, South Africa

ISBN 978-3-031-04854-8 ISBN 978-3-031-04855-5 (eBook)
https://doi.org/10.1007/978-3-031-04855-5

This Springer imprint is published by the registered company Springer Nature Switzerland AG
The registered company address is: Gewerbestrasse 11, 6330 Cham, Switzerland

Acknowledgment

Apart from the final review and other editorials as carried out by the editors, we would like to thank and appreciate our reviewers who were involved in the blinded review process. The reviewers listed below were constructive in their comments and we would like to say unequivocally that these comments led to substantial improvement in the quality of this book. Finally, we also thank our publisher and its publishing editors for their continuous support in the publication of this book.

Reviewers

Name: Abraham R Matamanda
Department: Department of Geography
Institution: University of the Free State, South Africa
Specialization: Human settlement planning and climate change adaptation in cities of the Global South
Email Address: MatamandaRA@ufs.ac.za
Name: Rotimi Obateru
Department: Department of Geography and Planning Sciences
Institution: Adekunle Ajasin University, Akungba-Akoko, Ondo State.
Area of specialization: Applied Geomorphology and Hydrology
Email Address: obaterurotimi@gmail.com
Name: Jay le Roux
Department: Department of Geography
Institution: University of the Free State, South Africa
Area of specialization: soil erosion mapping and modelling.
Email address: lerouxjj@ufs.ac.za
Name: Simbarashe Jombo
Department: Department of Geography
Institution: University of the Free State, South Africa
Email address: simbarashejombo@gmail.com

Area of specialization: Remote sensing and GIS (LiDAR, hyperspectral and multispectral data).

Name: Elizabeth M Rudolph
Department: Department of Geography
Institution: University of the Free State
Specialization: Geomorphology
Email Address: rudolphem@ufs.ac.za

Name: Dr. Philemon Tsele (PhD) Department: Department of Geography, Geoinformatics and Meteorology
Institution: University of Pretoria, Private Bag X20, Hatfield, 0028, South Africa
Specialization: Geoinformatics
Email Address: philemon.tsele@up.ac.za

Name: Mbulisi Sibanda
Department: Department of Geography, Environmental Studies, and Tourism
Institution: University of the Western Cape, South Africa
Specialization: GIScience and Earth Observation scientist
Email Address: msibanda@uwc.ac.za

Name: Toyin Fashae
Institution: University of Ibadan, Ibadan, Nigeria
Department: Geography
Specialization: Geomorphology, GIS and Remote Sensing
toyinafashae@yahoo.com

Name: Sifiso Xulu
Department: Geography
Institution: University of the Free State, QwaQwa Campus, South Africa
Specialization: Geospatial applications
Email Address: xulus@ufs.ac.za

Name: Kabir Peerbhay
Institution: Sappi Forests
Specialization: Spatial Technologies
Email Address: peerbhaykabir@gmail.com

Name: Naledzani Ndou
Department: GIS and Remote Sensing
Institution: University of Fort Hare, South Africa
Specialization: Geo-information Systems
Email Address: raschant@gmail.com

Introduction

Samuel Adelabu, Abel Ramoelo, Adeyemi Olusola, and Efosa Adagbasa

Montane environments are found in every continent on planet Earth. These areas are important biologically, as clearly portrayed by the Conference of Parties to the United Nations Conventions on Biological Diversity in 2004. The parties posited that montane environments are about the most biologically diverse parts of the Earth. A fact supported by the Conservation International by laying claim to the fact that 25 of the 34 world centers of greatest biodiversity hot spots are wholly or partly mountainous (see Price, 2013). These regions are of rugged terrain and have been defined as areas with an elevation of about 300 m and above over a radius of about 7 km (Wohl, 2018). These regions cover not less than 12% of the earth's surface and among other things provide various functions such as historical, cultural, religious, and environmental. Historically, these regions have been described as areas where man started domesticating plants and animals. Also, across the world, mountain ranges hold cultural eminence as places of tourist attractions, sports, and home to indigenous people. Montane environments have been deified across ages and time with various groups of people across the world objectifying mountains and worshiping them. In terms of environment, mountain regions serve as headwater catchment for most of the large rivers of the world (Price et al., 2013). Furthermore, the range of ecosystem services provided by the mountain ecosystem includes, but not limited to, meat, milk, wool, leather, maintenance of atmospheric composition and genetic library, amelioration of water, and conservation of soils (Kang et al., 2018), and it also provides shelter to those living on and around mountain environments. It is a

S. Adelabu · A. Olusola
Department of Geography, University of the Free State, Bloemfontein, South Africa

A. Ramoelo
Department of Geography, Geoinformatics and Meteorology, University of Pretoria, Pretoria, South Africa

E. Adagbasa
Department of Geography, University of the Free State, Phuthaditjhaba, South Africa

space for social interactions that allow for human-environment interactions. This human-environment interaction allows for the (re)production of goods and services. Due to the physiographic makeup of montane regions, that is, altitude, terrain, soil, and climate, montane environments are hotspots for biodiversity. The variety of plants and animals found within these environments is to a large extent endemic with great genetic diversity. Mountain biota (plants and animals) survive under the environmental conditions of their habitat because of their adaptability, which allows them to establish themselves and reproduce. It is precisely this ability to adapt to the specific characteristics of a given microsite, which has shaped one of the theories, is what partly explains the endemism found in the mountains through speciation.

From the foregoing, it is clear that montane regions or ecosystems are unique (Semala et al., 2022). Globally, there has been an increase in environmental awareness of various environmental issues. However, within the montane setting, environmental issues such as changing climate, habitat loss and fragmentation, population growth, agricultural activities, and natural hazards are burning issues (Atkinson and De Clercq, 2022; Das and Zhang, 2022, Onaolapo et al., 2022; Luliro et al., 2022). Although these issues are also peculiar to lowland environments, however, because of the physiography of montane environments and the highly sensitive nature of its ecosystems, changes or perturbations create almost irreversible reactions. The changing climate affects snow caps and glaciers on mountain tops by melting these age-long ice caps due to global warming (Boudhar et al., 2022). Also, the slower pace of recovery of natural regenerative processes, owing to colder temperatures, greatly increases potential for erosion, owing to steeper gradients and generally less fertile soil endangers this environment and soil fertility (Adagbasa et al., 2022; Nyawacha and Meta, 2022; Harrison and van Tol, 2022; Luliro et al., 2022). Furthermore, the changing climate is altering habitat makeup of various plants and animals, leading to migration of animals and extinction of some plants, which is a great challenge to the genetic pool of the region (Adagbasa et al., 2022). Besides, changing climate coupled with fires and other anthropogenic activities like overcultivation is leading to loss of carbon stocks in biomass of montane vegetation (Dipuo et al., 2022; Adagbasa et al., 2022; Onaolapo et al., 2022). These issues and many more impact on the livelihoods of mountain people. To the indigenous peoples and those whose livelihoods depend on the ecology of the mountains most often than not see this physical entity, mountain, not just as a natural resource but also as part of their existence (Sharma et al., 2019). To those living within and beyond, they understand that their well-being, to some extent their identity, especially for those living there, depends on careful stewardship of the montane ecosystems (Wang et al., 2019). However, in the light of the changing climate and its direct and indirect consequences, new and emerging socio-economic patterns within and around mountain environments are developing which not only affect those living within and around the mountain but also those whose livelihoods depend on the montane ecosystems. Addressing these issues requires careful planning and the need to understand various aspects of montane environments. As against lowland areas where intensive field studies can be carried out, montane areas due to their physiography and location limit the number of field studies that could be carried out. Some mountains are so remote that to understand the dynamics of such

environments requires remote sensing through the use of satellites or unmanned aerial vehicles (UAVs) (Semala et al., 2022). Remote sensing, in contrast with traditional approaches, such as field studies, offers spatial and temporal data that are convenient for mapping large areas at different spatial scales in a more vigorous, rapid, and efficient manner (Fajji, 2015). Globally, we know more about mountain ranges in Asia, North and South America, and Europe than the ones in Africa. Several studies and documentaries abound for the Himalayas, Andes, Alps, etc. (see Smethurst, 2000; Funnell and Price, 2003; Wester et al., 2019). Studies for these ranges increased in light of the changing climates and global warming. Some of these studies focused on sea-level rise, melting ice caps, coastal cities in the global north, and changing lifestyle for those living around these ranges (Anderson et al., 2020; Jorgenson and Ely, 2001; Wang et al., 2020). However, in Africa, besides the East-African Range (such as Kilimanjaro, Rwenzori), part of the Drakensberg and part of the high Atlas in North Africa (Smethurst, 2000; Thompson et al., 2002; Kaser et al., 2004; Jacobs et al., 2016; Teixell et al., 2003; Sebrier et al., 2006; Büscher, 2012), little is known about other montane environments. As portrayed by Smethurst (2000), little or nothing is known about the mountains in Madagascar, Cape Verde, and other countries. Furthermore, despite the array of information available for some mountain ranges in different parts of the world, global assessments such as the Intergovernmental Panel on Climate Change and the Millennium Ecosystem Assessment provide detailed information as regards mountain environments with respect to scientific and traditional indigenous knowledge (Wester et al., 2019). Besides, only four journals deal with mountain environments globally (the *Journal on Protected Mountain Areas Research*, *Sustainable Development of Mountain Territories*, *Mountain Research and Development*, and the *Journal of Mountain Science*). Therefore, this book will open up closed mountain areas of Africa and present new and emerging studies within and around known and unknown mountain ranges in Africa using remote sensing techniques. This will push further the frontier of knowledge in mountain studies and help shape further global assessments and policies. The 11 chapters presented in this book fall within the following thematic areas. These are:

1. Satellite Remote Sensing and Montane Vegetation
2. Satellite Remote Sensing and Mountain Hazards
3. Satellite Remote Sensing and Mountain Ecosystem Services
4. Satellite Remote Sensing of Mountain Geological and Geomorphic Surfaces
5. Satellite Remote Sensing and Mountain Energy Balance Modelling

The findings presented in this book will drive global policies and help strengthen these fragile ecosystems in Africa. With the impact of climate change already seen in various parts of the continent and especially in Sub-Saharan Africa, this book will help understand the role climate change is playing within mountain systems and the impact on those depending on them for their livelihoods either directly or indirectly.

Lastly, even though the studies covered in the book cannot touch every aspect of mountain systems, it is expected that enough would have been presented in the book to help drive policies and establish montane research units across the continent.

References

Adagbasa, G. E., Adelabu, S. A., & Okello, T. W. (2022). Ecological vulnerability assessment to Grassland fires in a protected mountainous area using remote sensing and GIS. In S. Adelabu, R. Abel, A. Olusola, & A. Efosa (Eds.), *Remote sensing of African mountains: Geospatial tools toward sustainability*. Springer.

Anderson, J. T., Wilson, G. S., Jones, R. S., Fink, D., & Fujioka, T. (2020). Ice surface lowering of Skelton Glacier, Transantarctic Mountains, since the Last Glacial Maximum: Implications for retreat of grounded ice in the western Ross Sea. *Quaternary Science Reviews*, *237*, 106305.

Atkinson, J., & De Clercq, W. (2022). Unravelling regional geodiversity: A grid-mapping approach to quantify geodiversity in the Uthukela District, Kwazulu-natal. In S. Adelabu, R. Abel, A. Olusola, & A. Efosa (Eds.), *Remote sensing of African mountains: Geospatial tools toward sustainability*. Springer.

Boudhar, A., Wassim Mohamed Baba, W. M., Marchane, A., Ouatiki, H., Bouamri, H., Hanich, L., & Chehbouni, A. (2022). Water resources monitoring over the Atlas Mountains in Morocco using satellite observations and Reanalysis data. In S. Adelabu, R. Abel, A. Olusola, & A. Efosa (Eds.), *Remote sensing of African mountains: Geospatial tools toward sustainability*. Springer.

Büscher, B. (2012). Payments for ecosystem services as neoliberal conservation: (Reinterpreting) evidence from the Maloti-Drakensberg, South Africa. *Conservation and Society*, *10*(1), 29–41.

Das, P., & Zhang, Z. (2022). Monitoring the wildfire activity and ecosystem response on Mt. Kilimanjaro using Earth Observation data and GIS. In S. Adelabu, R. Abel, A. Olusola, & A. Efosa (Eds.), *Remote sensing of African mountains: Geospatial tools toward sustainability*. Springer.

Dipuo, O. M., Olusola, A., & Adewale, S. A. (2022). Development of lightning hazard map for fire danger assessment over Mountainous Protected Area using geospatial technology. In S. Adelabu, R. Abel, A. Olusola, & A. Efosa (Eds.), *Remote sensing of African mountains: Geospatial tools toward sustainability*. Springer.

Fajji, N. G. (2015). *A remote sensing and GIS scheme for rangeland quality assessment and management in the North-West Province, South Africa* [Doctoral dissertation]. North-West University, South Africa.

Funnell, D. C., & Price, M. F. (2003). Mountain geography: A review. *The Geographical Journal, 169*(3), 183–190.

Harrison, R., & van Tol, J. (2022). Digital Soil Mapping for hydropedological purposes of the Cathedral Peak research catchments, South Africa. In S. Adelabu, R. Abel, A. Olusola, & A. Efosa (Eds.), *Remote sensing of African mountains: Geospatial tools toward sustainability*. Springer.

Jacobs, L., Dewitte, O., Poesen, J., Delvaux, D., Thiery, W., & Kervyn, M. (2016). The Rwenzori Mountains, a landslide-prone region? *Landslides*, *13*(3), 519–536.

Jorgenson, T., & Ely, C. (2001). Topography and flooding of coastal ecosystems on the Yukon-Kuskokwim Delta, Alaska: Implications for sea-level rise. *Journal of Coastal Research*, 124–136.

Kang, P., Chen, W., Hou, Y., & Li, Y. (2018). Linking ecosystem services and ecosystem health to ecological risk assessment: A case study of the Beijing-Tianjin-Hebei urban agglomeration. *Science of the Total Environment, 636*, 1442–1454.

Kaser, G., Hardy, D. R., Mölg, T., Bradley, R. S., & Hyera, T. M. (2004). Modern glacier retreat on Kilimanjaro as evidence of climate change: observations and facts. *International Journal of Climatology: A Journal of the Royal Meteorological Society*, *24*(3), 329–339.

Luliro, N. D., Dbumba, D. S., Nammanda, I., & Kisira, Y. (2022). Effect of climate variability and change on land suitability for Irish Potato Production in Kigezi Highlands of Uganda. In S. Adelabu, R. Abel, A. Olusola, & A. Efosa (Eds.), *Remote sensing of African mountains: Geospatial tools toward sustainability*. Springer.

Nyawacha, S. O., & Meta, V. K. (2022). Assessing the vulnerability of the Eastern Africa Highlands' soils to rainfall erosivity. In S. Adelabu, R. Abel, A. Olusola, & A. Efosa (Eds.), *Remote sensing of African mountains: Geospatial tools toward sustainability*. Springer.

Onaolapo, T. F., Okello, T. W., & Adelabu, S. A. (2022). Evaluating settlement development change, pre, and post-1994 in the Drakensberg mountains of Afromontane region, South Africa. In S. Adelabu, R. Abel, A. Olusola, & A. Efosa (Eds.), *Remote sensing of African mountains: Geospatial tools toward sustainability*. Springer.

Price, M. F. (2013). *Mountain geography: Physical and human dimensions*. University of California Press.

Price, M. F., & Kohler, T. (2013). Sustainable mountain development. In M. F. Price, A. C. Byers, D. A. Friend, T. Kohler, & L. W. Price (Eds.), *Mountain geography* (pp. 333–365). University of California Press.

Sébrier, M., Siame, L., Zouine, E. M., Winter, T., Missenard, Y., & Leturmy, P. (2006). Active tectonics in the moroccan high atlas. *Comptes Rendus Geoscience*, *338*(1–2), 65–79.

Semala, M., Olusola, A., Adelabu, S., & Ramoelo, A. (2022). Montane grasslands: Biomass estimations using remote sensing techniques in Africa. In S. Adelabu, R. Abel, A. Olusola, & A. Efosa (Eds.), *Remote sensing of African mountains: Geospatial tools toward sustainability*. Springer.

Sharma, E., Molden, D., Rahman, A., Khatiwada, Y. R., Zhang, L., Singh, S. P., … & Wester, P. (2019). Introduction to the hindu kush himalaya assessment. In *The Hindu Kush Himalaya Assessment* (pp. 1–16). Springer.

Smethurst, D. (2000). Mountain geography. *Geographical Review,* 90(1), 35–56

Teixell, A., Arboleya, M. L., Julivert, M., & Charroud, M. (2003). Tectonic shortening and topography in the central High Atlas (Morocco). *Tectonics*, *22*(5).

Thompson, L. G., Mosley-Thompson, E., Davis, M. E., Henderson, K. A., Brecher, H. H., Zagorodnov, V. S., … & Beer, J. (2002). Kilimanjaro ice core records: evidence of Holocene climate change in tropical Africa. *Science*, *298*(5593), 589–593.

Wang, Y., Wu, N., Kunze, C., Long, R., & Perlik, M. (2019). Drivers of change to mountain sustainability in the Hindu Kush Himalaya. In *The Hindu Kush Himalaya Assessment* (pp. 17–56). Springer.

Wang, Y., Zhang, T., Xiao, C., Ren, J., & Wang, Y. (2020). A two-dimensional, higher-order, enthalpy-based thermomechanical ice flow model for mountain glaciers and its benchmark experiments. *Computers & Geosciences*, 104526.

Wester, P., Mishra, A., Mukherji, A., & Shrestha, A. B. (2019). *The Hindu Kush Himalaya assessment: Mountains, climate change, sustainability and people* (p. 627). Springer Nature.

Wohl, E. (2018). Mountain environments. *obo* in environmental science. https://doi.org/10.1093/obo/9780199363445-0094

Contents

List of Figures

List of Tables

Chapter 1
Montane Grasslands: Biomass Estimations Using Remote Sensing Techniques in Africa

Semala Mathapelo, Adeyemi Olusola, Samuel Adelabu, and Abel Ramoelo

Abstract Grasslands are the least protected biome across the world. The range of ecosystem services provided by grassland biomes includes but is not limited to the sequestration of carbon. Most grasslands are threatened globally due to various direct and indirect anthropogenic factors. These anthropogenic factors considering changing climates are becoming amplified leading to the gradual or total destruction of global grassland communities. These transformations release carbon stocks sequestered in grassland biomes globally leading to the global accumulation of atmospheric carbon (CO_2). Even though several studies have presented carbon loss from various grasslands across the world due to various anthropogenic practices and natural disasters, there is still a gap in accounting for global carbon sink or loss from grassland biomes especially from the montane grassy environments as they are largely underrepresented. Mountainous areas are largely inaccessible due to rugged terrains and harsh weather conditions. Hence, this review aims to present existing approaches to studying biomass in montane grasslands and their challenges. The study concluded that the best approach to biomass estimation in montane grasslands especially in Africa lies in the use of active sensors fused with passive sensors especially those with the red-edge bands.

Keywords Biomass · Active sensors · Montane grasslands · Carbon · Africa

S. Mathapelo
Department of Geography, University of the Free State, QwaQwa, South Africa

A. Olusola (✉) · S. Adelabu
Department of Geography, University of the Free State, Bleomfontein Campus, South Africa

A. Ramoelo
Department of Geography, University of the Free State, Bleomfontein, South Africa

Department of Geography, Geoinformatics and Meteorology, University of Pretoria, Pretoria, South Africa

S. Adelabu et al. (eds.), *Remote Sensing of African Mountains*,
https://doi.org/10.1007/978-3-031-04855-5_1

1.1 Introduction

Grasslands are found the world over except in Antarctica; these grasslands can be divided into two: temperate and tropical. The temperate grasslands are called by different names such as prairies, steppes, velds and pampas. The tropical grasslands are largely referred to as savannas. Grassland biomes occupy about 20–40% of the whole land area on earth, and they have little or absence of trees (Egoh et al., 2011). From time immemorial, grasslands serve as sources of animal products and also home to indigenous people (Kang et al., 2007). Their role in the environment as regards the sustenance of ecosystem services and grounds for social interactions for animals is quite remarkable. Ecosystem services as defined by Daily (1997, p.3)

> are the conditions and processes through which natural ecosystems, and the species that make them up, sustain and fulfill human life … In addition to the production of goods, ecosystem services are the actual life-support functions, such as cleansing, recycling, and renewal, and they confer many intangible aesthetic and cultural benefits as well.

The range of ecosystem services provided by grassland biomes includes meat, milk, wool leather, maintenance of atmospheric composition and genetic library, amelioration of water and conservation of soils (Sala & Paruelo, 1997; Kang et al., 2007). Concerning ground for social interactions, grasslands are areas of large diverse biodiversity which allows for human-environment interactions (Kang et al., 2007). This human-environment interaction allows for the (re)production of goods and services. One major source of attraction from the interaction is the abundance of genetic resources available for humankind within grassland biomes (Sala & Paruelo, 1997). As pointed out by Sala & Paruelo (1997 p. 264):

> grasslands represent the natural ecosystem from where a large fraction of domesticated species originated, and where wild populations related to the domesticated species and their associated pests and pathogens still thrive [social interactions]. These areas are most likely to provide new strains that are resistant to diseases or contain new features important for humankind.

One of the important ecosystem services provided by grasslands is the maintenance of atmospheric composition in terms of carbon sequestration (Lal, 2008). Carbon sequestration is the process through which atmospheric carbon dioxide (CO_2) is secured in other long-lived carbon (C) pools to prevent them from being accumulated in the atmosphere (Lal, 2008). Sequestration of large quantities of C in grassland soils is very important with regard to maintaining the dynamics of the atmospheric carbon cycle (Fan et al., 2008). Whether below- or aboveground, the storage of carbon in grasslands is very important for the development of viable strategies for mitigating climate change at this scale. Most grasslands are threatened globally due to various direct and indirect anthropogenic factors such as an increase in the human population, deforestation, overgrazing, fires and invasive species to mention a few. These anthropogenic factors in light of changing climates are becoming amplified leading to the gradual or total destruction of global grassland communities (Kang et al., 2007). These transformations release carbon stocks sequestered in grassland biomes globally leading to the accumulation of

atmospheric carbon (CO_2). Even though several studies have presented carbon loss from various grasslands across the world due to various anthropogenic practices and natural disasters, there is still a gap in accounting for global carbon sink or loss from grassland biomes especially from the grasslands of the montane environments that are largely underrepresented (Ward et al., 2014).

Montane grasslands, like other lowland grasslands, are facing threats, but more importantly, the montane grassland soils face unique threats such as historical intensive use by humans, a greater amount of rainfall, snow cover, steep topography inhibiting widespread peatlands formation and natural disturbances such as soil erosion, rockfall, spring snow thaw and avalanches (Ward et al., 2014). Even though mountainous areas are largely inaccessible due to rugged terrains and harsh weather conditions. Human activities around this area by the "mountain people" and other people from nearby lowland areas imprint on this biome and damage this unique biodiversity. The damage most often than not is irreversible (Ward et al., 2014). The transformation of montane grasslands yields loss of carbon stock; unfortunately, their distribution, extent and volume are still of growing concern as these areas are yet to be extensively studied and accounted for in global carbon emissions as against their lowland counterparts (Ward et al., 2014). Understanding the carbon sequestration of montane grasslands requires a methodological design that can access remote areas with rugged terrains.

This study aims to evaluate global trends in biomass estimations of grasslands across montane environments using remote sensing techniques. To achieve this aim, the study will highlight growth in biomass estimation (above and below) studies across grassland biomes in montane environments using available satellites and sensors. Furthermore, the study will showcase emerging topics, trajectories and challenges in grassland biomass estimations in montane environments using remote sensing techniques. Even though in situ studies cannot be ruled out, estimation of biomass in remote environments using remote sensing techniques and tools is very germane to global carbon stock estimations and validation.

Remote sensing, in contrast with traditional approaches, offers spatial and temporal data that are convenient for mapping biomass at different spatial scales in a more vigorous, rapid and efficient manner (Fajji, 2015). Several studies have considered biomass estimation using geographic information systems (GIS) and remote sensing (RS) techniques (Fang et al., 2001; Baccini et al., 2004; Lu, 2006; de Castilho et al., 2006; Attarchi & Gloaguen, 2014; Dube & Mutanga, 2015; Chapungu et al., 2020). Very few have considered biomass estimation on montane vegetation (Attarchi & Gloaguen, 2014; Barrachina et al., 2015; Brovkina et al., 2017; Cho & Skidmore, 2009; Du et al., 2020; Massetti & Gil, 2020; Soenen et al., 2010; Sun et al., 2002). However, studies on biomass estimation on montane grasslands using GIS and remote sensing are still growing especially in areas outside China; the ones available are largely field-based studies (Ward et al., 2014) especially in Africa. Out of all these, only a few studies have considered biomass (above or below) estimation for grassland areas in montane environments (Fan et al., 2008; Gill et al., 2002). There is a need for contributions to biomass estimations in montane areas with improved studies focusing on below-ground biomass for montane grasslands. This

review is divided into the following sections: methodology, aboveground biomass and remote sensing, aboveground biomass (AGB) and RS, below-ground biomass and remote sensing, BGB and RS, grassland biomass estimations in montane environments with a sub-section on issues and challenges in Africa and finally the conclusion.

Biomass is related to many important components, such as carbon cycles, soil nutrient allocations, fuel accumulation and habitat environments in terrestrial ecosystems (de Castilho et al., 2006; Lu, 2006). Plants are responsible for biomass production through the process of photosynthesis. When plants are burned or transformed, the stored energy, in this case, carbon dioxide, CO_2, is released into the atmosphere. CO_2 is one of the most important greenhouse gases (GHGs) influencing global warming. Hence, biomass is very basic in understanding stocks of carbon in plant communities and most especially in montane grassland environments (Fan et al., 2008). Even though field measurements stand as one of the most important ways to estimate biomass especially in lowland areas, the situation in montane grasslands is rather different. The rugged terrain, altitudinal extent and remoteness of most montane areas render intensive field measurement for biomass estimation to be a laborious task. Therefore, the ability to measure and derive estimates of biomass remotely from observation platforms stands as one of the most unique ways to overcome this challenge. The ability to appropriately harness the utilities of remotely sensed products using remote sensing techniques will go a long way in ensuring improvement in biomass mapping in the light of the changing climates.

1.2 Methodology

1.2.1 Data Source

The study is approached from a global point of view. The data for this study were retrieved from the SCOPUS database. The SCOPUS database was used based on its reputation and wide acceptance. Hence, any paper published on the topic in any journal not indexed in SCOPUS would not have been retrieved. The data was downloaded in a *.bibtex* format, and it contains the title, authors, institutions, abstract, keywords, keywords plus and references, among other things (Fig. 1.1).

1.2.2 Data Retrieval

The dataset in *.bibtex* format as retrieved for this study from SCOPUS is based on the syntax “grasslands and remote sensing and mountains and biomass” or “grasses and biomass and mountain and remote sensing” or “highlands and grass and

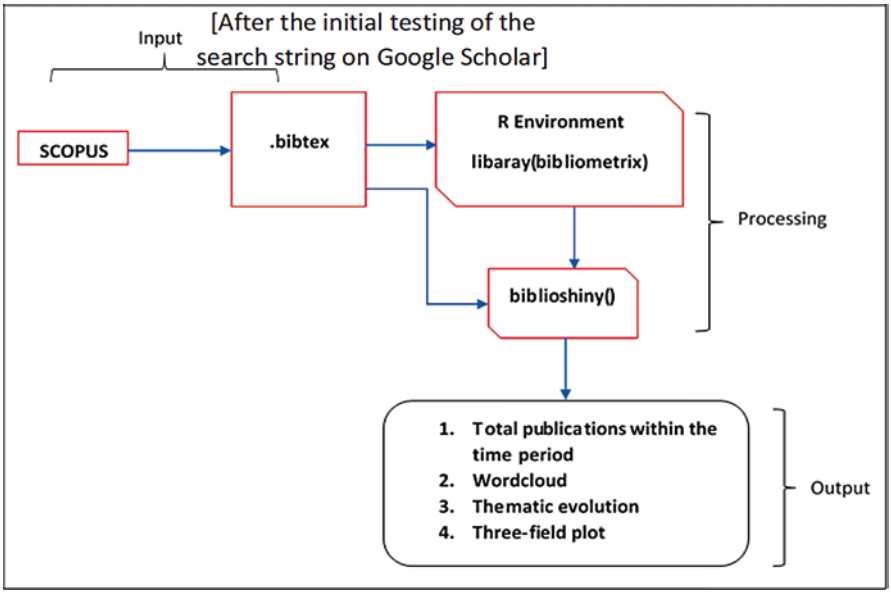

Fig. 1.1 Flowchart showing the methodology and outputs

biomass and earth observation". The choice of the search syntax is borne out of the focus of the study and careful identification of the mix of words on google scholar. The syntax used for the review was tested within Google Scholar for appraisal and stability. After careful sorting and to the satisfaction of the authors, we applied the same search protocol ([*grasslands and remote sensing and mountains and biomass*] or [*grasses and biomass and mountain and remote sensing*] *or* [*highlands and grass and biomass and earth observation*]) within the SCOPUS database.

This was essential to ensure that studies on the subject were not left out due to the choice of words. Hence, these strings of words form the focus of this study (Fig. 1.1). Therefore, any publication that is not solely on the use of remote sensing techniques for the estimation of grasslands in montane environments will not be retrieved by the search engine. Out of a total of four thousand three hundred and eighty-six (4386) papers published under the syntax "grasslands and remote sensing", only twenty-four (24) papers have been published so far using the "grasslands and remote sensing and mountains and biomass" or "grasses and biomass and mountain and remote sensing" *or* "highlands and grass and biomass and earth observation" syntax and indexed in SCOPUS (Fig. 1.1).

1.2.3 Data Analysis

The bibliometrix package in R (Aria & Cuccurullo, 2017) was used to analyse the data (Fig. 1.1) as retrieved from the SCOPUS database. The *.bibtex* format was converted into a bibliometrix file using the *convert2df* () function. The *convert2df* function converts the .bibtex format into a dataframe with variables such as but not limited to authors, countries, affiliations, references, keywords, co-authors and citations. After the conversion, the data was used to initiate the biblioshiny environment using the *biblioshiny* () function. The biblioshiny environment is a shiny app that provides a web interface for bibliometrix. From the biblioshiny app, document information, authors publication list, wordcloud, three-field plot and thematic evolution of keywords were generated (Fig. 1.1).

1.3 AGB and RS in Montane Grasslands

There has been considerable progress in the use of optical sensors in the estimation AGB of grasslands (Table 1.1). Optical remote sensing makes use of visible, near-infrared and short-wave infrared sensors to form images of the earth's surface by detecting the solar radiation reflected from targets on the ground. In simple terms, it makes use of natural radiation from the sun and provides a two-dimensional view of grasslands and other earth surface topographies. Most optical images such as Landsat and Sentinel-2 are freely accessible and affordable and have allowed a large number of studies to freely use the products from these optical sensors. AGB estimation in lowland grasslands has proved successful using either active or passive optical sensors (Niu & Ni, 2003; Ali et al., 2017; Guerini Filho et al., 2020).

Multispectral data such as the Landsat MSS, Landsat TM and Advanced Very High-Resolution Radiometer (AVHRR) has been successfully used in many different areas across the world for estimating grassland biomass (Niu & Ni, 2003; Nguyen et al., 2020); while some others have enhanced grassland biomass estimation with machine learning algorithms (Adepoju & Adelabu, 2020; Silveira et al., 2019), their use in montane grassland studies is largely constrained and remains limited (Table 1.1). These constraints are due to the regular cloud conditions that often restrain the acquisition of high-quality remotely sensed data by optical sensors (Mohd Zaki & Abd Latif, 2017; Xu et al., 2020). Furthermore, vegetation indices (VI) computed from these optical sensors reach a saturation level on high-density biomass estimation (Mutanga & Skidmore, 2004). In their study, on narrow-band vegetation indices, Mutanga and Skidmore (2004) posited that limited channels on multispectral images restrict the estimation of vegetal indices such as the Normalized Difference Vegetation Index (NDVI) because they asymptotically approach a saturation level after a certain biomass density due to growing seasons, a view upheld by several authors (see Mutanga & Skidmore, 2004).

Table 1.1 Biomass estimation: sensors, findings and references from 2009 to 2020

Sensor(s)	Elevation	Findings	References
Optical sensors			
Landsat (5, 7, 8)	Montane	Landsat archive is a great resource for reconstructing grassland areas, and Landsat improves the estimation of biomass	Kuang et al. (2020), Morley et al. (2019), Primi et al. (2016), Barrachina et al. (2015), Borrelli et al. (2015), Elias et al. (2015) and Chen et al. (2014)
MODIS	Montane	The capability of MODIS with or without climatic variables and VI provides a good estimate of biomass across montane environments	Zhang et al. (2018); Kuang et al. (2020), De Leeuw et al. (2019), Yang et al. (2016), Choler (2015), Maselli et al. (2013) and Yan et al. (2021)
RapidEye	Montane	RapidEye is identified as a suitable product for biomass estimation and an improvement against some other optical sensors	Magiera et al. (2017)
GeoEye	Montane	Applicability of GeoEye in biomass estimation was satisfactory	Morley et al. (2019)
Sentinel-1	Montane	As with other optical sensors, Sentinel-1 also provides a good estimate for biomass	Morley et al. (2019)
Systéme Pour lObservation de la Terre (SPOT)	Montane	It was established that the (SPOT) NDVI-biomass relationship can be quantified effectively and is a good indicator of biomass	Morley et al (2019) and Klinge et al (2018)
Airborne			
Unarmed aerial vehicle (UAVs) Multi-rotor UAV equipped with Micro-MCA12 Snap Airborne Visible and InfraRed Imaging Spectrometer (AVIRIS)	Montane	The study analyses the spatio-temporal changes in AGB using UAVs in Tianshan Mountain. The author posited that poor correlations exist between aboveground biomass and VIs, but these correlations improved remarkably after considering the terrain factors Furthermore, using the airborne AVIRIS, Ernst et al. (2003) discriminated against different grass species on the White-Inyo Range, Eastern California. This was later used to understand the relationship between vegetation and climate and geology	Ernst et al. (2003)

Despite the aforementioned limitations in the use of optical sensors, success has been recorded in the use of GeoEye, RapidEye, Sentinel, SPOT, Landsat and most especially Moderate Resolution Imaging Spectroradiometer (MODIS) (Table 1.1). The level of success recorded has been attributed to but not limited to the use of narrow-band vegetation indices computed from hyperspectral data and high spectral resolutions to estimate biomass (Zhang et al., 2020), especially with some results showing that modified vegetation indices calculated from the red-edge and near-infrared shoulder domains can successfully estimate biomass (Table 1.1) as compared to the standard red or infrared-based indices. Cho and Skidmore (2009) in their study conducted within the Majella National Park, Italy, a Mediterranean montane area, between 2004 and 2005 extracted vegetation indices (VIs) (narrow-band NDVI, modified soil-adjusted vegetation index, NSAVI, and normalized difference water index, NDWI) and also red-edge positions (REP) from HyMap image, an airborne hyperspectral imaging sensor. They concluded in their study that VIs are a weak predictor of grass/herb biomass within their study area. However, they concluded that narrow bands in the red-edge positions are more consistent predictors of biomass estimations in montane grasslands. The limitations regarding hyperspectral data sources include but are not limited to cost, availability, processing and high dimensionality.

Generally, whether it is hyperspectral or multispectral, Lu (2006) and Wu et al. (2016) affirmed that the use of moderate to coarse spatial resolution sensors such as Landsat, MODIS and AVHRR for AGB estimation especially in montane grassland results in poor forecast accuracy. This is because of the occurrence of mixed pixels composed with a mismatch between the size of sections and the pixel since the area consists of different landscapes. However, despite these limitations, passive optical sensors are still the first point of call for most AGB estimations because of availability, free-to-low-cost, coverage and spectral resolution.

1.4 BGB and RS in Montane Grasslands

Below-ground biomass (BGB) is the biomass totality of live roots except for those roots less than 2 mm in diameter. Live roots less than 2 mm in diameter are largely excluded because of the yet-to-be verified difference between these roots and soil organic matter. Globally, BGB accounts for about 20% of the total biomass. Therefore, the direct estimation of below-ground biomass is very important especially in estimating the total carbon pool and understanding carbon loss and storage for specific environments. Conventionally, the following methods are used in the estimation and monitoring of BGB. These are the excavation of roots, monolith for deep roots, soil core or pit for non-tree vegetation, root-to-shoot ratio and allometric equations (Fan et al., 2008; Peng et al., 2020). BGB estimations for most grassland studies have employed the above-listed methods or a combination of field-based studies (Fan et al., 2008; Peng et al., 2020).

Compared to AGB, BGB of grassland communities is still growing in the literature. The use of remote sensing techniques in the estimation of BGB is still growing even for lowland studies. Chapungu et al. (2020) estimated BGB of savanna grasslands using an indirect relationship between AGB and BGB and then comparing that with NDVI. In their study, they stated the limitations of multispectral data especially those obtained from Landsat images. They concluded that for grassland biomass estimation, multispectral sensors of Sentinel-2 and Worldview-3 hold great promise using the red-edge region. For montane environments, BGB estimations for grasslands are few and far in between. There is a need for studies on BGB estimations for montane grasslands using remote sensing techniques to fully understand these unique ecosystems and their dynamics.

1.5 Grasslands Biomass Estimation in Montane Environments: Global Knowledge

Globally, the state of knowledge with regard to biomass estimations in montane environments is just growing. The first paper emerged on the global scene in 2003 (Table 1.2). The highest number of papers, five (5) in total, was published in the year 2015 and then three published in the year 2018; every other year had less than three publications (Table 1.2). The growth of papers in biomass estimation of grasslands in montane environments has not been very great, and the reasons could be but not limited to the terrain, available sensors and the importance attached to this ecosystem. From these studies, the platform for data extraction has been mainly from space (satellites), while only two studies have made use of airborne instruments (Sun et al., 2018).

On the global scene, some authors have contributed greatly to the subject matter. These authors such as Magiera, A., Feilhauer, H., Waldhardt, R., Wiesmair, M., Otte, A, Barrachina, M and Zhang, Y (Fig. 1.3), have published at least two papers on the subject matter. Across the available studies, most of the keywords outside grasslands, remote sensing and biomass have been on but not limited to some parts of China and Italy.

Attempting a spatio-temporal evolution of these keywords reveals how over time (2003–2020), there has been growth in the direction of studies on grasslands, biomass and remote sensing in montane environments (Fig. 1.2). Studies involving carrying capacity, ecosystems and spatial distribution entered the narrative of studies on grasslands within montane environments using remote sensing in 2016. Since 2016, these words have stayed to date. However, there has been little concern about below-ground biomass. The focus has been on aboveground biomass, primary production of grasslands within these environments. The most prominent sensor has been the MODIS, while the only machine learning tool observed between the period is the random forest (Fig. 1.3).

Table 1.2 Progression of publications from 2003 to 2020

Year	No and title(s)
2003	1. Reindeer Pasture Biomass Assessment Using Satellite Remote Sensing 2. Relationships among vegetation, climatic zonation, soil, and bedrock in the central White-Inyo Range, eastern California: A ground-based and remote-sensing study
2009	1. Influences of changing land use and CO_2 concentration on ecosystem and landscape level carbon and water balances in mountainous terrain of the Stubai Valley, Austria
2010	1. Spatial Analysis of Fire Potential in Iran Different Region by Using RS and GIS 2. Development of new vegetation indexes, shadow index (si) and water stress trend (wst)
2011	1. The correlation analysis between herbage yield and ecoclimatic factors and carbon storage accounting of desert grassland in Xinjiang, China
2013	1. Simulation of grassland productivity by the combination of ground and satellite data
2014	1. The application of grassland aboveground biomass estimating model in Karst mountainous area
2015	1. Estimating above-ground biomass on mountain meadows and pastures through remote sensing 2. The implications of fire management in the andean paramo: A preliminary assessment using satellite remote sensing 3. Land conversion dynamics in the borana rangelands of southern Ethiopia: An integrated assessment using remote sensing techniques and field survey data 4. Growth response of temperate mountain grasslands to inter-annual variations in snow cover duration 5. 2015 8th International Workshop on the Analysis of Multitemporal Remote Sensing Images, Multi-Temp 2015
2016	1. Monitoring of grassland herbage accumulation by remote sensing using MODIS daily surface reflectance data in the Qingnan Region 2. From Landsat to leafhoppers: A multidisciplinary approach for sustainable stocking assessment and ecological monitoring in mountain grasslands
2017	1. Modelling biomass of mountainous grasslands by including a species composition map 2. Natural mowing grassland resource distribution and biomass estimation based on remote sensing in Hulunber
2018	1. Mapping Plant Functional Groups in Subalpine Grassland of the Greater Caucasus 2. Climate effects on vegetation vitality at the treeline of boreal forests of Mongolia 3. Estimating aboveground biomass of natural grassland based on multispectral images of Unmanned Aerial Vehicles.
2019	1. Application of the MODIS MOD 17 Net Primary Production product in grassland carrying capacity assessment 2. Quantifying structural diversity to better estimate change at mountain forest margins
2020	1. A remote sensing monitoring method for alpine grasslands desertification in the eastern Qinghai-Tibetan Plateau 2. Spatial distribution pattern of NPP of Xinjiang grassland and its response to climatic changes

1.6 Issues and Challenges in Africa

The issues and challenges surrounding African grasslands can be conceptually captured using the DPSIR (Drivers, Pressures, State, Impact and Response) Framework (Agyemang et al., 2007). The grasslands of Africa are savannas asides from the velds of Southern Africa. The savanna in Africa is the most extensive in the world

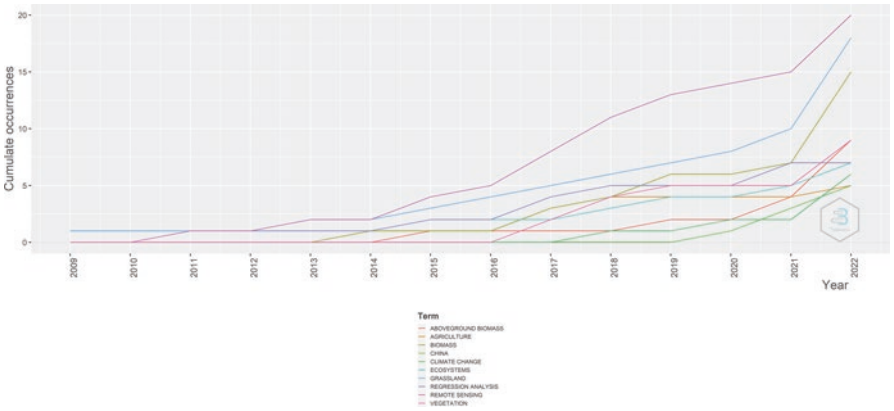

Fig. 1.2 Thematic evolution describing the focus of studies from 2003 to 2020

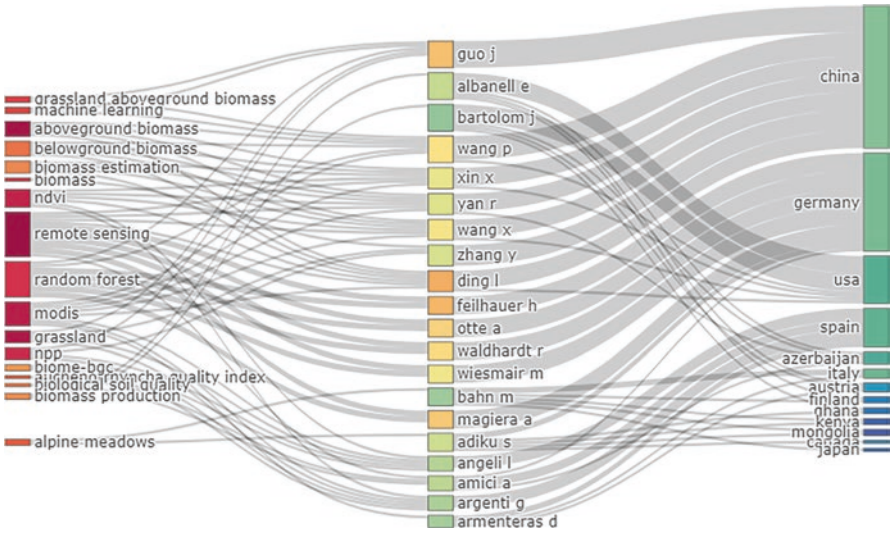

Fig. 1.3 Three-field plot showing keywords (left), authors (middle) and keyword plus (right)

covering almost half of the continent. Grasslands of Africa (savanna and the velds) form a significant component of Africa's terrestrial ecosystem covering not less than 30% of the land area and contribute about 20% of the total terrestrial primary productivity. In Africa and most especially in the southern part of the continent, grasslands are said to be an entirely important source of livestock forage, which does support the entire livelihood of the community depending and relying on it as well as the wildlife population (Schmidt and Skidmore 2001; Xu and Guo 2015).

However, before delving headlong into the challenges and issues, a background into existing studies will be provided. Few studies have been carried out on the

estimation of grassland biomass in lowlands of the African environments using remote sensing techniques (Fajji, 2015; Shoko et al., 2016; Sibanda et al., 2016; Timothy et al., 2016; de Leeuw et al., 2019; Dingaan & Tsubo, 2019; Naidoo et al., 2019). Studies within the highlands across African environments have been on forest biomass (Adagbasa et al., 2020; Adagbasa et al., 2019; Adepoju & Adelabu, 2019), while studies focusing on grassland biomass using remote sensing techniques in montane environments are few. From the sampled dataset, none of the existing papers focused on Africa. This shows a key knowledge gap as regards carbon sequestration and loss across montane environments in Africa (Fig. 1.2). Even though studies have been carried out within montane environments in Africa which suggests that the basic requirement and datasets required for grassland studies are available, reasons for the low turnout on montane grassland and biomass estimation using remote sensing remain yet unsolved.

As with other biomes of the world, the *drivers* of African grasslands are largely human populations, livelihood patterns, wildlife and landuse/landcover. These drivers put a strain on the grassland communities and ecosystem provisioning. These drivers create *pressures* on the grassland community through various human activities such as fires, urbanization, cultivation, climate change, grazing and invasive species (Balima et al., 2020; Gallego-Zamorano et al., 2020; Newbold et al., 2017; Waters et al., 2019) and, as a result, alter the *state* of the grassland biome completely. The *state* of the African grassland community at present is an accumulation of pressures over the years. Across the continent, the grassland community in some quarters has witnessed gradual destruction, while some have been completely wiped out. The gradual change or changes being witnessed across African grassland environments is a major contributor to total carbon loss into the atmosphere (Chapungu et al., 2020). The use of satellite data has proved useful in the understanding of pressures and state. It has helped in detecting patterns of both interannual and seasonal variations of the land surface features as a result of various pressures such as fires (Adagbasa, Adelabu, Okello, et al. 2019; Adelabu et al., 2018; Adepoju & Adelabu, 2019), anthropogenic activities (direct and indirect) (Adeola et al. 2020) and consequences of climate change (Propastin et al., 2006) such as drought, dehydration, instabilities in rainfall patterns (Balas et al., 2007) and high temperature (Xiao & Moody, 2004). These climatic variables and other pressures including anthropogenic are products that are fully captured from remotely sensed platforms at various resolutions and are disseminated daily, hourly, seasonally and monthly, based on the observing satellites, sensors, their orbits and objectives (Wang et al., 2003). These techniques can be applied over Africa with a more focused and concerted effort. The *impact* of these increases the total amount of greenhouse gases (GHGs) being released into the atmosphere. There is therefore a need to respond by arresting the threat to grassland communities not only to save the community but also to preserve the entire environment and forestall the increasing impact of climate change. The *response* of governments and stakeholders such as conservationists, park rangers, environmentalists, academia and the communities is to work together and be involved in the co-production of knowledge and sustainable methods that would help save the grasslands of Africa. Therefore, adequate and enhanced environmental

monitoring using remotely sensed products and techniques (Table 1.1) proves to be a reliable means of monitoring the impact, variations and dynamics of the changing African grassland communities especially the montane grasslands of Africa (Booth & Tueller, 2003).

Therefore, one major way out is the effective use of remote sensing techniques and geographic information systems, in a more coordinated manner which includes but not limited to the establishment of montane research units in various zones of the continents such as the Afromontane Unit in South Africa, to focus on montane activities across these zones in Africa. Together, these units using remotely sensed products and ground-based datasets to monitor, map and understand more closely the montane grassland biome will eventually help in the conservation and monitoring of grasslands in Africa and contribute to the global atmospheric storage of carbon. This will go a long way in the conservation and protection of biodiversity within the grassland biomes in Africa. The stability and the resilience of the ecosystem largely depend on this to ensure the continued supply of ecosystem services from this threatened biome, in quality and quantity as and when needed.

1.7 Conclusion

Firstly, this study has shown that the difficulty in accessing montane areas due to reasons such as terrain could be one of the reasons for the low output in terms of publication on montane grassland studies, despite the fact that these ecosystems are covered by a variety of vegetation types that are largely unique to their environments and some of these grasses are yet to be fully classified, especially in Africa. Therefore, there is still a lot to be done by improving on studies on montane grasslands especially the below-ground biomass using remote sensing techniques. As already highlighted in the study, remote sensing platforms offer a solution since it is a technology that offers information in very high resolutions and is independent of topographic conditions.

Optical sensors with either wider or special spectral bands such as Sentinel-2, RapidEye and Worldview have great potentialities in biomass estimation. These optical satellites when fused with either RADAR or LiDAR could provide enhanced information on biomass estimations in mountainous regions especially in the red-edge positions. Other positions along the electromagnetic spectrum such as the red and near-infrared are also of importance but more restricted and sensitive to weather conditions making satellites such as the NOAA, AVHRR, MODIS and Landsat of limited use.

Summarily, for biomass estimations (above or below), the use of active sensors holds great promise and opens a world of opportunities. However, cost especially for these active sensors stands to be an issue. Sentinel-1, radar, when fused with optical sensors has immense capabilities to offer in the estimation of biomass especially in montane environments. Even though studies using remotely sensed products to estimate below-ground biomass of montane grasslands are very few globally,

the inherent characteristics of the sensors and their applications in lowland areas show that their application in montane areas cannot be overemphasized. Radar images have longer wavelengths; hence, they can penetrate further than optical sensors, and coupled with the fact that some radar images are freely available makes it even better for montane environments in Africa. The emergence of Sentinel satellite missions provides unlimited radar products at no cost. Also, Worldview-2 and Worldview-3 and RapidEye satellite missions provide datasets with multispectral channels that can be fused with radar images to improve the quality of biomass estimations across montane environments. This in essence provides a way to improve studies on montane biomass grassland estimations across the world and especially in Africa.

References

Adagbasa, E. G., Adelabu, S. A., & Okello, T. W. (2020). Development of post-fire vegetation response-ability model in grassland mountainous ecosystem using GIS and remote sensing. *ISPRS Journal of Photogrammetry and Remote Sensing, 164*, 173–183. https://doi.org/10.1016/j.isprsjprs.2020.04.006

Adagbasa, E. G., Adelabu, S. A., & Okello, T. W. (2019). Application of deep learning with stratified K-fold for vegetation species discrimination in a protected mountainous region using Sentinel-2 image. *Geocarto International, 37*(1), 142–162. https://doi.org/10.1080/10106049.2019.1704070

Adelabu, S. A., Adepoju, K. A., & Mofokeng, O. D. (2018). Geocarto International Estimation of fire potential index in mountainous protected region using remote sensing Estimation of fire potential index in mountainous protected region using remote sensing. *Taylor & Francis, 35*(1), 29–46. https://doi.org/10.1080/10106049.2018.1499818

Adeola, F. O., Gbenga, A. E., Oludapo, O. A., & Oluseyi, O. R. (2020). Land use/land cover change and land surface temperature of Ibadan and environs, Nigeria. *Environmental Monitoring and Assessment, 192*(2), 1–8. https://doi.org/10.1007/s10661-019-8054-3

Adepoju, K. A., & Adelabu, S. A. (2020). Improving accuracy evaluation of Landsat-8 OLI using image composite and multisource data with Google Earth Engine. *Remote Sensing Letters, 11*(2), 107–116. https://doi.org/10.1080/2150704X.2019.1690792

Adepoju, K. A., & Adelabu, S. A. (2019). Assessment of fuel and wind drivers of fire risk in protected mountainous grassland of South Africa. In *IGARSS 2019-2019 IEEE international geoscience and remote sensing symposium* (pp. 867–870). IEEE. https://doi.org/10.1109/igarss.2019.8900100

Agyemang, I., McDonald, A., & Carver, S. (2007). Application of the DPSIR framework to environmental degradation assessment in northern Ghana. *Natural Resources Forum, 31*(3), 212–225. https://doi.org/10.1111/j.1477-8947.2007.00152.x

Ali, I., Cawkwell, F., Dwyer, E., & Green, S. (2017). Modeling managed grassland biomass estimation by using multitemporal remote sensing data-a machine learning approach. *IEEE Journal of Selected Topics in Applied Earth Observations and Remote Sensing, 10*(7), 3254–3264. https://doi.org/10.1109/JSTARS.2016.2561618

Aria, M., & Cuccurullo, C. (2017). bibliometrix: An R-tool for comprehensive science mapping analysis. *Journal of Informetrics, 11*(4), 959–975.

Attarchi, S., & Gloaguen, R. (2014). Improving the estimation of above ground biomass using dual polarimetric PALSAR and ETM+ data in the Hyrcanian mountain forest (Iran). *Remote Sensing, 6*(5), 3693–3715. https://doi.org/10.3390/rs6053693

Baccini, A., Friedl, M. A., Woodcock, C. E., & Warbington, R. (2004). Forest biomass estimation over regional scales using multisource data. *Geophysical Research Letters, 31*(10), L10501. https://doi.org/10.1029/2004GL019782

Balas, N., Nicholson, S. E., & Klotter, D. (2007). The relationship of rainfall variability in West Central Africa to sea-surface temperature fluctuations. *International Journal of Climatology: A Journal of the Royal Meteorological Society, 27*(10), 1335–1349.

Balima, L. H., Nacoulma, B. M. I., Bayen, P., Kouamé, F. N. G., & Thiombiano, A. (2020). Agricultural land use reduces plant biodiversity and carbon storage in tropical West African savanna ecosystems: Implications for sustainability. *Global Ecology and Conservation, 21*, e00875. https://doi.org/10.1016/j.gecco.2019.e00875

Barrachina, M., Cristóbal, J., & Tulla, A. F. (2015). Estimating above-ground biomass on mountain meadows and pastures through remote sensing. *International Journal of Applied Earth Observation and Geoinformation, 38*, 184–192. https://doi.org/10.1016/j.jag.2014.12.002

Borrelli, P., Armenteras, D., Panagos, P., Modugno, S., & Schütt, B. (2015). The implications of fire management in the Andean páramo: a preliminary assessment using satellite remote sensing. *Remote Sensing, 7*(9), 11061–11082.

Booth, D. T., & Tueller, P. T. (2003). Rangeland monitoring using remote sensing. *Arid Land Research and Management, 17*(4), 455–467.

Brovkina, O., Novotny, J., Cienciala, E., Zemek, F., & Russ, R. (2017). Mapping forest aboveground biomass using airborne hyperspectral and LiDAR data in the mountainous conditions of Central Europe. *Ecological Engineering, 100*, 219–230. https://doi.org/10.1016/j.ecoleng.2016.12.004

Chapungu, L., Nhamo, L., & Gatti, R. C. (2020). Estimating biomass of savanna grasslands as a proxy of carbon stock using multispectral remote sensing. *Remote Sensing Applications: Society and Environment, 17*, 100275. https://doi.org/10.1016/j.rsase.2019.100275

Chen, B., Zhang, X., Tao, J., Wu, J., Wang, J., Shi, P., ... & Yu, C. (2014). The impact of climate change and anthropogenic activities on alpine grassland over the Qinghai-Tibet Plateau. *Agricultural and Forest Meteorology, 189*, 11–18.

Cho, M. A., & Skidmore, A. K. (2009). Hyperspectral predictors for monitoring biomass production in Mediterranean mountain grasslands: Majella National Park, Italy. *International Journal of Remote Sensing, 30*(2), 499–515. https://doi.org/10.1080/01431160802392596

Choler, P. (2015). Growth response of temperate mountain grasslands to inter-annual variations in snow cover duration. *Biogeosciences, 12*(12), 3885–3897.

Daily, G. C. (1997). *Nature's services (vol. 3, issue 5)*. https://doi.org/10.1017/CBO9781107415324.004

de Castilho, C. V., Magnusson, W. E., de Araújo, R. N. O., Luizão, R. C. C., Luizão, F. J., Lima, A. P., & Higuchi, N. (2006). Variation in aboveground tree live biomass in a central Amazonian Forest: Effects of soil and topography. *Forest Ecology and Management, 234*(1–3), 85–96. https://doi.org/10.1016/j.foreco.2006.06.024

de Leeuw, J., Rizayeva, A., Namazov, E., Bayramov, E., Marshall, M. T., Etzold, J., & Neudert, R. (2019). Application of the MODIS MOD 17 Net Primary Production product in grassland carrying capacity assessment. *International Journal of Applied Earth Observation and Geoinformation, 78*, 66–76. https://doi.org/10.1016/j.jag.2018.09.014

Dingaan, M. N. V., & Tsubo, M. (2019). Improved assessment of pasture availability in semi-arid grassland of South Africa. *Environmental Monitoring and Assessment, 191*(12), 1–12. https://doi.org/10.1007/s10661-019-7918-x

Du, Y., He, W., Zhou, J., Ma, S., Yuan, J., & Wang, Y. (2020). Dynamic changes of aboveground biomass of vegetation in Qaidam Basin. In *IOP conference series: Earth and environmental science* (Vol. 428, p. 012086). IOP Publishing.. https://doi.org/10.1088/1755-1315/428/1/012086

Dube, T., & Mutanga, O. (2015). Evaluating the utility of the medium-spatial resolution Landsat 8 multispectral sensor in quantifying aboveground biomass in uMgeni catchment, South Africa. *ISPRS Journal of Photogrammetry and Remote Sensing, 101*, 36–46. https://doi.org/10.1016/j.isprsjprs.2014.11.001

Egoh, B. N., Reyers, B., Rouget, M., & Richardson, D. M. (2011). Identifying priority areas for ecosystem service management in South African grasslands. *Journal of Environmental Management, 92*(6), 1642–1650. https://doi.org/10.1016/j.jenvman.2011.01.019

Elias, M., Hensel, O., Richter, U., Hülsebusch, C., Kaufmann, B., & Wasonga, O. (2015). Land conversion dynamics in the Borana rangelands of Southern Ethiopia: an integrated assessment using remote sensing techniques and field survey data. *Environments, 2*(1), 1.

Ernst, W. G., Van de Ven, C. M., & Lyon, R. J. P. (2003). Relationships among vegetation, climatic zonation, soil, and bedrock in the central White-Inyo Range, eastern California: A ground-based and remote-sensing study. *Geological Society of America Bulletin, 115*(12), 1583–1597.

Fajji, N. G. (2015). *A remote sensing and gis scheme for rangeland quality assessment and management in the north west province, South Africa*. http://repository.nwu.ac.za/handle/10394/24952

Fan, J., Zhong, H., Harris, W., Yu, G., Wang, S., Hu, Z., & Yue, Y. (2008). Carbon storage in the grasslands of China based on field measurements of above- and below-ground biomass. *Climatic Change, 86*(3–4), 375–396. https://doi.org/10.1007/s10584-007-9316-6

Fang, J., Chen, A., Peng, C., Zhao, S., & Ci, L. (2001). Changes in forest biomass carbon storage in China between 1949 and 1998. *Science, 292*(5525), 2320–2322. https://doi.org/10.1126/science.1058629

Gallego-Zamorano, J., Benítez-López, A., Santini, L., Hilbers, J. P., Huijbregts, M. A. J., & Schipper, A. M. (2020). Combined effects of land use and hunting on distributions of tropical mammals. *Conservation Biology, 34*(5), 1271–1280. https://doi.org/10.1111/cobi.13459

Gill, R. A., Kelly, R. H., Parton, W. J., Day, K. A., Jackson, R. B., Morgan, J. A., Scurlock, J. M. O., Tieszen, L. L., Castle, J. V., Ojima, D. S., & Zhang, X. S. (2002). Using simple environmental variables to estimate below-ground productivity in grasslands. *Global Ecology and Biogeography, 11*(1), 79–86. https://doi.org/10.1046/j.1466-822X.2001.00267.x

Guerini Filho, M., Kuplich, T. M., & Quadros, F. L. F. D. (2020). Estimating natural grassland biomass by vegetation indices using Sentinel 2 remote sensing data. *International Journal of Remote Sensing, 41*(8), 2861–2876. https://doi.org/10.1080/01431161.2019.1697004

Kang, L., Han, X., Zhang, Z., & Sun, O. J. (2007). Grassland ecosystems in China: Review of current knowledge and research advancement. *Philosophical Transactions of the Royal Society B: Biological Sciences, 362*(1482), 997–1008. https://doi.org/10.1098/rstb.2007.2029

Kuang, Q., Yuan, Q. Z., Han, J. C., Leng, R., Wang, Y. S., Zhu, K. H., ... & Ren, P. (2020). A remote sensing monitoring method for alpine grasslands desertification in the eastern Qinghai-Tibetan plateau. *Journal of Mountain Science, 17*(6), 1423–1437.

Lal R (2008) Carbon sequestration. In Philosophical transactions of the royal society B: Biological sciences (Vol. 363, 1492, 815–830). Royal Society. https://doi.org/10.1098/rstb.2007.2185

Lu, D. (2006). The potential and challenge of remote sensing-based biomass estimation. *International Journal of Remote Sensing, 27*(7), 1297–1328. https://doi.org/10.1080/01431160500486732

Magiera, A., Feilhauer, H., Waldhardt, R., Wiesmair, M., & Otte, A. (2017). Modelling biomass of mountainous grasslands by including a species composition map. *Ecological Indicators, 78*, 8–18.

Maselli, F., Argenti, G., Chiesi, M., Angeli, L., & Papale, D. (2013). Simulation of grassland productivity by the combination of ground and satellite data. *Agriculture, Ecosystems & Environment, 165*, 163–172.

Massetti, A., & Gil, A. (2020). Mapping and assessing land cover/land use and aboveground carbon stocks rapid changes in small oceanic islands' terrestrial ecosystems: A case study of Madeira Island, Portugal (2009–2011). *Remote Sensing of Environment, 239*, 111625. https://doi.org/10.1016/j.rse.2019.111625

Mohd Zaki, N. A., & Abd Latif, Z. (2017). Carbon sinks and tropical forest biomass estimation: A review on role of remote sensing in aboveground-biomass modelling. *Geocarto International, 32*(7), 701–716. https://doi.org/10.1080/10106049.2016.1178814

Morley, P. J., Donoghue, D. N., Chen, J. C., & Jump, A. S. (2019). Quantifying structural diversity to better estimate change at mountain forest margins. *Remote Sensing of Environment, 223*, 291–306.

Mutanga, O., & Skidmore, A. K. (2004). Narrow band vegetation indices overcome the saturation problem in biomass estimation. *International Journal of Remote Sensing, 25*(19), 3999–4014.

Naidoo, L., van Deventer, H., Ramoelo, A., Mathieu, R., Nondlazi, B., & Gangat, R. (2019). Estimating above ground biomass as an indicator of carbon storage in vegetated wetlands of the grassland biome of South Africa. *International Journal of Applied Earth Observation and Geoinformation, 78*, 118–129. https://doi.org/10.1016/j.jag.2019.01.021

Newbold, T., Boakes, E. H., Hill, S. L. L., Harfoot, M. B. J., & Collen, B. (2017). The present and future effects of land use on ecological assemblages in tropical grasslands and savannas in Africa. *Oikos, 126*(12), 1760–1769. https://doi.org/10.1111/oik.04338

Nguyen, T. H., Jones, S., Soto-Berelov, M., Haywood, A., & Hislop, S. (2020). Landsat time-series for estimating forest aboveground biomass and its dynamics across space and time: A review. *Remote Sensing, 12*(1), 1–25. https://doi.org/10.3390/RS12010098

Niu, Z., & Ni, S. (2003). Study on models for monitoring of grassland biomass around Qinghai Lake assisted by remote sensing. *Dili Xuebao/Acta Geographica Sinica, 58*(5), 695–702. http://en.cnki.com.cn/Article_en/CJFDTotal-DLXB200305006.htm

Peng, F., Xue, X., You, Q., Sun, J., Zhou, J., Wang, T., & Tsunekawa, A. (2020). Change in the trade-off between aboveground and belowground biomass of alpine grassland: Implications for the land degradation process. *Land Degradation and Development, 31*(1), 105–117. https://doi.org/10.1002/ldr.3432

Peter, K. (2004). *The DPSIR framework*, *10*.

Primi, R., Filibeck, G., Amici, A., Bückle, C., Cancellieri, L., Di Filippo, A., ... & Piovesan, G. (2016). From Landsat to leafhoppers: a multidisciplinary approach for sustainable stocking assessment and ecological monitoring in mountain grasslands. *Agriculture, Ecosystems & Environment, 234*, 118–133.

Propastin, P., Muratova, N., & Kappas, M. (2006). Reducing uncertainty in analysis of relationship between vegetation patterns and precipitation. In *7th International Symposium on Spatial Accuracy Assessment in Natural Resources and Environmental Sciences* (pp. 5–7).

Sala, O. E., & Paruelo, J. M. (1997). Ecosystem services in grasslands. *Nature's services: Societal dependence on natural ecosystems*, 237–251.

Schmidt, K. S., & Skidmore, A. K. (2001). Exploring spectral discrimination of grass species in African rangelands. *International Journal of Remote Sensing, 22*(17), 3421–3434.

Shoko, C., Mutanga, O., & Dube, T. (2016). Progress in the remote sensing of C3 and C4 grass species aboveground biomass over time and space. *ISPRS Journal of Photogrammetry and Remote Sensing, 120*, 13–24. https://doi.org/10.1016/j.isprsjprs.2016.08.001

Sibanda, M., Mutanga, O., & Rouget, M. (2016). Comparing the spectral settings of the new generation broad and narrow band sensors in estimating biomass of native grasses grown under different management practices. *GIScience and Remote Sensing, 53*(5), 614–633. https://doi.org/10.1080/15481603.2016.1221576

Silveira, E. M. O., Silva, S. H. G., Acerbi-Junior, F. W., Carvalho, M. C., Carvalho, L. M. T., Scolforo, J. R. S., & Wulder, M. A. (2019). Object-based random forest modelling of aboveground forest biomass outperforms a pixel-based approach in a heterogeneous and mountain tropical environment. *International Journal of Applied Earth Observation and Geoinformation, 78*, 175–188. https://doi.org/10.1016/j.jag.2019.02.004

Soenen, S. A., Peddle, D. R., Hall, R. J., Coburn, C. A., & Hall, F. G. (2010). Estimating aboveground forest biomass from canopy reflectance model inversion in mountainous terrain. *Remote Sensing of Environment, 114*(7), 1325–1337. https://doi.org/10.1016/j.rse.2009.12.012

Sun, G., Ranson, K. J., & Kharuk, V. I. (2002). Radiometric slope correction for forest biomass estimation from SAR data in the Western Sayani Mountains, Siberia. *Remote Sensing of Environment, 79*(2–3), 279–287. https://doi.org/10.1016/S0034-4257(01)00279-6

Sun, Y., Yi, S., & Hou, F. (2018). Unmanned aerial vehicle methods makes species composition monitoring easier in grasslands. *Ecological Indicators, 95*, 825–830.

Timothy, D., Onisimo, M., Cletah, S., Adelabu, S., & Tsitsi, B. (2016). Remote sensing of aboveground forest biomass: A review. *Tropical Ecology, 57*(2), 125–132. https://pdfs.semanticscholar.org/3531/03ff6537860bd72676d2e64e691473753610.pdf

Wang, J., Liu, X., Christopher, S. A., Reid, J. S., Reid, E., & Maring, H. (2003). The effects of non-sphericity on geostationary satellite retrievals of dust aerosols. *Geophysical Research Letters, 30*(24). https://doi.org/10.1029/2003GL01869

Ward, A., Dargusch, P., Thomas, S., Liu, Y., & Fulton, E. A. (2014). A global estimate of carbon stored in the world's mountain grasslands and shrublands, and the implications for climate policy. *Global Environmental Change, 28*(1), 14–24. https://doi.org/10.1016/j.gloenvcha.2014.05.008

Waters, C. M., McDonald, S. E., Reseigh, J., Grant, R., & Burnside, D. G. (2019). Insights on the relationship between total grazing pressure management and sustainable land management: Key indicators to verify impacts. *Rangeland Journal, 41*(6), 535–556. https://doi.org/10.1071/RJ19078

Wu, J., Wurst, S., & Zhang, X. (2016). Plant functional trait diversity regulates the nonlinear response of productivity to regional climate change in Tibetan alpine grasslands. *Scientific reports, 6*(1), 1–10.

Xiao, J., & Moody, A. (2004). Photosynthetic activity of US biomes: Responses to the spatial variability and seasonality of precipitation and temperature. *Global Change Biology, 10*(4), 437–451.

Xu, D., & Guo, X. (2015). Some insights on grassland health assessment based on remote sensing. *Sensors, 15*(2), 3070–3089.

Xu, K., Su, Y., Liu, J., Hu, T., Jin, S., Ma, Q., Zhai, Q., Wang, R., Zhang, J., Li, Y., Liu, H., & Guo, Q. (2020). Estimation of degraded grassland aboveground biomass using machine learning methods from terrestrial laser scanning data. *Ecological Indicators, 108*, 105747. https://doi.org/10.1016/j.ecolind.2019.105747

Yang, Y., Wang, Z., Li, J., Gang, C., Zhang, Y., Zhang, Y., ... & Qi, J. (2016). Comparative assessment of grassland degradation dynamics in response to climate variation and human activities in China, Mongolia, Pakistan and Uzbekistan from 2000 to 2013. *Journal of Arid Environments, 135*, 164–172.

Yan, K., Pu, J., Park, T., Xu, B., Zeng, Y., Yan, G., ... & Myneni, R. B. (2021). Performance stability of the MODIS and VIIRS LAI algorithms inferred from analysis of long time series of products. Remote Sensing of Environment, 260, 112–438.

Zhang, F., Huo, Y., Cobb, A. B., Luo, G., Zhou, J., Yang, G., ... & Zhang, Y. (2018). Trichoderma biofertilizer links to altered soil chemistry, altered microbial communities, and improved grassland biomass. Frontiers in microbiology, 9, 848.

Zhang, X., Chen, X., Tian, M., Fan, Y., Ma, J., & Xing, D. (2020). An evaluation model for aboveground biomass based on hyperspectral data from field and TM8 in Khorchin grassland, China. *PLoS One, 15*(2), e0223934. https://doi.org/10.1371/journal.pone.0223934

Chapter 2
Unravelling Regional Geodiversity: A Grid-Mapping Approach to Quantify Geodiversity in the uThukela District, KwaZulu-Natal

Jonathan T. Atkinson and Willem P. De Clercq

Abstract The interpretation and integrated application of geodiversity has undergone significant theoretical and applied undulation to establish its own identity beyond its initial generic application linked to geological diversity and biodiversity conservation. Geodiversity (abiotic complexity) has not received the same level of attention as biodiversity (biotic complexity) despite its intrinsic and indivisible linkages to ecosystem and landscape richness characterisation. Therefore, it must have its potential explored. The present work outlines the findings of a semi-quantitative assessment of geodiversity in the entire uThukela District Municipality (UTDM) using a grid-mapping approach of surrogate environmental variables. Foremost this work aims to provide a first approximation methodology for geodiversity index (*GDIx*) quantification adapted to a regional context with scaling-up potential to a national level. We present a proper application of the concept by producing a regional, 11,500 km^2*GDIx* map highlighting the richness of selective (limited) abiotic elements at the landscape scale. We evaluate the contribution of seven ensuing partial diversity covariates that consider hydrographic, lithostratigraphic, pedological, climatic, topographic, solar morphometric and geomorphometric information to obtain a final *GDIx* calculated from the sum of these partial thematic indices. It is expected that the *GDIx* digital coverage will be a flexible decision support tool, even for the most agnostic of users, allowing straightforward interpretation regardless of specialist background. Beyond the regional merits for decision-makers and practitioners, this research's novelty is its contribution to unravelling local application enigmas and cementing specific affirmations regarding *GDIx* quantification

J. T. Atkinson (✉)
Farm Services Unit, Meridian Group, Lilongwe, Malawi

Stellenbosch Department of Soil Science, Matieland, Stellenbosch, South Africa
e-mail: jonathan.atkinson@meridiangsl.com

W. P. De Clercq
Stellenbosch University Water Research Unit, Matieland, Stellenbosch, South Africa
e-mail: wpdc@sun.ac.za

S. Adelabu et al. (eds.), *Remote Sensing of African Mountains*,
https://doi.org/10.1007/978-3-031-04855-5_2

optimisation gained with GIS. One of the primary outputs is a simple cartographic representation of ranked diversity importance of the quality of geodiversity for the entire UTDM that is easily understandable by a varied audience. Therefore, the *GDIx* map(s) should be considered first as a tool for integrated natural resource management, monitoring and reporting at a regional level. This will facilitate land and biodiversity management recommendations and action programmes in an integrated approach to environmental management and geoconservation given the structural ties between geodiversity and biodiversity.

Keywords Geodiversity · Geodiversity index · Pedodiversity · Sustainable land management

2.1 Introduction

The interpretation and integrated application of geodiversity have systematically undergone an evolutionary adaptation in the context of geoscience since its genesis between 1991 and 1993, admittedly to the benefit of a broader scientific audience (Araujo & Pereira, 2018). First introduced at the International Symposium on the Conservation of Geological Heritage (Panizza, 2007) and then further unpacked during the Malvern Conference of Geological and Landscape Conservation (Sharples, 1993; Sharples, 1995) and (Serrano & Ruiz-Flaño, 2007); the concept of geodiversity has undergone significant theoretical and applied undulation in an attempt to establish its own identity beyond its initial generic application linked to geological diversity and biodiversity conservation (Pellitero et al., 2015). It is well accepted that both geodiversity and biodiversity are concepts that emerged from the 1992 World Biodiversity Convention in Rio de Janeiro, Brazil, and has since been embraced by numerous countries (Brilha, 2005; Gray, 2008). Owing to its usefulness as a driving mechanism for habitat variation and how widely it can be employed, the convenience of the geodiversity concept has gained reputable exposure beyond that of the inaugural application centred on geological site (geosite) heritage conservation (Sharples, 1993) and pedodiversity (Ibáñez et al., 1995; Alba Alonso et al., 1998; Thwaites, 2000). Most notably, recent studies highlight additional contributions in the disciplines of biodiversity and ecosystem development (Parks & Mulligan, 2010; Gordon et al., 2012), geomorphodiversity (Zhang et al., 2003), geotourism (Serrano & González Trueba, 2011), geoconservation (Gray, 2013), environmental policy management and even geodiversity action plans (Burek & Potter, 2006; Prosser et al., 2011). Of particular relevance to the present study are the works by Serrano and Ruiz-Flaño (2007), Benito-Calvo et al. (2009), Hjort and Luoto (2010), Araujo and Pereira (2018) and Betard and Peulvast (2019), highlighting how the combination of geological, geomorphological, climatic and hydrological information can be used to quantify geodiversity at a regional scale.

Geodiversity (abiotic complexity) has arguably not received the same attention as its biological counterpart (biotic complexity), despite its intrinsic and indivisible linkages to both ecosystems and landscape richness (Pellitero et al., 2015). Natural ecosystem diversity is understood to be the combination of these two constituents: biological and physical complexity of nature is necessary to determine the landscape individuality for a region, country and even continent (Kostrzewski, 2011; Santos et al., 2017). Manosso and de Nóbrega (2016) further point out that like biodiversity, geodiversity is not a constant but is instead adapted to a given moment, place or region. While it is necessary to acknowledge the synergies between bio- and geodiversity, it is equally important to recognise that geodiversity is of inherent value in itself. Geodiversity is a significant driver of many environmental processes that require further affirmation on its characterisation, spatial distribution and systematisation of mapping techniques to better quantify and evaluate the full scope of its capability and preservation (Manosso & de Nóbrega, 2016; Zwoliński et al., 2018). The recent work by Atkinson et al. (2020) demonstrates that geomorphic classification and delineation need a better representation in discrete landform mapping endeavours in South Africa. Using modern geographic technologies and incorporating better base maps of topography into landform mapping process (Miller & Schaetzl, 2014) is the centrepiece of this directive, moving away from an ad hoc to a more formal and systematic approach to landscape character assessment (Wascher, 2005). Landscape character is defined here as the distinctive, recognisable and consistent pattern of elements in the landscape that differentiate one landscape from another (Swanwick, 2002). Hence, this definition identifies individual landscape elements that constitute the landscape and enables systematic comparison of areas according to their landscape character (Galatowitsch et al., 2009).

Given the broad scope of geodiversity application, it is not surprising that there is limited lingua franca for defining the concept and its methodological assessment. Several pragmatic and mainstream definitions for geodiversity, notably that of Sharples (1993), Dixon (1996), Kozlowski (2004) and Zwoliński (2008), dominate the progressive geodiversity pedagogy. However, this study follows the definition(s) of the concept of geodiversity endorsed by Gray (2004) as a departure point for scope of assessment: "The natural heterogeneity (diversity) of geological (rocks, minerals, fossils), geomorphological (landforms, topography, physical processes), soil and hydrological features. It includes their assemblages, structures, systems and contributions to landscapes", and Ruban (2010) considers the assessment of geodiversity "as a numerical expression of geocentric entity diversity". For reasons of clarity, consistency and simplicity, it is necessary to acknowledge the interrelationship of geodiversity with the following commonly used concepts (adapted after (Crofts et al., 2020):

- *Geoconservation*, the conservation of geodiversity for its intrinsic, ecological and geoheritage value.
- *Geoheritage is an element of geodiversity, whether it is singular or combined, that has significant value* for intrinsic, scientific, educational, cultural, spiritual, aesthetic, ecological or ecosystem reasons and therefore deserves conservation.

- *Geotope*, geomorphological and/or geologic associations within a particular spatial area. A geotope is the geologic equivalent of an ecotope.

Knight et al. (2015) caution that the use of these different terms may lead to a cause of confusion and limitations in potential geodiversity application in the context of digital geomorphological mapping. While the nature of "heritage" differs considerably among people, between places and over time, it invariably stems from nature and culture, and our attachments to it are universal (Lowenthal, 2005). This concept is well defined in the Digne Declaration (Crofts et al., 2020) "Our history and the history of the Earth cannot be separated. Its origins are our origins, its history is our history, and its future will be our future". The pluriform manifestations of geoheritage and geoconservation appear universal and straightforward. However, there are a myriad of tensions that can arise when defining landscape heritage. These include defining where values, objectives and expertise belong, and whom the intended beneficiaries are for protecting it can be challenging to resolve (Graham et al., 2000; Rassool, 2013). Fortunately, there is no shortage of international agreements or conventions and national regulations and guidelines for heritage management in South Africa.

Many organisations, including the International Union for Conservation of Nature and Natural Resources (IUCN), the International Union of Geological Sciences (IUGS) and UNESCO, contribute to landscape conservation in various ways, including a geodiversity component. Specific to South Africa, two key parliamentary statutes aim to regulate the utilisation and ownership of geological resources, i.e. the Geoscience Act (GSA, 2010) and the National Heritage Resource Act, 1999 (NHRA, 1999). The NHRA, in particular, aims to address South Africa's imbalances in the representation and management of its heritage following apartheid and introduce a heritage management system that is reflective of its cultural diversity and constitutional democracy (Deacon, 2015). That being said, while the NHRA coordination, through the South African Heritage Resources Agency (SAHRA), serves to protect South Africa's valuable cultural heritage resources, two notable caveats remain unresolved: first, if geological specimens cannot meet the criteria of being cultural heritage or rare artefacts, then ideally they cannot fall within the ambit of the NHRA (Cairncross, 2011). This, of course, limits the interdisciplinary contributions of geodiversity beyond archaeological and paleontological considerations. Disciplines such as sustainable land management, natural resource management or even integrated environmental management would instead consider pedological and geomorphological diversity rather than cultural value and archaeological rarity high on the developmental agenda. In fact, S24(3) of the National Environmental Management Act (NEMA, 2008) has already made provision for identifying and managing geographical areas of importance in South Africa. Currently, NEMA only prioritises geographical regions for renewable energy production. However, suppose a readily accessible, accurate and repeatable approach is demonstrated to provide a pragmatic solution to quantify geodiversity. In that case, a similar strategy may be considered a primer for prioritising regions with high-value agricultural land, water catchment conservation or even ecosystem-based

services and resilience. For a synthesis of legislative and management context of landscapes and geoheritage sites in South Africa, readers are referred to Grab and Knight et al. (2015).

Generally, it is understood that geoheritage features must have unique geological, cultural or geomorphological values (Gray, 2013). Although a descriptive version of geodiversity is useful for geoconservation, all relevant management activities require a numerical expression of geodiversity quantification (Ruban, 2010). This is the second major limitation of geodiversity assessment in South Africa. No formative approach still exists to characterise priority patterns or exclusion patterns numerically or geospatially (Cocks et al., 2018), i.e. areas characterised by rich or poor geodiversity and low or high significance. Recently Kori et al. (2019) piloted the application of a Geomorphodiversity Index in the Soutpansberg range, South Africa, using the geodiversity assessment criteria proposed by Zwoliński et al. (2018). Their geospatial quantification of geodiversity provides a baseline for the present study, with substantive semblances regarding the recognition of geodiversity factors. The present and aforementioned referenced studies diverge, however, in the application concerning the quantification of geodiversity, i.e. geodiversity based on feature richness and abundance.

This divergence of methods remains a challenge to both geodiversity's applied and theoretical unanimity and further extends to its valuation, both numerically and descriptively. Pereira et al. (2013) conveniently diagnose several key methodological points that remain unresolved: these include which criteria to use to assess geodiversity? How to rationalise scale-factor dependencies, i.e. how does the size of the area under analysis influence the type of criteria, and how should the results for the given methodology then be presented? Following Ruban (2010), numerous quantitative methods for geodiversity assessment have been proposed in the last decade. According to Zwoliński et al. (2018), geodiversity assessment procedures are relatively subjective and informed by the observer's knowledge and experience. Equally, these procedures can be selected and adapted to the object or phenomenon being analysed. Church (2011) further cautions that geodiversity studies are beset by the same methodological issues analogous to scientific observation in geomorphology: sampling, measurement, scales, scaling, classification and residual errors. Research out of South America (Serrano & Ruiz-Flaño, 2007; Benito-Calvo et al., 2009; Pereira et al., 2013; dos Santos et al., 2020) and Europe (Zwolinski, 2018) present the most state-of-the-art interdisciplinary approaches for geospatial, mathematical and statistical geo-indexed geodiversity assessment and geo-visualisation. The benefits of employing quantitative and geospatial methods to geodiversity assessment should be apparent. Melelli et al. (2017) conveniently outline these benefits: first, quantitative approaches are both repeatable and objective, allowing for valuable comparisons of areas in different geographical backdrops. Second, ranking geodiversity using a theoretical geodiversity index (*GDIx*) facilitates practical gridded planimetric geo-visualisation and cartographic approaches in a geographical information system (GIS), allowing areas of similar *GDIx* values to be harmonised. By the same token, representing *GDIx* as a numerically ranked grid-based digital dataset would allow overlaying the *GDIx* with other spatial covariate information of

identical grid size, reaching a *GDIx* value per areal sample unit and allowing the comparison of *GDIx* values in different cells of the grid as well as identifying areas of low or high geodiversity. Our point of departure for this research is the understanding that geodiversity is increasingly recognised to underpin and deliver essential ecosystem services (landscape functioning) linking people, landscapes and their heritage to the broader benefit of the natural and built environment as outlined in the MEA (2005). Comer et al. (2015) showcased that land units with high geodiversity are relatively resistant to degrading living conditions and well equipped to cope with disturbances such as climatic changes than low-geodiversity land units. Therefore, most important to decision-makers is prioritising the endogenous linkages and mapping the spatial variability between geodiversity and geological, hydrogeological, topographic, climatic, geomorphological and pedological covariates. This presents a far more holistic approach to mitigating cross-cutting issues of current concern, including habit loss and food insecurity in the face of increased natural and anthropogenic pressures linked to economic development (Grab & Knight, 2015).

In fact, Lilburne et al. (2020) poignantly reaffirm this didactic outlook. They state that the growing demand on land-based industries and land managers to balance the need for economic prosperity with a greater focus on sustainable landscape management is best achieved through the use of comprehensive land information systems that can assess the benefits, impacts and trade-offs of land use decisions at varying temporal and spatial scales. While the authors are aware of the numerous geodiversity studies conducted internationally (see Zwoliński et al. (2018) for a thorough review), only a select few have attempted to quantify South Africa's geodiversity importance, notably the work by Kori et al. (2019). Typically, most national studies on geodiversity have focused heavily on the importance of geosite (Ruban, 2010) diversity for heritage preservation (Knight et al., 2015). Therefore, the present work aims to perform a semi-quantitative assessment of geodiversity in the entire uThukela District Municipality located in KwaZulu-Natal, South Africa. The specific application of quantitative geodiversity assessment is yet to be fully explored in the Southern Africa context, where various landscape pattern-process functions inevitably influence a unique set of soil-landscape and pedo-hydro-geomorphic processes (Partridge et al., 2010; Grab & Knight, 2015; Holmes et al., 2016). Foremost this work seeks to provide a first approximation methodology for geodiversity assessment adapted to the regional context with possible scaling-up potential to a national level. We present a proper application by producing a *GDIx* map highlighting the richness of selective (limited) abiotic elements at a landscape scale. The *GDIx* digital dataset would then be a flexible decision support tool, even for the most agnostic users, allowing straightforward interpretation regardless of specialist background. A key consideration of our research is thus ensuring synoptic replicability across the landscape. In this regard, we attempt to control model simplicity at minimal expense to represent each input element (partial index) diversity. We apply a modified methodology developed by Pereira et al. (2013) and further refined by Araujo and Pereira (2018). Our methodology describes the degree of geodiversity as objectively as possible and then maps its distribution from a panoptic context. More specifically, we employ a two-pronged approach as follows: first,

we leverage a suite of geospatial analytical tools offered by GIS platforms to overlay a regular grid onto different thematic covariate categories that consider hydrographic, geological, pedological, climate, topographic, atmospheric and geomorphological information to obtain a final *GDIx* calculated from these partial thematic indexes.

Beyond the relative regional merits for decision-makers and practitioners, the novelty of this research is possibly its contribution to unravelling certain application enigmas for the discipline. We aim to cement specific affirmations regarding optimisation gained with GIS, outline limitations due to feature scale, define appropriate abiotic feature selection and highlight ease of cartographic interpretability. The authors believe that the study's findings are pursuant to the broader international discussion on the evolution of quantitative geodiversity assessment methods as a valuable, holistic and replicable spatial decision support tool.

2.2 Materials and Methods

2.2.1 Regional Settings

The study site is the entire uThukela District Municipal area located between the Kingdom of Lesotho and the western boundary of the coastal Province of KwaZulu-Natal (KZN), South Africa, with the seat for the municipality situated in the town of Ladysmith (*28°33′35″S 29°46′50″E*) (Fig. 2.1). Approximately 11,500 km^2 in extent, the UTDM provides a valuable case for designing a geodiversity assessment map in a mesoscale context. The region presents an eclectic combination of high-value natural resources with competing demands at different scales. Cox et al. (2015) highlight the competition for using resources between local users (livelihoods) and agricultural production and international demands from the tourism sector and biodiversity conservation necessary for maintaining sound natural systems. Furthermore, the area also includes a rich cultural heritage left by the indigenous San People. The rock art of the Maloti-Drakensberg Park is the largest and most concentrated group of rock paintings in Africa, south of the Sahara. It is outstanding both in quality and diversity of subject (UNESCO, 2000). The region is almost entirely rural. The dominant land use in private and tribal lands is commercial and small-scale agriculture, respectively (EKZNW, 2010). Most small-scale farmers practise extensive livestock grazing, dryland cropping and some vegetable gardening, while private agricultural operations are of large scale, more diverse, more productive and strongly commercially oriented.

The topographic expression of the UTDM is broadly diversified from high mountains in the southwestern region of the province, becoming more undulating as it forms part of the Thukela catchment and drains to marine estuaries and coastal dunes towards the Indian Ocean in the east. The Drakensberg, the highest lying component of the study domain, includes three altitudinal zones (the Montane zone, the Subalpine zone and the Alpine zone) extending from approximately 1300–3500 m above sea level, which encompasses the steepest altitudinal gradient in the District.

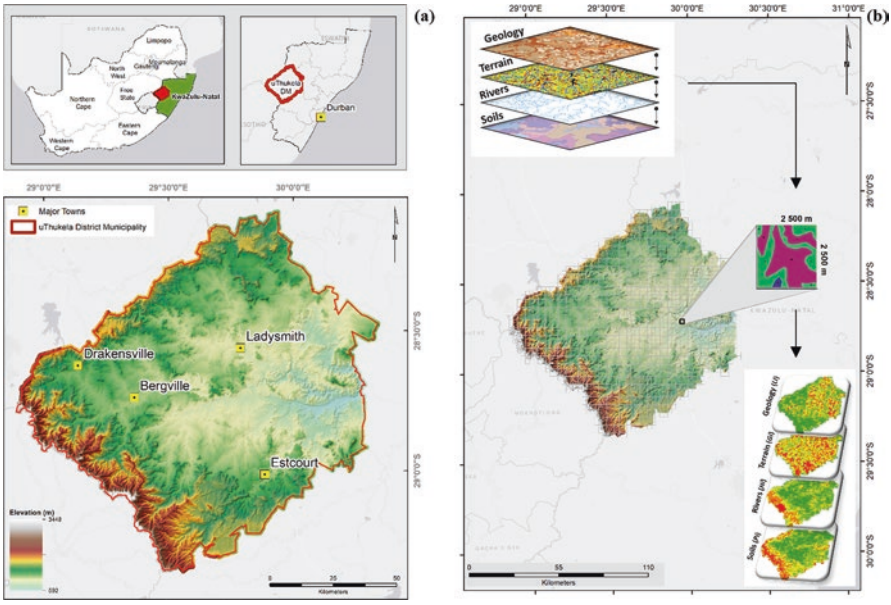

Fig. 2.1 (**a**) Map showing the uThukela District Municipality (UTDM) situated in the western region of KwaZulu-Natal, South Africa (DEM Source: CGIAR, 2014). (**b**) The conceptual workflow uses gridded datasets to derive geodiversity sub-index data layers for the UTDM region overlaid with the 2.5 × 2.5 km sample grid

Elliot and Escott (2015) characterise the landscape as an assortment of gently undulating hills through to a rolling and partly broken landscape across a notable altitudinal gradient extending through the district (600–1300 m). In the higher altitude regions, typical terrain morphological features include rocky, rugged slopes and terraces, including mountainous areas incised by river gorges, a variety of narrow and broad valleys, plateaus with sharp hills, steep ravines and escarpment slopes, high mountain ridges separated by cavernous valleys, prominent cliff faces, complex mountain topography and steep basalt rock faces and terraces. In the lower declivity regions, meandering stream channel and paludal floodplains with drier ephemeral stream and semi-arid alluvial fans and aeolian dunes are most prevalent (Botha & Singh, 2012).

The Drakensberg mountain range encompasses a wide range of geological formations. These include a diversity of Karoo Supergroup rocks, including Stormberg basalts, tillite of the Dwyka formation, as well as Ecca and Beaufort Group formations. Geological formations are typically either sedimentary or igneous in origin. The region is mainly dominated by sandstone, shale, mudstone, dolerite, quartzite, dolomite, granite, diabase and basalt saprolitic material. Moreover, altitudinal variations highly influence geological exposure, especially for the well-layered Karoo Supergroup (Elliot & Escott, 2015). The geological and geomorphological diversities are reflected in the pedodiversity of the area in terms of pedon-depth, topsoil depth, drainage, fertility and soil texture. Typical soil groups include, in varying

spatial assemblages and without limitation: *Histosols*, *Gleysols*, *Vertisols*, *Umbrisols*, *Fluvisols*, *Luvisols*, *Lixisols*, *Planosols*, *Plinthosols*, *Ferralsols*, *Arenosols*, *Leptosols*, *Cambisols* and *Stagnosols*. The district is also strategically significant as it makes up the principal catchment area for the Thukela River. Two major impoundments occur along the Thukela River within the central-western regions: Woodstock Dam and Spioenkop Dam. Another critical natural impoundment, namely, Wagendrift Dam, occurs along the Boesmans River within the southern area of the UTDM. This rich biodiversity and cultural value of the Drakensberg is the basis for its World Heritage Status and includes both the uKhahlamba National Park and the Maloti-Drakensberg Trans-frontier Peace Park between Lesotho and South Africa, not to mention wetland areas of Ramsar Conservation status as well. It's worth noting that all World Heritage sites are designated as Protected Areas, which means that mining or prospecting are not permitted within the property or proclaimed buffer zone. Further, any unsuitable development that may adversely affect the property is prohibited by the South African and Lesotho Ministers responsible for Environment and Culture (UNESCO, 2000).

2.2.2 Geodiversity Classification

Digital inventories of landscape resources are vital for landscape management, as one cannot protect that which is unknown (Jackson et al., 2019). The quantification of geodiversity for UTDM is calculated using the geodiversity index (*GDIx*) methodology developed by Araujo and Pereira (2018) with minor modifications. The approach is based on the theoretical definition of partial numerical indices estimated from selected thematic geo-informational coverages representing the main (direct and indirect) geodiversity elements segmented within a regular grid overlay. The grid-based framework provides a simple solution for assessing the degree of georichness. It avoids the ordinal classification and overrating of any element by considering each part's quantification as equally important aggregates to the final *GDIx*. Holistically then, the *GDIx* is estimated from the sum of the partial indices calculated from the discrimination of occurrences (count) in each grid cell. Hjort and Luoto (2010) further emphasise the benefits of a grid-based *GDIx* approach in that it enables an objective subdivision of geospatial richness, creating units of identical dimensions, allowing direct comparison of results to explore the relationship of geodiversity with a diverse range of spatial abiotic or biotic variables. The implementation of the *GDIx* assessment is further explained in the forthcoming subtopics.

2.2.2.1 Grid Resolution

Geodiversity cannot be understood without the proper definition of scale relating to the areas under observation and the elements targeted for assessment (Serrano & Ruiz-Flaño, 2007). For this study, we applied a regular Cartesian grid of

2500 × 2500 m resolution using ArcGIS Desktop 10.5 (ESRI, 2021), hereafter ArcMap, generating 2042 grid squares. This approach is considered the most pragmatic parametrisation for optimal differentiation of maximum range between the highest and lowest partial indices and ultimately *GDIx* values for the UTDM. Moreover, the grid resolution of the *GDIx* map is defined considering the map scale(s)/resolution of the input geospatial layers used to perform the assessment and enabled the inclusion of coarse-scaled thematic map data (Table 2.1). Similarly to Kozlowski (2004) and Benito-Calvo et al. (2009), the mesoscale (1:750000 map scale) application of data is based on prioritising the minimum detectable feature range of elements of geodiversity as well as the overall extent of the UTDM study area. Due to the significant diversity within a landscape, finding an objective measurement unit of geodiversity quantification and at the same time giving comparable results remains an ongoing subject in the study of geodiversity. The grid resolution selected for quantifying geodiversity in the UTDM follows the recommended grid resolution of 100–2500 m (with a map scale of between 1:500000 and 1:1000000) for regions between 2500 and 10,000 km^2.

2.2.2.2 Geodiversity Partial Index Classification

After using the vector (polygon) grid design, we implemented an overlay function to calculate seven theoretical numerical partial indices based on the following geodiversity elements: hydrographic, geological, pedological, geomorphological, climatic, atmospheric and topographic diversity within the UTDM region. Broadly, we applied a bilateral approach to separately quantify each sub-partial index on the format of each geospatial data layer, i.e. raster or vector format. This step is mandatory considering the differences in quantifying phenomena of either a discrete or continuous nature. All datasets analysed in the diversity quantification were reprojected to transverse Mercator projection with a 31° meridian and WGS 84 Datum. For the vector-based sub-partial datasets, the quantification is based on the variety (richness) and count (abundance) (Ruban, 2010) of the different elements representing geodiversity (Serrano et al., 2009; Araujo & Pereira, 2018). The primary assumption is that a higher occurrence or variety of features per grid cell would represent a corresponding degree of geodiversity. Importantly, we assessed the geodiversity classes directly by computing the primary indicators of geodiversity such as geological classes and landforms and using surrogate factors that are considered reflections of geodiversity, such as topographical or climatic variability (Pellitero et al., 2015). The utility of the grid quantification approach is to express, in the most harmonious way possible, all of these aspects without overrating any particular sub-partial element (Araujo & Pereira, 2018). For the analysis of geodiversity, we considered only the *count* of relative frequency and the *variety* of each element within the sample area and avoided qualitative ranking, or weighting, based on the intrinsic, or perceived, importance of each landscape component. In doing so, we minimised the subjectivity of the final geodiversity output, a common caveat with many other evaluation methods (Silva et al., 2013).

Table 2.1 Fundamental components of input data, and their sub-types, used for quantitative assessment of geodiversity in UTDM

Partial geodiversity index	Sub-partial data layer(s)	Resolution/ scale	Source	Format	Geodiversity relevance	Determination of diversity
Hydrographic (*Hi*)	Groundwater recharge	1.7 km	Schulze et al. (2007)	Raster	Variability in annual baseflow	Modal zonal statistic of mean annual baseflow (mm) per grid cell
	Stream density	1:500,000	Dept. of Water Affairs, DWA (2006)	Vector	Stream density	Sum of stream length per grid cell
Lithological (*Li*)	Lithostratigraphic	1:250,000	Council for GeoSciences, CGS (2000)	Vector	Geological richness	Count of different lithostratigraphic formations per grid cell
	Paleo-sensitivity	1:250,000	Council for GeoSciences, CGS (2000)	Vector	Geological sensitivity	Count of different paleo-sensitivity classes per grid cell
Pedological (*Pi*)	Land type soil association	1:250,000	Institute for Soil, Climate and Water, ARC (2003)	Vector	Pedological richness	Count of different soil classes per grid cell
	Profile soil depth	1:250,000	Institute for Soil, Climate and Water, ARC (2003)	Vector	Soil depth >800 mm	Count of features >800 mm soil depth
Climatic (*Ci*)	Rainfall intensity	1.7 km	Schulze and Maharaj (2007)	Raster	Variability in monthly rainfall concentration	Modal zonal statistic of rainfall concentration index (%) per grid cell
	Rainfall variability	1.7 km	Schulze and Maharaj (2007)	Raster	Variability in mean annual precipitation	Modal zonal statistic of the coefficient of variation (%) of precipitation per grid cell
	Diurnal temperature variability	1.7 km	Schulze and Maharaj (2007)	Raster	Variability in daily temperature	Modal zonal statistic of the mean monthly temperature range (T_{max}–T_{min}°C) per grid cell

(continued)

Table 2.1 (continued)

Partial geodiversity index	Sub-partial data layer(s)	Resolution/ scale	Source	Format	Geodiversity relevance	Determination of diversity
Topographic (*Ti*)	Terrain ruggedness index	90 m	Created for this study using SRTM 3 arc second DEM	Raster	Topographical variability	Modal zonal statistic of terrain ruggedness values per grid cell
	Terrain surface classification	90 m	Created for this study using SRTM 3 arc second DEM	Raster	Relief richness	Modal zonal statistic of terrain surface classification values per grid cell
Geomorphometric (*Gi*)	Geomorphon	90 m	Created for this study using SRTM 3 arc second DEM	Vector	Landform richness	Count of different geomorphon features per grid cell
Solar morphometric (*Si*)	Solar radiation variability	1.7 km	Schulze and Chapman (2007)	Raster	Variability in daily solar insolation	Modal zonal statistic of mean daily solar radiation (MJ/m^2/day) per grid cell

Furthermore, this provides a segway for the final geodiversity map to provide an objective and unprejudiced regional, albeit theoretical, interpretation of geodiversity within the UTDM. For all contributing raster-format datasets, the challenge is defining a central measure of quantification to represent each sample unit, i.e. grid cell. Therefore, we use a *Zonal Statistic* geoprocessing approach, implemented in ArcMap Desktop, to determine each grid cell's most commonly occurring (mode) aggregated value. This data generalisation approach provides a simplistic yet still regionally representative solution for aligning the various multi-resolution raster datasets to the unified geodiversity sample grid area.

While all elements are considered equal shareholders in the final diversity assessment, each sub-partial index constitutes a distinct set of variables (Table 2.1): *hydrographic index* (two sub-partial covariates), *topographic index* (two sub-partial covariates), *lithological index* (two sub-partial covariates), *pedological index* (two sub-partial covariates), *geomorphological* aspects (one sub-partial covariate variables), *climatic index* (two sub-partial covariates) and *solar morphometric index* (one sub-partial covariate). Therefore, each partial index combines either one or several geospatial layers normalised (Eq. (2.1)) to a scale of 0–0.5 or 0 and 1.0 where single covariates are analysed.

$$X_{\text{norm}} = \frac{\left(X_{\text{i}} - X_{\text{min}}\right)}{\left(X_{\text{max}} - X_{\text{min}}\right)} \tag{2.1}$$

A brief description of each of the seven partial indices, and their contributed sub-partial indices, including the geoprocessing steps, are described in detail below and graphically represented in Figs. 2.2 and 2.3.

The *hydrographic index* (*Hi*) is evaluated by considering both surface and subterranean hydrological contributions to geodiversity. For the sub-partial index diversity calculation of surface waters, we used the 1:500000 national vector dataset (DWA, 2006) of the perennial stream network. We augmented this coverage with a higher resolution 1:50000 national vector river network (NGI, 2018) to include non-perennial streams for quantifying drainage density (km/km^2) for each grid cell. Drainage density is useful for describing drainage basin morphometry by estimating the stream channel's length per unit area, indicating how well or how poorly a watershed is drained by stream channels (Horton, 1932). All values are then normalised to a scale of 0 and 0.5. A score of 0 is assigned to squares, in which no hydrological elements are represented, while a score of 0.5 indicates high drainage density. To complement drainage density, *mean* annual baseflow (mm), i.e. the dry weather and non-rainy season streamflow sourced from the groundwater stores, was also assessed. The baseflow coverage has been empirically generated for South Africa on a 1′ × 1′ (1.7 × 1.7 km) spatial resolution using 50 years of historical climate data. We resampled the baseflow coverage to 90 m resolution using a bilinear interpolation approach in ArcMap to allow interoperability with the remaining datasets, specifically the topographic raster surface, derived from the three-arc second Shuttle Radar Transfer Mission (SRTM) DEM. The ArcMap *Zonal Statistic*

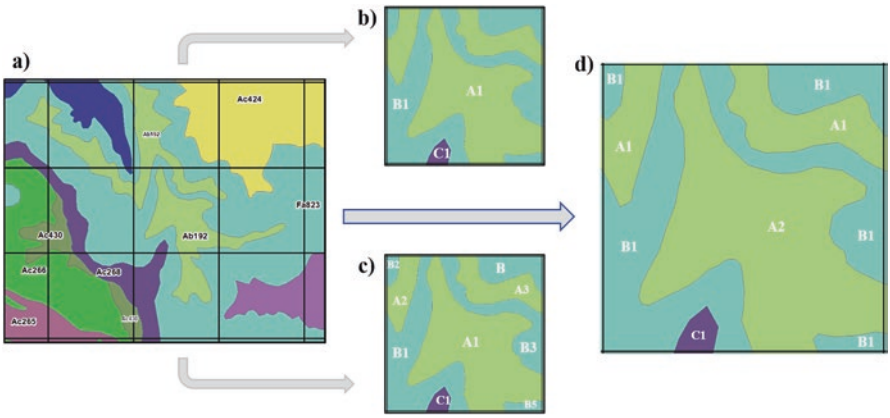

Fig. 2.2 Concept of the geodiversity quantification of vector datasets in the 2.5 × 2.5 km grid. (**a**) Overview map showing vector soil association(s) in a 3 × 3 window range. (**b**) Counting the number of soil forms per grid cell is too conservative with only three soil form features counted and full abundance of soil features not quantified. (**c**) Counting the number of vector features per grid cell is too liberal with a total of 9 soil form features counted. Duplication of similar features resulting in an overestimation of geodiversity per grid cell. (**d**) Counting the number of vector features per network cell per spatially contiguous element.: "Goldilocks case" of quantifying vector feature diversity resulting in four soil form features per grid

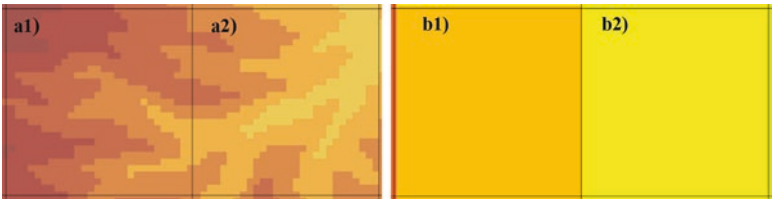

Fig. 2.3 Concept of the geodiversity quantification of raster datasets in the 2.5 × 2.5 km grid. (**a**) SRTM 90 m elevation for two grid cells (**a1**) having an elevation height range of 413 m and (**a2**) having an elevation height range of 345 m. Grids highlighted in (**b1**) and (**b2**) have been generalised using the Zonal Statistical modal value for elevation calculated for each grid cell resulting in new elevation grid values of 375 m and 305 m, respectively, for the geodiversity index calculation

function was then used to calculate the modal raster baseflow within each 6.25 km^2 grid cell. Like drainage density, baseflow values were normalised to 0 and 0.5. The final *Hi* partial index value is calculated as the sum of the partial drainage density diversity and baseflow diversity with values ranging from 0 to1.

The *lithological index* (*Li*) is calculated as the sum of the lithostratigraphic and paleo-sensitivity sub-partial indices, both derived using a digitised 1:250,000 geological series map courtesy of the South African Council for Geoscience (CGS, 2000) with minor modifications. The lithostratigraphic map is a special-purpose vector polygon dataset depicting the 12 dominant lithostratigraphic units and geologic strata in the UTDM. Following the method outlined by Araujo and Pereira

(2018), the lithological units were first homogenised to eliminate duplication of polygons of the same classification within each cell. This was done using a unique numerical ID assigned to each lithological unit and then "exploding" the dataset before intersecting the layer with the spatial grid, with each grid cell itself having a unique identifier, finally "dissolving" on unique grid ID and summarising on feature count to calculate the sum of differentiated lithological features within each cell. The paleo-sensitivity and geological heritage (Lavin, 2013) sub-partial index provides a valuable assessment for tentatively outlining paleontologically sensitive areas in the UTDM and adds a necessary degree of quantification to the geological sub-index calculation and thus final *GDIx*. The paleo-sensitivity sub-partial dataset is based on the same 12 lithological classes as above but ranked according to their paleo-sensitivity using a six-class classification (unknown to very high). The paleo-sensitivity diversity was computed by counting the number of occurrences of different sensitivity classes within each grid cell, following the same procedures used to calculate the lithological heterogeneity. While this geoprocessing analysis was wholly automated in a GIS, a crucial step was the manual inclusion of same-ID and non-contiguous features as part of the feature count. This approach was considered a "goldilocks" approach to avoid over- or underestimating feature count per grid cell. Since the *Li* comprises two sub-partial vector layers, each layer was normalised to 0 and 0.5 and then summed to a scale of 0–1.0 for the final lithological index. Figure 2.2 outlines the geospatial approach used to derive the sub-partial indices for all vector datasets. Simultaneously, Fig. 2.2d represents the optimised estimation based on the goldilocks concept for each grid cell's feature count and variety.

For the *pedological index* (*Pi*), two sub-partial indices, soil pattern and soil depth >800 mm, were analysed using the 1:250,000 Land Type Survey (LTS) digital soil inventory dataset (ARC, 2003). The land types of South Africa have been comprehensively mapped over South Africa for agricultural purposes. Each land type shows an accepted degree of uniformity concerning terrain form, soil pattern and climate. In total, the LTS contains information for 28 broad soil pattern groups (association) classified according to the Soil Classification: A Binomial System for South Africa (MacVicar et al., 1977). The soil pattern sub-partial index facilitates tracing the pedological diversity in the UTDM. Following the same grid-geoprocessing procedure, as outlined for *Li*, the information for 15 soil patterns for the entire UTDM was analysed with the count of soil class per grid normalised to 0 and 0.5. The soil depth sub-partial index was derived by selecting all soils with a depth >800 mm (given to a depth of 1500 mm) in the LTS dataset.

Soil depth refers to total profile depth and not effective rooting depth highlighting limitations due to physical rather than chemical impediments (Schulze et al., 2007). This definition, therefore, denotes the depth to which plant roots can be active. Polygons where soil depth is >800 mm were all equally weighted and assigned the maximum value of 0.5. All remaining polygons were assigned a value of 0 and then summed with soil pattern index scores for the combined final *Pi* values ranging from 0 to 1.

The *climatic index* (*Ci*) assessed the contribution of two sub-partial indices: rainfall and temperature diversity. Rainfall diversity was evaluated by rainfall

concentration and rainfall variability, while daily max-min temperature variability was considered a suitable surrogate contributor to geodiversity in the UTDM. Rainfall concentration, instead of MAP, is a good determinant of how concentrated (severe) rainfall events are throughout the year, which provides a complete perspective of the influence of events on the landscape. Schulze and Maharaj (2007) represent rainfall concentration, calculated per quaternary catchment, for South Africa on a 1′ × 1′ (1.7 × 1.7 km) spatial resolution using 50 years of historical data. The raster coverage delineates high rainfall regions as locations that receive all their rainfall in 1 month. In contrast, low rainfall concentration regions receive the same rain for each month of the year. Therefore, the higher the concentration index, the less spread the rainfall season is over time (whether it is a high or low rainfall area or in a winter or summer rainfall region). To complement the effects of rainfall concentration, we likewise quantified the coefficient of variation (CV) of annual precipitation for the UTDM. MAP maps do not showcase the natural year-to-year rainfall variability within a region. The CV (%) is a more suited index to express precipitation with high/low CV values corresponding to high and low inter-annual rainfall variability, respectively. The sub-partial temperature diversity was represented by the regional diurnal temperature range (Schulze & Maharaj, 2007). Very simply, the diurnal temperature range is the difference between the maximum and minimum temperatures on a given day. Unlike MAT, which is a reasonable indicator for continentality, the selection of mean monthly diurnal temperature range is a valuable index to assess the influence of temperature diversity related to a broad range of local anthropocentric and natural process phenomena such as inter alia, land cover/use change, climate change, thermoperiodism and photosynthesis, i.e. the response of plants to diurnal temperature ranges (Schulze & Maharaj, 2007). As with *Hi*, both *Ci* sub-partial indices were resampled to 90 m and using the *Zonal Statistics* to calculate the modal rainfall concentration per grid cell. The rainfall concentration and rainfall CV were first normalised to a scale of 0 and 0.25 and then combined to derive an index of 0–0.5. The geoprocessing of the diurnal temperature range followed suit with *Zonal Statistic* values rescaled to 0 and 0.5. Both rainfall diversity and temperature diversity sub-partial indices were tallied resulting in a final *Ci* diversity score between 0 and 1.

Topographic index (*Ti*) is calculated as a collective of the terrain ruggedness index (TRI) and terrain surface texture (TST) sub-partial indices with both datasets derived from two mosaiced and void-filled three-arc second SRTM DEM V4.1 (Jarvis et al., 2008) scenes with a resolution of 90 m for the entire UTDM region. The simplest definition of TST (Bennett & Mattsson, 1999) is that it represents the amplitude and frequency of topographic relief features of a surface and provides one of many useful surrogates for assessing topographic diversity (Benito-Calvo et al., 2009). Consequently, large roughness diversity values indicate a substantial dispersion of slope gradient and slope aspect with short slope lengths. In contrast, small values indicate a homogenous orientation of slopes with minor variations and long slope lengths (Hjort & Luoto, 2010). At the same time, Riley et al. (1999) consider TRI an expression of terrain heterogeneity, quantitatively indicating how undulated, broken, rugged or dissected the landscape is between a grid cell and its

eight neighbouring cells and an ideal indicator for assessing land surface ruggedness. The inclusion of TRI and TST is supported by the decisive role of both parameters on the energy flows (exposure to sunlight, humidity) and material flows (water, sediments on the slopes) and the diversity and distribution of landforms and processes (Serrano & Ruiz-Flaño, 2007). These two sub-partial indices collectively provide a far more pragmatic contribution of topographic variability to geodiversity than only evaluating solitary altitudinal and declivity gradients. To quantify the resulting *Ti*, we calculated the *Zonal Statistics* for each sample grid resolution as outlined before. Using Eq. (2.1), we rescaled the modal values for TRI and TST to 0 and 0.5 respectively. Both sub-partial indices were then summed representing the final *Ti* diversity between 0 and 1 per grid cell.

For the *geomorphometric index* (*Gi*), we leveraged the utility of the geomorphon (geomorphological phonotypes) mapping approach to provide a general-purpose geomorphometric map for the UTDM using the previously processed 90 m resolution SRTM DEM. Moving beyond simple topographic heterogeneity measures, the geomorphon approach's utility (Jasiewicz & Stepinski, 2013) is the low-cost characterisation of landform features, which we consider a reasonable standard of landform richness. Geomorphons are analogous to textons (Julesz, 1981) of a landscape. Their extraction from a DEM comes at a small computational cost considering that they simultaneously represent quantitative and stratified terrain attributes and landform types. The geomorphon approach's product is the stratification of the landscape into ten unique but recognisable landform elements: *Peak*, *Ridge*, *Shoulder*, *Spur and Slope*, *Hollow*, *Foot slope*, *Valley*, *Pit* and *Flat* terrain morphological units. Recently, Atkinson et al. (2020) successfully applied the geomorphon approach to soil-landscape characterisation to a smaller region within the UTDM.

For this reason, we decided to implement the scale-independent approach to a larger regional area such as the UTDM. Similar to Bailey et al. (2017) and Atkinson et al. (2020), we used the geomorphometric algorithm "*r.geomorphon*" extension in GRASS GIS 7.4.1 (GRASS Development Team, 2016) to delineate the landform coverage data from the SRTM DEM using the pattern recognition approach. Geomorphon features were then vectorised to polygons and then further homogenised to eliminate duplication of the same feature with multiple polygons of the same geomorphon unit "dissolved" to eliminate redundant features from the diversity quantification. The quantification of the geomorphon sub-partial index followed the same methodology as previously outlined for vector datasets, namely, that of soils and geological material, except for the single sub-partial *Gi* values normalised directly to 0 and 1.

Finally, we evaluated *solar morphometric diversity* (*Si*) through the contribution of monthly mean solar radiation variability (MJ/m^2/day), using the solar radiation raster grid developed by Schulze and Chapman (2007) at $1' \times 1'$ (1.7×1.7 km) resolution using 50 years of historical data for South Africa. Solar radiation, the exogenous component of the surface thermal regime, is a suitable morphometric replacement for slope aspect with added computational benefits. First, the estimation of solar radiation is more sophisticated. It considers inputs such as latitude, atmospheric properties and temporal frequency, which account for differences in

topographic shadowing (from adjacent hills) and slope gradient (Thompson et al., 2012). Second, Van Niel et al. (2004) demonstrated that solar radiation derived directly from a DEM is less affected by DEM error than aspect and slope. Finally, unlike the slope aspect, solar radiation considers the measurable quantity of direct sunlight rather than merely the cardinal representation of solar insolation. Schulze and Chapman (2007) record solar radiation as monthly means of daily solar radiation variability. To derive a yearly average, we used the ArcMap *Raster Calculator* (Spatial Analyst Tools) to cascade the 12-monthly datasets and calculate the annual average for the UTDM region. The solar radiation sub-partial index followed the same geoprocessing protocol applied to the previous raster datasets: first generalising the solar radiation dataset from 1700 m to 90 m and then summarising the sample grid values by *Zonal Statistics* to calculate the modal radiation variability per 2500 m grid cell. The solar radiation sub-partial index was then normalised directly to 0 and 1.0 with grid cells approaching 1.0 displaying higher *Si* diversity.

The final *GDIx* score for each grid square is the sum of the seven sub-partial indices of diversity (Eq. (2.3)). Following Araujo and Pereira (2018), we reclassified the resultant seven-class *GDIx* grid values to an equal interval five-class model using, Eq. (2.2), to distinguish the following *GDIx* classes: Class 1 (0–1) = very low; class 2 (1–2) = low; class 3 (2–3) = medium; class 4 (3–4) = high; and class 5 (4–5) = very high based on the minimum and maximum values obtained (Betard & Peulvast, 2019) (Fig. 2.4h).

$$Y_{\text{new}} = \left(\frac{\left(X_{\text{i}} - X_{\text{min}}\right)}{\left(X_{\text{max}} - X_{\text{min}}\right)} \right) n_{\text{upper limit}} \tag{2.2}$$

$$G_{\text{diversity}} = H_{\text{i}} + P_{\text{i}} + L_{\text{i}} + C_{\text{i}} + T_{\text{i}} + G_{\text{i}} + S_{\text{i}} \tag{2.3}$$

2.2.2.3 Geodiversity Partial Index Classification

While the final grid map may be functional as a regional representation of geodiversity, the tessellated grid results do not offer further opportunity to interrogate the geodiversity-landscape relationships within the UTDM. To better visualise the *GDIx* as a smooth continuous surface, we followed a similar protocol to Argyriou et al. (2016) and Araujo and Pereira (2018) with modifications as follows:

1. We resampled our original 2500 m grid to 500 m, generating a centroid for each new grid cell. This resulted in 25 centroids at 500 m compared to 1 centroid at 2500 m grid resolution.
2. We then used the centroid points in an optimised ordinary kriging interpolation method (with standard model parametrisation) in ArcMap *Geostatistical Wizard*, using a maximum of five and a minimum of two neighbours within a four-sector range to generate intermediate values between the geodiversity centroid values.
3. The final output is a more detailed spatially continuous raster surface of geodiversity distribution for the UTDM.

4. To further capitalise on the spatially detailed interpolated geodiversity surface, we generated a histogram to highlight the distribution, range and class intervals of the *GDIx* values for the UTDM.

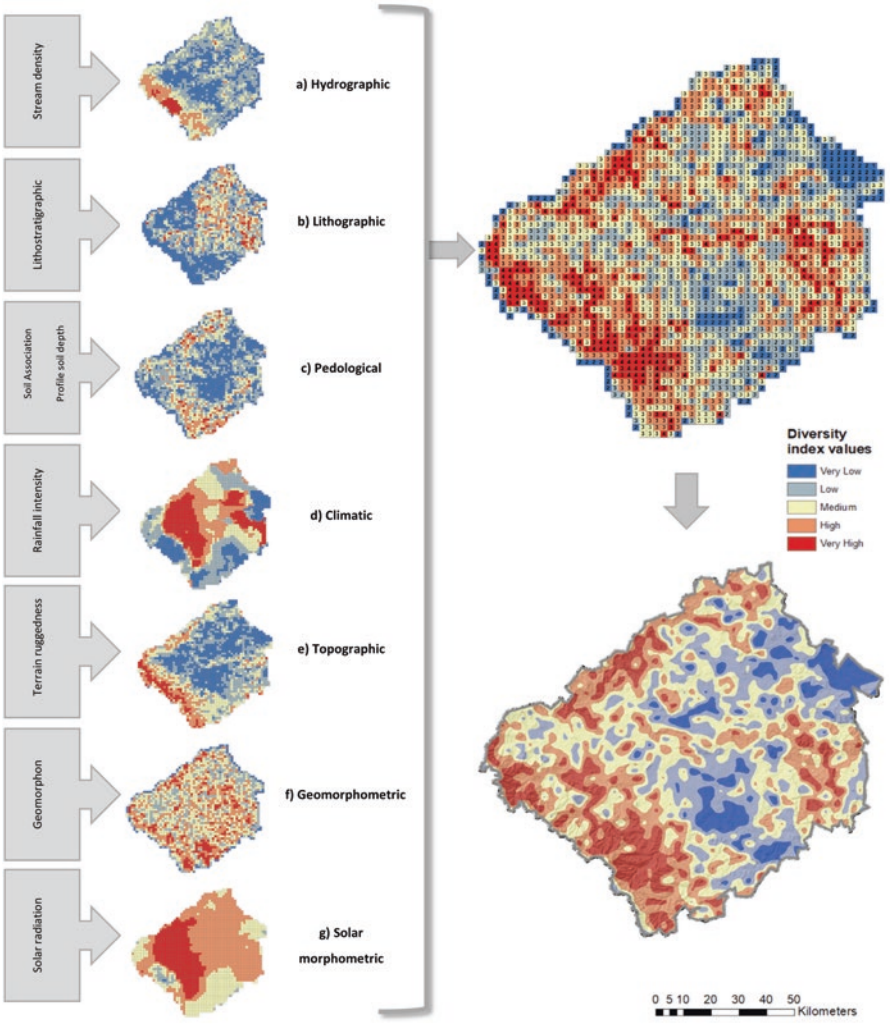

Fig. 2.4 Calculation of geodiversity index applied to UTDM as the sum of seven sub-indices: *Hi*, *Pi*, *Li*, *Ci*, *Ti*, *Gi* and *Si*. The final thematic geodiversity layer is interpolated using a geostatistical interpolation approach to provide a smooth surface of diversity and rescaled and classified to a five-class scale of theoretical geodiversity index. (**a**) Hydrographic diversity index. (**b**) Lithographic diversity index. (**c**) Pedological diversity index. (**d**) Climatic diversity index. (**e**) Topographic diversity index. (**f**) Geomorphometric diversity index. (**g**) Solar morphometric diversity index. (**h**) *GDIx* grid. (**i**) Modelled *GDIx*

2.3 Results and Discussion

2.3.1 UTDM Sub-partial Diversity Quantification

The final geodiversity map resulting from the interaction of the seven partial diversity index datasets evaluated for the entire UTDM is presented in Fig. 2.4h. The methodology used for quantifying the partial index diversity for both vector and raster datasets proved to effectively highlight the richness and abundance of features for the respective partial sub-indices. In particular, the topographical, pedological and geological diversity estimation, as well as the geomorphometric diversity quantification, all showed strong associations with regions in the northern, southern and western areas of the UTDM characterised by the Drakensberg mountain range, higher altitude, complex terrain and associated increased diversity of soil and geological material. Consequently, these partial index covariate datasets strongly influence the final *GDIx* map with medium partial index diversity areas randomly distributed throughout the UTDM. Notably, despite using a moderate-resolution spatial layer of soil association, the pedological partial index displayed a surprisingly high pedological diversity. The eastern and western regions of the UTDM are known to be pedologically diverse, predominantly due to topographic and climatic influence. Our findings are aligned with similar findings by Kori et al. (2019), who found that their final geomorphological diversity map was strongly influenced by geology, slope and soils in the Soutpansberg range in South Africa. This would suggest that despite differences in the quantification approaches to geodiversity estimation, i.e. factor maps (Kori et al., 2019) or partial index maps, as presented in this study, the influence of selected covariates for driving geodiversity remains relatively systematic regardless of regionality. These results present inspiring opportunities for further testing the quantification approach to geodiversity mapping in other country regions to further validate the influence of physical environmental covariates. Identifying landscape units is an integral part of understanding a given portion of land's behaviour, functioning and dynamics and how these interrelationships drive geodiversity in the landscape. Specifically, this study has shown that the topographical (terrain character), pedological (soil character) and lithostratigraphic (geological and paleo-sensitivity character) diversity, as well as the geomorphometric (landform character) diversity quantification, are all highly invested in the final *GDIx* valuation, having a distinctive spatial clustering in the northern, southern and western areas of the UTDM.

The climatic and solar morphometric partial indices exhibited a categorical clustering of high diversity regions closest to the Drakensberg with a gradual decrease in diversity clustering in an easterly direction towards the lower altitude homogenous coastal region. The pockets of high solar and climatic diversity in the central and eastern areas of UTDM may be attributed to the known seasonal climatic variability associated with the humid coastal region and the adjacent interior Mist belt, which forms a band through the entire KZN Midlands, and consequently a central region of the UTDM. Surprisingly, the hydrographic partial index layer did not

perform as expected, considering the high stream density calculated for the region. An average stream density of 2.3 km per grid (6.25 km^2), with a maximum density of 7.46 km, was recorded for the UTDM with the highest values conditioned by the Drakensberg catchment basin(s) and fluvial drainages within closed valleys in the central and eastern regions of the study site. Like Betard and Peulvast (2019), surface waters' contribution dominates the diversity estimation in areas of high stream density and baseflow and show less influence in low baseflow regions. Likewise, Manosso and de Nóbrega (2016) highlight that, indirectly, sets of elements with the highest number of variables significantly influence the overall quantification index process. This is an unavoidable caveat of the numerical method of counting feature richness and abundance using a grid-based approach. By default, features with the most occurrence (count) will register as more diverse, while other elements become reflections of conditions contributing to the overall diversity. The major drawback of numerical approaches is the lack of distinction between the description and the evaluation of nature. The valuation of nature must be defined in its own right. Likewise, indicators of diversity may be of great interest as value criteria. Additional value criteria should be included if these indicators are designed to measure a part of the total variety. For quantitative approaches, it is particularly problematic when the absence/presence of a limited set of value indicator(s) is exclusively used to represent the lack/abundance of geodiversity value.

A pragmatic solution for future geodiversity estimations using a gridded approach may need to avoid using sub-partial indices altogether to derive partial indexes of geodiversity and instead use individual datasets, i.e. soil form, geology, baseflow and stream density, independently as partial index layers. This may resolve the shortcomings of the obligatory normalisation approach between datasets of varying scales (spatial and measurement) while maximising the representation of diversity features at a partial index level for overall geodiversity representation. Similar methods were adopted by Hjort and Luoto (2010), who evaluated 74 different types of elements of geodiversity in Northern Finland and Manosso and de Nóbrega (2016), who considered 15 features of geodiversity to calculate the geodiversity from landscape units of the Cadeado Region in Paraná, Brazil. Alternatively, future analyses may further benefit from introducing a weight factor for each sub-partial index, particularly for those sub-index features used for *Hi*, where there is an apparent spatial bias of feature richness and abundance that influences feature diversity. The introduction of an attribute weighting factor may also address the "edge effect" limitations expected from coarse resolution datasets that do not necessarily show much diversity over small distances within the landscape, i.e. Koppen-Geiger climate classification (Conradie, 2013). In these instances, the diversity quantification is limited to the adjoining climatic-class boundaries with a minimal intra-feature variation. However, as Santos et al. (2017) point out, introducing a weighting factor for each element may be challenging without introducing subjectivity into the diversity analysis leading to an imbalance in the final results. Qualitative assessment methods based on knowledge and expert experiences such as descriptive documentary (Panizza, 2009), expert classification (Kozlowski, 2004) and values and benefits (Gordon & Barron, 2013) have successfully been used for systematic geodiversity

evaluation, albeit with limited applicability and repeatability beyond the spatial regions of interest. The solution to these limitations is to ensure maximum data representation and a more detailed spatial variation of parameters at minimal expense to data quality. In regard to climatic diversity, rather than introducing a weighting's factor to the methodology, the authors applied a rudimentary but effective downscaling approach, suggested by Vajda and Venäläinen (2003) and Hjort et al. (2012), to resample the 1.7 × 1.7 km resolution climatic sub-partial indices to a 90 × 90 m resolution using a bilinear interpolation approach with an overall R^2 prediction of 96%. Rescaling the sub-partial climatic index to a more acceptable resolution allowed for improved climatic diversity representation with higher-density natural class breaks (Jenks) for each respective sub-partial climate variable.

2.3.2 Geodiversity Index Map for UTDM

Despite particular methodological challenges, which represent similar issues of the current discourse on geodiversity quantification (Santos et al., 2017), the final geodiversity map presents an exciting product that highlights the integrated analysis of the physical environment and the richness in abiotic elements distributed throughout the UTDM area. The components of geodiversity were analysed using two sets of informative diversity indices: feature *richness* representing the number of fundamental elements within the feature space or sample grid and feature *abundance* representing the frequency of sub-partial diversity elements within each grid cell (Ferrer-Valero, 2018). The *GDIx* score of each grid square is the sum of all the previously outlined partial indices: *Hi*, *Pi*, *Li*, *Ci*, *Ti*, *Gi* and *Si*, with each index representing an element of geodiversity with values of the final *GDIx* in the range of 1 and 5 (Fig. 2.4) based on the minimum and maximum values categorised into five-class equal intervals.

The areas with the highest geodiversity concentration are in the eastern, central and western parts of the UTDM, with smaller pockets of high diversity scattered throughout the region. In the west region, the Drakensberg mountain range stands out as the dominant feature of *Li*, *Gi*, *Ti*, *Pi* and surprisingly *Si* diversity, where there are diverse landforms and many exposed lithostratigraphic features. More precisely, the highest values of the topographic, geomorphometric, pedological and solar morphometric partial indices (3–5 points) are associated with the ensuing morphological contrast between the central region and the diversified relief of the Drakensberg mountain range in the west. Similarly, the diverse lithostratigraphic and paleosensitivity variety justifies the high geodiversity values east of the UTDM. A total of seven of the eleven lithostratigraphic elements were identified in the eastern region of the UTDM comprised of a mix of alluvial and colluvial material as well as agglomerates of Masotcheni Basalt and Karoo Dolerite with sedimentary surface intrusions of shale, sandstone, siltstone and mudstone of the Vryheid, Estcourt and Volksrust formations, respectively. In such areas, the regions of high paleosensitivity (fossil heritage) were positively associated with the corresponding

lithological diversity signalling that the eastern part of the UTDM is characterised by diverse fossil heritage from geological formations.

Large portions to the northeast and southeast regions of the UTDM are characterised by low to medium geodiversity, with primary diversity influenced by the *Gi* partial index of varying geomorphon abundance. Consequently, this same region was marked by a moderate to intermittent high surface water sub-partial index normalised score (0.4–0.5) and low underground sub-partial index normalised score (0.1–0.25), resulting in the low-medium final *Hi* partial index scores due to the scale-abundance-quantification paradox of selected sub-partial indices outlined in the previous section. A key observation regarding the *GDIx* for the UTDM is an association of medium-high index values (>3) for higher altitude regions above 1450 m a.s.l. with lower index values characterised by lower-lying areas below 1220 m a.s.l. For these regions, the results suggest that the *GDIx* distribution is closely linked to the topographic arrangement of the UTDM: where the amplitude of terrain relief is high, *GDIx* shows the highest values; in contrast, the lowest *GDIx* values uniformly define the dominant flat areas of the region. Pellitero et al. (2015) observed similar trends in glacial landforms and attributed this relationship to the increasingly active landform, geological and soil processes at higher altitudes.

The entire UTDM region of approximately 11,500 km^2 was divided into 2042 separate 6.25 km^2 grids (Fig. 2.4h). However, while the grid format may be useful for block diversity quantification, it is not readily applicable to visualise the final *GDIx* results as a continuous surface or interoperable with other spatial datasets for supplementary spatial analysis. Following the methodology outlined by Santos et al. (2017), we performed grid-to-point conversion of the *GDIx* values, after which these points were interpolated using an ordinary kriging approach, resulting in a predicted continuous surface ($R^2 = 0.96$) of *GDIx* class distribution throughout the UTDM region (Fig. 2.4i). The results presented in Table 2.2 have been derived from the interpolated *GDIx* surface and provide the most meaningful outcomes of key descriptive metrics related to the frequency distribution and selected fragmentation class metrics for each *GDIx* class. The first significant observation is that low-medium *GDIx* areas cover approximately 600,000 ha (or 60%), while high-very high *GDIx* occupies almost 400,000 ha (14%) of the study area. This result suggests that while there are specific features of high diversity – geodiversity hotspots or loci – the region is dominated by low-medium overall geodiversity. These results are further contextualised by considering the outputs of selected patch metrics (McGarigal et al., 2009) calculated for each *GDIx* class. A total of 131 low diversity patches compared to 77 high and 70 very high *GDIx* classes were detected within the UTDM.

Interestingly, despite the lower patch number for the high-very high *GDIx* classes, the higher *GDIx* classes recorded larger mean patch sizes, by a factor of 2, compared to the lower-valued *GDIx* class. Moreover, the mean perimeter-to-area ratio, which represents shape complexity, suggests that the high-very high *GDIx* patches are less complex in shape, or the amount of patch area exposed to edges is lower, not as pronounced as the low-medium *GDIx* class. The perimeter-to-area ratio values for the low-medium *GDIx* values also suggest that these regions are

Table 2.2 Categorisation of frequency of selected landscape metrics summarised by geodiversity class

Geodiversity index	Geodiversity class	Area (ha)	Mean patch size (ha)	Mean perimeter/area ratio (shape complexity)	Number of patches	Area ratio (%)	Cumulative frequency (%)
0–1	Very low	92 452	1 566	80.4	59	8.1	8.1
1–2	Low	252 339	1 926	166.7	131	22.2	30.4
2–3	Medium	343 644	3 818	150.9	90	30.3	60.7
3–4	High	288 287	3 743	70.6	77	25.4	86.1
4–5	Very high	156 387	2 234	49.8	70	13.8	100

characterised by *GDIx* patches with elongated shapes or indented and are generally small patches and therefore have higher perimeter-to-area ratios than the larger-shaped and unbroken edges of the high *GDIx* patches (Helzer & Jelinski, 1999).

2.4 Future Work

The methodology presented in the study is, in fact, a subnational adaptation of the method(s) proposed by Araujo and Pereira (2018). Our findings, therefore, confirm the application of their approach within a regional southern Africa, something which has not been tested before. A significant advantage of our study is that we introduce additional sub-index covariates to detail a richer perspective of local geodiversity in the UTDM. We propose a methodology that simultaneously considers abiotic feature richness and abundance that can be readily developed and deployed in many proprietary or open-source GIS platforms. While this chapter aims not to describe the full geodiversity of the UTDM, the approach developed in this work has one main disadvantage: the quantification and prediction of geodiversity do not consider the combined geovalues and products of the regions' physical resources. This study has focused on limiting any considerations of geodiversity's intrinsic value, i.e. the belief that some things (in this case, nature's geodiversity) are of value simply for what they are rather than what they can be used for by humans (utilitarian value). Both Gray (2013) and Wilson (1994) point out that it is the most challenging value to describe since it involves ethical and philosophical dimensions of the relationships between society and nature. Instead, this study aimed to highlight the utility of adopting an objective quantitative approach to geodiversity valuation based on the functional value, or utilitarian interpretations, of the supporting surrogates that contribute to landscape diversity. Nevertheless, to fully meet end-user's needs, it may be necessary to translate this kind of quantitative geodiversity

information into qualitative maps that explicitly address the importance of geoheritage and geoconservation of geotopes or geomorphological features within UTDM. Therefore, in addition to functional and scientific values of geodiversity, future studies may consider evaluating other overlapping potentialities such as cultural, aesthetic and economic values of geodiversity, which are equally as important and may provide a full range of local and regional geodiversity (Gray, 2013; Araujo & Pereira, 2018). Nevertheless, the evaluation of geodiversity should focus on the conservation of resources and their management, which are vital to the development of human activities (Benito-Calvo et al., 2009). In this context, the method presented herein provides a reliable and user-friendly approach to unravelling geodiversity in KZN, but there is still much left to do.

The links between geodiversity and biodiversity are irrefutable (Melelli et al., 2017). However, these links must be adequately understood in developing effective management responses to human pressures and climate change (Gordon & Barron, 2013). What is exceptionally high on the development agenda is better understanding the interrelationship between geodiversity and biodiversity in dynamic environments, where natural processes (e.g. floods, erosion and deposition) maintain habitat diversity and ecological functions and how these links can drive environmental policy reforms in South Africa. South Africa is known for its progressive and innovative environmental legislation that reflects the natural, physical, economic and psychological importance of the environment to humans (Grab & Knight, 2015). An exciting approach to evaluating geodiversity importance may need to consider how an ecosystem-based approach to resource management can provide a framework for developing a much better integration of geodiversity, biodiversity and landscape management. This will provide a means of realising geodiversity's broader values and benefits through its contribution and functionality in delivering ecosystem services. From a national perspective, including areas of high geodiversity into systematic conservation planning may also provide a useful platform to address a range of contemporary policy, strategy and landscape-action sustainability issues: What geodiversity does a country have and can we map it? What is the condition of geodiversity across the landscape? Where and how should a country act first to manage and mitigate geodiversity importance? The concept of "conserving natures stage" is defined by Lawler et al. (2015) as a concept that encapsulates the idea that maintaining a varied physical landscape will enable diverse ecological processes to operate, protecting and promoting landscape diversity. Failure to acknowledge such responses may cross essential geomorphic and ecological thresholds that initiate land degradation and increase human risk and vulnerability to natural hazards.

2.5 Conclusion

To date, only one other landmark study has successfully investigated the influence of environmental factors on geodiversity mapping in South Africa (Kori et al., 2019). This work was the first attempt KZN to produce a full extent geodiversity

map for the uThukela District Municipality (UTDM) using a geospatial index approach to objectively quantify the influence of physical environmental factors on landscape geodiversity. The proposed contribution of partial environmental indices, readily obtained from various open-source platforms (Table 1.1) and harmonised to a spatial resolution of 90 m to successfully produce a 90 m geodiversity map for UTDM, can become a reference for inclusive geomorphological mapping for KZN.

This study assessed and mapped geodiversity by quantifying seven primary components of geodiversity importance based on the hydrographic lithostratigraphic, pedological, climatic, topographic, atmospheric and geomorphological diversity across the landscape. The semi-quantitative methodology for assessing geodiversity relies heavily on the approach outlined by Araujo and Pereira (2018), with minor modifications related to sample grid resolution (resolution of 2500 m × 2500 m) and the specific quantification of feature richness and abundance from varying spatial data formats, using a data scale of 1:250,000. The methodology used in this study relies on the input of numerous spatial datasets of varying data format, scale and measurement scale. The results of this study provide a valuable resource to evaluate the limitations of data normalisation necessary for geodiversity score standardisation when constructing the geodiversity analysis.

By adapting well-known methods of numerical geodiversity quantification, this study attempted to provide a regional GDIx map for the entire UTDM. In the regional approach, surrogate partial indices are evaluated as explanatory variables for the contributions to the GDIx rankings on a spatial basis. The methodology used for quantifying the *GDIx*, using both vector and raster datasets, proved to be effective in highlighting the richness and abundance of features for the respective partial sub-indices. The main results of the geodiversity analysis are categorised and graphically represented into five classes from very low to very high geodiversity. The topographical, pedological and geological diversity estimation and the geomorphometric diversity quantification showed strong associations with regions in the northern, southern and western areas of the UTDM characterised by the Drakensberg mountain range, higher altitude, complex terrain and associated increased diversity of soil and geological material. A key finding is that these partial indices consequently strongly influence the final regionalisation of geodiversity with areas of medium partial index diversity randomly distributed throughout the UTDM. These high-index-value regions of geodiversity indicate that these areas should be prioritised from a land management perspective. A key consideration of this research is highlighting a simplistic, objective and replicable numerical approach for deriving a *GDIx* product at a landscape level, with rudimentary technical expectations placed on the end-user, at minimal expense to representing the reality of each input element (partial index) diversity.

There is no superior approach to geodiversity quantification and representation. While the methodology presented in this study provides a pragmatic approach for geodiversity assessment, further adaptions based on personal user preference and research objectives such as sampling grid resolution, method of geodiversity assessment and quantification, spatial data analysis, the scale of analysis and application of the final product provide an opportunity for further exploration. Importantly, it

must be emphasised that the present study's geodiversity results merely represent the diversity (richness and abundance) concerning the observed partial indices for the region where no other studies on geodiversity have been undertaken from this perspective. Therefore, the concept of geodiversity is somewhat "flexible" in that future studies may indeed consider a new suite of partial indices for geodiversity quantification. We must point out that geodiversity assessment's future adaptations may benefit from systematic improvements to the present methodology. Firstly, the inclusion of other surrogate elements of intrinsic geodiversity importance, such as detailed lithostratigraphic resource data or improved soil classifications for the region or further, includes climatic variables, beyond those applied in this study, since increasingly more studies on climate change vulnerability assessment and adaptive management are being conducted at the scale of landscapes.

The last decade has seen a significant increase in the quality of landscape indices through the application of geoinformatics research aimed directly at assessing geodiversity. Over this period, land surface analysis and classification have seen rapid improvements in the rate and quality of geomorphometric computational approaches, a key factor for the utility of digital geomorphic mapping. In truth, the substantive contribution of geographical information systems (GIS) and remote sensing (RS) has provided a platform for users to digitally access environmental information readily at different spatial scales and levels of sophistication. This has contributed significantly to providing new information about the mechanisms that underlie the current patterns of geodiversity. RS further provides a segway to endless opportunities to merge knowledge from different domains (e.g. software, mathematics, engineering, geomorphology) to study landscapes in a more interdisciplinary manner. GIS systems provide a solid platform to synoptically explore the parameters driving geodiversity and promote a systematic digital approach to accurately mapping landforms and geomorphic systems with different climate, geological and topographic settings. Specifically, advances in RS of land surface terrain features and geospatial modelling systems that support numerical modelling of surface biophysical processes have reformed traditional geomorphic analyses and mapping. Pioneering techniques, such as these, may benefit future geodiversity research since the focus is on integrating quantitative topographic information, on a cell-by-cell (gridded format) basis, with some form of geospatial platform with an ever-increasing reliance on geostatistical approaches and artificial intelligence to describe the dynamic landscape and topographic change, patterns and complexity. These digital systems, data and tools, often referred to as geomorphic decision support systems (GDSS), are increasingly favoured for their contributions to diagnostic assessments and terrain modelling to achieve enhanced interpretations of scale, patterns, processes and diversity of landscape features and systems. A final consideration beyond the present study's scope is the possible application of digital hexagonal grids, rather than the standard fishnet grid, for the numeric quantification of the GDIx in a GIS environment. A significant advantage of using hexagonal grids is that they offer reduced edge effect since they provide the lowest perimeter-to-area ratio of any regular tessellation of a sampled plane. Hexagonal sampling may offer increased benefit to users' intent on using vector-based abiotic variables for geodiversity quantification

since hexagons can better fit curved surfaces than squares across large areas such as landscapes. This may regulate the independencies and respective influences of abiotic variables on overall geodiversity contributions.

The present study is expected to intellectually incentivise future studies on geodiversity in South Africa as persistent environmental pressures will soon demand maps that express this concept to become more frequent as decision support tools. If prioritised as a significant element for adaptive management, the *GDIx* assessment presented in this study can inform many kinds of planning and decision-making supporting sustainable development. It implicitly considers the diversity contributions of seven critical abiotic components related to geology, soils, climate, hydrology, atmospheric, topography and geomorphology to overall landscape geodiversity importance. One of the primary outputs is a simple cartographic representation of ranked diversity importance of the quality of geodiversity for the entire UTDM that is easily understandable by a varied audience. Therefore, the *GDIx* map(s) should be considered first as a tool for integrated natural resource management, monitoring and reporting at a regional level. Given the structural ties between geodiversity and biodiversity, this will facilitate leveraging usable land and biodiversity management recommendations and action programmes in an integrated approach to environmental management and geoconservation.

References

Alba Alonso, S., Ibáñez Martí, J. J., Lobo Aleu, A., & Zucarello, V. (1998). Pedodiversity and global soil patterns at coarse scales. *Geoderma, 83*, 171–192.

Araujo, A. M., & Pereira, D. Í. (2018). A new methodological contribution for the geodiversity assessment: Applicability to Ceará State (Brazil). *Geoheritage, 10*(4), 591–605.

ARC. (2003). *1:250,000 scale land type survey of South Africa*. ARC.

Argyriou, A. V., Sarris, A., & Teeuw, R. M. (2016). Using geoinformatics and geomorphometrics to quantify the geodiversity of Crete, Greece. *International Journal of Applied Earth Observation and Geoinformation, 51*, 47–59.

Atkinson, J., de Clercq, W., & Rozanov, A. (2020). Multi-resolution soil-landscape characterisation in KwaZulu Natal: Using geomorphons to classify local soilscapes for improved digital geomorphological modelling. *Geoderma Regional, 22*, 1–18.

Bailey, J. J., Boyd, D. S., Hjort, J., Lavers, C. P., & Field, R. (2017). Modelling native and alien vascular plant species richness: At which scales is geodiversity most relevant? *Global Ecology and Biogeography, 26*(7), 763–776.

Benito-Calvo, A., Pérez-González, A., Magri, O., & Meza, P. (2009). Assessing regional geodiversity: The Iberian Peninsula. *Earth Surface Processes and Landforms, 34*(10), 1433–1445.

Bennett, J. M., & Mattsson, L. (1999). *Introduction to surface roughness and scattering*. Optical Society of America.

Betard, F., & Peulvast, J. P. (2019). Geodiversity hotspots: Concept, method and cartographic application for geoconservation purposes at a regional scale. *Environmental Management, 63*(6), 822–834.

Botha, G. A., & Singh, R. (2012). *Geology, geohydrology and Development Potential Zonation of the uThukela District Municipality: Specialist contribution towards the Environmental Management Framework*. Council for Geoscience.

Brilha, J. (2005). *Geological heritage and geoconservation: Nature conservation in its geological aspect*. Braga.
Burek, C. V., & Potter, J. (2006). Local geodiversity action plans: Setting the context for geological conservation. In *0967-876X*. Peterborough.
Cairncross, B. (2011). The National Heritage Resource Act (1999): Can legislation protect South Africa's rare geoheritage resources? *Resources Policy, 36*(3), 204–213.
CGS. (2000). *Cartographic Material: 2828 Harrismith, 2928 Drakensberg, 2930 Durban, 2830 Richards Bay*. In: C.f. Geosciences (Ed.). 1:250 000 Geological Series (South Africa Geological Survey). Council for Geosciences, Pretoria
Church, M. (2011). Observations and experiments. In *The SAGE Handbook of Geomorphology*. Sage.
Cocks, M., Vetter, S., & Wiersum, K. F. (2018). From universal to local: perspectives on cultural landscape heritage in South Africa. *International Journal of Heritage Studies, 24*(1), 35–52.
Comer, P. J., Pressey, R. L., Hunter, M. L., Jr., Schloss, C. A., Buttrick, S. C., Heller, N. E., Tirpak, J. M., Faith, D. P., Cross, M. S., & Shaffer, M. L. (2015). Incorporating geodiversity into conservation decisions. *Conservation Biology, 29*(3), 692–701.
Conradie, D. C. U. (2013). Appropriate passive design approaches for the various climatic regions in South Africa. In L. Van Wyk (Ed.), *The Green Building Handbook, the Essential Guide* (pp. 101–117). Alive2Greean.
Cox, D., Oosthuizen, S., & Dickens, C. (2015). *Moving from Integrated Water Resources Management (IWRM) to Integrated Natural Resources Management (INRM): A proposed framework for INRM at District Scale in South Africa*. Institute of Natural Resources.
Crofts, R., Gordon, J., Brilha, J., Gray, M., Gunn, J., Larwood, J., Santucci, V., Tormey, D., & Worboys, G. (2020). *Guidelines for geoconservation in protected and conserved areas*. International Union for Conservation of Nature (IUCN).
Deacon, J. (2015). Great expectations: Archaeological sites and the national heritage resources act (act 25 of 1999). *The South African Archaeological Bulletin*, 220–223.
Dixon, G. (1996). *Geoconservation: An international review and strategy for Tasmania*. Parks and Wildlife Service.
dos Santos, F. M., Bacci, D. L. C., Saad, A. R., & da Silva Ferreira, A. T. (2020). Geodiversity index weighted by multivariate statistical analysis. *Applied Geomatics, 12*(3), 361–370.
DWA. (2006). *South African dams and river line shapefiles mapped at 1:500 000*. In: S.A. Department of Water Affairs (Ed.).
EKZNW. (2010). *2008 KZN Province Land Cover Mapping (from SPOT5 Satellite imagery circa 2008)*. Ezemvelo KwaZulu-Natal Wildlife.
Elliot, F., & Escott, B. (2015). *UThukela District municipality: Biodiversity sector plan*. Ezemvelo KZN Wildlife.
ESRI. (2021). *ArcGIS 10.5*. Environmental Systems Research Institute Inc..
Ferrer-Valero, N. (2018). Measuring geomorphological diversity on coastal environments: A new approach to geodiversity. *Geomorphology, 318*, 217–229.
Galatowitsch, S., Frelich, L., & Phillips-Mao, L. (2009). Regional climate change adaptation strategies for biodiversity conservation in a midcontinental region of North America. *Biological Conservation, 142*(10), 2012–2022.
Gordon, J. E., & Barron, H. F. (2013). The role of geodiversity in delivering ecosystem services and benefits in Scotland. *Scottish Journal of Geology, 49*(1), 41–58.
Gordon, J. E., Barron, H. F., Hansom, J. D., & Thomas, M. F. (2012). Engaging with geodiversity—Why it matters. *Proceedings of the Geologists' Association, 123*(1), 1–6.
Grab, S., & Knight, J. (2015). *Landscapes and landforms of South Africa*. Springer International Publishing.
Graham, B., Ashworth, G. J., & Tunbridge, J. E. (2000). *A geography of heritage: Power. Culture and economy*. Routledge.
GRASS Development Team. (2016). *Geographic Resources Analysis Support System (GRASS) software*. Open Source Geospatial Foundation. Retrieved from http://grass.osgeo.org

Gray, M. (2004). *Geodiversity: Valuing and conserving abiotic nature*. John Wiley & Sons.
Gray, M. (2008). Geodiversity: A new paradigm for valuing and conserving geoheritage. *Geoscience Canada, 35*(2), 51–59.
Gray, M. (2013). *Geodiversity: Valuing and conserving abiotic nature*. Wiley.
GSA. (2010). Geoscience amendment act, 16 of 2010. In C. F. Geoscinence (Ed.), *Gazette No. 33837*. South Africa Government Printers.
Helzer, C. J., & Jelinski, D. E. (1999). The relative importance of patch area and perimeter–area ratio to grassland breeding birds. *Ecological Applications, 9*(4), 1448–1458.
Hjort, J., & Luoto, M. (2010). Geodiversity of high-latitude landscapes in northern Finland. *Geomorphology, 115*(1–2), 109–116.
Hjort, J., Heikkinen, R. K., & Luoto, M. (2012). Inclusion of explicit measures of geodiversity improve biodiversity models in a boreal landscape. *Biodiversity and Conservation, 21*(13), 3487–3506.
Holmes, P. J., Grab, S. W., & Knight, J. (2016). South African geomorphology: Current status and new challenges. *South African Geographical Journal, 98*(3), 405–416.
Horton, R. E. (1932). Drainage-basin characteristics. *Eos, Transactions American Geophysical Union, 13*(1), 350–361.
Ibáñez, J., De-Alba, S., Boixadera, J., King, D., Jones, R., & Thomasson, A. (1995). The pedodiversity concept and its measurement: Application to soil information systems. In *European land information systems for agro-environmental monitoring* (pp. 181–195).
Jackson, C., Mofutsanyana, L., & Mlungwana, N. (2019). A risk-based approach to heritage management in South Africa. In *International Archives of the Photogrammetry, Remote Sensing & Spatial Information Sciences*.
Jarvis, A., Reuter, H. I., Nelson, A., & Guevara, E. (2008). *Hole-illed Seamless SRTM Data V4*. International Centre for Tropical Agriculture (CIAT).
Jasiewicz, J., & Stepinski, T. F. (2013). Geomorphons—A pattern recognition approach to classification and mapping of landforms. *Geomorphology, 182*, 147–156.
Julesz, B. (1981). Textons, the elements of texture perception, and their interactions. *Nature, 290*(5802), 91.
Knight, J., Grab, S., & Esterhuysen, A. B. (2015). Geoheritage and geotourism in South Africa. In S. Grab & J. Knight (Eds.), *Landscapes and landforms of South Africa* (pp. 165–173). Springer International Publishing.
Kori, E., Onyango Odhiambo, B. D., & Chikoore, H. (2019). A geomorphodiversity map of the Soutpansberg range, South Africa. *Landform Analysis, 38*, 13–24.
Kostrzewski, A. (2011). The role of relief geodiversity in geomorphology. *Geographia Polonica, 84*(Special Issue Part 2), 69–74.
Kozlowski, S. (2004). Geodiversity. The concept and scope of geodiversity. *Przegląd Geologiczny, 52*, 833–837.
Lavin, J. (2013). *Palaeontological sensitivity map of South Africa*. In: SAHRA (Ed.). https://sahris.sahra.org.za/content/how-use-palaeontological-fossil-sensitivity-map/, Cape Town
Lawler, J. J., Ackerly, D. D., Albano, C. M., Anderson, M. G., Dobrowski, S. Z., Gill, J. L., Heller, N. E., Pressey, R. L., Sanderson, E. W., & Weiss, S. B. (2015). The theory behind, and the challenges of, conserving nature's stage in a time of rapid change. *Conservation Biology, 29*(3), 618–629.
Lilburne, L., Eger, A., Mudge, P., Ausseil, A. G., Stevenson, B., Herzig, A., & Beare, M. (2020). The Land Resource Circle: Supporting land-use decision making with an ecosystem-service-based framework of soil functions. *Geoderma, 363*, 114134.
Lowenthal, D. (2005). Natural and cultural heritage. *International Journal of Heritage Studies, 11*(1), 81–92.
MacVicar, C. M., de Villiers, J. M., Loxton, R. F., Verster, E., Lambrechts, J. J. N., Merryweather, F. R., Le Roux, J., & van Rooyen, T. H. (1977). *Soil classification – A binominal system for South Africa*. Department of Agricultural Technical Services.

Manosso, F. C., & de Nóbrega, M. T. (2016). Calculation of geodiversity from landscape units of the Cadeado Range region in Paraná, Brazil. *Geoheritage, 8*(3), 189–199.

McGarigal, K., Tagil, S., & Cushman, S. A. (2009). Surface metrics: An alternative to patch metrics for the quantification of landscape structure. *Landscape Ecology, 24*(3), 433–450.

MEA. (2005). *Millennium ecosystem assessment: Ecosystems and human well-being*. Island.

Melelli, L., Vergari, F., Liucci, L., & Del Monte, M. (2017). Geomorphodiversity index: Quantifying the diversity of landforms and physical landscape. *Science of the Total Environment, 584*, 701–714.

Miller, B. A., & Schaetzl, R. (2014). The historical role of base maps in soil geography. *Geoderma, 230*, 329–339.

NEMA. (2008). *National Environmental Management Act, 63 of 2008*. In: S.A. Department of Environmental Affairs (Ed.), Gazette No.19519, Pretoria, South Africa Government Printers.

NGI. (2018). *Hydrological polygon and river line shapefiles mapped from the 1:50 000 topographical maps*. In: DRDLR:NGI (Ed.), Cape Town.

NHRA. (1999). *National Heritage Resources Act 25 of 1999*. In: S.A. Department of Arts and Culture (Ed.), Government Gazette, 506(19974), Pretoria, South Africa Government Printers.

Panizza, M. (2007). *Geodiversity, geological heritage and geotourism*, Geomorphorsites, Geoparks and Geotourism, Lesvos.

Panizza, M. (2009). The geomorphodiversity of the Dolomites (Italy): A key of geoheritage assessment. *Geoheritage, 1*(1), 33–42.

Parks, K., & Mulligan, M. (2010). On the relationship between a resource-based measure of geodiversity and broad-scale biodiversity patterns. *Biodiversity and Conservation, 19*(9), 2751–2766.

Partridge, T., Dollar, E., Moolman, J., & Dollar, L. (2010). The geomorphic provinces of South Africa, Lesotho and Swaziland: A physiographic subdivision for earth and environmental scientists. *Transactions of the Royal Society of South Africa, 65*(1), 1–47.

Pellitero, R., Manosso, F. C., & Serrano, E. (2015). Mid-and large-scale geodiversity calculation in fuentes carrionas (nw spain) and serra do cadeado (paraná, brazil): Methodology and application for land management. *Geografiska Annaler: Series A, Physical Geography, 97*(2), 219–235.

Pereira, D. I., Pereira, P., Brilha, J., & Santos, L. (2013). Geodiversity assessment of Paraná State (Brazil): An innovative approach. *Environmental Management, 52*(3), 541–552.

Prosser, C. D., Bridgland, D. R., Brown, E. J., & Larwood, J. G. (2011). Geoconservation for science and society: Challenges and opportunities. *Proceedings of the Geologists' Association, 122*(3), 337–342.

Rassool, C. (2013). Towards a critical heritage studies. *Material Religion, 9*(3), 403–404.

Riley, S. J., DeGloria, S. D., & Elliot, R. (1999). Index that quantifies topographic heterogeneity. *Intermountain Journal of Sciences, 5*(1–4), 23–27.

Ruban, D. A. (2010). Quantification of geodiversity and its loss. *Proceedings of the Geologists' Association, 121*(3), 326–333.

Santos, D. S., Mansur, K. L., Gonçalves, J. B., Junior, E. R. A., & Manosso, F. C. (2017). Quantitative assessment of geodiversity and urban growth impacts in Armação dos Búzios, Rio de Janeiro, Brazil. *Applied Geography, 85*, 184–195.

Schulze, R. E., & Maharaj, M. (2007). *Rainfall concentration*. WRC.

Schulze, R. E., & Chapman, R. D. (2007). *Estimation of daily solar radiation over South Africa*. WRC.

Schulze, R. E., Horan, M. J. C., Lumsden, T. G., & Warburton, M. L. (2007). *Recharge to the groundwater store and Baseflow*. Water Research Commission.

Serrano, E., & Ruiz-Flaño, P. (2007). Geodiversity: A theoretical and applied concept. *Geographica Helvetica, 62*(3), 140–147.

Serrano, E., & González Trueba, J. J. (2011). Environmental education and landscape leisure. Geotourist map and geomorphosites in the Picos de Europa National Park. *Geojournal of Tourism and Geosites, 8*(2), 295–308.

Serrano, E., Ruiz-Flaño, P., & Arroyo, P. (2009). Geodiversity assessment in a rural landscape: Tiermes-Caracena area (Soria, Spain). *Memorie Descrittive Della Carta Geoligica d'Italia, 87*, 173–180.

Sharples, C. (1993). *A methodology for the identification of significant landforms and geological sites for geoconservation purposes*. Forestry Commission Tasmania.

Sharples, C. (1995). Geoconservation in forest management principles and procedures. *Tastforest Hobart, 7*, 37–50.

Silva, J. P., Pereira, D. I., Aguiar, A. M., & Rodrigues, C. (2013). Geodiversity assessment of the Xingu drainage basin. *Journal of Maps, 9*(2), 254–262.

Swanwick, C. (2002). *Landscape Character Assessment: Guidance for England and Scotland*. Department of Landscape University of Sheffield.

Thompson, J. A., Roecker, S., Grunwald, S., & Owens, P. R. (2012). Digital soil mapping: Interactions with and applications for hydropedology. In H. Lin (Ed.), *Hydropedology: Synergistic integration of soil science and hydrology*. Academic Press.

Thwaites, R. N. (2000). From biodiversity to geodiversity and soil diversity. A spatial understanding of soil in ecological studies of the forest landscape. *Journal of Tropical Forest Science, 12*(Part 2), 388–405.

UNESCO. (2000). *United nations educationa, scientific and cultural organisation.*https://whc.unesco.org/en/list/985/

Vajda, A., & Venäläinen, A. (2003). The influence of natural conditions on the spatial variation of climate in Lapland, northern Finland. *International Journal of Climatology: A Journal of the Royal Meteorological Society, 23*(9), 1011–1022.

Van Niel, K. P., Laffan, S. W., & Lees, B. G. (2004). Effect of error in the DEM on environmental variables for predictive vegetation modelling. *Journal of Vegetation Science, 15*(6), 747–756.

Wascher, D. M. (2005). Landscape character: Linking space and function. Final ELCAI Project Report, Landscape Europe. In *European landscape character areas e typology, cartography and indicators for the assessment of sustainable landscapes* (pp. 1–4).

Wilson, C. (1994). *Earth heritage conservation*. Open University.

Zhang, X., Chen, J., Zhang, G., Tan, M., & Ibáñez, J. (2003). Pedodiversity analysis in Hainan Island. *Journal of Geographical Sciences, 13*(2), 181–186.

Zwolinski, Z. (2018). *Spatial scales of geodiversity and landform taxonomic hierarchy*. Geoheritage and Conservation: Modern Approaches and Applications Towards the 2030 Agenda.

Zwoliński, Z. (2008). *Designing a map of the geodiversity of landforms in Poland* (pp. 18–22). IAG and AIGEO International Meeting Environmental Analysis and Geomorphological Mapping for a Sustainable Development.

Zwoliński, Z., Najwer, A., & Giardino, M. (2018). Methods for assessing geodiversity. In E. Reynard & J. Brilha (Eds.), *Geoheritage: Assessment, protection, and management* (pp. 27–52). Elsevier.

Chapter 3
Monitoring the Wildfire Activity and Ecosystem Response on Mt. Kilimanjaro Using Earth Observation Data and GIS

Priyanko Das, Zhenke Zhang, and Hang Ren

Abstract Forest fires play an important role in environmental problems that influence climate change. It is essential to map the burnt areas and monitor vegetation's regrowth to investigate the relationship between climate change and wildfire events in the mountain area. The present study provides remote sensing technology to monitor the extent of wildfire and vegetation reconstruction on Mt. Kilimanjaro. Active fire information on 11 October 2020 was obtained from MODIS optical sensor and masked the burn area. Estimating NBR, dNBR, and BAIS2 using Sentinel-2 data provides detailed information of active fires and burn severity concerning MODIS imagery. Results indicate that 398.89 ha is in higher severity condition within the burn area of 7011.30 ha. LAI and NDVI were used to detect the damage of vegetation in this reserve forest. LAI and NDVI report that a large area of vegetation was lost, where LAI decreased from 0.83 to 0.34 and NDVI decreased from 0.28 to 0.22, respectively, in this fire event. After the post-fire, the time series of LAI showed a positive vegetation reconstruction trend, which also depends on the climatic condition. We conclude that the dry climatic condition and local human activity cause this wildfire event. However, human activity management and control will reduce the forest fire events in this reserve forest.

Keywords Climate change · dNBR · BAIS2 · LAI · NDVI

P. Das · Z. Zhang (✉) · H. Ren
Center for African Studies, School of Geographic and Oceanographic Sciences, Nanjing University, Nanjing, China
e-mail: zhangzk@nju.edu.cn; renhangnju@smail.nju.edu.cn

S. Adelabu et al. (eds.), *Remote Sensing of African Mountains*,
https://doi.org/10.1007/978-3-031-04855-5_3

3.1 Introduction

Forest fire is crucial for short and long-term changes in the forest ecosystem, vegetation structure modification, and significant greenhouse gas sources (Poletti et al., 2019). The forest fire has a global impact on damages to our livelihood, such as desertification, soil erosion, and landslide (Kurnaz et al., 2020). Also, the burning of forests can damage the various ecosystem components such as plant species, soil organic layer, increased landslide, animal death, and pollution (Oliveira-Júnior et al., 2020). Drought severity may trigger the fire regimes worldwide under the climate change condition (Filipponi, 2018). Since 1992 (Rio earth summit), many countries have adopted forest fire management strategies and balanced ecological factors to reach sustainable development goals (Hislop et al., 2020).

Satellite earth observation data is commonly used to detect the burn area information based on the vegetation fire reflectance (Roteta et al., 2019). Several researchers (Fornacca et al., 2018; Scholtz et al., 2020; Veraverbeke & Hook, 2013; Wu et al., 2020) adopted different satellite data from various sensors such as AVHRR (Advanced Very High-Resolution Radiometer), MODIS (Moderate Resolution Imaging Spectroradiometer), Medium Resolution Imaging Spectrometer (MERIS), or SPOT to monitor the regional and global forest fire activity (Shan et al., 2017). Liu et al. (2020) analyzed the GEOS-Chem chemical transport model to detect the smoke-induced health impact using five global inventories datasets – GFAS (Global Fire Assimilation system), GFED (Global Fire Emission Database), FINN (Fire Inventory from NCAR), FEER (Fire Energetics and Emission Research), and QFED (Quick Fire Emissions datasets) for equatorial Asia. Recent studies by Seydi et al. (2021) reported that wildfires affected areas and classified the land cover map with 91.02% accuracy using MODIS Sentinel-2 imageries. Similarly, Liu et al. (2019) collected the MODIS product (MCD64A1) with a 500 m resolution to detect the small burned area with 40% accuracy. Most of the satellite data are based on coarse resolution sensors, including MODIS (250–500 m), and it is challenging to detect the small fires using the size of the pixels. However, high-resolution satellite sensors such as LANDSAT-OLI (30 m) and Sentinel-2 (10 m) make possible to estimate the burn area information on a smaller region.

In general, several methods have been developed for mapping the burn areas from these medium and high-resolution satellite images (Govedarica et al., 2020). Most previous studies used vegetation indices (e.g., NDVI – Normalized Difference Vegetation Index) to discriminate the burn areas from vegetation (González-Alonso & Merino-de-Miguel, 2009). However, these indices could not differentiate carbon to charcoal from fire-affected regions and may not be applicable for burnt area mapping. The use of near-infrared (NIR) and shortwave infrared (SWIR) reflectance is more appropriate for burn mapping and provides more substantial burn area discrimination (Fernández-Manso et al., 2016). Therefore, Normalized Burn Ratio (NBR) (Carlà et al., 2009) and threshold-based classification of Normalized Burn Ratio difference (dNBR) (Govedarica et al., 2020) were developed and widely used for burn severity mapping. Burn Area Index (BAI) also detects the charcoal signal

in post-fire images and discriminates the burn areas compared to other indexes (González-Alonso & Merino-de-Miguel, 2009). Filipponi (2018) presented the newly developed Burn Area Index for Sentinel-2 (BAIS2) based on the spectral properties of Sentinel-2 bands. The BAIS2 detects the post-fire mapping at 20 m resolution and shows good performance on a small scale. However, this work aims to evaluate the capabilities of MODIS and Sentinel-2 imagery for burn severity mapping and vegetation reconstruction on Africa's highest mountain (Mt. Kilimanjaro).

The fire activity in Africa from the last millennium provides the origin of more fire-tolerant flora. Without it, the African savannas may develop woodlands (Catarino et al., 2020). According to the national park service (TANAPA), the wildfire incident on 11 October 2020 at Mt. Kilimanjaro has destroyed most vegetation and threatened the mountain ecosystem (Hemp, 2020). Mt. Kilimanjaro forest is an important natural resource providing ecological services such as tourism, honey collection, and other economic activity (Poletti et al., 2019). In this contrast, monitoring wildfire activity, damage assessment, and vegetation reconstruction on Mt. Kilimanjaro is essential. The increasing human population living in the mountain-surrounding region depends on natural forest resources (Poletti et al., 2019). This population creates more pressure on Mt. Kilimanjaro for driving forest products during the dry season, which later causes a forest fire. A few studies from the local survey found that the higher temperature and dry climatic conditions increased forest fire intensity (Kilungu et al., 2019).

This paper adopted a newly developed burned area index (BAIS2) algorithm estimated from Sentinel-2 imagery for active fire detection in Kilimanjaro Mountain. Also, this study presents the capabilities of MODIS and Sentinel-2 imagery for burn severity mapping. Pre- and post-fire NBR algorithm is applied to Sentinel-2 data and estimate the Differenced Normalized Burn Ratio (dBNR). The Leaf Area Index (LAI) and Normalized Difference Vegetation Index (NDVI) are estimated to monitor damage assessment and post-fire vegetation recovery after the wildfire incident.

3.2 Study Area

Africa's highest mountain, Mt. Kilimanjaro (5895 meters), is located in the border of Kenya and Tanzania with an extent from 2°50′–3°20'S to 37°00′–37°35′E (Fig. 3.1). Hans Meyer is the first geographer who reached the mountain summit in 1889 and was a famous tourist spot for hiking. The forest area was declared a national park in 1973 and UNESCO's World Heritage site in 1989. However, forest ecosystems and biodiversity are important habitats for species diversity in this reserve belt. There are 900 species in the forest belt and 2500 species in the whole mountain.

The climate condition is affected by two rainy seasons – short rain (March to May) and long rain (November to December). The forest belt received 3000 mm, where the lower slope received 1500–2000 mm and southern 900 mm (Hemp,

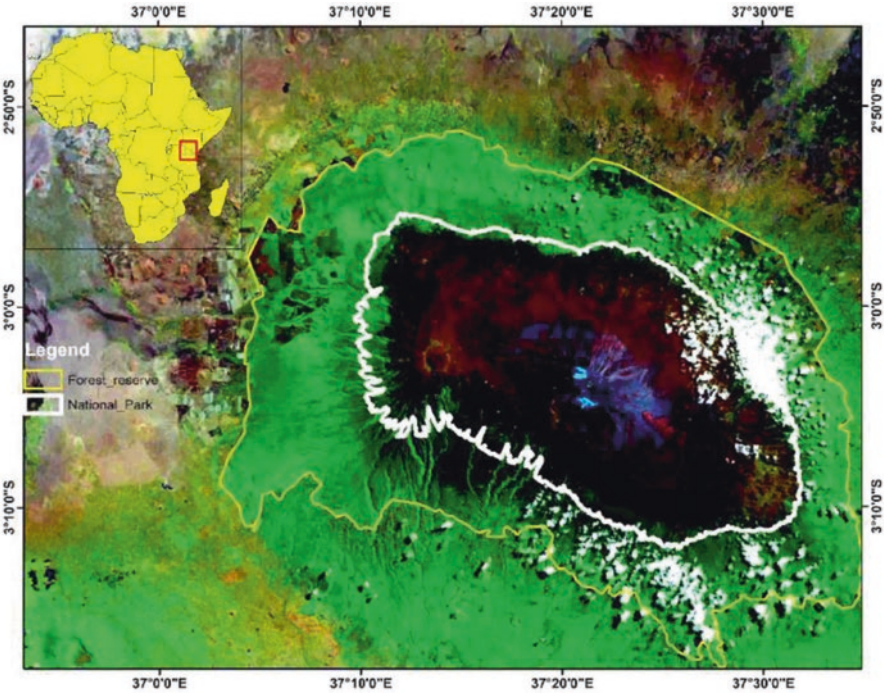

Fig. 3.1 Location map of Mt. Kilimanjaro

2006). Also, the savanna plain's annual temperature is more than 25 °C, and it's less than −5 °C on the Mt. summit (Detsch et al., 2016).

3.3 Materials and Methods

3.3.1 Datasets

The vegetation zonation information is obtained from the European Space Agency (ESA) website (https://www.esa.int/SPECIALS/Eduspace_Global_EN/). The boundary layer for Reserve Forests and National Parks was taken from the following webpage. This boundary was a mask with the final output to determine the burn area and vegetation recovery monitoring.

The Moderate Resolution Imaging Spectroradiometer (MODIS) collection of six burn area products (MCD64A1) was obtained to monitor fire activity in the small region (Giglio et al., 2018). The sensor provides daily global fire monitoring services based on surface reflectance. The product is grided with a 500 m resolution containing information per pixel burn area (Table 3.1) compared to collection 5 (C5 MCD64A1) (Scholtz et al., 2020). Giglio et al. (2009) improved the burn area

Table 3.1 Properties of Sentinel-2 and MODIS satellite data used in this study

Sentinel-2				MODIS		
Band no	Band name	Central bandwidth	Resolution (m)	Product name	Retrieved data	Resolution (m)
B01	C/A	0.421	60	MCD64A1	Burn area monthly	500
B02	Blue	0.490	10			
B03	Green	0.560	10	MCD15A2H	LAI	500
B04	Red	0.665	10			
B05	Red-edge 1	0.705	20	MOD 13A1	NDVI	500
B06	Red-edge 2	0.740	20			
B07	Red-edge 3	0.783	20			
B08	NIR	0.842	10			
B8a	NIR narrow	0.865	20			
B11	SWIR 1	1.610	20			
B12	SWIR 2	2.190	20			

approach to observe fire activity using MODIS channels 5 and 7 and estimate temporal texture. In addition, Leaf Area Index (LAI) datasets are obtained from MODIS level 4 (version 6) 8-day composite with 500 m spatial resolution (MCD15A2H) (Myneni et al., 2015). Similarly, the Normalized Difference Vegetation Index (NDVI) was retrieved from the MODIS Level 3 composite with 500 m resolution. This dataset is freely available and downloaded from the NASA lpdaac website (https://lpdaac.usgs.gov/) (Table 3.1). Although the algorithm (MODIS LAI/FPAR algorithm) combines the best pixel available from the sensor, the study used MODIS LAI and NDVI products to monitor the post-fire vegetation recovery.

The high-resolution Sentinel-2 image was used in this study to identify the burn area and obtained from ESA (European Space Agency), Sentinel Scientific Data Hub (https://scihub.copernicus.eu/). This Multispectral Instrument (MSI) includes an optical sensor with 13 spectral bands at different spatial resolutions (10–60 m) (Table 3.1). The datasets provide accurate post-fire mapping and analysis of the wildfire extent in a small area. The two Sentinel-2 images are selected from 08 October 2020 (pre-fire) and 15 October 2020 (post-fire).

3.4 Method

The monthly MODIS burnt area product (MCD64A1) was used to determine the burn area and mask this area at Mt. Kilimanjaro reserve forest. The algorithm generated a burn-sensitive vegetation index (VI) (Eq. 3.1) and created a dynamic

threshold value in the composite data (Giglio et al., 2009). Afterthought, the burn area was classified into an active fire region and unburned in October 2020. The VI is defined

$$VI = \left(\text{band}\,5 - \text{band}\,7\right) / \left(\text{band}\,5 + \text{band}\,7\right) \tag{3.1}$$

where band 5 and band 7 are atmospherically corrected surface reflectance in MODIS infrared channels.

In the second stage, the two Sentinel images with less cloud were pre-processed in QGIS. The semi-automatic plugin separated the actual reference from the atmospheric reflectance by applying the DOS atmospheric correction. The cloud mask tool was used to mask the cloud pixel from the NBR and dNBR images. The corrected bands were processed to estimate the Normalized Burn Ratio (NBR) pre- and post-fire (Eq. 3.2).

$$NBR = \left(\rho nir - \rho swir\right) \Big/ \left(\rho nir + \rho swir\right) \tag{3.2}$$

where the ρnir represents the near-infrared (NIR) band and $\rho swir$ represents the shortwave infrared (SWIR) in respected satellite data (Sentinel-2).

After estimating the pre- and post-fire NBR, it is necessary to calculate their difference to obtain the dNBR (Difference Normalized Burn Ratio) value (Eq. 3.3). However, the dNBR image is classified into unburned to high severity based on their spectral reflectance value. After estimating the dNBR, we will mask the cloud and remove it to calculate the burn severity area.

$$\text{dNBR} = \left(Pre - NBR - \text{Post} - NBR\right) \tag{3.3}$$

The study also introduces the new burned area index from Sentinel-2 (BAIS2) for burnt area mapping (Eq. 3.4). This new method uses high-resolution S2 MSI characteristics and, combined with the band, is suitable for post-fire monitoring (Filipponi, 2018). The BAIS2 was estimated using the following equation

$$\text{BAIS2} = \left(1 - \sqrt{B06 * B07 * B8A \Big/ B04}\right) * \left(B12 - B8A \Big/ \sqrt{B12 + B8A} + 1\right) \tag{3.4}$$

where the B06 and B07 represent the red-edge-2 and red-edge-3 and 8A represents the NIRn2. Similarly, the B04 defines the red band, and B12 presents the SWIR 2 band in Sentinel-2 image.

The MODIS Leaf Area Index (LAI) product defines the one-sided green leaf area per unit ground area. Similarly, the NDVI product provides greenness and minimizes canopy-soil variation. MODIS vegetation indices (LAI, NDVI) were derived from daily bidirectional surface reflectance and atmospherically corrected and

removed pixels with no data. This vegetation index monitors vegetation damage and post-fire vegetation recovery from September to February.

3.5 Results and Discussion

3.5.1 Active Fire Detection on Mt. Kilimanjaro

The reserve forest reported fire on 11 October 2020 and monitored this fire activity using MODIS MCD64A1 product. Detecting the active fire in the mountain region is a key component for managing biomass loss (Szpakowski & Jensen, 2019). The MCD64A1 detects the most burnt area (approximately 90%) compared with other products throughout the year (Humber et al., 2019). The spatial plot (Figure 3.3a) shows the active fire region, where the Julian days range between 291 and 297. The total 7011.30 hectors burn area was obtained from the MCD64A1 product and masked this area to estimate the dNBR and vegetation indices.

The output of dNBR and BAIS2 was estimated from high-resolution Sentinel-2 imagery. The Sentinel-2 image showed better severity classification and burn area compared to MCD64A1 due to spatial differences. Therefore, high-resolution imagery gives good performance for burn area classification in a small region. The band 8 (NIR) of the Sentinel-2 image shows the high spectral reflectance before the fire event and down significantly after the event. Similarly, the lower spectral reflectance of the unburned area shown in band 12 (SWIR) increased after the fire (Fig. 3.2). Figure 3.3b describes the burn severity classes based on the indices using Sentinel-2 bands. The dNBR severity classes for Sentinel-2 were retrieved and classified based on the dNBR scale range (Table 3.2) with a reference image of MCD64A1. The figures show the large proportion of burn area is moderate to very high severity, and few pixel areas are unburned to low severity (Fig. 3.3b). Due to TOA's (Top of the Atmosphere) correction, the burn area's missing pixel value is present. The statistic of each severity class (Table 3.2) indicates that the 1890.211 ha unburned area only remains in the total area of 7011.30 ha.

The present BAIS2 (Burn Area Index Sentinel-2) is a novel method for post-fire monitoring and discriminating burn severity levels at a small scale (Filipponi, 2018). The vegetation red-edge spectral is the best radiance-based descriptors of chlorophyll in vegetation. The BAIS2 is calculated based on the B05 (red-edge 1), mainly associated with chlorophyll content. Similarly, B07 and B08 (red-edge 2 and 3) are closed to NIR, representing the leaf structure. The BAIS2 (Fig. 3.3c) results show the fire-affected area, where the highest value of 1.72 indicates the active fire on the studied region. The value nearby 1 demonstrates the high severity burn area as per the classification of dNBR (Fig. 3.3b). This spectral information also allows monitoring fire active regions in Mt. Kilimanjaro.

Monitoring the small fire using high-resolution Sentinel imagery, the SWIR is the most helpful band to obtain the fire changes region and lowest reflectance value

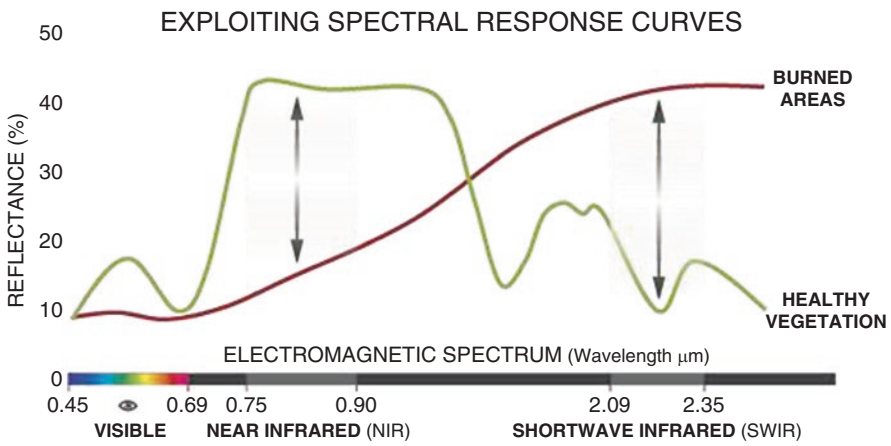

Fig. 3.2 Spectral reflectance curve for comparison of healthy vegetation and burned areas. (Source: US Forest service)

in healthy plants (Fig. 3.2). However, the red-edge spectral band shows burn severity classification and active fire monitoring (Fernández-Manso et al., 2016). To estimate burn area, severity classes using MODIS data could not classify the severity index. The resulting output from high-resolution Sentinel-2 imagery showed a reasonable separation and more detail of the burn area than MODIS 500 m product at a small region.

3.6 Post-fire Monitoring and Vegetation Loss at Mt. Kilimanjaro

The vegetation recovery after the fire must be investigated to determine the long-term impact on the forest ecosystem (Szpakowski & Jensen, 2019). Vegetation recovery after the fire event depends on the soil, temperature, precipitation, and vegetation structure. The LAI (Leaf Area Index) and NDVI (Normalized Difference Vegetation Index) responses were used to determine the temporal pattern of vegetation dynamics. However, vegetation recovery takes a long time, which differs from the burning season (Lacouture et al., 2020).

The LAI is an important ecological parameter and vegetation indices (VIs) for post-fire vegetation loss and recovery assessment. The spatial image of LAI (Fig. 3.4) describes the two conditions – before the fire event (20–30 September 2020) and after the fire (8–15 October 2020). It clearly showed on the map that the LAI was reduced significantly after the fire event. The results indicate that LAI's mean value declined from 0.83 (before the fire) to 0.34 (after the fire) in the burn area.

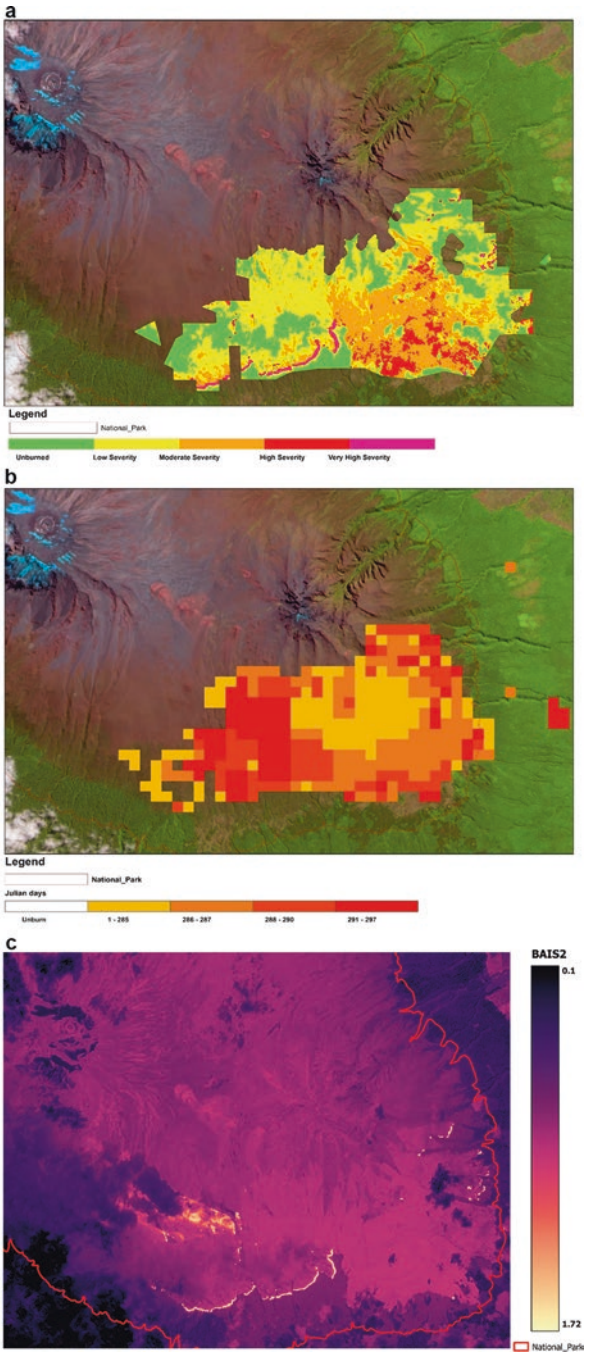

Fig. 3.3 Mt. Kilimanjaro Forest fire 11 October 2020. (**a**) MODIS burnt area and Julian days detected by MCD64A1 during 01 October 2020 to 31 October 2020 and true color composite Sentinel-2 image on 17 August 2017. (**b**) dNBR (difference normalized burn ratio) for burn severity classes during 08 October 2020 to 15 October 2020 and true color composite Sentinel-2 image on 17 August 2017. (**c**) Monitoring burn area after the post-fire event by BAIS2 (burn area index from Sentinel-2) on 15 October 2020

Table 3.2 dNBR classification and statistic estimated from the Sentinel-2 during 08 October 2020 to 15 October 2020

Segment classes [dNBR]	Area [ha]	dNBR spectral range
Unburn	1890.211	< 0.1
Low severity	2719.1	0.1–0.269
Moderate severity	1929.01	0.27–0.439
High severity	398.89	0.44–0.659
Very high severity	74.09	0.66–1.3

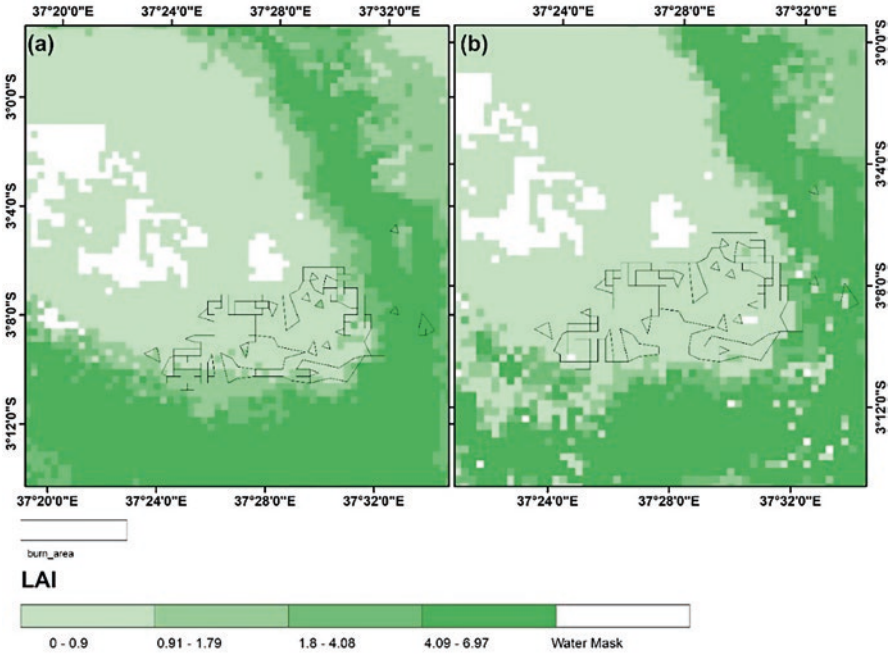

Fig. 3.4 Eight-day composite of LAI at Mt. Kilimanjaro. (**a**) Before fire (22–30 September 2020). (**b**) After fire event (8–15 October 2020) and burn area retrieved from MODIS (MCD64A1)

Vegetation present on the earth's surface is measured by various vegetation indices such as NDVI, LAI, Enhanced Vegetation Index (EVI), Global Environmental Monitoring Index (GEMI), etc. (Das et al., 2020). However, green vegetation has strong absorption of radiant energy in the red band and high reflectance in the NIR band (Fornacca et al., 2018). Therefore, NIR reflectance was used for detecting the damage of vegetation loss and regeneration of vegetation. Calculating the NDVI is more accessible compared with other vegetation indices such as GEMI, EVI, etc. There was a significant difference between NDVI spatial imagery on 7 October 2020 and 15 October 2020 (Fig. 3.5). Spatial variation of NDVI showed a large area of green vegetation was lost after the fire event concerning MODIS burn product.

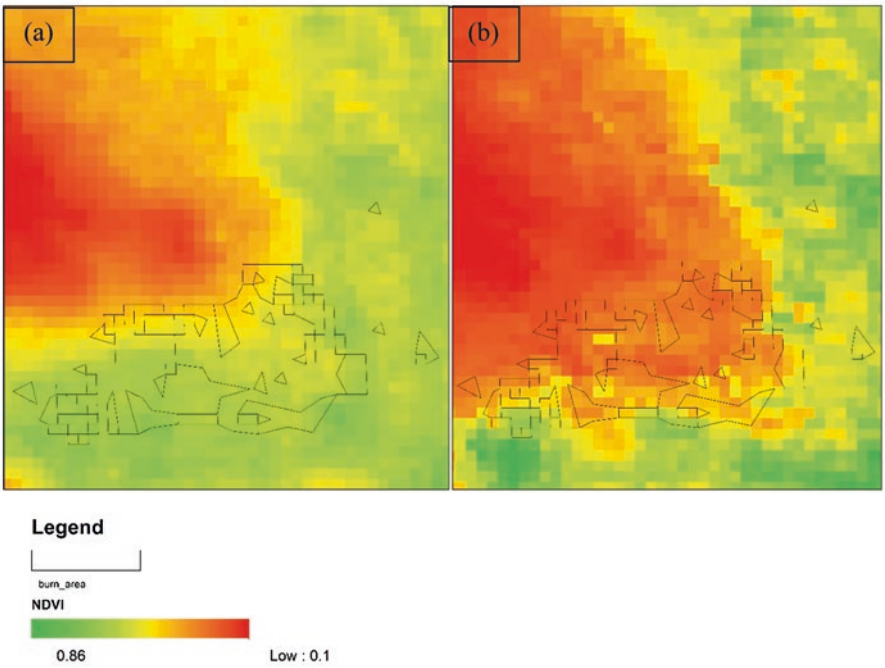

Fig. 3.5 Eight-day composite of NDVI at Mt. Kilimanjaro. (**a**) Before fire (22–30 September 2020). (**b**) After fire event (8–15 October 2020) and burn area retrieved from MODIS (MCD64A1)

The results demonstrate that the mean value of NDVI decreased from 0.28 (before the fire) to 0.22 (after the fire).

Although the growth of NDVI is significantly affected by temperature, this NDVI increased faster at a higher temperature and is delayed at a lower temperature (Lacouture et al., 2020). It is also noted that the NDVI cannot differentiate the different plant spices at moderate resolution. However, high-resolution satellite-derived NDVI can recognize the diverse plant diversity and loss of every species.

It is important to estimate the vegetation re-growth rates and how they vary with the burn area index (Franks et al., 2013). This study extracted the burn area's pixel value from BAIS2 and VIs using MODIS 500 m resolution. Figure 3.6 demonstrates the negative correlation between the burn area index (BAIS2) and vegetation indices (LAI and NDVI), retrieved from the MCD64A1 burn area patches. The correlation between the BAIS2 and VIs was relatively strong, with the value of R2 = 0.8 and R2 = 0.63.These results from the MCD64A1 burn area patches suggest that the intensity of vegetation indices declines with an increased burn area rate, which identifies the damage of forest and vegetation re-growth (Fig. 3.7a).

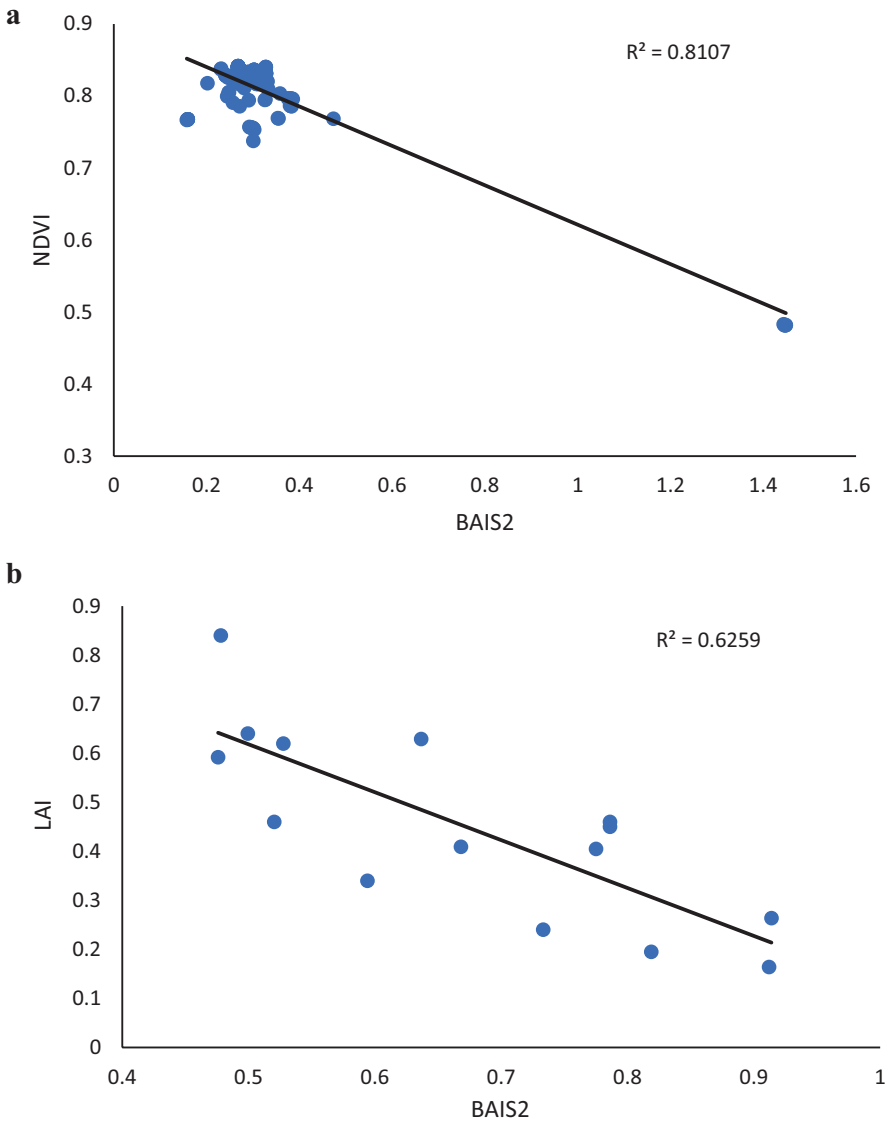

Fig. 3.6 Correlation between burn area index (BAIS2) and vegetation indices (VIs). (**a**) NDVI vs BAIS2. (**b**) LAI vs BAIS2 during 1 September 2020–10 February 2020

3.7 Vegetation Reconstruction

The methodology was adopted to monitor vegetation reconstructing for the studied area under the time series shown in Fig. 3.7. Implementing MODIS 8-day composite vegetation indices (LAI) showed gradual changes in the time series analysis

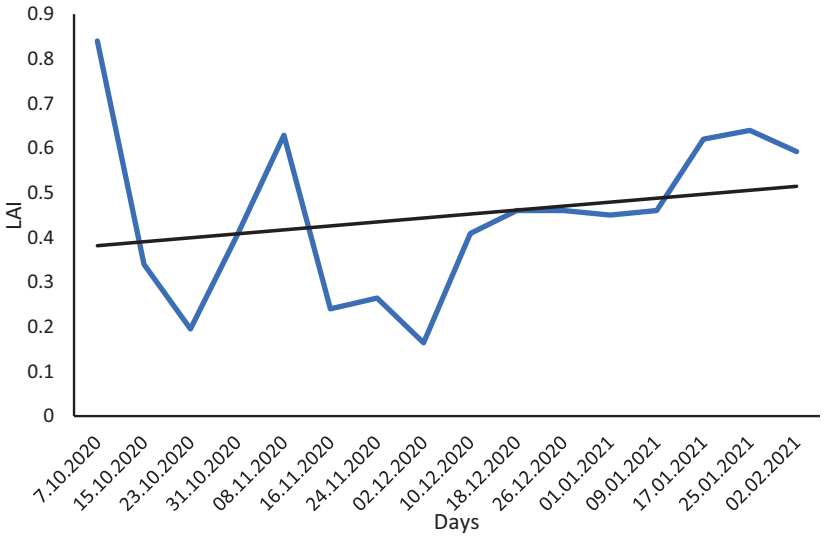

Fig. 3.7 Mt. Kilimanjaro Leaf Area Index LAI trend from 7 October 2020 to 2 February 2021

(Fig. 3.7). The temporal changes in vegetation recovery are detectable at all the MODIS VIs images. The sudden drop was reported in the LAI time series from 7 October to 2 December (due to the fire event). Although the results demonstrate the significant increasing linear trend in LAI values after the post-fire event, the resulting output indicates that the diverse vegetation loss and vegetation recovers after the fire event take a long time (at least 100 years) to grow. However, human activity can affect vegetation reconstruction of the burn area at the upper site.

Global climate change increased the temperature, which developed the dry climatic condition to dry vegetation more quickly and later the fire. Also, the wildland-urban interface (WUI) or urban exposer on this dry vegetation has great concern for wildfire activity (Turco et al., 2019). The fire intensity also depends on the regional weather condition, such as declining moisture rate, increased wind speed, or fuel load (Flannigan et al., 2006). Chen et al. (2014) developed a drought index to determine the number of dry days from the total precipitation, significantly impacting a forest fire. Similarly, Abatzoglou and Williams (2016) found the anthropogenic climate change effect on forest fire and estimated the human-made climate change contribution on 4.2 million ha of forest fire across the United States. In this similar contrast, the dry climatic condition and human activity on Mt. Kilimanjaro increased wildfire frequency. From the last century, climate change has affected Mt. Kilimanjaro with the changes in precipitation and higher temperature (Kilungu et al., 2019). Previous studies suggest that the precipitation on Mt. Kilimanjaro has declined by 600–1200 mm from the last 100 years (Hemp, 2009). Therefore, a declining rainfall pattern and increasing temperature create a drier climatic condition on this mountain region, impacting a forest fire. Hemp (2005) found that the fire intensity has increased under the drier climatic condition on the slope of

Kilimanjaro and changed the vegetation dynamics. However, the results indicate that the most fire event on Mt. Kilimanjaro results from human activity such as honey collectors and tourism.

3.8 Conclusion and Recommendation

This paper estimates the burn area trend and vegetation reconstruction using freely available satellite data in a small-scale region. The novel methodology (BAIS2) is based on a spectral index with active fire at Mt. Kilimanjaro, demonstrated in previous research (Filipponi, 2018). These high-resolution satellite imageries detected the burn area in a small region of the mountain ecosystem and found a real-time solution. Although, the Sentinel-2 imagery did not find the specific species in the diverse ecosystem. The thermal character was detected in the proposed algorithm, which takes place on the active fire. The estimation of burn severity from high-resolution imagery allows for the assessment of fire damage. The monitoring of vegetation degradation and re-growth using MODIS vegetation indices (NDVI, LAI) was also presented in this study. In addition, long time series for burn area detection will improve the understanding of spatial features in the reserve forest. However, including field data enhanced the wildfire information.

It is important to isolate and incorporate the deep river valley below the national park to protect the diverse ecosystem. Also, it is essential to connect the wildlife corridor between Amboseli, Kenya, and Mt. Kilimanjaro, which helps the migration of animals and controls wildfire (Hemp, 2009). This work suggests that prevention of fire activity is more reliable than fighting with fire.

Acknowledgments The authors express thanks to anonymous for their constructive comments and advice.

Conflicts of Interest The authors declare no conflicts of interest.

Funding This research was funded by "Integrated management for sustainable utilization of water resources in East Africa Great Lakes basin (No. 2018YFE0105900)" and the project commissioned by the National Key R&D program of China [No. 2018YFE0105900].

References

Abatzoglou, J. T., & Williams, A. P. (2016). Impact of anthropogenic climate change on wildfire across western US forests. *Proceedings of the National Academy of Sciences, 113*(42), 11770–11775. https://doi.org/10.1073/pnas.1607171113

Carlà, R., Santurri, L., Bonora, L., & Conese, C. (2009). Multitemporal burnt area detection methods based on a couple of images acquired after the fire event. In C. M. U. Neale & A. Maltese (Eds.). https://doi.org/10.1117/12.832908

Catarino, S., Romeiras, M. M., Figueira, R., Aubard, V., Silva, J. M. N., & Pereira, J. M. C. (2020). Spatial and temporal trends of burnt area in Angola: Implications for natural vegetation and protected area management. *Diversity, 12*(8), 307. https://doi.org/10.3390/d12080307

Chen, F., Niu, S., Tong, X., Zhao, J., Sun, Y., & He, T. (2014). The impact of precipitation regimes on Forest fires in Yunnan Province, Southwest China. *The Scientific World Journal, 2014*, 1–9. https://doi.org/10.1155/2014/326782

Das, P., Vamsi, K. S., & Zhenke, Z. (2020). Decadal variation of the Land Surface Temperatures (LST) and Urban Heat Island (UHI) over Kolkata City projected using MODIS and ERA-interim DataSets. *Aerosol Science and Engineering, 4*(3), 200–209. https://doi.org/10.1007/s41810-020-00067-1

Detsch, F., Otte, I., Appelhans, T., Hemp, A., & Nauss, T. (2016). Seasonal and long-term vegetation dynamics from 1-km GIMMS-based NDVI time series at Mt. Kilimanjaro, Tanzania. *Remote Sensing of Environment, 178*, 70–83. https://doi.org/10.1016/j.rse.2016.03.007

Fernández-Manso, A., Fernández-Manso, O., & Quintano, C. (2016). SENTINEL-2A red-edge spectral indices suitability for discriminating burn severity. *International Journal of Applied Earth Observation and Geoinformation, 50*, 170–175. https://doi.org/10.1016/j.jag.2016.03.005

Filipponi, F. (2018). BAIS2: Burned area index for Sentinel-2. *Proceedings, 2*(7), 364. https://doi.org/10.3390/ecrs-2-05177

Flannigan, M. D., Amiro, B. D., Logan, K. A., Stocks, B. J., & Wotton, B. M. (2006). Forest fires and climate change in the 21st century. *Mitigation and Adaptation Strategies for Global Change, 11*(4), 847–859. https://doi.org/10.1007/s11027-005-9020-7

Fornacca, D., Ren, G., & Xiao, W. (2018). Evaluating the best spectral indices for the detection of burn scars at several post-fire dates in a mountainous region of Northwest Yunnan, China. *Remote Sensing, 10*(8), 1196. https://doi.org/10.3390/rs10081196

Franks, S., Masek, J. G., & Turner, M. G. (2013). Monitoring forest re-growth following large scale fire using satellite data-A case study of Yellowstone National Park, USA. *European Journal of Remote Sensing, 46*(1), 551–569. https://doi.org/10.5721/EuJRS20134632

Giglio, L., Boschetti, L., Roy, D. P., Humber, M. L., & Justice, C. O. (2018). The Collection 6 MODIS burned area mapping algorithm and product. *Remote Sensing of Environment, 217*, 72–85. https://doi.org/10.1016/j.rse.2018.08.005

Giglio, L., Loboda, T., Roy, D. P., Quayle, B., & Justice, C. O. (2009). An active-fire based burned area mapping algorithm for the MODIS sensor. *Remote Sensing of Environment, 113*(2), 408–420. https://doi.org/10.1016/j.rse.2008.10.006

González-Alonso, F., & Merino-de-Miguel, S. (2009). Integration of AWiFS and MODIS active fire data for burn mapping at regional level using the Burned Area Synergic Algorithm (BASA). *International Journal of Wildland Fire, 18*(4), 404. https://doi.org/10.1071/WF07081

Govedarica, M., Álvarez-Taboada, F., & Kokeza, Z. (2020). Near real-time burned area mapping using Sentinel-2 data. 15.

Hemp, A. (2005). Climate change-driven forest fires marginalize the impact of ice cap wasting on Kilimanjaro. *Global Change Biology, 11*(7), 1013–1023. https://doi.org/10.1111/j.1365-2486.2005.00968.x

Hemp, A. (2006). The Banana Forests of Kilimanjaro: Biodiversity and conservation of the Chagga Homegardens. *Biodiversity and Conservation, 15*(4), 1193–1217. https://doi.org/10.1007/s10531-004-8230-8

Hemp, A. (2009). Climate change and its impact on the forests of Kilimanjaro. *African Journal of Ecology, 47*, 3–10. https://doi.org/10.1111/j.1365-2028.2008.01043.x

Hemp, A. (2020). Fires shaped Mount Kilimanjaro's unique environment, now they threaten it. Down to earth. https://www.downtoearth.org.in/blog/africa/

Hislop, S., Haywood, A., Jones, S., Soto-Berelov, M., Skidmore, A., & Nguyen, T. H. (2020). A satellite data driven approach to monitoring and reporting fire disturbance and recovery across boreal and temperate forests. *International Journal of Applied Earth Observation and Geoinformation, 87*, 102034. https://doi.org/10.1016/j.jag.2019.102034

Humber, M. L., Boschetti, L., Giglio, L., & Justice, C. O. (2019). Spatial and temporal intercomparison of four global burned area products. *International Journal of Digital Earth, 12*(4), 460–484. https://doi.org/10.1080/17538947.2018.1433727

Kilungu, H., Leemans, R., Munishi, P. K. T., Nicholls, S., & Amelung, B. (2019). Forty years of climate and land-cover change and its effects on tourism resources in Kilimanjaro National Park. *Tourism Planning & Development, 16*(2), 235–253. https://doi.org/10.1080/21568316.2019.1569121

Kurnaz, B., Bayik, C., & Abdikan, S. (2020). Forest fire area detection by using Landsat-8 and Sentinel-2 satellite images: A case study in Mugla, Turkey [Preprint]. In Review. https://doi.org/10.21203/rs.3.rs-26787/v1.

Lacouture, D. L., Broadbent, E. N., & Crandall, R. M. (2020). Detecting vegetation recovery after fire in a fire-frequented habitat using normalized difference vegetation index (NDVI). *Forests, 11*(7), 749. https://doi.org/10.3390/f11070749

Liu, T., Marlier, M. E., Karambelas, A., Jain, M., Singh, S., Singh, M. K., … DeFries, R. S. (2019). Missing emissions from post-monsoon agricultural fires in northwestern India: Regional limitations of MODIS burned area and active fire products. *Environmental Research Communications, 1*(1), 011007. https://doi.org/10.1088/2515-7620/ab056c

Liu, T., Mickley, L. J., Marlier, M. E., DeFries, R. S., Khan, M. F., Latif, M. T., & Karambelas, A. (2020). Diagnosing spatial biases and uncertainties in global fire emissions inventories: Indonesia as regional case study. *Remote Sensing of Environment, 237*, 111557. https://doi.org/10.1016/j.rse.2019.111557

Myneni, R., Knyazikhin, Y., & Park, T. (2015). MOD15A2H MODIS Leaf Area Index/FPAR 8-Day L4 Global 500m SIN Grid V006. NASA EOSDIS Land Processes DAAC. https://doi.org/10.5067/MODIS/MOD15A2H.006

Oliveira-Júnior, J. F. de, Teodoro, P. E., da Silva Junior, C. A., Baio, F. H. R., Gava, R., Capristo-Silva, G. F., … Costa, M. da S. (2020). Fire foci related to rainfall and biomes of the state of Mato Grosso do Sul, Brazil. Agricultural and Forest Meteorology, 282–283, 107861. doi: https://doi.org/10.1016/j.agrformet.2019.107861.

Poletti, C., Dioszegi, G., Nyongesa, K. W., Vacik, H., Barbujani, M., & Kigomo, J. N. (2019). Characterization of forest fires to support monitoring and management of Mount Kenya Forest. *Mountain Research and Development, 39*(3). https://doi.org/10.1659/MRD-JOURNAL-D-18-00104.1

Roteta, E., Bastarrika, A., Padilla, M., Storm, T., & Chuvieco, E. (2019). Development of a Sentinel-2 burned area algorithm: Generation of a small fire database for sub-Saharan Africa. *Remote Sensing of Environment, 222*, 1–17. https://doi.org/10.1016/j.rse.2018.12.011

Scholtz, R., Prentice, J., Tang, Y., & Twidwell, D. (2020). Improving on MODIS MCD64A1 burned area estimates in grassland systems: A case study in Kansas Flint Hills tall grass prairie. *Remote Sensing, 12*(13), 2168. https://doi.org/10.3390/rs12132168

Seydi, S. T., Akhoondzadeh, M., Amani, M., & Mahdavi, S. (2021). Wildfire damage assessment over Australia using Sentinel-2 imagery and MODIS land cover product within the Google earth engine cloud platform. *Remote Sensing, 13*(2), 220. https://doi.org/10.3390/rs13020220

Shan, T., Wang, C., Chen, F., Wu, Q., Li, B., Yu, B., … Wu, W. (2017). A burned area mapping algorithm for Chinese FengYun-3 MERSI satellite data. *Remote Sensing, 9*(7), 736. https://doi.org/10.3390/rs9070736

Szpakowski, D., & Jensen, J. (2019). A review of the applications of remote sensing in fire ecology. *Remote Sensing, 11*(22), 2638. https://doi.org/10.3390/rs11222638

Turco, M., Jerez, S., Augusto, S., Tarín-Carrasco, P., Ratola, N., Jiménez-Guerrero, P., & Trigo, R. M. (2019). Climate drivers of the 2017 devastating fires in Portugal. *Scientific Reports, 9*(1), 13886. https://doi.org/10.1038/s41598-019-50281-2

Veraverbeke, S., & Hook, S. J. (2013). Evaluating spectral indices and spectral mixture analysis for assessing fire severity, combustion completeness and carbon emissions. *International Journal of Wildland Fire, 22*(5), 707. https://doi.org/10.1071/WF12168

Wu, Z., He, H. S., Keane, R. E., Zhu, Z., Wang, Y., & Shan, Y. (2020). Current and future patterns of forest fire occurrence in China. *International Journal of Wildland Fire, 29*(2), 104. https://doi.org/10.1071/WF19039

Chapter 4
Ecological Vulnerability Assessment to Grassland Fires in a Protected Mountainous Area Using Remote Sensing and GIS

E. Adagbasa, Samuel Adelabu, and T. W. Okello

Abstract Natural disturbances such as wildfire can be a major and positive driver of ecosystem dynamics by changing forest structure and altering species composition. However, depending on the fire's magnitude and frequency of occurrence, it becomes negative to the ecosystem. This study, therefore, established a model to predict ecological vulnerability to fire in a protected mountainous ecosystem. The model assessed the ecosystem's vulnerability to fire with the response of soil and vegetation. The response of soil was generated using a modified RUSLE model, while the vegetation response was derived from a vegetation response ability model developed by a previous study. Validation was done using correlation analysis between the presence and abundance of two known species (S. *plumosum* and E. *curvula*) and the vulnerability class. The correlation results showed a strong positive relationship of $r = 0.68$ for S. *plumosum* and $r = 0.82$ for *E. curvula*. The model results showed that 12% of the study area has high ecological vulnerability to fire and 60% and 26% have medium and low ecological vulnerability, respectively. The results indicate that about 74% of the park has medium to high vulnerability, which suggests the need for park managers to use post-fire restoration strategies in these areas to prevent long-term soil erosion and the loss of particular vegetation species.

Keywords Remote sensing · GIS · Wildfires · Soil erosion · RUSLE

E. Adagbasa (✉)
Department of Geography, The University of the Free State, Phuthaditjhaba, South Africa
e-mail: Adagbasa.EG@ufs.ac.za

S. Adelabu
Department of Geography, The University of the Free State, Bloemfontein, South Africa
e-mail: AdelabuSA@ufs.ac.za

T. W. Okello
Department of Biological and Environmental Sciences, Walter Sisulu University, Mthatha Campus, South Africa
e-mail: tokello@wsu.ac.za

S. Adelabu et al. (eds.), *Remote Sensing of African Mountains*,
https://doi.org/10.1007/978-3-031-04855-5_4

4.1 Introduction

The state of the ecosystem is important for human survival and development (Qiu et al., 2007). However, the conditions of ecosystems around the world are gradually depleting due to natural and anthropogenic disturbances (Peters et al., 2013). Natural and anthropogenic disturbances can be regarded as drivers of ecosystem change. Natural disturbances such as wildfire can be a major and positive driver of ecosystem dynamics, changing forest structure and altering species composition (Duguy et al., 2012; Peters et al., 2013). Conversely, depending on the magnitude and frequency, wildfire can become a negative driver of ecosystem dynamics (Cohen et al., 2016; Thompson et al., 2015).

Globally, 200–500 Mha of savannahs, woodland, shrubland, grassland, and other vegetation burn annually from wildfires (Goldammer & Mutch, 2001). The occurrence, spread, and magnitude of wildfires are influenced by climate, vegetation structure, and land use (Lavorel & Steffen, 2004), which can cause sizable variations in the construction and functioning of ecosystems (Dale et al., 2001). Vegetation changes caused by fire might bring about ecological degradation, impact on the atmosphere, biogeochemical cycles, and various ecosystems services such as carbon sequestration, soil fertility, grazing value, biodiversity conservation, and tourism (Lavorel et al., 2007).

Fire limits sustainable economic development globally and in Southern Africa when little or no attention is paid to the challenges of fire management, which results in increasingly large losses (Dlamini, 2011). Most of South Africa has seasonal precipitation and a dry time of year, which can last for five or more months (Forsyth et al., 2010). The eastern part of the country receives enough precipitation for grasses to grow and fuel to support fire every year or two. It implies that wildfires are frequent and inevitable (Forsyth et al., 2010).

Ecological vulnerability can be defined as the failure of an ecosystem to endure the effects of stressors over time and space (Williams & Kapustka, 2000). Forsyth et al. (2010) classified wildfire risk in South Africa into 13 fire-ecology types using ecological information from various studies and MODIS images. The authors focused on economic, social, and environmental vulnerability to produce a risk map. The economic and social vulnerability used vegetation as an indicator, while the consequences of frequent wildfires were used as an indicator of environmental vulnerability. They concluded that 40% of the eastern part of the country, which is grassland and savannah, had the highest risk from wildfires. The authors recorded the effect of frequent fire on the environment but did not take the effect of fire on the interaction of abiotic and biotic factors in the ecosystem into consideration. A complete assessment of ecological vulnerability should take into consideration both the biotic and abiotic components and their interrelationships with the different organization levels (Ippolito et al., 2010). This type of assessment is impracticable, which reduces the assessments that have been conducted (Turner et al., 2003). The response and recovery time of two main ecosystem components have been used by serval studies (soil and vegetation) to model ecological vulnerability to fire (Chuvieco,

2012; Duguy et al., 2012; Rodrigues et al., 2014; Viedma et al., 1997). Viedma et al. (1997) estimated the ecosystem recovery rate on the Mediterranean coast of Spain using Landsat 5 TM satellite images. They observed that normalized differential vegetative index (NDVI) was suitable for mapping burnt areas, and they then used a nonlinear regression analysis between NDVI and the time elapsed since the fire to assess the recovery time. Chuvieco (2012), Duguy et al. (2012), and Rodrigues et al. (2014) focused on short-term and medium-term vulnerabilities to fire in the Mediterranean region of Spain. They attributed the short-term vulnerabilities to soil erosion and the medium-term to the recovery time of plant communities after wildfires. These studies estimated the time required to restore vegetation to pre-fire conditions using map algebra, remote sensing, and a geographical information system.

Analyzing different ecological processes requires various process-specific resilience assessments with several temporal scales (Lavorel, 1999). Soil erosion by water is likely to occur some months after being exposed to fire, while vegetation cover recovery is still poor (Pausas & Vallejo, 1999). The soil is exposed to direct raindrops due to the loss of vegetation, which leads to an increase in soil erosion. The increased soil erosion will cause a decrease in soil organic matter and soil-rich nutrients necessary for vegetation recovery, also affecting other related ecosystem services. Re-establishing pre-fire plant communities takes a few years, even decades, depending on pre-existing vegetation, fire regime, and environmental conditions (Baeza et al., 2002; Keeley, 2009). Therefore, it is important for an integrated fire management strategy that brings together these factors to predict the vulnerability of the ecosystem in the short term after the fire.

Recently, several methods linking remote sensing and GIS have assessed particular post-fire processes (e.g., erosion) on a small scale to support post-fire management (Adagbasa et al., 2020b; Bisson et al., 2008; Ruiz-Gallardo et al., 2004). The significance of remote sensing and GIS in post-fire vegetation recovery analysis using fire severity and environmental factors has also been explored in recent studies (Adagbasa et al., 2018a; Rodrigues et al., 2014; Viana-Soto et al., 2017). Arianoutsou et al. (2011) presented a GIS-based multi-criteria evaluation approach for a comprehensive ecological knowledge-based assessment of the post-fire recovery ability of *Pinus halepensis* forests. Adagbasa et al. (2020a) developed a vegetation response ability model from remote sensing data by integrating environmental factors (elevation, aspect, rainfall, land surface temperature, soil, and fire severity), vegetation adaptive strategies (flowering months, water requirements, resprouter/seeders), and ecological class (increaser or decreaser). This study, therefore, presents a model adapted from Chuvieco (2012) and Duguy et al. (2012) for assessing short-term ecological vulnerability to wildfires in grassland through the responses of soil and vegetation using remote sensing and GIS. The model will be helpful for resource management and nature conservation decision-making because it will illustrate the ecological vulnerabilities to fires and contribute to environmental management plans. It will assist park managers in monitoring remote mountainous regions with limited ground monitoring coverage. The model will also aid in the development of suitable mitigation strategies against grassland fires that endanger biodiversity.

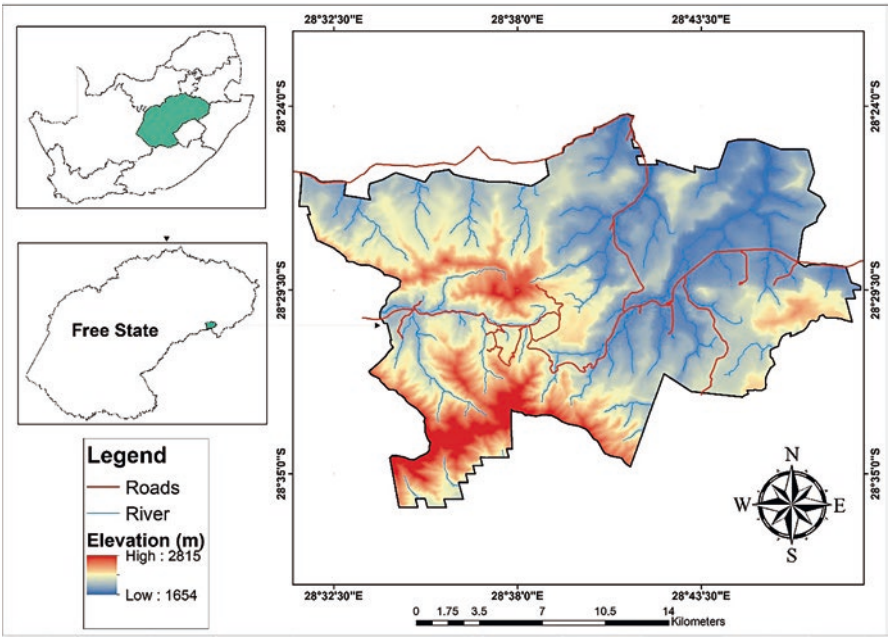

Fig. 4.1 Study area

4.2 Study Area

The study was conducted at the Golden Gate Highlands National Park (340 km^2), in the Eastern Free State, South Africa (Fig. 4.1). The park is in the Eastern Highveld region with dry seasons from June to August, showers, hail, thunderstorms from October and April, snow in winter, and an annual rainfall of 800 mm. The park is also home to several endemic and threatened plant and animal species, making it an important biodiversity hotspot. *Eragrostis* and *T. triandra* are two of the most common plants in the park (Adagbasa et al., 2019; Sanpark, 2012). The montane biome provides a wide range of ecosystem goods and services to people inside and outside the region and local communities (Sanpark, 2012). Nevertheless, the park is threatened by numerous problems, including veldt fires, invasive alien species (IAS), poaching, overgrazing, and overfishing of resources, especially medicinal plants.

4.3 Methodology

This study adapt and integrated the vegetation response ability model of Adagbasa et al. (2020a), erosion susceptibility model by Adagbasa et al. (2020b), and invasive vegetation species extracted from vegetation species discrimination map by

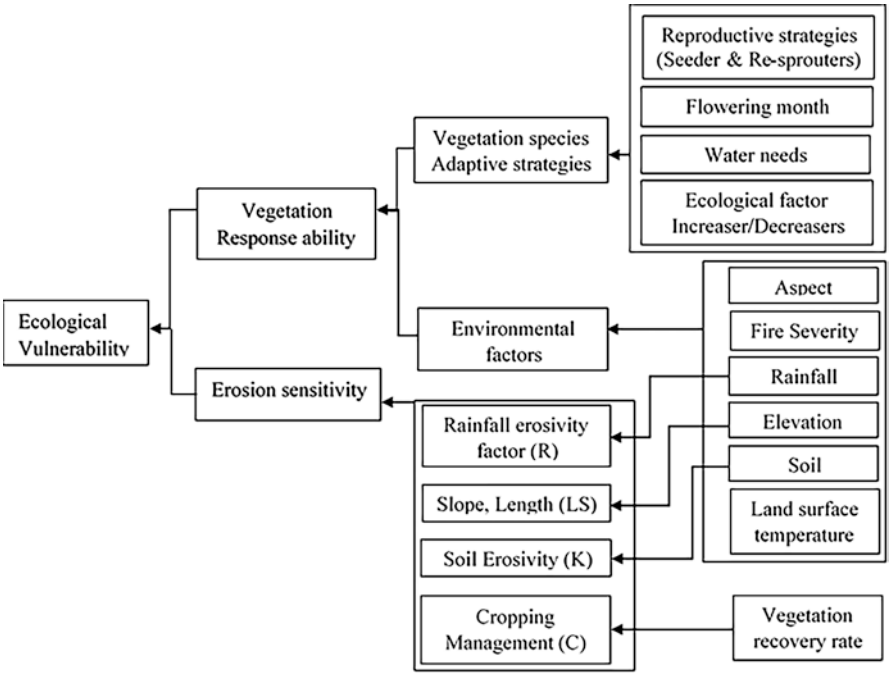

Fig. 4.2 Ecological vulnerability model

Adagbasa et al. (2019) to determine the ecological vulnerability using GIS and remote sensing as shown in Fig. 4.2.

4.3.1 Erosion Sensitivity

The Universal Soil Loss Equation (USLE) is by far the most widely used soil erosion modelling technique for any environment (Breetzke et al., 2013; Le Roux et al., 2008; Vetter, 2007). The model estimates soil loss using a set of variables, including soil erodibility, slope length, slope steepness, and cover management practice. The model was modified by Renard et al. (1997), referred to as the Revised Universal Soil Loss Equation (RUSLE), and has been used with GIS for modelling soil loss in different areas (Bizuwerk et al., 2003; Breetzke et al., 2013; Le Roux et al., 2008). The USLE also accounts for differences in vegetation types and land management practices in estimating the quantity of soil that could be lost from a unit area. The RUSLE model adapted by Adagbasa et al. (2020b) was used for this study. The model takes into account the same environmental factors of the RUSLE model, but with modifications to the crop management C-factor. The rainfall erosivity factor was based on the product of the total impact of the kinetic energy in MJ.mm/ha·h·yr. (E) of a raindrop and the (I_{30}) maximum 30-minute rainfall intensity in mm/h for a

given storm. The EI_{30} was obtained from a local rainfall station located 165 km away from the study area with a similar climate and topography. Thirty years average annual rainfall data were obtained from the 500 m resolution Climate Hazards Group Infrared Precipitation with Stations daily dataset available on the Google Earth Engine (GEE) platform.

The soil erodibility factor (K) was computed using soil samples collected at a depth of 5 cm from 100 plots using stratified random sampling (Adagbasa et al., 2020b). The soil samples were taken to a laboratory to determine soil particle sizes (Gee & Or, 2002) and organic matter content using the loss on the ignition process (Konen et al., 2002; Robertson, 2011; Schulte & Hopkins, 1996). The nomograph method (Wischmeier & Smith, 1978) was used to determine soil structure and permeability. The LS-factor was derived from a 30 m Shuttle Radar Topographic Mission (SRTM) using the stream power formula proposed by Moore & Burch (1986) and a later revised by Mitasova & Mitas (1999). Francis & Thornes (1990) stated that the minimum vegetation protective cover needed to protect soil from erosion is about 40% below which high erosion process occurs. Therefore, the C-factor was computed by first using the formula proposed by (Lin et al., 2004) to determine the vegetation recovery rate (VRR) after fire using the red edge NDVI derived from Sentinel-2 image. Secondly, the equation proposed by Lin et al. (2002) was used to calculate the linear reverse of the red edge NDVI to derive the C-factor. The erosion sensitivity was categorized into soil-loss classes with 0–5 as very low, 5–12 as low, 12–25 as moderate, 25–60 as high, 60–150 as very high, and greater than 150 as extremely high.

4.3.2 Vegetation Response Ability

Vegetation response ability to fire is important for recovery. It determines how fast a plant species can sprout and recruit (Paula & Pausas, 2008). The ability for vegetation to return to its pre-fire condition after a fire is regarded as post-fire vegetation recovery (Bartels et al., 2016; Chuvieco, 2012). The adapted model from Adagbasa et al. (2020a) integrated environmental factors (elevation, aspect, rainfall, land surface temperature (LST), and soil) and vegetation adaptive strategies (flowering months, water requirements, respouter/seeders, and ecological class (increaser or decreasers)) with five severity. The vegetation response ability was classified into low, medium, and high based on the adaptive vegetation strategy and favorable environmental factors for plant growth. An adaptive strategy like facultative seeders was classified as having high response ability, because they recovered faster to pre-fire conditions compared to obligated seeders (medium) or resprouters (low) (Chuvieco, 2012; Pausas & Keeley, 2014). Some grass species have adapted to flowering early and storing water underground to reduce the amount of water needed to regrow and recover, thus allowing them to flower earlier in spring than other plants (Wyk, 2003). Vegetation that flowered between August and April was classified as high, September

and May as medium, and March and May as low. Locations with low, medium, or high response ability were classified according to Adagbasa et al. (2020a).

4.3.3 Ecological Vulnerability

The ecological vulnerability was derived by integrating the vegetation response ability and erosion sensitivity. The resulting image was a 500 m resolution map, which classified ecological vulnerability into high (low response ability and high to extremely high soil loss), medium (medium response ability and medium to low soil loss), and low (high response ability and low to very low soil loss).

4.3.4 Validation

Ecological models are generally difficult to validate (Rykiel & Edward, 1996), with the NDVI technique the most used (Bisson et al., 2008; Dı'az-Delgado et al., 2002, 2003; Riaño et al., 2002; Viedma et al., 1997). Pe'rez-Cabello et al. (2002) recommended that by assessing the reconstruction process of various forest communities, observations should be carried out on the NDVI changes in burned plots over 3–5 years. Duguy et al. (2012) applied the same method to evaluate their model over 3 years. However, this method may not work in a grassland ecosystem. Grass species in South Africa have adapted to fire and require a few months to recover to pre-fire conditions (Forsyth et al., 2010), and the changes in mean NDVI may not show the true recovery. It is because recovery to pre-fire conditions in a grassland ecosystem depends on the vegetation species' response ability and the influence of other factors like the rate of soil erosion and the succession of invasive and increaser species (Adagbasa et al., 2020a). Increaser and invasive species tend to suppress other species and regenerate to pre-fire conditions within 6 months after the fire. The NDVI values from the pre-fire and post-fire conditions may show full recovery, but an increaser or invasive species may have replaced the original plant community. This study, therefore, used the spatial distribution of two known species, *Seriphium plumosum* and *Eragrostis curvula*, to evaluate the validity of the model. The study assumed that there would be a positive relationship between the spatial distribution of these species and the level of ecological vulnerability. Increasers and invasive vegetation species threaten native vegetation species and water resources, because they grow faster, consume more water, and spread more than the native species (Curhes et al., 2009; Rebelo et al., 1997). The encroachment of these vegetation species tends to alter ecosystems' balance, thereby making them more ecologically vulnerable to fire. Recent studies on grassland ecosystems have shown the impact of invasive plants such as *S. plumosum*, also known as "Slangbos" (Dubula et al., 2016; Mashalane & Adjorlolo, 2016; Snyman, 2009). The plant promotes fire, kills native grass species, and transforms grazing grasslands into degraded shrublands

(Mashalane & Adjorlolo, 2016; Snyman, 2009). *E. curvula* is termed an increaser II species, which increases profusely on overexploited soils (Mansour et al., 2012). It is the most dominant species within the study area, found around lower elevations (Adagbasa et al., 2019). *E. curvula* regenerates early and recovers to pre-fire conditions after the fire and can survive for long dry seasons. It grows quickly, spreads fast, and can easily suppress other species by preventing their regeneration. This species usually increase fire frequency and severity because of its very high fuel load (Curhes et al., 2009; Firn, 2009).

S. plumosum and *E. curvula* were extracted from the vegetation species map of the study area created by Adagbasa et al. (2019) using the structured query language (SQL) tool of ArcMap 10.5. Their study applied a multi-layer perceptron (MLP) deep neural network and stratified K-fold to discriminate grass species using post-fire Sentinel-2 MSI images from November 2017 to April 2018. All the bands of the Sentinel-2 images were resampled to 10 m resolution using the nearest neighbor resampling technique and linear mapping function. Fifty-three species were identified, and 12 were dominant and included *E. curvula* and *S. plumosum*. The abundance of both species was calculated by counting the number of 10 m pixels for each species located within 500 m resolution for each ecological vulnerability class. Spearman's correlation analysis was then used to determine the relationship between percentage species abundance and vulnerability categories. The strength of the relationship was gauged using Cohen's standards, where coefficients between 0.10 and 0.29 signified a small effect size, 0.30 and 0.49 signified a moderate effect size, and above 0.50 indicated a large effect size (Cohen, 1988).

4.4 Results and Discussion

The study area experienced an average yearly soil erosion of 13 t/ha·yr., with about 21% of the study area experiencing low to extremely high soil loss from water erosion (Adagbasa et al., 2020b). The vegetation recovery index used as the C-factor showed that 34% of the vegetation was fully recovered to pre-fire conditions 6 months after the last fire with medium to very low soil loss and that 48% of the vegetation had high response ability, 43% medium, and 9% low response ability (Adagbasa et al., 2020b).

Figure 4.3 shows the spatial distribution of *S. plumosum* with 5.3% coverage and *E. curvula* with 38% coverage, making up 43.3% of the study area. *S. plumosum* was mostly found in the northeastern and central parts of the study area, along the roads, northwestern boundary, and a few patches to the western part. It confirms the results of the predicted spatial distribution of the species done by Adepoju et al. (2019). These locations also experience high fire severity (Adagbasa et al., 2018b), low to medium vegetation response ability, and human activities. *S. plumosum* is not abundant in the west-central and southern part of the study area. These parts are predominantly mountain ridges with high elevations. *E. curvula*, which is the most dominant species, is found all over the study area, with the exception of high

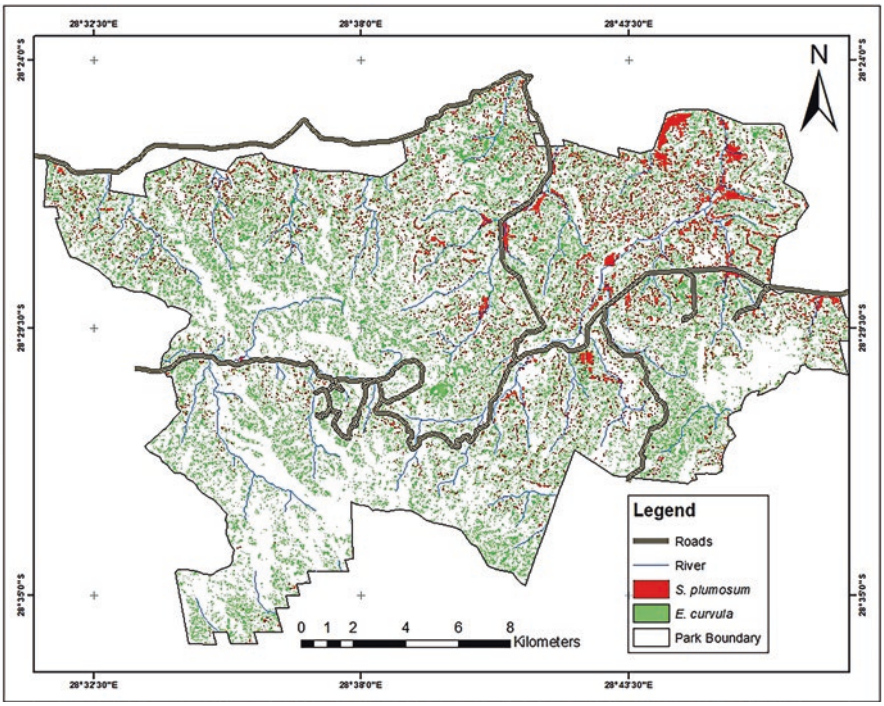

Fig. 4.3 Spatial distribution of S. *plumosum* and *E. curvula* extracted from vegetation species map (Adagbasa et al., 2019)

elevations where it is sparse. Recent studies have revealed that an ecosystem with increaser species like *E. curvula* being the most dominant compared to other species indicates a degrading environment (Wet, 2017).

The results of the ecological vulnerability show that 14% of the study area had a high vulnerability, 60% with medium vulnerability, and 26% with low vulnerability, as shown in Fig. 4.4 and Table 4.1. The northeastern part has 31% of the high ecological vulnerability, probably because that part experienced low to medium vegetation response ability and low to high soil loss. The vegetation recovery might be slow due to the effects of post-fire soil degradation resulting in soil nutrient losses (Duguy et al., 2012). The location also experienced less rainfall, high land surface temperature, and high fire frequency and severity (Adagbasa et al., 2020a). A quarter (25%) of high ecological vulnerability was distributed around the southern part of the study area. The southern part also experienced low vegetation response ability and high to very high soil loss. Although it experienced high rainfall, it also frequently experienced high fire severity. Fire severity directly relates to high soil losses, increasing land degradation, potentially impacting the vegetation regeneration process (De Luis et al., 2003; Scott et al., 2009).

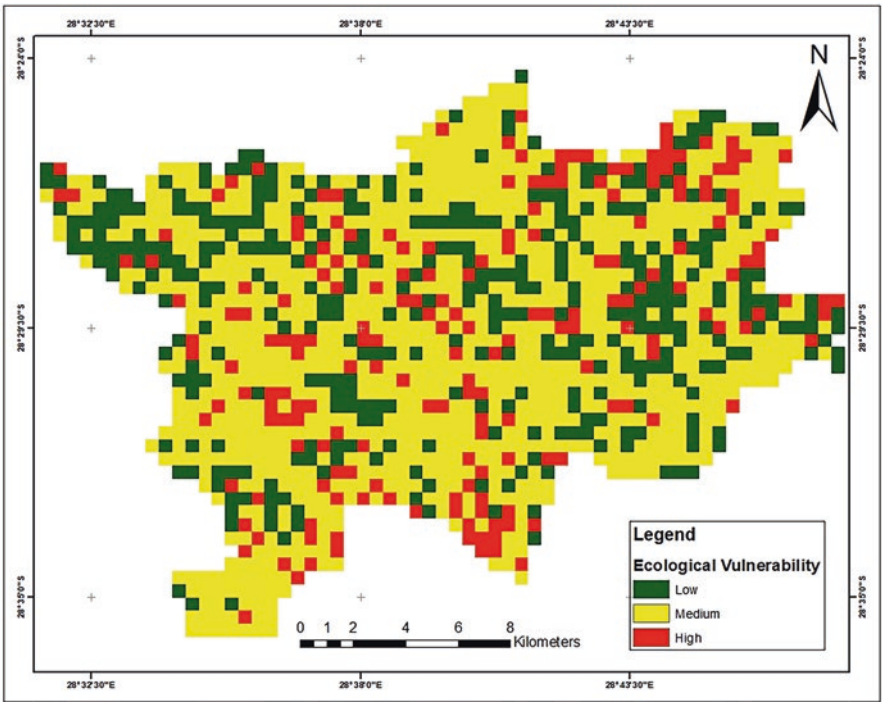

Fig. 4.4 Ecological vulnerability to fire

Table 4.1 Area coverage of ecological vulnerability in square kilometers

Category	Km^2
Low	80.14
Medium	186.53
High	44.00

4.5 Ecological Vulnerability Validation

The correlations were examined at an alpha value of 0.05. A significant positive correlation was observed between *S. plumosum* and ecological vulnerability ($r_s = 0.68$, $p < .001$). The correlation coefficient between *S. plumosum* and ecological vulnerability was 0.68, indicating a large effect size (the confidence intervals were computed using $\alpha = 0.05$; $n = 193{,}762$). This correlation indicated that as the abundance of *S. plumosum* increased, the ecological vulnerability from low to high tended to increase. Figure 4.5a presents the scatterplot of the correlation.

A significant positive correlation was also seen between *E. curvula* and ecological vulnerability ($r_s = 0.82$, $p < .001$). The correlation coefficient between *E. curvula* and ecological vulnerability was 0.82 (the confidence intervals were computed

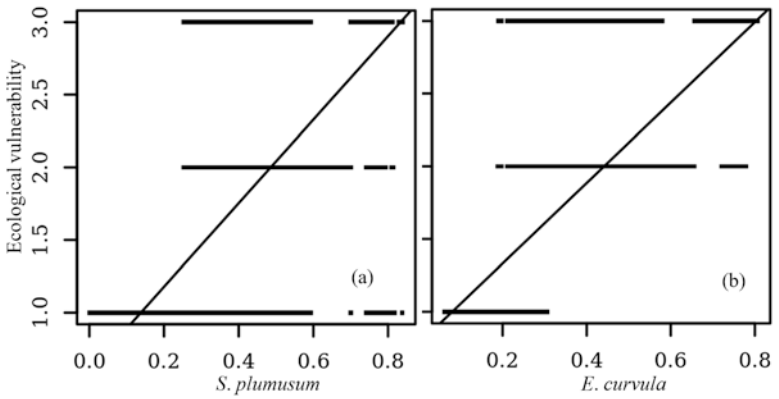

Fig. 4.5 (**a**) Correlation between *S. plumosum* and ecological vulnerability. (**b**) Correlation between *E. curvula* and ecological vulnerability. The value on the Y-axis presents the vulnerability categories. 1.0 represents low vulnerability, 2.0 medium, and 3.0 high vulnerability. The X-axis represents the species abundance

using $\alpha = 0.05$; $n = 781479$), indicating a great effect size. This correlation indicated that as *E. curvula* increased, the ecological vulnerability from low to high tended to increase (Fig. 4.5b).

It is clear from the correlation analysis that both species had a positive relationship with the vulnerability of the areas they were present in abundance. It confirms that both species thrive in overexploited and degrading lands (Mansour et al., 2012; Mashalane & Adjorlolo, 2016; Snyman, 2009).

4.6 Conclusion

This study developed a method to assess the ecological vulnerability of a protected mountainous ecosystem to wildfire. The response of soil and vegetation was used to evaluate the ecological vulnerability of the region to wildfire. A modified RUSLE model was utilized to create the soil response, whereas a vegetation response ability model designed by previous research was used to generate the vegetation response. This study showed that 12% of the study area had a high ecological vulnerability to fire, 60% medium, and 26% low ecological vulnerability. The ecological vulnerability of the study area showed the urgency for park managers to carry out post-fire restoration management practices on the areas with medium to high vulnerability, which comprised 74% of the park. The risk of lasting soil erosion and the loss of some vegetation species should be prevented. Finally, the research findings have also shown the extent of the park's ecological vulnerabilities to fires and can help with improving conservation environmental management plans. This study, therefore, recommends that park managers use the model to aid in creating biodiversity-friendly mitigation strategies for grassland fires that endanger the ecosystem.

Acknowledgments The authors acknowledge the National Research Foundation for funding under the Thuthuka funding tool (UID 106921), South African National Parks, and the Afromontane Research Unit (ARU).

References

Adagbasa, E. G., Adelabu, S., & Okello, T. (2018a). Assessment of short term inter-annual post fire vegetation recovery using Land Surface Temperature (LST). *South African Geographers, 1*, 605–631.

Adagbasa, E. G., Adelabu, S., & Okello, T. (2018b). Spatio-temporal assessment of fire severity in a protected and mountainous ecosystem. *IGARSS 2018 IEEE International Geoscience and Remote Sensing Symposium, 2018*, 6572–6575. https://doi.org/10.1109/IGARSS.2018.8518268

Adagbasa, E. G., Adelabu, S. A., & Okello, T. W. (2019). Application of deep learning with stratified K-fold for vegetation species discrimation in a protected mountainous region using Sentinel-2 image. *Geocarto International, 37*, 1–21. https://doi.org/10.1080/10106049.2019.1704070

Adagbasa, E. G., Adelabu, S. A., & Okello, T. W. (2020a). Development of post-fire vegetation response-ability model in grassland mountainous ecosystem using GIS and remote sensing. *ISPRS Journal of Photogrammetry and Remote Sensing, 164*, 173–183. https://doi.org/10.1016/j.isprsjprs.2020.04.006

Adagbasa, E. G., Adelabu, S. A., & Okello, T. W. (2020b, 26 Sept.-2 Oct. 2020). *Small Scale Soil Erosion Susceptibility Modelling in A Protected Mountainous Grassland Using Sentinel-2, Field, and Climate Data.* Paper presented at the IGARSS 2020 - 2020 IEEE International Geoscience and Remote Sensing Symposium.

Adepoju, K., Adelabu, S., & Mokubung, C. (2019). *Mapping Seriphium Plumosum encroachment in Mountainous Grassland using species distribution modelling.* Paper presented at the World Environmental Conservation Conference, Department of Ecotourism and Wildlife Management Federal University of Technology, Akure.

Arianoutsou, M., Koukoulas, S., & Kazanis, D. (2011). Evaluating post-fire forest resilience using GIS and multi-criteria analysis: An example from Cape Sounion National Park, Greece. *Environmental Management, 47*(3), 384–397.

Baeza, M. J., Luis, M. D., Raventos, J., & Escarre, A. (2002). Factors influencing fire behaviour in shrublands of different stand ages and the implications for using prescribed burning to reduce wildfire risk. *Journal of Environmental Management, 65*, 199–208.

Bartels, S. F., Chen, H. Y. H., Wulder, M. A., & White, J. C. (2016). Trends in post-disturbance recovery rates of Canada's forests following wildfire and harvest. *Forest Ecology and Management, 361*, 194–207. https://doi.org/10.1016/j.foreco.2015.11.015

Bisson, M., Fornaciai, A., Coli, A., Mazzarini, F., & Pareschi, M. T. (2008). The vegetation resilience after fire (VRAF) index: Development, implementation and an illustration from central Italy. *International Journal of Applied Earth Observation and Geoinformation, 10*(3), 312–329.

Bizuwerk, A., Taddese, G., & Getahun, Y. (2003). Application of GIS for modeling soil loss rate in Awash river basin, Ethiopia. In *International Livestock Research Institute (ILRI), Addis Ababa, Ethiopia* (pp. 1–11).

Breetzke, G., Koomen, E., & Critchley, W. (2013). GIS-assisted modelling of soil erosion in a South African catchment: Evaluating the USLE and SLEMSA approach. *Water Resources Planning, Development and Management*, 53.

Chuvieco, E. (2012). *Remote sensing of large wildfires: In the European Mediterranean Basin.* Springer Science & Business Media.

Cohen, J. (1988). *Statistical power analysis for the social sciences*.

Cohen, W., Yang, Z., Stehman, S., Schroeder, T., Bell, D., & Masek, J. (2016). Forest disturbance across the conterminous United States. The emerging dominance of forest decline. *Forest Ecology and Management, 360*, 242–352.

Curhes, S., Leigh, C., & Walton, C. (2009). *Weed risk assessment: African lovegrass Eragrostis curvula*.

Dale, V., Joyce, L., McNulty, S., Neilson, R., Ayres, M., Flannigan, M., … Wotton, B. (2001). Climate change and forest disturbances. *Bioscience, 51*, 723–734.

De Luis, M., González-Hidalgo, J., & Raventós, J. (2003). Effects of fire and torrential rainfall on erosion in a Mediterranean gorse community. *Land Degradation & Development, 14*(2), 203–213.

Dı'az-Delgado, R., Lloret, F., Pons, X., & Terradas, J. (2002). Satellite evidence of decreasing resilience in Mediterranean plant communities after recurrent wildfires. *Ecology, 83*(88), 2293–2303.

Díaz-Delgado, R., Lloret, F., & Pons, X. (2003). Influence of fire severity on plant regeneration by means of remote sensing imagery. *International Journal of Remote Sensing, 8*(null), 1751.

Dlamini, W. M. (2011). Application of Bayesian networks for fire risk mapping using GIS and remote sensing data. *GeoJournal, 76*(3), 283–296.

Dubula, B., Tefsamichael, S. G., & Rampedi, I. T. (2016). Assessing the potential of remote sensing to discriminate invasive Seriphium plumosum from grass. *South African Journal of Geomatics, 5*(2), 201–213.

Duguy, B., Alloza, J. A., Baeza, M. J., De la Riva, J., Echeverria, M., Ibarra, P., … Vallejo, R. V. (2012). Modelling the ecological vulnerability to forest fires in Mediterranean ecosystems using geographic information technologies. *Environmental Management, 50*(6), 1012–1026. https://doi.org/10.1007/s00267-012-9933-3

Firn, J. (2009). African lovegrass in Australia: a valuable pasture species or embarrassing invader? *TG: Tropical Grasslands, 43*(2), 86.

Forsyth, G., Kruger, F., & Le Maitre, D. (2010). National veldfire risk assessment: Analysis of exposure of social, economic and environmental assets to veldfire hazards in South Africa. *National Resources and the Environment CSIR, Fred Kruger Consulting cc*.

Francis, C., & Thornes, J. (1990). Runoff hydrographs from three Mediterranean vegetation cover types. In *Vegetation and erosion. Processes and environments* (pp. 363–384). Wiley.

Gee, G. W., & Or, D. (2002). 2.4 Particle-size analysis. *Methods of soil analysis part, 4*(598), 255–293.

Goldammer, J. G., & Mutch, R. (2001). *Global Forest Fire Assessment.* Retrieved from Rome.

Ippolito, A., Sala, S., Faber, J., & Vighi, M. (2010). Ecological vulnerability analysis: A river basin case study. *Science of the Total Environment, 408*(418), 3880–3890.

Keeley, J. E. (2009). Fire intensity, fire severity and burn severity: a brief review and suggested usage. *International Journal of Wildland Fire, 18*(1), 116–126.

Konen, M. E., Jacobs, P. M., Burras, C. L., Talaga, B. J., & Mason, J. A. (2002). Equations for predicting soil organic carbon using loss-on-ignition for north central US soils. *Soil Science Society of America Journal, 66*(6), 1878–1881.

Lavorel, S. (1999). Ecological diversity and resilience of Mediterranean vegetation to disturbance. *Diversity and Distributions.*, 3–13.

Lavorel, S., Flannigan, M. D., Lambin, E. F., & Scholes, M. C. (2007). Vulnerability of land systems to fire: Interactions among humans, climate, the atmosphere, and ecosystems. *Mitigation and Adaptation Strategies for Global Change, 12*(1), 33–53.

Lavorel, S., & Steffen, W. (2004). Cascading impacts of land use through time. In *Global change and the earth system: A planet under pressure* (pp. 186–188). Springer.

Le Roux, J., Morgenthal, T., Malherbe, J., Pretorius, D., & Sumner, P. (2008). Water erosion prediction at a national scale for South Africa. *Water SA, 34*(3), 305–314.

Lin, C.-Y., Lin, W.-T., & Chou, W.-C. (2002). Soil erosion prediction and sediment yield estimation: the Taiwan experience. *Soil and Tillage Research, 68*(2), 143–152.

Lin, C.-Y., Lo, H.-M., Chou, W.-C., & Lin, W.-T. (2004). Vegetation recovery assessment at the Jou-Jou Mountain landslide area caused by the 921 Earthquake in Central Taiwan. *Ecological Modelling, 176*(1-2), 75–81.

Mansour, K., Mutanga, O., Everson, T., & Adam, E. (2012). Discriminating indicator grass species for rangeland degradation assessment using hyperspectral data resampled to AISA Eagle resolution. *ISPRS Journal of Photogrammetry and Remote Sensing, 70*, 56–65.

Mashalane, M. J., & Adjorlolo, C. (2016). *Integrating remote sensing and geostatistics in mapping Seriphium plumosum (bankrupt bush) invasion.*

Mitasova, H., & Mitas, L. (1999). *Multiscale soil erosion simulations for land use management, in landscape erosion and evolution modeling*. Springer. (ISBN978-1-4613-5139-9).

Moore, I. D., & Burch, G. J. (1986). Physical basis of the length-slope factor in the universal soil loss equation 1. *Soil Science Society of America Journal, 50*(5), 1294–1298.

Paula, S., & Pausas, J. G. (2008). Burning seeds: germinative response to heat treatments in relation to resprouting ability. *Journal of Ecology, 96*(3), 543–552. https://doi.org/10.1111/j.1365-2745.2008.01359.x

Pausas, J. G., & Keeley, J. E. (2014). Evolutionary ecology of resprouting and seeding in fire-prone ecosystems. *New Phytologist, 204*(1), 55–65.

Pausas, J. G., & Vallejo, V. R. (1999). The role of fire in European Mediterranean ecosystems. In *Remote sensing of large wildfires* (pp. 3–16). Springer.

Pe'rez-Cabello, F., Echeverrı'a, M., Ibarra, P., & De la Riva, J. (2002). Estudio experimental de la dina'mica ambiental postincendio en. *Aportaciones a la Geomorfologı'a el incendio de Agu¨ero.*, 307–314.

Peters, E. B., Wythers, K., Bradford, J., & Reich, P. B. (2013). Influence of disturbance on temperate forest productivity. *Ecosystems, 16*, 95–110.

Qiu, P. H., Xu, S. J., Xie, G. Z., Tang, B. N., Bi, H., & Yu, L. U. (2007). Analysis of the ecological vulnerability of the western Hainan Island based on its landscape pattern and ecosystem sensitivity. *Acta Ecologica Sinica, 27*, 1257–1264.

Rebelo, A., Cowling, R., Richardson, D., & Pierce, S. (1997). *Vegetation of Southern Africa*. Cambridge University Press.

Renard, K. G., Foster, G. R., Weesies, G., McCool, D., & Yoder, D. (1997). *Predicting soil erosion by water: a guide to conservation planning with the Revised Universal Soil Loss Equation (RUSLE)* (Vol. 703). United States Department of Agriculture.

Riaño, D., Chuvieco, E., Ustin, S., Zomer, R., Dennison, P., Roberts, D., & Salas, J. (2002). Assessment of vegetation regeneration after fire through multitemporal analysis of AVIRIS images in the Santa Monica Mountains. *Remote Sensing of Environment, 79*(1), 60–71.

Robertson, S. (2011). Direct estimation of organic matter by loss on ignition: methods. *SFU Soil Science Lab, Burnaby 11p*.

Rodrigues, M., Ibarra, P., Echeverría, M., Pérez-Cabello, F., & de la Riva, J. (2014). A method for regional-scale assessment of vegetation recovery time after high-severity wildfires. *Progress in Physical Geography, 38*(5), 556–575. https://doi.org/10.1177/0309133314542956

Ruiz-Gallardo, J. R., Castaño, S., & Calera, A. (2004). Application of remote sensing and GIS to locate priority intervention areas after wildland fires in Mediterranean systems: a case study from south-eastern Spain. *International Journal of Wildland Fire, 13*(3), 241–252.

Rykiel, J., & Edward, J. (1996). Testing ecological models: the meaning of validation. *Ecological Modelling, 90*(3), 229–244.

Sanpark. (2012). *Golden Gate Highlands National Park Management Plan*.

Schulte, E., & Hopkins, B. (1996). Estimation of soil organic matter by weight loss-on-ignition. In *Soil organic matter: Analysis and interpretation* (soilorganicmatt) (pp. 21–31).

Scott, D. F., Curran, M. P., Robichaud, P. R., & Wagenbrenner, J. W. (2009). Soil erosion after forest fire. In *Fire effects on soils and restoration strategies* (pp. 193–212): CRC Press, Boca Raton, Florida, United States.

Snyman, H. (2009). Seriphium plumosum. *Newsletter of the Grassland Society of Southern Africa, 9*, 43.

Thompson, M., Gilbertson-Day, J., & Scott, J. (2015). Integrating pixel and polygon-based approaches to wildfire risk assessment: Application to a high-value watershed on the Pike and San Isabel National Forests, Colorado, USA. *Environmental Modeling and Assessment, 21*(21), 21–15.

Turner, B., Kasperson, R., Matson, P., McCarthy, J., Corell, R., & Christensen, L. (2003). A framework for vulnerability analysis in sustainability science. *Proceedings of the National Academy of Sciences of the United States of America, 100*(114), 8074–8079. https://doi.org/10.1073/pnas.1231335100

Vetter, S. (2007). Soil erosion in the Herschel district of South Africa: Changes over time, physical correlates and land users' perceptions. *African Journal of Range & Forage Science, 24*(2), 77–86. https://doi.org/10.2989/AJRFS.2007.24.2.4.158

Viana-Soto, A., Aguado, I., & Martínez, S. (2017). Assessment of post-fire vegetation recovery using fire severity and geographical data in the mediterranean region (Spain). *Environments, 4*(4), 90. https://doi.org/10.3390/environments4040090

Viedma, O., Meliá, J., Segarra, D., & García-Haro, J. (1997). Modeling rates of ecosystem recovery after fires by using Landsat TM data. *Remote Sensing of Environment, 61*(3), 383–398.

Wet, F. D. (2017). *Veld Condition Assessment and Management.* Retrieved from http://bezhoek.co.za/wp-content/uploads/Veld-Condition-Management-2015.pdf

Williams, L., & Kapustka, L. (2000). Ecosystem vulnerability: a complex interface with technical components. *Environmental Toxicology and Chemistry, 19*(14), 1055–1058.

Wischmeier, W. H., & Smith, D. D. (1978). Predicting rainfall erosion losses: a guide to conservation planning (No. 537). United States Department of Agriculture Science and Education Administration, Washington, D.C., United States of America.

Van Wyk, B. (2003). Southern African Grasslands: Aspects of their biodiversity, dynamics and management. In Timber Plantations: Impact, Future Visions and Global Trends conference. Nelspruit, South Africa.

Chapter 5
Natural Hazards Magnitude, Vulnerability, and Recovery Strategies in the Rwenzori Mountains, Southwestern Uganda

Bernard Barasa, Bob Nakileza, Frank Mugagga, Denis Nseka, Hosea Opedes, Paul Makoba Gudoyi, and Benard Ssentongo

Abstract Tropical mountain environments witness unprecedented occurrences of natural hazards that directly and indirectly threaten human lives and hard-earned properties. Existing literature reveals limited efforts underpinning the magnitude of natural hazards including the vulnerabilities and recovery efforts in the Rwenzori Mountain. This chapter aimed at examining the magnitude of natural hazards and prevailing vulnerability in Mt. Rwenzori. It also explored the possible recovery strategies that could be undertaken by local authorities and other stakeholders. The study adopted a multi-hazard approach. The main natural hazards considered in this chapter are drought, earthquake, floods, hailstorm, landslides, lightning, and windstorms. Different hazard severity methods were applied depending on the type of natural hazard analysed. Droughts were analysed using the Standard Precipitation Index. The earthquake hazard was computed using the Probabilistic Seismic Hazard Assessment (PSHA) technique. Landslide hazards were assessed using a Spatial Multi-Criteria Evaluation (SMCE) method to create a semi-quantitative landslide susceptibility index. Lightning hazard was assessed using the thunderstorm counts recorded at a local weather station. Windstorm studies relied on wind speed data for the period 2002–2018 obtained from a weather station. Similarly, records registered at this weather station were also used to estimate hailstorm incidences. Floods were mapped using the HEC-RAS model. Vulnerability was assessed qualitatively based on the elements exposed and the nature of hazard. The results revealed that the area experiences moderate to high intensity of earthquakes and landslides. Much of the area experiences low incidences of floods and droughts. However, high incidences

B. Barasa (✉) · P. Makoba Gudoyi
Kyambogo University, Department of Geography, Kyambogo – Kampala, Uganda

B. Nakileza · F. Mugagga · D. Nseka · H. Opedes
Makerere University, Department of Geography, Geoinformatics and Climatic Sciences, Kampala, Uganda

B. Ssentongo
Makerere University, Department of Environmental Management, Kampala, Uganda

S. Adelabu et al. (eds.), *Remote Sensing of African Mountains*,
https://doi.org/10.1007/978-3-031-04855-5_5

of flash floods have been witnessed in Kasese and Ntoroko districts. Hailstorms and windstorms are moderately intensive. The elements most affected by various natural hazards include people, buildings, schools, roads, and croplands. Continued occurrence of natural hazards will wreck more havoc and retard efforts towards achieving sustainable development in such a fragile mountain ecosystem. This result should trigger continuous debates on resettlement, disaster policy reforms, land use planning, early warning systems and budgetary allocations. Therefore, any recovery strategies under such complex multi-hazard scenario should involve balanced short- to long-term recovery planning.

Keywords Drought · Earthquake · Flood · Hailstorm · Landslide · Lightning · Mt. Rwenzori

5.1 Introduction

Natural hazards constitute to the representation of an ever-present intrinsic force with threats to society. Although hazards and disasters have been used interchangeably, they are different. According to Montz et al. (2017), a natural hazard characterizes the likelihood of an event (not the actual event itself) arising from natural processes and/or interaction of mankind and extreme natural events. For instance, by establishing settlements, infrastructure, and/or farmland on floodplains, human beings expose themselves to natural hazards. Upon occurrence is when these events become disasters (Twigg, 2015). A disaster is an event that overwhelms the community's ability and capacity to cope, requiring external assistance (Montz et al., 2017; Twigg, 2015). The extent of the impact of a disaster caused is determined by the level of vulnerability of communities.

Disasters manifest in different forms depending on the associated natural hazard events. Globally, these have been categorized as geophysical, climatological, meteorological, hydrological, and biological hazards. Disasters like landslides, drought, cyclones, floods, and disease epidemics respectively have been experienced across different timescales and space the world over. Over 83% of all natural disasters are triggered by extreme weather- and climate-related events, specifically, floods, storms, and heatwaves (IFRC, 2020). Though not the focus of this study, it is worth noting that man-made hazards such as conflicts arising from wars result in disasters like famine and human displacement (IFRC, 2019; Montz et al., 2017; Wisner et al., 2014). Mountains including Rwenzori have not been spared from such man-made disasters.

The magnitude and intensity of losses accruing from natural hazards is alarming. More than 1.7 billion people around the world have been affected by climate-related disasters with more than 410,000 fatalities over the past 10 years (IFRC, 2020). Most of the fatalities have majorly been experienced in developing countries where

the level of disaster preparedness is very limited (Dilley et al., 2005; Guha-Sapir et al., 2004). The magnitude of disasters in Sub-Saharan Africa isn't comparable to the huge losses experienced by the rest of the continent and Europe (Dilley et al., 2005; Montz et al., 2017; Wisner et al., 2014). Nonetheless, Nigeria, Burkina Faso, Ethiopia, Kenya and Uganda have been reported to have a relatively high mortality risk from multiple hazards based on total area and percentage population in areas at risk (Dilley et al., 2005).

Like the rest of the East African mountainous environments, the frequency and rate of natural disaster occurrence in Uganda is on the rise with impacts weighing heavily on the livelihoods and economy (Bagonza, 2014; Scuderi et al., 2019). In Uganda, the long-term damage to buildings arising from landslides is highest in eastern and western mountainous areas which exceeds $850,000 annually and flooding that affects at least 45,000 people (World Bank, 2019). Mount Rwenzori situated in western Uganda is among the most affected regions in the country by natural disasters (Mertens et al., 2018). The major disasters recorded on the slopes of Mount Rwenzori included landslides, storms, floods, and drought in the districts of Bundibugyo, Kasese, and Kabarole (Katutu et al., 2019; Mertens et al., 2018). Several households were noted to be more vulnerable and lost a lot of property in terms of housing structures and farm plantations among other livelihoods.

Vulnerability refers to the unfavourable conditions, including physical, social, economic, and environmental factors that increase the susceptibility of elements at risk to the impact of hazards (UNISDR, 2015a, 2015b). Vulnerability is related to predisposition, susceptibilities, fragilities, weaknesses, deficiencies or lack of capacities that favour adverse effects on the exposed elements. Vulnerability assessment is the systematic examination of elements at risk that are susceptible to damage from the effects of natural hazards.

Several recovery strategies in response to natural hazards have been initiated by the local governments and other stakeholders. For instance, recovery strategies against landslides have been explored although with varying level of success. Efforts have been made in enhancing deeper infiltration of rain water through planting trees and reforestation on depleted slope zones of Mount Rwenzori and relocation of population from floodplains and other disaster-prone areas (Katutu et al., 2019). Existing literature reveals limited efforts underpinning the nexus of magnitude of natural hazards, the vulnerabilities, and recovery efforts in the Rwenzori Mountain. This chapter, therefore, aimed at examining the magnitude of natural hazards and prevailing vulnerability in Mt. Rwenzori region. It also explored the possible recovery strategies that could be undertaken by local and other authorities. The study adopted a multi-hazard approach in analysing the vulnerabilities of elements exposed to the hazards. The main hazards considered in this chapter were drought, earthquakes, floods, hailstorms, landslides, lightning, and windstorms. The objectives of this chapter were (i) to examine the magnitude and vulnerability of natural hazards experienced in Mt. Rwenzori and (ii) to ascertain the appropriate disaster recovery strategies to natural hazards in the Rwenzori Mountains.

5.2 Materials and Methods

5.2.1 Description of Study Area

The study was conducted in the Mountain Rwenzori region at the border between Uganda and the Democratic Republic of Congo (Fig. 5.1). The study area is situated between latitudes 0.3858° N and longitudes 29.8717° E. Mount Rwenzori traverses five districts, i.e. Bundibugyo, Bunyangabu, Kabarole, Kasese, and Ntoroko. The

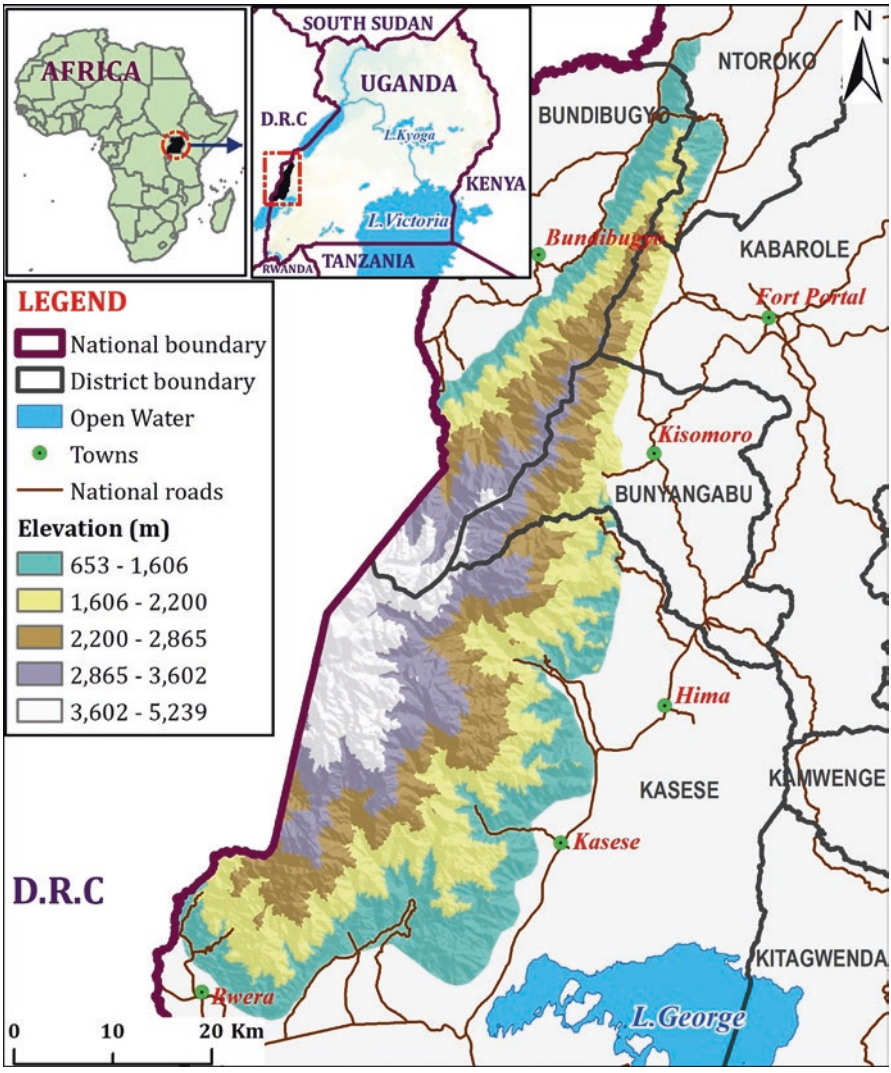

Fig. 5.1 Location of Mountain Rwenzori in Uganda

topography of the mountain ranges between 653 m and 5239 m above sea level (Fig. 5.1). The major rivers that drain the mountain include Nyamwamba, Nyamagasani, Kanyampara, Mubuku, Ruimi, Kahera, Rukoki, and Lamia. The vegetation of the mountain is characterized by afro alpine moorland, Afromontane rain forest, combretum wooded grasslands, edaphic wooded grasslands, evergreen bushlands and thickets, montane ericaceous, Afromontane bamboo, and *Hagenia abyssinica* forest. The mountain has unique alpine flora that includes many species endemic to the Albertine rift in the higher altitude zones, and these include giant heathers, groundsels, and lobelias.

The mountain experiences an alpine climate with high rainfall patterns ranging between 1000 mm and 2800 mm. The Ugandan part of Mt. Rwenzori can receive heavy rains any time of the year, but the rainiest periods are from Mid-March to May and from September to mid-December (Van Damme & Eggermont, 2011). Temperature and precipitation changes with altitude. For example, at the base of the mountain (1250 m.a.s.l), mean annual temperature and precipitation are about 24 °C and 1150 mm, respectively; at 3300 m.a.s.l, mean annual temperature and precipitation are about 12.5 °C and 2600 mm, respectively; at 4000 m.a.s.l, temperature and precipitation drop to about 7 °C and 2000 mm, respectively; above 4300 m.a.s.l, precipitation is mainly received as snow and temperature drops further to about 4 °C and can reach 0 °C at 4600 m.a.s.l (Osmaston, 1989; Roller et al., 2012). The ecosystem is inhabited by about 1,665,900 people (Bundibugyo 263,800; Bunyangabu 195,100; Kabarole 337,800; Kasese 793,200 and Ntoroko 76,000) as per UBOS (2020).

5.2.2 Natural Hazards in Mountain Rwenzori

The main natural hazards considered for investigation were drought, earthquakes, floods, hailstorms, landslides, lightning, and windstorms. The data sources and methods for analysing each hazard are described below.

Drought Hazard Drought occurs when there is an extended period of an abnormal deficiency in precipitation relative to what is considered normal (Eslamian et al., 2017). Meteorological drought is the mostly experienced. Compounding factors such as poverty and inappropriate land uses increase the vulnerability of people to drought. In this study, drought was assessed using the Standard Precipitation Index (SPI). Precipitation data (1995–2018), used in the computation of SPI, was acquired from the Kasese weather station. This period was selected due to consistent data availability. The drought classification system developed by McKee et al. (1993) was used to define drought intensities resulting from the SPI (Table 5.1).

Earthquake An earthquake is a result of a sudden release of energy in the Earth's crust that creates seismic waves. At the Earth's surface, earthquakes manifest themselves by shaking and sometimes displacement of the ground. Earthquakes can also

Table 5.1 Standard Precipitation Index and Drought Intensity Scale

SPI Index	Drought Intensity Scale
2.0+	Extremely wet
1.5–1.99	Very wet
1.0–1.49	Moderately wet
−99 to 0.99	Near normal
−1.0 to −1.49	Moderately dry
−1.5 to −1.99	Severely dry
−2 and less	Extremely dry

Source: Adopted from McKee et al. (1993)

trigger landslides and occasionally volcanic activity. The earthquake hazard was computed using the Probabilistic Seismic Hazard Assessment (PSHA) technique (Ordaz et al., 2013). The PSHA uses the Poisson distribution model and has been recognized as the most appropriate seismicity modelling tool in the context of insufficient data records in the region. This method involved building a catalogue from seismic data with a unified magnitude that provides information on the location and frequency of earthquake occurrence during the past 10 years and delineating seismic source zones based on geological and seismological evidence (faults). The Modified Mercalli Intensity (MMI) was then used to standardize the earthquake hazard for Mt. Rwenzori.

Flood Hazard A flood is a temporary overflow of a normally dry area due to surface water run-off, abnormal erosion, and unusual built-up, among others. Mt. Rwenzori sometimes experiences floods that are riverine in nature. The rivers that experience high inundation levels include Nyamwamba and Mubuku. The flood inundation extents in Mt. Rwenzori were delineated using the HEC-GeoRAS tool using rainfall (2020), land use (2020), Digital Elevation Model (DEM) of 30 m spatial resolution, and stream geometry datasets. Efforts were made to make sure recent datasets were utilized. Rainfall data was obtained from the Uganda National Meteorological Authority, land use was created from downloaded Landsat 8 (20 m) imagery filtered and subjected to supervised classification algorithm, while the SRTM DEM was downloaded, filled, and used. The flood extents were then categorized into flood hazard intensities based on water depth, i.e. very high (>2 m), high (1.5 m–2 m), moderate (1 m–1.5 m), and low (0.5 m–1 m). The results were validated by stakeholders in four regions of Uganda in well-organized workshops.

Hailstorm Hazard Hail is a form of solid precipitation that occurs when rising air in a thunderstorm lifts water droplet high into the atmosphere where temperatures are below freezing. This causes the water droplets to turn into hailstones before falling down to earth. Data for the number of hail days between 2000 and 2018 was obtained from the Kasese weather station due to availability and appropriate consistency. The incidences were collated with data from the DesInventar database

(https://www.desinventar.net/). The data was cleaned and processed using ordinary kriging interpolation technique to produce the spatial hailstorm hazard map of Mt. Rwenzori. The hailstorm hazard was categorized into intensities basing on the number of hail days in a year.

Landslide Hazard Landslides are the sudden movement of soil material down a slope under the influence of gravity. Some of the triggering factors of landslides include rainfall, earthquakes, stream erosion, changes in groundwater, volcanic activity, and increased human activities, among others. In this study, landslides were assessed using a Spatial Multi-Criteria Evaluation (SMCE) method to create a semi-quantitative landslide susceptibility index. The datasets/factors considered in the analysis included ASTER DEM (30 m), rainfall, land use/cover, lithology, and Peak Ground Acceleration (PGA). The factors were assigned a range of scores and weights to assess their influence in the occurrence of landslides. The landslide susceptibility index was used to standardize the landslide hazard of Mt. Rwenzori.

Lightning Hazard Uganda has one of the highest rates of lightning strike deaths in the world (Mary & Gomes, 2012). The frequencies and severities of lightning incidences have increased, resulting in significant loss of life and property. Uganda is not equipped with lightning flash counter network or a lightning detection system, and thus the thunder-heard day is the most appropriate parameter that can be used in lightning-related studies. Thunder day is when thunder is heard at a given location. Data on thunder days was obtained from the Kasese weather station for the period 2007 to 2018 due to availability and consistency. This data was supplemented with the Overshooting Tops (OT) data from the NASA Spin-Enhanced Visible Infrared Imager (SEVIRI). The interpolation technique was used to determine the OT counts and flash density in Mt. Rwenzori. The lightning hazard for Mt. Rwenzori was categorized basing on flashes per square kilometre per year.

Windstorm Hazard A windstorm is a storm with very strong wind but little or no rain. Winds can be classified based on their strength and direction. To map the windstorm hazard in Mt. Rwenzori, wind speed data for the period 2002–2018 was obtained from the Kasese weather station due to data availability, and this was interpolated to assess the spatial distribution. The Beaufort wind scale was used to classify the windstorm hazard basing on the wind speed and the respective impact and severity.

5.2.3 Elements at Risk in Mountain Rwenzori

The elements at risk in the Mt. Rwenzori that were considered for analysis included buildings, health centres, schools, police posts, road network, water sources, and croplands. These were selected due to data availability in the ecosystem. These are provided in Table 5.2 below and their sources.

Table 5.2 Sources of data considered in the analysis

Elements	Data types	Data source
Buildings	Polygon	OpenStreetMap (2020)
Croplands	Polygon	National Forestry Authority (2020)
Police posts	Point	Uganda Police Force (2020)
Health centres	Point	Ministry of Health (2020)
Road network	Line	Uganda National Roads Authority (2020)
Schools	Point	Ministry of Education and Sports (2020)
Water sources	Point	Ministry of Water and Environment (2020)

Table 5.3 Elements at risk in Mountain Rwenzori ecosystem by districts

	Elements at Risk									
	Buildings		Croplands		Road network		Schools		Water sources	
Districts	No	%	Area (Km^2)	%	Length (km)	%	No	%	No	%
Bundibugyo	14,182	13.6	0.7	2.3	129.0	6.0	24	8.5	94	7.6
Bunyangabu	3530	3.4	2.4	7.6	25.1	1.2	9	3.2	38	3.1
Kabarole	3212	3.1	2.2	6.9	28.2	1.3	6	2.1	26	2.1
Kasese	81,402	78.0	24.5	78.7	1915.6	89.7	243	85.6	1052	84.7
Ntoroko	2075	2.0	1.4	4.4	36.6	1.7	2	0.7	32	2.6
Total	104,401	100	31.2	100	2134.5	100	284	100	1242	100

As per the elements at risk, a total of 104,401 buildings are situated on the slopes and foots of Mt. Rwenzori with the biggest portion of them in Kasese district (78%) and the least percentage (2%) in Ntoroko district (Table 5.3). There are about 138,154 croplands covering an area of 31.2 km^2 on the slopes of Mt. Rwenzori. Still, the biggest percentage portion of croplands, 78.7%, is located in Kasese district, and the least portion, 2.3%, is in Bundibugyo district. A total of 32 health centres found in the Mt. Rwenzori region are situated in Kasese (30) and Bundibugyo (2) districts. There are eight police posts on the foot slopes of Mt. Rwenzori in Kasese (seven) and Bundibugyo (one) districts (Fig. 5.2). There is about 2134.4 km of road network that traverses the foot slopes of Mt. Rwenzori. Most of the road network (89.7%) on Mt. Rwenzori is found in Kasese district. There is also a total of 284 schools on the foot slopes mostly (243) situated in Kasese district. A total of 1242 water sources were established on the foot slopes of Mt. Rwenzori with most of them, 84.7%, located in Kasese district. The types of water sources that exist in Mt. Rwenzori include deep boreholes, kiosks, protected springs, public stand posts, rainwater harvesting tanks, shallow wells, and yard taps for public use. Of these, protected springs are the most common (56.9%).

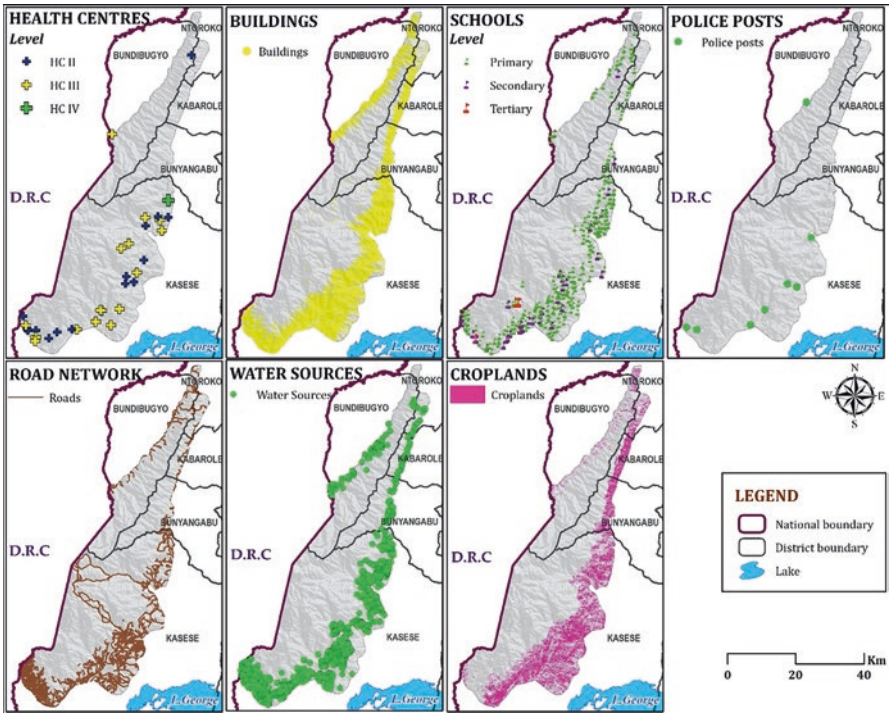

Fig. 5.2 Natural hazards experienced in Mountain Rwenzori

5.2.4 Disaster Recovery Assessment

Purposive key informant interviews were conducted at the regional and district levels. These were selected because of their expertise and experience in post-disaster recovery assessment and management. As a first step, these were contacted, and meeting schedules were set for either face to face or virtual. In either case, a key informant guide was used to guide the interviewing process that lasted between 1 and 2 hours. These were asked questions regarding the impacts of disasters, recovery interventions implemented in the short and long terms, and lessons learned among others. The interviewed stakeholders were from government ministries, departments, and agencies such as the Ministry of Works and Transport, Ministry of Health, and NGOs such as Red Cross and World Vision, among others.

The selection of disaster recovery interventions implemented in the short-, medium-, and long-term periods was based on the following criteria:

1. Potential to cause humanitarian impact
2. Potential to improve sustainable livelihoods
3. Incorporation of marginal group (pro-poor, vulnerable, and gender) agendas
4. Restoration and rebuilding of critical infrastructure and services
5. Inclusiveness of public and private sector recovery needs

5.3 Results

5.3.1 Spatial Exposure Profile of Hazards in Mt. Rwenzori

Mountain Rwenzori region is exposed to very low (1298.6 km^2), low (536.6 km^2), and moderate (70.5 km^2) drought hazard (Fig. 5.3). The biggest part of the mountain, 68.1%, is exposed to very low drought hazard; however, there is a portion in Kasese and Ntoroko districts that is exposed to moderate drought hazard (3.7%). The earthquake hazard coverage is characterized with Modified Mercalli Intensity (MMI) of VIII and Peak Ground Acceleration (PGA) range of 0.34–0.62. The ecosystem is exposed to low (4.2 km^2), moderate (1.2 km^2), high (2.9 km^2), and very high (2.6 km^2) flood hazard. Thirty-eight percent of Rwenzori Mountain is disproportionately exposed to low and very high flood hazard intensity particularly in Kasese and Bunyangabu districts (Fig. 5.3). In Kasese district, the sub-counties exposed to very high flood hazard intensity include Bugoye, Bulembia Division, Bwesumbu, Kilembe, Kyarumba, Kyondo, and Maliba, whereas in the Bunyangabu district, Kabonero sub-county is exposed to very high flood hazard intensity.

Mountain Rwenzori is also exposed to moderate (1848.3 km^2) and high (59.9 km^2) hailstorm hazard of Uganda (Fig. 5.3). The biggest part of the mountain, 96.9%, is exposed to moderate hailstorm hazard intensity in the districts of Kasese, Bunyangabu, Kabarole, and Bundibugyo. The biggest portion of the high hailstorm hazard intensity (71.8%) is located in Ntoroko district in the sub-counties of Butungama, Bweramule, Karugutu, and Karugutu town council. The mountain is exposed to low (26.9 km^2), moderate (440.5 km^2), and high (1425.1 km^2) landslide hazard of Uganda (Fig. 5.3). However, 1.9 km^2 of Rwenzori Mountain is not prone to landslides. The biggest part of the mountain, 75.2%, is exposed to high landslide hazard intensity majorly in Kasese, Bundibugyo, and Bunyangabu districts.

Rwenzori Mountain is exposed to very low (445.3 km^2), low (1228.5 km^2), moderate (185.9 km^2), and high (48.4 km^2) lightning hazard of Uganda (Fig. 5.3). The biggest part of the mountain, 64.4%, is exposed to low lightning hazard intensity; however, there is a portion (2.5%) in Bundibugyo and Ntoroko districts that is exposed to high lightning hazard intensity. In Bundibugyo district, the sub-counties exposed to high lightning hazard intensity include Bukonzo, Burondo, Kasitu, Mabere, Ngamba, and Ntandi Town Council, while in Ntoroko, Karugutu sub-county is exposed to high lightning hazard intensity of Uganda. Rwenzori Mountain is also exposed to high (47.6 km^2) and very high (1858.3 km^2) windstorm hazard of Uganda (Fig. 5.3). The biggest portion of the mountain (97.5%) is exposed to very high windstorm hazard intensity. The districts highly exposed are Kasese, Bunyangabu, Bundibugyo, and Kabarole.

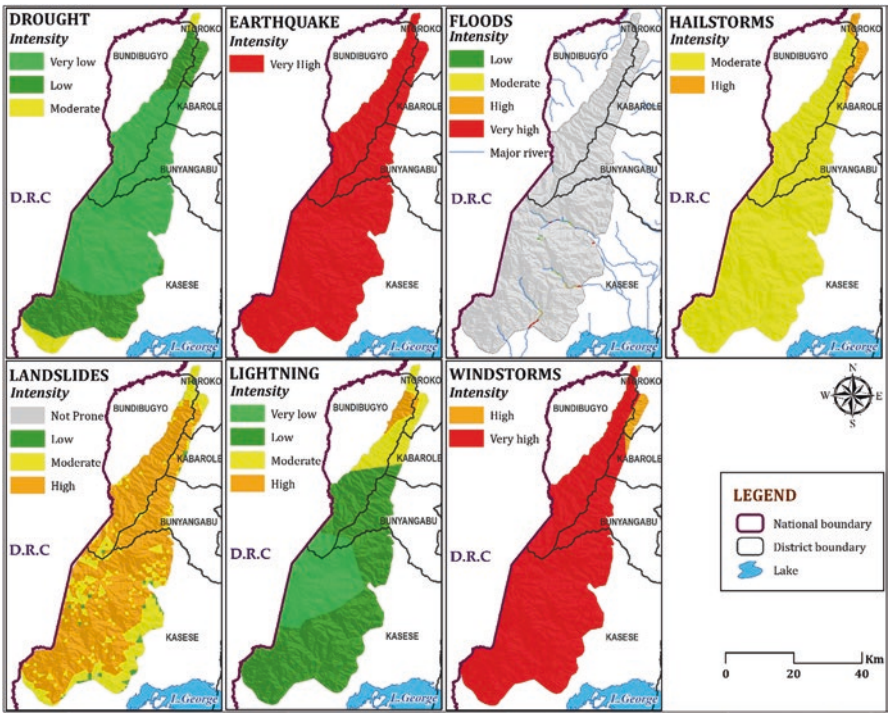

Fig. 5.3 Elements at risk in Mountain Rwenzori

5.3.2 Vulnerability of Elements to Natural Hazards in Mt. Rwenzori

In this study, due to limited data on the elements at risk, vulnerability was computed basing on the location of the elements and the intensity of the hazard.

The sensitivity of elements at risk to hazards were defined in reference to hazard intensities. Elements located in "very low" and "low" were categorized to be with low vulnerability, whereas elements found in "moderate", "high", and "very high" intensities of any natural hazard were classified to be with high vulnerability. This vulnerability assessment methodological approach was adopted from the National Risk and Vulnerability Atlas of Uganda 2019. This is partly due to limited data available on the vulnerability status of elements at risk. Sensitivity of elements at risk is presented in Table 5.4.

Table 5.4 Sensitivity of elements to natural hazards

Hazards	Elements sensitive to the hazard
Drought	Croplands and water sources
Earthquake	Buildings, croplands, health centres, police posts, road network, schools, and water sources
Floods	Buildings, croplands, health centres, police posts, road network, schools, and water sources
Hailstorms	Croplands
Landslides	Buildings, croplands, health centres, police posts, road network, schools, and water sources
Lightning	Buildings, health centres, police posts, and schools
Windstorms	Buildings, croplands, health centres, police posts, and schools

5.3.2.1 Elements Vulnerable to Drought Hazard

About 2.6 km^2 of croplands (translating into 9763 croplands) (7.1%) and 222 water sources (17.9%) are highly vulnerable to drought hazard in Mt. Rwenzori. Most of the highly vulnerable water sources are public stand posts (49.5%). The highly vulnerable water sources are found in Kasese district in the sub-counties of Bwera, Ihandiro, Karambi, Kisinga, Kitholhu, Mpondwe-Lhubiriha, Munkunyu, and Nyakiyumbu. The croplands that are highly vulnerable to drought are located in Bundibugyo, Kasese, and Ntoroko districts. In Bundibugyo district, they are found in Burondo sub-county, while in Kasese district, they are situated in Bwera, Ihandiro, Karambi, Kisinga, Kitholhu, Lake Katwe, Muhokya, Munkunyu, and Nyakiyumbu sub-counties; and in Ntoroko district, they are located in Bweramule and Karugutu sub-counties. Figure 5.4 shows the croplands and water sources that are vulnerable to drought hazard.

5.3.2.2 Elements Vulnerable to Earthquake Hazard

A total of 104,401 buildings (100%), 138,154 croplands (31.2 km^2) (100%), 32 health centres (100%), 8 police posts (100%), 2134.4 km of road network (100%), 284 schools (100%), and 1242 water sources (100%) are highly vulnerable to earthquake hazard on the slopes of Mt. Rwenzori. These elements are Kasese, Bunyangabu, Bundibugyo, Kabarole, and Ntoroko districts as shown in Fig. 5.5.

5.3.2.3 Elements Vulnerable to Flood Hazard

The elements that are highly vulnerable to flood hazard in Mt. Rwenzori include 1093 buildings (1.1%), 2318 croplands (0.3 km^2) (1.7%), 3 health centres (9.4%), 1 police station (12.5%), 33.3 km of road network (1.6%), 9 schools (3.2%), and 15 water sources (1.2%). These elements are located in Bundibugyo, Bunyangabu, and Kasese districts (Fig. 5.6). In Bundibugyo district, the highly vulnerable elements

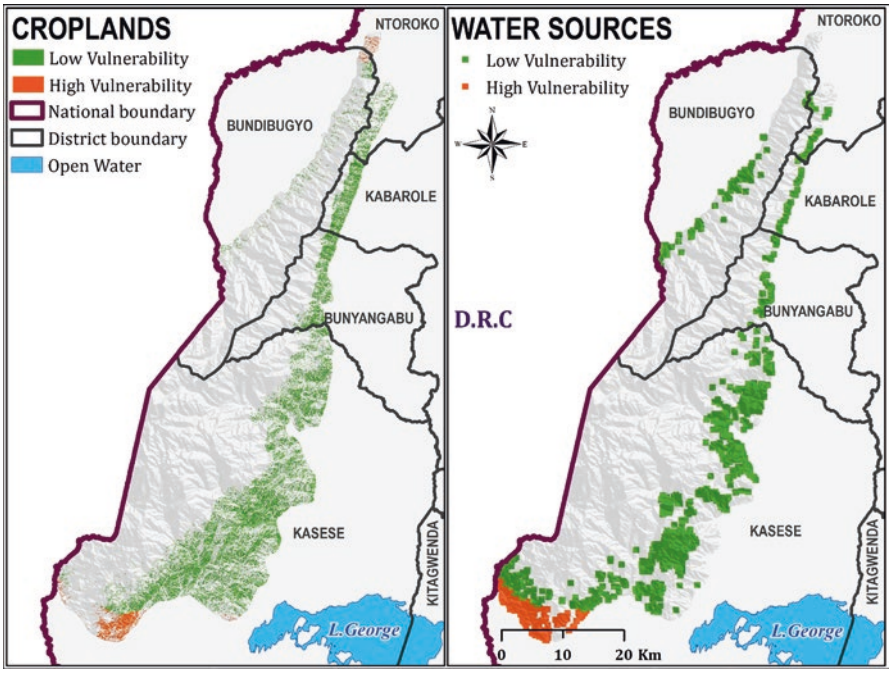

Fig. 5.4 Elements that are vulnerable to drought hazard in Mt. Rwenzori

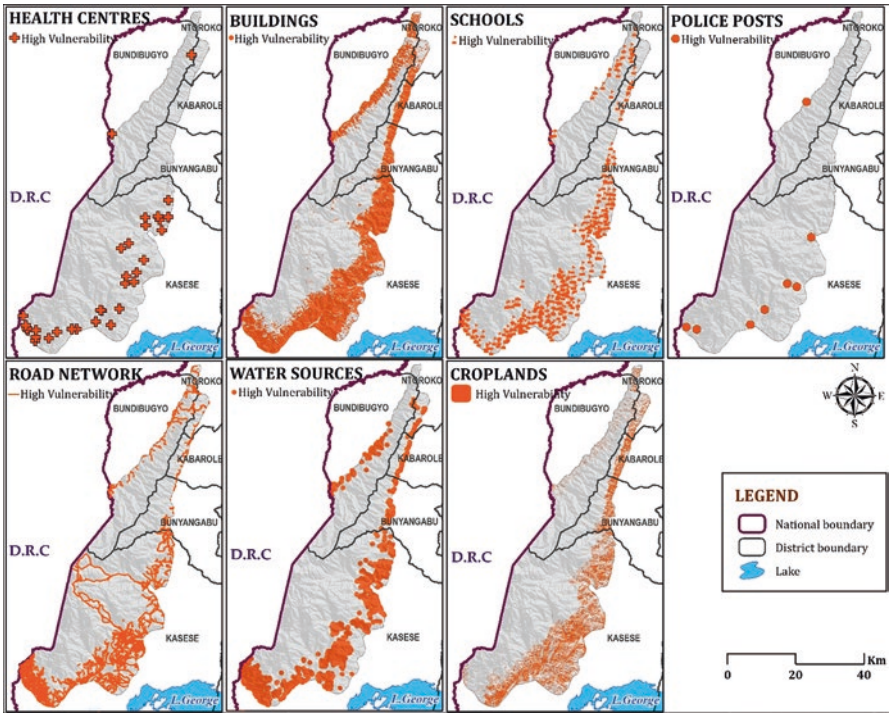

Fig. 5.5 Elements that are vulnerable to earthquake hazard in Mt. Rwenzori

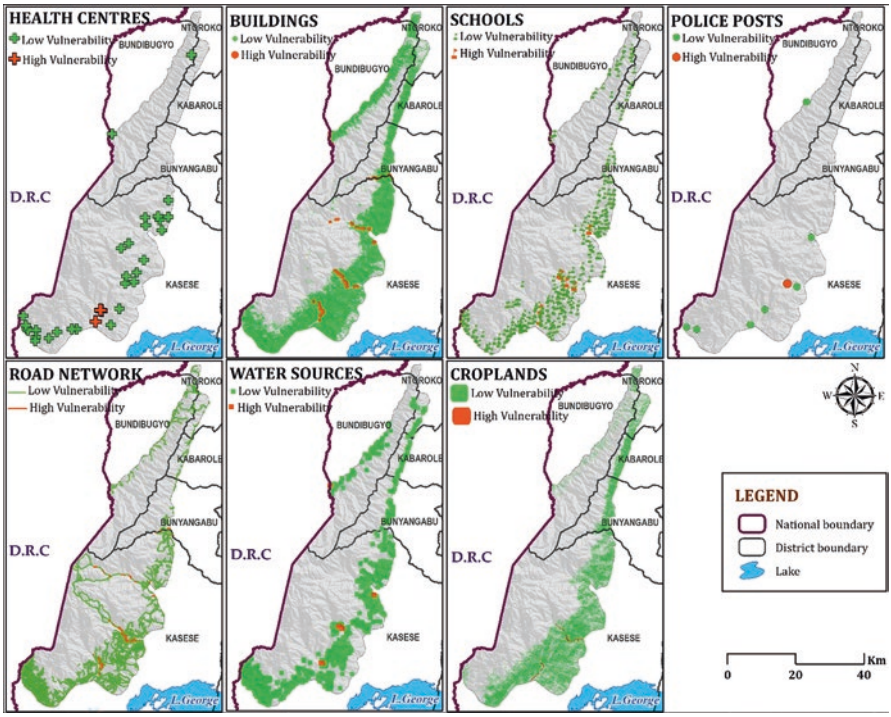

Fig. 5.6 Elements that are vulnerable to flood hazard in Mt. Rwenzori

are located in Sindila sub-county, while in Bunyangabu district, they are situated in Kabonero sub-county; and in Kasese district, they are found in Bugoye, Bulembia division, Bwesumbu, Kilembe, Kyarumba, Kyondo, and Maliba.

The health centres that are highly vulnerable to floods include Kyondo Health Centre III, Kyarumba Health Centre III, and Kyarumba Phc Health Centre III, all located in Kasese district. The Kilembe police post is highly vulnerable to flood hazard and is located in Bulembia division, Kasese district. Seven (7) primary schools (Mughete, Kaghema, Road Barrier, Katiiri, Kyanjuki, Kyanya, and Kyanya SDA) and 2 secondary schools (Mt. Rwenzori Girls and Kilembe Senior) located in Kasese district are also highly vulnerable to flood hazard in Mt. Rwenzori. The highly vulnerable water sources in Mt. Rwenzori include protected springs (3), public stand posts (11), and rainwater harvesting tank (1).

5.3.2.4 Element Vulnerable to Hailstorm Hazard

A total of about 138,154 croplands (100%) in Mt. Rwenzori in the districts of Bunyangabu, Bundibugyo, Kabarole, Kasese, and Ntoroko are highly vulnerable to hailstorm hazard (Fig. 5.7).

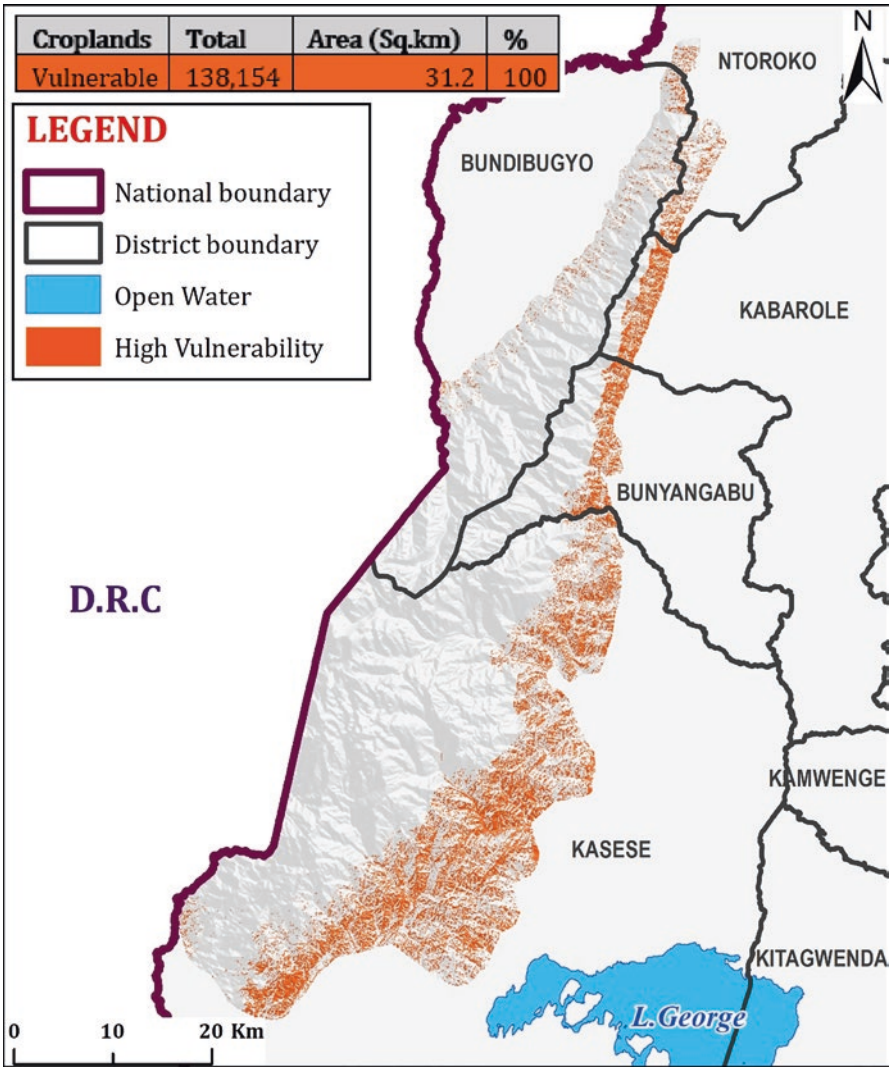

Fig. 5.7 Croplands that are vulnerable to hailstorm hazard in Mt. Rwenzori

5.3.2.5 Elements Vulnerable to Landslide Hazard

The elements that are highly vulnerable to landslides in Mountain Rwenzori include 100,678 buildings (96.4%), 134,964 croplands (30 km^2) (96.6%), 31 health centres (96.9%), 7 police posts (87.5%), 2044.9 km of road network (96.1%), 270 schools (95.1%), and 1178 water sources (94.9%). The highly vulnerable elements are spread across Mt. Rwenzori in the districts of Bundibugyo, Bunyangabu, Kabarole, Kasese, and Ntoroko (Fig. 5.8).

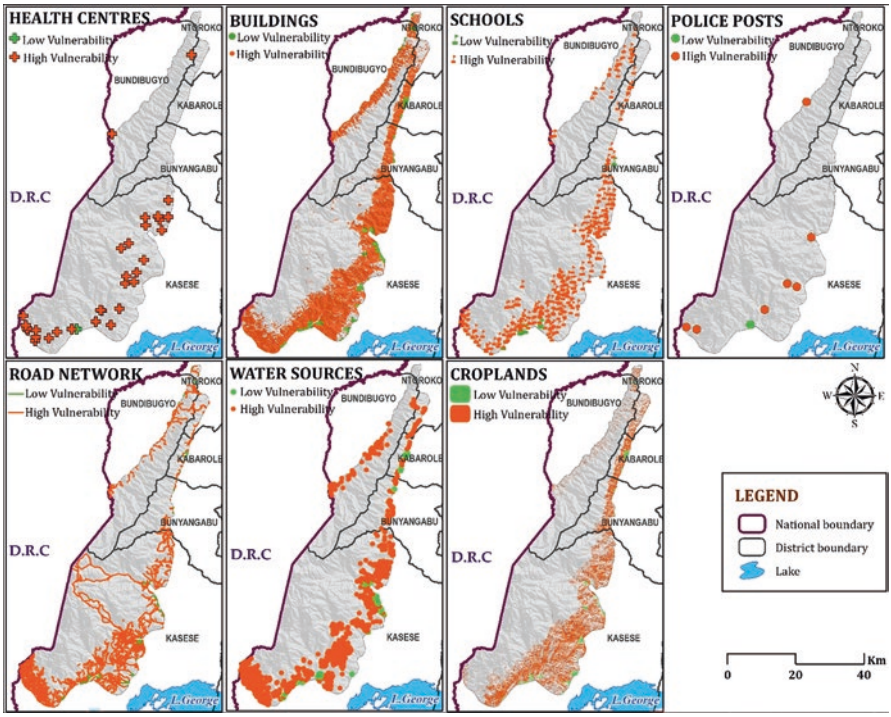

Fig. 5.8 Elements that are vulnerable to landslide hazard in Mt. Rwenzori

5.3.2.6 Elements Vulnerable to Lightning Hazard

The elements that are highly vulnerable to lightning hazard include 14,787 buildings (14.2%), 1 health centre (3.1%), 1 police post (12.5%), and 27 schools (9.5%) (Fig. 5.9). In Bundibugyo district, the highly vulnerable buildings are located in the sub-counties of Bukonzo, Burondo, Harugale, Kasitu, Mabere, Nduguto, Ngamba, and Ntandi Town Council, while in Kabarole district, they are found in Bukuuku, Karago Town Council, Karangura, and Kichwamba sub-counties. In Ntoroko district, the highly vulnerable buildings are located in the sub-counties of Butungama, Bweramule, Karugutu, and Karugutu Town Council.

Kyondo Health Centre II situated in Kasitu sub-county; Bundibugyo district is a highly vulnerable health centre. Harugale police post is also highly vulnerable to lightning hazard, and this is located in Harugale sub-county, Bundibugyo district. In Bundibugyo district, the schools that are highly vulnerable to lightning hazard are found in the sub-counties of Bukonzo, Burondo, Kasitu, Mabere, Ngamba, and Ntandi Town Council; in Kabarole and Ntoroko districts, the highly vulnerable schools are located in Karangura and Butungama sub-counties, respectively.

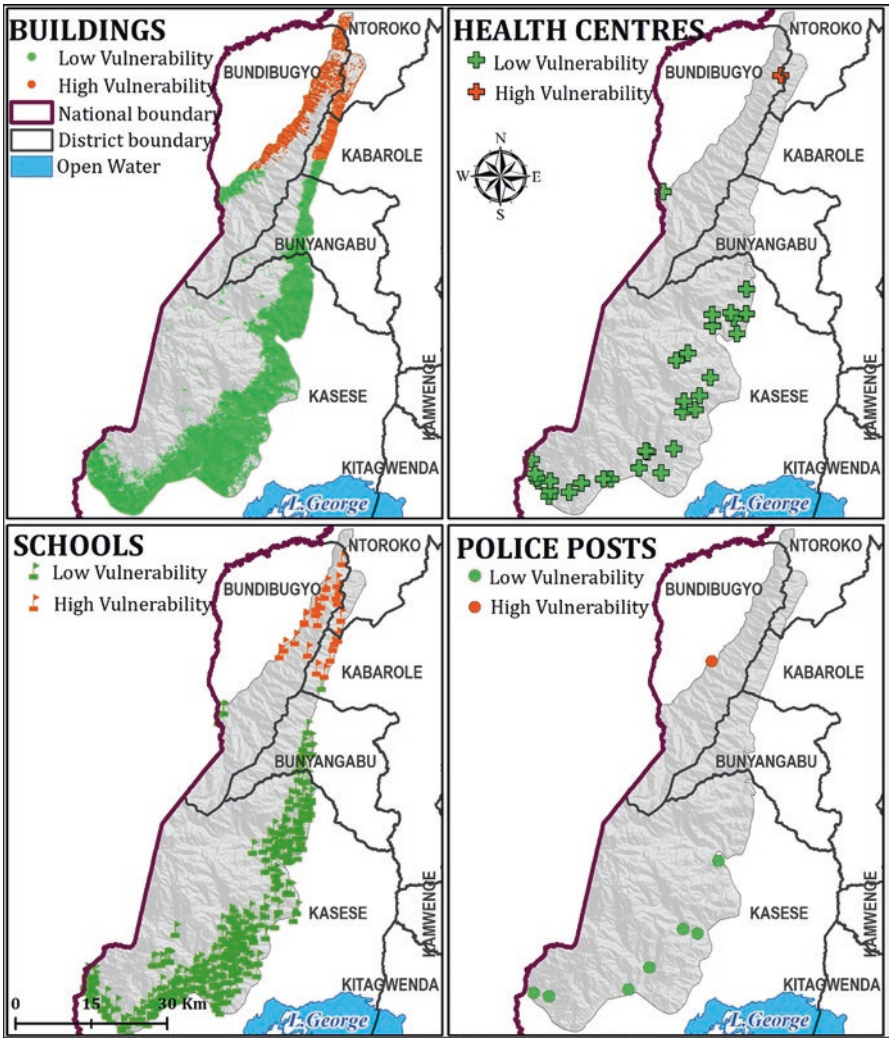

Fig. 5.9 Elements that are vulnerable to lightning hazard in Mt. Rwenzori

5.3.2.7 Elements Vulnerable to Windstorm Hazard

The elements that are highly vulnerable to windstorm hazard in Mt. Rwenzori include 104,401 buildings (100%), 138,154 croplands (31.2 k m^2) (100%), 32 health centres (100%), 8 police posts (100%), and 284 schools (100%). These elements in the districts of Kasese, Bunyangabu, Bundibugyo, Kabarole, and Ntoroko are shown in Fig. 5.10.

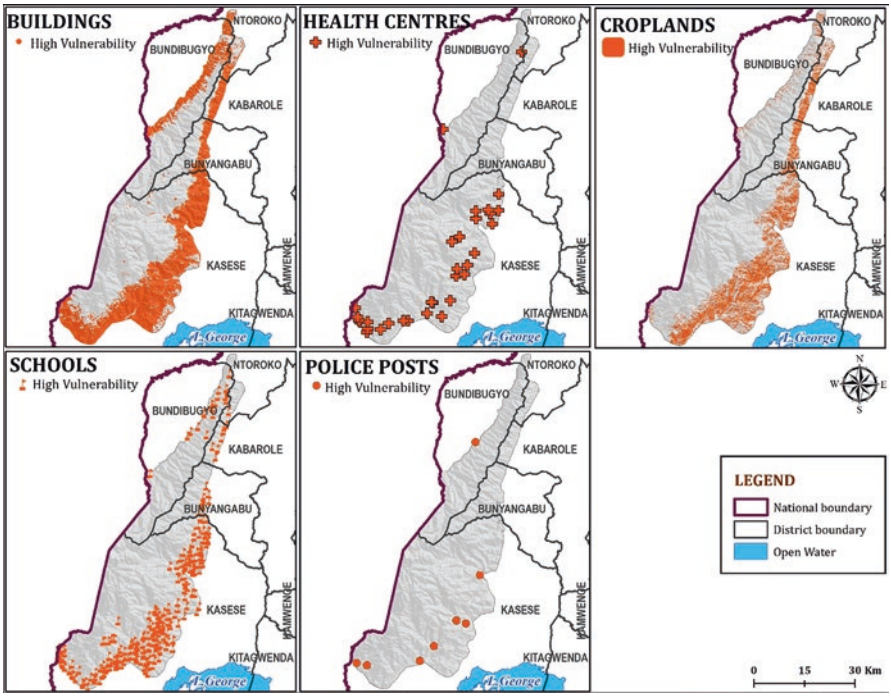

Fig. 5.10 Elements that are vulnerable to windstorm hazard in Mt. Rwenzori

5.3.3 Disaster Recovery Strategies to Natural Hazards in the Rwenzori Mountains

The strategies are a reciprocal of the elements at risk (buildings, croplands, police posts, health facilities, road network, schools, and water sources) affected by studied hazards in the Rwenzori mountains. The recovery strategies per element are as follows.

5.3.3.1 Buildings

The housing sector is highly sensitive to flooding, landslides, and earthquake hazards. There is a need to support the rapid disaster recovery assessments planned by the sector, improve the re-establishment of social networks and community hosting facilities, and build capacity of responsible authorities to promote, supervise, and guide planning and construction processes of recovery national structures.

In the long term, support the development of housing prototype plans to be used in the reconstruction of buildings that are disaster-resilient model houses; strengthen the quality control monitoring mechanisms in the house constructions; testing of

building materials and undertaking geotechnical designs and development of bills of quantities; support supervision of the contractors in the implementation recovery interventions; and ensure reconstruction of strong reinforced and retrofitted housing units. Support the operationalization of developed earthquake-resistant construction guidelines to strengthen buildings in the prone corridor; increase trainings for the skilled and unskilled labour in the earthquake disaster-prone areas to learn how to build resilient buildings; and strengthen awareness on the building and safety regulations and construction of demonstration houses during the trainings. There is a need support the development of site master plans and detailed physical development plans of the affected disaster areas to help communities build back better.

In addition, strengthen the housing development committees such as the Uganda National Building Review Board to ensure that housing activities are compliant with the established guidelines and engage local communities in the development schemes of hazard-proof construction if the modified disaster-resilient housing designs are to be accepted. There is a need to consider voluntary relocation of the most affected households and those in disaster-prone areas to avoid future calamities and provide financing guarantees to secure and increase private sector investments in real estate and hence attract joint ventures and partnerships.

5.3.3.2 Croplands

Ensure timely procurement and supply of production inputs for the affected enterprises in the affected communities; provide the affected communities with farm inputs like fertilizers, pesticides, and equipment like ox-ploughs, tractors, and spray pumps to boost production; procure and replace damaged beehives; planting of drought-tolerant and early-maturing crop varieties; and supply fast-maturing seed varieties mainly maize, beans, and sweet potatoes and agriculture inputs such as agrochemicals and fertilizers. Offer credit to poor agricultural households at affordable rates; provide technical and advisory support to the affected farmers; promote household implementation of small-scale irrigations facilities; and strengthen the already established or engage farmers using the farmer field schools model9+.

Construct silos to communities to increase food security; construct small-scale irrigation schemes; strengthen the provision of extension services; popularize government livelihood programmes such as Operation Wealth Creation, youth livelihood fund, etc.; transport extension staff to offer technical services to the farmer communities; and protect, restore, and improve the livelihoods of affected communities. Sensitize communities about the Sustainable Land and Water Management (SLWM) techniques such as cover cropping, terracing, and mulching. Also, empower communities to establish firebreaks in areas prone to seasonal bushfires. Promote avenues for household income diversification, and support the implementation of soil and water conservation technologies that are climate-smart and integrated pest management.

In the long term, strengthen the integration of disaster risk management into development plans and support the development of community resilience plans.

Financial/capital investments should support community engagement in the promotion of climate-smart agriculture, particularly soil and water conservation structures. Support should also be extended to agricultural credit and insurance services and communities that require machinery for post-harvest handling, e.g. bean sorters and maize huller machines and maize mills to store farm produce. Strengthen community infrastructure through the construction of wells, dams, water ponds, etc. Enhance structures to enable farmers to adopt surface irrigation. There is a need to enforce the construction of contours to control water run-off in the areas that are fragile such as hilly area; support tree planting initiatives that can be integrated into farming systems to increase farm production; and provide support for improved breeding of pest- and disease-resistant seed varieties.

5.3.3.3 Police Posts

Strengthen training on emergency response to equip the officers with the basic knowledge that is required to save life and property; engage in continuous monitoring and sensitization engagements with members of the community; and support the engineering brigade of army, together with the construction unit of the Uganda Police Force and the Mechanical Unit of Uganda Prison Services, to increase their capability to construct houses and other infrastructure for the disaster victims. Strengthen the capacities of the national identification system to capture all and non-citizens of Uganda, births, and deaths; support the development of a village registration system to avoid false claims at the disaster recovery stage; and strengthen community policing initiatives and prosecution units so that the criminals are apprehended. Also, support security mechanisms to regularly enforce policies and ensure that there are adhered to.

5.3.3.4 Health Facilities

There is gap to promote government's initiative to distribute mosquito nets as one of the most cost-effective preventative measures for malaria control and advocate for an increase in the budget to the National Medical Stores and health supplies. In Uganda, the recommended government budget allocation is 7.2% which is still far from the 15% target. More support is needed to provide mobile toilets at evacuation centres, camps, and settlements, install community water and rainwater harvesting tanks, construct at least six stance latrines at the affected health facilities, and de-silt affected health facilities. Strengthen the development and dissemination of health standard operating materials astride the country. Many Standard Operating Procedures have already been established, however there is still limited implementation and adherence to them and development of procedures that support efficiency and smooth operations of multisectoral stakeholders during the handling of complex disaster incidences. Restock affected health facilities with medical and

equipment supplies, deal with malnutrition, supply malaria treatment kits and mosquito nets to the most affected areas with higher malaria burden, supply temporary medical treatment facilities (tents), provide ambulances to health facilities (i.e. health centres and hospitals), set up tents, and provide emergency drugs.

Support the health sector in the training of staff, for example, surveillance, contact tracing, quarantine, laboratory and border post health, and basic emergency care; restock affected health facilities with medical and equipment supplies; deal with malnutrition; supply malaria treatment kits and mosquito nets to the most affected areas with higher malaria burden; supply temporary medical treatment facilities (tents); and provide ambulances to health facilities (i.e. HCII, HCIII, and hospitals).

Plan and support the upgrading of the health facilities with better wage provision to attract and retain human resource personnel; support the recruitment of health workers because the health worker (doctors, nurse, and midwives) population ratio of 1.92 health workers per 1000 population is still below the World Health Organization recommendation of 2.8 per 1000 population to achieve healthcare. Strengthen household health inspections, recruit more health staff to strengthen psychosocial support to communities and health workers, recruit more medical workers, and conduct training and placement of volunteers. Support the enactment of the National Health Insurance Bill 2019 that seeks to create a National Health Insurance Scheme, and increase numbers of health facilities to increase access to quality health services; there is also need to renovate and expand regional health facilities to improve on the secondary care services and construct more modern pallet space warehouse for the National Medical Store. There is a need to establish specialized health rehabilitation centres, construct and rehabilitate completely damaged health facilities and staff houses, and relocate and construct hospitals in risky areas.

Advocate for the operationalization and maintenance of the National Laboratory Information Management System, develop a Comprehensive Community Health Promotion Program Strategy, support the development and implementation of a Comprehensive Health Communication Strategy for the Health Sector, and advocate for more funding to be increased to improve research in the recovery of outbreaks. Strengthen the integration processes of mainstreaming DRR in the District Development Plans, projects, and programmes, among others, and integrate health issues in disaster risk reduction strategies.

5.3.3.5 Road Network

Provide support for full rehabilitation of the affected roads including drainage works; reconstruction of affected road sections; grading, reshaping, and gravelling of affected roads including drainage systems; desilting and removing boulders from the affected rivers; replacement of the broken and swept away timber bridges; repair of approaches and construction of gabion protection; replacement of the damaged guard rails; and removal of displaced material blocking watercourses. Strengthen

community sensitization on the dangers of over-cultivation along the slopes that are sensitive to landslides, and provide financial support to the emergency fund so that the recovery interventions are attended too within a short period.

There is need to increase district infrastructure development funding to facilitate the renovation of partially damaged roads caused by floods and other disasters. Additional support should be provided for the maintenance budgets for the already existing road equipment. Support carrying out detailed investigations and designs of new bridges and roads to be constructed, demarcation of road reserves and planting of trees, and repair of damaged water supply systems. Strengthen the localized monitoring system of roads along with the mapped wetlands systems for easier reconstruction and support the conducting of detailed road engineering designs to avoid duplication and waste of resources in reconstruction of damaged roads.

5.3.3.6 Schools

Urgency is needed to improve academic and non-academic staffing in the affected schools; the communities in collaboration with the education department at district level should put in place an emergency committee to see how and where to relocate learners for continuity of learning. Mobilization of teachers to support the learners relocated to safer schools. Support relocation of learners to safer schools and flat areas so that learning can continue; establishment of tents and permanent and semi-permanent structures for the affected learners; and coding of schools affected by the disasters. Supply lower and old-age dual desks for primary and secondary schools, procure assorted textbooks and chairs, supply assorted laboratory equipment and wooden cupboards destroyed, provide food and non-food items to the affected learners, and strengthen emergency funding structures especially at the districts to support implementation and monitoring of short-term recovery interventions in the education sector.

Support continued learning in established temporal structures established to ensure that the teaching syllabus is completed, set up school disaster management committees to empower the students about disaster mitigation and management in schools and communities, and support budgetary allocations meant to help the sector recovery from disasters and monitoring of funding initiatives especially at the district levels.

Provide additional funds to the sector, commit and set aside additional funding to address cases of collapsed and damaged structures in the short term, and provide funding for the dissemination of disaster risk information in lower, upper, and post-primary schools. Increase rehabilitation, construction, and equipping of educational facilities with learning resources; construction of classrooms, laboratories, libraries, and offices affected and construction of stance VIP toilets and latrines affected; and installation of lightning arrestors on buildings in all schools. Strengthen the training

of teachers, pupils, and school managers on WASH issues and disaster risk management and training teachers in psychosocial support for the affected schools. Support the integration of DRR in learning areas such as social sciences, geography, and science subjects like biology and training and capacity building of technical staff on mainstreaming disaster risk management and interpretation of disseminated early warning messages. Relocate schools to new safer and flat areas for landslide victims; in these new areas, more facilities should be established (primary, secondary, and vocational institutions), and the established structures should be strong and retrofitted.

5.3.3.7 Water Sources

Strengthen already constructed floodwalls, construction, and rehabilitation of destroyed and damaged water sources to increase access to safe water services; rehabilitation of shallow wells, boreholes, and springs that were swept away by storms; and creation of bigger banks on the valley tanks to check storm waters. Strengthen enforcement of environmental laws, formulation of by-laws, and ordinance enactment which will help in the enforcement of environmental laws and increase vigilance and law enforcement; support the review and enactment of wetland bill as well as the issuance of water permits.

Support sensitization of the communities on river bank restoration and management; training on soil and water conservation programmes, e.g. construction of trenches and check dams; training of environmental inspectors in ecological integrity and sustainability of the green and brown environment; mass mobilization of communities to plant trees; carrying out of regular water quality tests; conducting public radio talk shows on environmental protection and conservation; continuous community sensitization on disaster risk reduction measures, e.g. soil and land management in highland and low land areas; and training and empowering of communities to use biogas as an alternative source of clean energy to prevent tree cutting for charcoal burning. Support the development of wetland and catchment/micro-catchment management plans and strengthen water user, wetland, and catchment management committees. Promote construction of valley tanks and deep boreholes to conserve water for the dry season; formation of water user committees; installation of solar-powered water pumps to enable semi-automatic water distribution in the urban centres; protection of water sources; desilting of valley tanks; monitoring water sources for possible drying up; and planting of drought-resistant trees to moderate the microclimate.

5.4 Discussion

5.4.1 The Magnitude and Vulnerability of Natural Hazards Experienced in Mt. Rwenzori

Study findings reveal that Mountain Rwenzori region is exposed to several potential hazard processes including droughts, earthquakes, floods, hailstorms, landslides, lightning, and windstorm hazards (Fig. 5.3). The findings are in line with several other studies which indicated landslides, droughts, severe flash flood, hailstorms, lightening, thunderstorms, and earthquakes, among others, as the dominant hazards within the Rwenzori region (Bwambale et al., 2018; Kabenge et al., 2017; Katutu et al., 2019). Exposure to hazards shows the degree to which the elements at risk are actually located in an area affected by a particular hazard event (Ronald & Mary, 2016). In mountainous areas like the Rwenzori region, floods, landslides, earthquakes, and other hazards can occur and cause complex interactions (Cardona et al., 2012). The two annual rainfall seasons received in the Rwenzori region during the months of March to May and September to December (NEMA, 2016) normally trigger landslides and floods (Jacobs et al., 2015; UNDP, 2013).

Although disasters such as droughts, floods, landslides, and hailstorms occur regularly in the Rwenzori region, the frequency and intensity of such weather-related hazards is, however, increasing due to climate change (Jacobs et al., 2016). Due to the fact that most of these disasters are related to precipitation (NEMA, 2018), this study establishes that there is high disaster occurrence during the months of heavy rainfall especially May and October. The major disasters associated high rainfall seasons in the region include flash floods, landslides, and storms (Mertens et al., 2018; Mathieu et al., 2019). On the other hand, the dry seasons which occurs during the months of January, June, and July are often associated with low disaster occurrence (NEMA, 2016). This study establishes that landslides, flash floods, and windstorms are the most frequent disasters in the Rwenzori region that cause a lot of damage to socioeconomic infrastructures and loss of lives. The management of these disasters should therefore be given top priority in solving. The elements at risk in Mt. Rwenzori that were considered for analysis included buildings, health centres, schools, police posts, road network, water sources, and croplands.

In this study, vulnerability was computed basing on the location of the elements and the intensity of the hazard. The sensitivity of elements to different natural hazards in the Rwenzori region was established (Table 5.3). The vulnerability of the affected socioeconomic and ecological systems determines the actual amount of damage of a specific event (Cardona et al., 2012). The more exposed an element is to a hazard event, the more susceptible it becomes to its forces and impacts (Ronald & Mary, 2016). The vulnerability of a community to a hazardous event increases due to settlements along the hazard path, occurrence of vulnerable group, and cultivation along the hazard event path (Al Abdullah et al., 2020). The vulnerability of elements at risk is also high due to topographical position of elements at risk along the hazard path (Katutu et al., 2019; Mertens et al., 2018). This study establishes

that, due to the steep topography, intense rainfalls, deep soil profiles, and high population densities, the Rwenzori region is highly vulnerable to geo-hazards.

5.4.1.1 Elements Vulnerable to Drought Hazard

Globally, droughts cause significant property damage (Michael et al., 2019). In the Rwenzori region, drought is very severe in the area in the months of January, June, and July. Although the intensity and spatial character of drought event changes from month to month or season to season, they normally take 2 to 3 months to become established but may then persist for months or years (Mertens et al., 2018; Montz et al., 2017). The costs of drought are not evenly distributed between years because they frequently occur in clusters (Katutu et al., 2019; NEMA, 2018). Droughts are associated with diverse economic, social, and environmental impacts (Michael et al., 2019). Drought often results in mass displacements of population. The direct impacts of drought include shortage of water and food. It is likely to have a long-term environmental, economic, and health impact on the population. This study establishes that community vulnerability to drought in the Rwenzori region is escalating at a significant rate and therefore calls for urgent attention to increase their resilience.

5.4.1.2 Elements Vulnerable to Earthquake Hazard

The study findings reveal that the most vulnerable elements to earthquake hazards in the Rwenzori region include buildings, croplands, health centres, police posts, road network, schools, and water sources (Fig. 5.5). According to the NEMA (2016), earthquakes have been more frequent in the Rwenzori region over the past 10 years. Basing on the history, their destructive effects can greatly exceed the scale of the effects of landslides and windstorms. It has been reported that severe earthquakes occurred in the Rwenzori region during the years 1966 and 1994, causing loss of lives and destruction of socioeconomic infrastructures (NEMA, 2018). Earthquakes in the Rwenzori region are associated with secondary events such as landslides, debris flows, and flooding. According to Storchak et al. (2015), it is difficult for people to control earthquakes. Communities are, however, able to reduce the negative impact of secondary hazards that arise from this phenomenon especially landslides and flooding (Weatherill et al., 2016).

5.4.1.3 Elements Vulnerable to Flood Hazard

The study established that flooding causes increased water levels in rivers of the region due to high precipitation amounts received throughout the year. In the Rwenzori region, flooding is often characterized by increased volumes of river water regime normally influenced by rain water accumulating in the catchment

during the wet season (Bwambale et al., 2018). This is in line with what has been reported elsewhere that flash floods result in an irregular transitory increase of water levels in rivers (Roxana et al., 2018). Flash floods are triggered by intensive precipitation in catchments associated with comparatively high flow velocities (Al Abdullah et al., 2020). Flash floods have been reported to be more frequent in Rwenzori slopes because of several flooding spots along rivers like Nyamwamba and Mubuku (Jacobs et al., 2017; Kabenge et al., 2017). According to Liesbet et al. (2016), flash flooding of river Nyamwamba has been attributed to diversion of the river course in the past to create space for infrastructure construction in Kilembe mines. This is a feedback mechanism, where the river normally regains back its natural course of flow during periods of heavy rains. Musoke (2015) further notes that continuous deforestation is another factor contributing to flooding in this region. There is need to, therefore, construct flood defence structures such as levees and reservoirs to prevent damage caused by such disasters.

5.4.1.4 Element Vulnerable to Hailstorm Hazard

Hailstorms are a frequent phenomenon in the Rwenzori region (NEMA, 2016). The economic losses from hailstorms are very significant every year (NEMA, 2018). Hailstorms can destroy crops and damage buildings and cars (Cecil & Blankenship, 2012; Munich, 2013). They also cause injury or kill humans and wildlife caught out in the open (Lamiur et al., 2020; Sioutas et al., 2009). Hailstorms are perceived as a potential threat to sustainable agriculture in the Rwenzori region (NEMA, 2016). This study established that due to the increased damage from hailstorms, farmers in Rwenzori region might stop farming and choose non-farming income sources as mitigation strategies. It can, therefore, be concluded that hailstorms pose a great obstacle to sustainable agriculture and hence a threat to poverty reduction in the Rwenzori region.

5.4.1.5 Elements Vulnerable to Landslide Hazard

Landslides are the most common disasters in the Rwenzori region (NEMA, 2018). They pose the most frequent danger to communities in the region. This can be attributed to the interaction of natural factors including prolonged and heavy rainfall and its exceptionally steep topography associated with human activities especially continuous cultivation, deforestation, and poor construction designs. Because landslides often occur as a result of intense rainfall, they are often referred to as "secondary hazards" (Mertens et al., 2018). They are a major hazard in many mountainous and highland regions (Jacobs et al., 2016). Their sizes and speed, the elements at risk, and the vulnerability of the affected populations quite often determine their impact on the environment and humans (Nseka et al., 2021). The study found out that landslides cause fatalities and functional damage to socioeconomic infrastructure, as well as serious disruptions to community's organization thus affecting

community livelihoods. Landslide risk is controlled by the vulnerability of people exposed and the hazard characteristics (Mertens et al., 2016). In the Rwenzori region, the study established that community vulnerability is constrained by unsafe living conditions.

5.4.1.6 Elements Vulnerable to Lightning Hazard

According to Altaratz et al. (2010) and NEMA (2018), many forms of labour-intensive work are far from lightning safety. Many people are involved in labour-intensive agriculture, fishing in open boats, and walking to market or inside schools during daytime without recourse to safety in an appropriate building or vehicle hence making themselves vulnerable to lighting attacks. During the night, many people live in lightning-unsafe dwellings without adequate wiring, plumbing, or metal structural components that can carry lightning into the ground without affecting individuals inside. One should always assume they are not lightning-safe (Clark et al., 2017; Finney et al., 2018). This is because they will likely not surround a person inside with a certain path for lightning to follow. A fire can be sparked whenever lightning strikes a natural or man-made feature (Bell et al., 2009; Garolera et al., 2016; NEMA, 2016). The fire hazard can be increased when dry lightning sparks, and there is no rain falling to douse the flames (Altaratz et al., 2017). Wildfires can be directly related to lightning and other weather-related elements, although they are not actual weather phenomenon (Finney et al., 2018).

5.4.1.7 Elements Vulnerable to Windstorm Hazard

Windstorms are one of the most common and most noticeable weather events of our atmosphere. This study establishes that windstorms pose hazardous effects that most concern communities in the Rwenzori region compared to other natural hazards. Windstorms can cause a tremendous amount of damage although they can be fairly small. Severe windstorms can cause injury or death and can also result in substantial property damage. Windstorms may cause power and telecommunication disruption which may seriously impair the emergency management capabilities of the affected communities.

5.4.2 The Appropriate Disaster Recovery Strategies to Natural Hazards in the Rwenzori Mountains

Disaster recovery includes the coordinated efforts and processes to implement the immediate, medium, and long-term holistic regeneration of a community following a disaster (McEntire, 2015). In this study, disaster recovery interventions entail a

developmental as well as a remedial process consisting activities minimizing the spread, the impacts of the disasters, regeneration of social, emotional, economic, natural and built environments future needs (Norman, 2006). For the studied elements at risk, their recovery strategies are hereby discussed below:

5.4.2.1 Buildings

The long-term recovery actions should be aimed at not only building community resilience, but also ensuring society housing sustainability (Adie, 2001; Ingram et al., 2006; Mikoš, 2013; Deshmukh and Hastak, 2014). Short-term recovery of buildings should include the provision of temporary shelter, provision of shelter repair kits, and demolition of partially/totally destroyed houses, while medium- and long-term actions should focus on training to build back safer, shelter construction, awareness raising activities for housing construction in disaster-free areas, community-based disaster risk management, hazard mapping, early warning system training, and disaster risk awareness raising in disaster-prone communities, among others (Adie, 2001; Ingram et al., 2006; UN, 2017).

5.4.2.2 Croplands

Recovery actions should aim at restoring vital production and supply chains in the shortest time possible. Under emergencies situation, recovery teams should ensure the food needs of the extremely vulnerable households, including orphans, those headed by a female and/or child, elderly, disabled (Katutu et al., 2019; Kumar et al., 2020). The focus should be on livelihood re-establishment for resettled households, creation of community productive assets, agricultural inputs including seeds, fertilizers and tools, restocking lost livestock head, rebuilding productive assets and stocks to support the ability of affected individuals to earn a living in the longer term, training in non-environmentally degrading farming techniques, rehabilitation and creation of community assets in resettled areas and disaster-prone areas to support livelihoods and promote community-level resilience to flooding, augmented Social Safety Nets and support to revise the Government's Social Protection Policy (Mikoš, 2013).

5.4.2.3 Police Posts

The police force forms part of the search and rescue team following a disaster, cases of human rights violations like gender-based violence increase during disasters since people start to shelter in temporal houses and camps (Deshmukh & Hastak, 2014; UN, 2017). Recovery actions should therefore aim at activating community-based protection mechanisms for identification, referral of and response to child

protection cases in the communities, protecting the affected population particularly women and girls from Gender-Based Violence (GBV) in emergency situations and providing comprehensive and multi-sectoral services for the survivors, Short term measures can include establishment of temporal structures for coordinating police operations and activities while long-term actions should focus of rebuilding following sustainability principles (Garnett & Moore, 2010).

5.4.2.4 Health Facilities

In the health sector, it is necessary to conduct reorientation of rural public health emergency management committees on emergency management, procure vehicles and motorbikes for public health emergency response in the districts, organize safe collection and treatment of medical waste (infectious waste, human body parts, pharmaceuticals, sharps, and needles), and install treatment facilities for the above, e.g. incinerators, theatres etc (Garnett & Moore, 2010; UN, 2017). It is also important to procure medical equipment and supplies to provide essential sexual and reproductive health services including equipment for emergency obstetric care, conduct mapping on human resources/health personnel in the health facilities and provide recommendations for health personnel distribution to provide services based on the facility type, and conduct trainings for the healthcare providers on the specific sexual and reproductive health services/intervention based on the needs. Ensure sector coordination for example WASH and infrastructure for provision of basic infrastructure facilities for the affected health facilities (electricity, running water, waste management), and conduct training of trainers on community-based surveillance in districts affected (Rubin et al., 1985; Ingram et al., 2006; Paquay et al., 2021).

5.4.2.5 Road Network

Both technical and non-technical skill teams are necessary to implement the various actions of recovery especially in the road network infrastructure (Mikoš, 2013; Paquay et al., 2021). Recovery actions for the road sector should thus be directed toward establishing a central technical capacity, undertaking slope stabilization works, implementing a build back better principles for the roads, and developing a master waste management plan for the road debris (Haigh & Sutton; Mair et al., 2016; UN, 2017). Long-term recovery actions should begin with repair or replacement of roads and bridges so that communities quickly, and with increasing resolve to re-establish utilities, provide access and create reconstruction policies (Garnett & Moore, 2010; Deshmukh and Hastak, 2014; Mair et al., 2016; Singh & Bartlett, 2018). Road network recovery actions need to be implemented by a technical team that should support the rehabilitation of prioritized roads and bridges in order to facilitate connectivity and accessibility between communities (UN, 2017).

5.4.2.6 Schools

The resilient recovery interventions ideal for this sector should include strengthening linkages with security forces to determine schools in safe areas for potential rehabilitation, placement of children attending camp schools into regular schools after relocation from the camp, rehabilitation, and supply of furniture to damaged schools. Given that children may be moving to various locations, it will be important to determine how to fast-track their enrolment into their new schools, social mobilization to raise awareness for affected children to reintegrate into schools, placement of approved teachers from schools that are closed into other schools, psychosocial support for children and teachers, and early learning access for children 3–5 years integrated into recovery interventions (Adie, 2001; UN, 2017).

5.4.2.7 Water Sources

Recovery interventions should aim at trucking of safe drinking water to the displaced people in the camp and affected communities, drilling of boreholes in the affected communities, construction/installation of households/communal rain water harvest system in the affected communities and institutions, support the rehabilitation of WASH facilities and waste management services in healthcare facilities, and promotion of sanitation and hygiene practices in the affected communities (Mair et al., 2016). Furthermore, care should be taken to ensure provision of adequate sanitation, hygiene promotion and sanitation, access to safe water for drinking and cooking, provision of adequate sanitation, hygiene promotion, and sanitation with a particular focus on the hygiene needs of women (McEntire, 2015; Mikoš, 2013; UN, 2017).

5.5 Conclusion

Mt. Rwenzori experiences moderate to high intensity of earthquakes and landslides. Much of the area experiences low incidences of floods and droughts. However, high incidences of flash floods have been witnessed in Kasese and Ntoroko districts. Hailstorms and windstorms are moderately intensive. The elements most exposed and affected by various natural hazards included people, buildings, schools, roads, and croplands. Floods mostly impacted roads, croplands, and buildings, particularly those located adjacent to rivers in the mid- to low-lying areas. Landslides affected the population and residential buildings in highland areas. Continued occurrence of natural hazards will wreck more havoc and retard efforts toward achieving sustainable development in such a fragile mountain ecosystem. For instance, to reduce the vulnerability of buildings to hazards, there is a need to strengthen the housing development committees such as the National Building Review Board to oversee if the housing activities are compliant with the established guidelines and engage local

communities in the development schemes of hazard-proof construction if the modified disaster-resilient housing designs are to be accepted. In crop production, support should be extended to agricultural credit and insurance services and communities that require machinery for post-harvest handling. In the health sector, support the upgrading of the health facilities at all levels with better wage provision to attract and retain human resource personnel.

References

Adie, C. E. (2001). *Holistic disaster recovery: Ideas for building local sustainability after a natural disaster*. Diane Publishing.

Al Abdullah, B., Islam, M., & Paul, S. (2020). Flood hazard, vulnerability and risk assessment for different land use classes using a flow model. *Earth Systems and Environment, 4*, 225–244. https://doi.org/10.1007/s41748-019-00141-w

Altaratz, O., Koren, I., Yair, Y., & Price, C. (2010). Lightning response to smoke from Amazonian fires. *Geophysical Research Letters, 37*, L07801.

Altaratz, O., Kucienska, B., Kostinski, A., Raga, G. B., & Koren, I. (2017). Global association of aerosol with flash density of intense lightning. *Environmental Research Letters, 12*, 114037.

Bagonza, R. A. (2014). *Gender and vulnerability to disasters and disaster/climate risk management in Uganda: A participatory characterisation* (Issue December). https://reliefweb.int/sites/reliefweb.int/files/resources/8. Gender %26 Vulnerability to Disasters In Uganda – study.pdf

Bell, T. L., Rosenfeld, D., & Kim, K.-M. (2009). Weekly cycle of lightning: Evidence of storm invigoration by pollution. *Geophysical Research Letters, 36*, L23805.

Bwambale, B., Muhumuza, M., & Nyeko, M. (2018). Traditional ecological knowledge and flood risk management: A preliminary case study of the Rwenzori. *Jàmbá: Journal of Disaster Risk Studies, 10*(1), a536. https://doi.org/10.4102/jamba.v10i1.536

Cardona, O. D., van Aalst, M. K., Birkmann, J., Fordham, M., McGregor, G., Perez, R., Pulwarty, R. S., Schipper, E. L. F., & Sinh, B. T. (2012). Determinants of risk: Exposure and vulnerability. In C. B. Field, V. Barros, T. F. Stocker, D. Qin, D. J. Dokken, K. L. Ebi, M. D. Mastrandrea, K. J. Mach, G.-K. Plattner, S. K. Allen, M. Tignor, & P. M. Midgley (Eds.), *Managing the risks of extreme events and disasters to advance climate change adaptation* (A special report of working groups I and II of the Intergovernmental Panel on Climate Change (IPCC)) (pp. 65–108). Cambridge University Press.

Cecil, D. J., & Blankenship, C. B. (2012). Toward a global climatology of severe hailstorms as estimated by satellite passive microwave imagers. *Journal of Climate, 25*, 687–703. [CrossRef] 4.

Clark, S. K., Ward, D. S., & Mahoowald, N. M. (2017). Parameterization based uncertainty in future lightning flash density. *Geophysical Research Letters, 44*, 2893–2901.

Deshmukh, A., & Hastak, M. (2014). Enhancing post disaster recovery by optimal infrastructure capacity building. *International Journal of Research in Engineering and Technology, 3*(28), 5–12.

Dilley, M., Chen, R. S., Deichmann, U., Lerner-Lam, A., Arnold, M., Agwe, J., Buys, P., Kjekstad, O., Lyon, B., & Yetman, G. (2005). *Natural disaster hotspots: A global risk analysis. World bank disaster risk management series (Issue 5)*. The World Bank Group.

Eslamian, S., Ostad-Ali-Askari, K., Singh, V. P., Dalezios, N. R., Ghane, M., Yihdego, Y., & Matouq, M. (2017). A review of drought indices. *International Journal of Constructive Research in Civil Engineering (IJRCRE), 3*(4), 48–66.

Finney, D. L., Doherty, R. M., Wild, O., Stevenson, D. S., Mackenzie, I. A., & Blyth, A. M. (2018). A projected decrease in lightning under climate change. *Nature Climate Change, 8*, 210–213.

Garnett, J. D., & Moore, M. (2010). Enhancing disaster recovery: Lessons from exemplary international disaster management practices. *Journal of Homeland Security and Emergency Management, 7*(1).

Garolera, A. C., Madsen, S. F., Nissim, M., Mayers, J. D., & Jolboell, J. (2016). Lightning damage to wind turbine blades from wind farms in the US. *IEEE Transactions on Power Delivery, 31*, 1043–1049.

Guha-Sapir, D., Hargitt, D., & Hoyois, P. (2004). Thirty years of natural disasters 1974-2003: The numbers. Presses univ. de Louvain

IFRC. (2019). Annual report 2019. International Federation of Red Cross and Red Crescent Societies, Geneva, Switzerland. 1-155

IFRC. (2020). World Disasters Report 2020: Come Heat or High Water. In *World Disaster Report 2020*. https://media.ifrc.org/ifrc/world-disaster-report-2020%0ACover

Ingram, J. C., Franco, G., Rumbaitis-del Rio, C., & Khazai, B. (2006). Post-disaster recovery dilemmas: Challenges in balancing short-term and long-term needs for vulnerability reduction. *Environmental Science & Policy, 9*(7–8), 607–613.

Jacobs, L., Dewitte, O., Poesen, J., Delvaux, D., Thiery, W., & Kervyn, M. (2015). The Rwenzori Mountains, a landslide-prone region? *Landslides, 13*, 519. https://doi.org/10.1007/s10346-015-0582-5

Jacobs, L., Maes, J., Mertens, K., Sekajugo, J., Thiery, W., & van Lipzig, N. (2016). Reconstruction of a flash flood event through a multi-hazard approach: Focus on the Rwenzori Mountains, Uganda. *Natural Hazards, 84*, 851–876. https://doi.org/10.1007/s11069-016-2458-y. [Google Scholar].

Jacobs, L., Maes, J., Mertens, K., Sekajugo, J., Thiery, W., van Lipzig, N., et al. (2017). Flash floods in the Rwenzori Mountains – Focus on the May 2013 multi-hazard Kilembe event. In N. Mikoš, M. Casagli, Y. Yin, & K. Sassa (Eds.), *Advancing culture of living with landslides: Volume 4 diversity of landslide forms* (pp. 631–641). Springer International Publishing. https://doi.org/10.1007/978-3-319-53485-5_73. [Google Scholar].

Kabenge, M., Elaru, J., Wang, H., & Li, F. (2017). Characterizing flood hazard risk in data-scarce areas, using a remote sensing and GIS-based flood hazard index. *Natural Hazards, 89*, 1369–1387. https://doi.org/10.1007/s11069-017-3024-y. [Google Scholar].

Katutu, R., Nyamweha, B. R., Kabaseke, C., Koojo, M. S., & Kervyn, M. (2019). Study of natural disasters and of their impact on the environmental condition Rwenzori Mountain region. *Technogenic and Ecological Safety, 5*, 31–37. https://doi.org/10.5281/zenodo.2582759

Kumar, J. S., Kumar, S., Choksi, M., & Zaveri, M. A. (2020). Collaborative data acquisition and processing for post disaster management and surveillance related tasks using UAV-based IoT cloud. *International Journal of Ad Hoc and Ubiquitous Computing, 34*(4), 216–232.

Lamiur, R., Onitsuka, K., Basu, M., Shimizu, N., & Hoshino, S. (2020). Rapid emergence and increasing risks of hailstorms: A potential threat to sustainable agriculture in Northern Bangladesh. *Sustainability, 12*, 5011.

Liesbet, J., Maes, J., Mertens, K., Sekajugo, J., Thiery, W., van Lipzig, N., Poesen, J., Kervyn, M., & Dewitte, O. (2016). Reconstruction of a flash flood event through a multi-hazard approach: Focus on the Rwenzori Mountains, Uganda. *Natural Hazards: Journal of the International Society for the Prevention and Mitigation of Natural Hazards, 84*(2), 851–876.

Mair, J., Ritchie, B. W., & Walters, G. (2016). Towards a research agenda for post-disaster and post-crisis recovery strategies for tourist destinations: A narrative review. *Current Issues in Tourism, 19*(1), 1–26.

Mary, A. K., & Gomes, C. (2012). Lightning accidents in Uganda. In *2012 International Conference on Lightning Protection (ICLP)* (pp. 1–6). IEEE.

McEntire, D. A. (2015). An evaluation of risk management and emergency management. Relying on the concept of comprehensive vulnerability management for an integrated perspective. In *Risk Governance* (pp. 201–210). Springer, Dordrecht.

McKee, T. B., Doesken, N. J., & Kleist, J. (1993). The relationship of drought frequency and duration to time scales. In *Proceedings of the 8th conference on applied climatology* (Vol. 17 (22), pp. 179–183). American Meteorological Society.

Mertens, K., Jacobs, L., Maes, J., Kabaseke, C., Maertens, M., Poesen, J., Kervyn, M., & Vranken, L. (2016). The direct impact of landslides on household income in tropical regions: A case study on the Rwenzori Mountains in Uganda. *Science of the Total Environment, 550*, 1032. https://doi.org/10.1016/j.scitotenv.2016.01.171

Mertens, K., Jacobs, L., Maes, J., Poesen, J., Kervyn, M., & Vranken, L. (2018). Disaster risk reduction among households exposed to landslide hazard: A crucial role of coping appraisal? *Land Use Policy, 75*, 77–91. https://doi.org/10.1016/j.landusepol.2018.01.028

Michael, H., Isabel, M., Anderson, C. C., Min, A., Renaud, F. G., Walz, Y., Siebert, S., & Sebesvari, Z. (2019). Drought vulnerability and risk assessments: State of the art, persistent gaps, and research agenda. *Environmental Research Letters, 14*, 083002.

Mikoš, M. (2013). Risk management and mountain natural hazards. In *2nd Professional & Scientific Conference Water Management Days* (pp. 245–268).

Munich. (2013). *Munich reinsurance company annual report 2012*. Munich RE, Munich, Germany.

Montz, E. B., Tobin, A. G., & Hagelman, R. R. I. (2017). *Natural hazards: Explanation and integration* (2nd ed.). The Guilford Press.

Musoke R. (2015). *Secrets of Kasese's river of death – The Independent [05.06.2015]. The Independent 1–2*., viewed 01 July 2016 from https://www.independent.co.ug/secrets-kaseses-river-death/

NEMA (National Environment Management Authority). (2016). *State of environment report for Uganda for 2015/16*. National Environment Management Authority. http://www.nemaug.org

NEMA (National Environment Management Authority). (2018). *State of environment report for Uganda for 2017/18*. National Environment Management Authority. http://www.nemaug.org

Norman, S. (2006). New Zealand's holistic framework for disaster recovery. *The Australian Journal of Emergency Management, 21*(4), 16–20.

Nseka, D., Mugagga, F., Opedes, H., Ayesiga, P., Wasswa, H., Mugume, I., Nimusiima, A., & Nalwanga, F. (2021). The damage caused by landslides in socio-economic spheres within the Kigezi highlands of South Western Uganda. *Journal of Environmental & Socio-economic Studies, 9*(1), 23–34. https://doi.org/10.2478/environ-2021-0003

Ordaz, M., Martinelli, F., D'Amico, V., & Meletti, C. (2013). CRISIS2008: A flexible tool to perform probabilistic seismic hazard assessment. *Seismological Research Letters, 84*(3), 495–504.

Osmaston, H. (1989). Glaciers, glaciations and equilibrium line altitudes on the Ruwenzori. Quaternary and Environmental Research on East African Mountains, 31, 104.

Paquay, M., Chevalier, S., Sommer, A., Ledoux, C., Gontariuk, M., Beckers, S. K., … Ghuysen, A. (2021). Disaster management training in the euregio-meuse-rhine: What can we learn from each other to improve cross-border practices? *International Journal of Disaster Risk Reduction, 56*, 102134.

Roller, S., Wittmann, H., Kastowski, M., & Hinderer, M. (2012). Erosion of the Rwenzori Mountains, East African Rift, from in situ-produced cosmogenic10Be. *Journal of Geophysical Research: Earth Surface, 117*(F3).

Roxana, T.'ı., Zêzereb, J. L., & Lazara, G. (2018). Identification of elements exposed to flood hazard in a section of Trotus River, Romania. *Geomatics, Natural Hazards and Risk, 9*(1), 950–969. https://doi.org/10.1080/19475705.2018.1486891

Ronald, L. H., & Mary, A. C. (2016). *Lightning occurrence and social vulnerability, atmospheric hazards – Case Studies in modeling, communication, and societal impacts*, Jill S. M. Coleman, IntechOpen. https://doi.org/10.5772/63001.

Rubin, C. B., Saperstein, M. D., & Barbee, D. G. (1985). *Community recovery from a major natural disaster*. FMHI Publications. Paper 87.

Scuderi, R., Tesoriere, G., & Fasone, V. (2019). Natural events and performance of micro firms: the impact of floods on shops in Uganda. *Economia Politica, 36*(2), 609–627. https://doi.org/10.1007/s40888-019-00152-w

Singh, R., & Bartlett, D. (Eds.). (2018). *Natural hazards: Earthquakes, volcanoes, and landslides*. CRC Press.

Sioutas, M., Meaden, T., & Webb, J. D. C. (2009). Hail frequency, distribution and intensity in Northern Greece. *Atmospheric Research, 93*, 526–533. [CrossRef] 5.

Storchak, D., et al. (2015). The ISC-GEM global instrumental earthquake catalogue (1900–2009): Introduction. *Physics of the Earth and Planetary Interiors, 239*, 48–63. 5.

Twigg, J. (2015). Good practice review 9: disaster risk reduction. *Gender, Development and Disasters*, 156–177. https://doi.org/10.4337/9781782548232.00014

UN. (2017). United Nations plan of action on disaster risk reduction for resilience. Towards a Risk-informed and Integrated Approach to Sustainable Development, United Nations, New York, USA, 1–13.

UNDP. (2013). *Study of the flooding in Rwenzori Mountain for effective disaster risk management* [WWW Document], UNDP Uganda, viewed 12 June 2017, from http://www.ug.undp.org/content/dam/uganda/docs/UNDPUg2014Kasese%20Flooding%20Study2_FINAL.pdf [Google Scholar].

UNISDR. (2015a). Proposed updated terminology on disaster risk reduction: A technical review. *Community, environment and disaster risk management*. https://doi.org/10.1108/S2040-7262(2011)0000007007.

UNISDR. (2015b). *A technical review on the updated terminology on disaster risk reduction*. United Nations Office for Disaster Risk Reduction, August 2015.

UBOS. (2020). Statistical Abstract 2020. Uganda Bureau of Statistics, Kampala, Uganda

Van Damme, K., & Eggermont, H. (2011). The Afromontane Cladocera (Crustacea: Branchiopoda) of the Rwenzori (Uganda–DR Congo): Taxonomy, ecology and biogeography. *Hydrobiologia, 676*(1), 57–100.

Weatherill, G., Pagani, M., & Garcia, J. (2016). Exploring earthquake databases for the creation of magnitude-homogeneous catalogues: Tools for application on a regional and global scale. *Geophysical Journal International, 206*(3), 1652–1676.

Wisner, B., Blaikie, P., Cannon, T., & Davis, I. (2014). At risk: natural hazards, peoples vulnerability and disasters. In *At risk: Natural hazards peoples vulnerability and disasters*. https://doi.org/10.4324/9780203714775.

World Bank. (2019). Disaster risk profile: Uganda. The International Bank for Reconstruction and Development, The World Bank Group, Washington, USA.

Chapter 6
Assessing the Vulnerability of the Eastern Africa Highlands' Soils to Rainfall Erosivity

Seth O. Nyawacha and Viviane K. Meta

Abstract The highland areas of the Eastern Africa region are the most productive areas agriculturally, acting as the main food basket for the region. Over the years, these areas have undergone increased population pressure coupled with urbanization leading to substantive decline in agricultural land. The increased pressure on the productive areas is also threatening the existence of ecosystem and other natural habitats such as forests and wetlands. Ultimately, the over-cultivation of land is leading to loss of soil nutrients depended on by plants due to soil erosion and soil leaching. As a result, soil becomes degraded after losing its quality and productivity by reducing infiltration rates, water-holding capacity, nutrients, organic matter, soil biota, and soil depth. Soil erosion also has an impact on ecosystem services such as water quality and quantity, biodiversity, and agricultural productivity. This study, therefore, seeks to assert the hypothesis that African mountains are susceptible to soil erosion, as a result to rainfall erosivity, by modelling using the Revised Universal Soil Loss Equation (RUSLE). The model is developed using five variables, i.e. rainfall erosivity factor (*R*), soil erodibility factor (K), slope length and steepness factor (LS), cover management factor (*C*), and conservation practice factor (*P*) for the estimation of the areas susceptible to soil loss in the Eastern Africa Highlands (Fenta et al., 2020). This study seeks to answer the validity of the hypothesis that the Eastern African Mountains (highlands) are susceptible to high soil erosion levels contributed by the geomorphological nature, rainfall, soil, and the influence of vegetation cover using earth observation datasets within a GIS environment.

Keywords Soil degradation · Soil erosion · Land susceptibility · Soil vulnerability · Soil Erodibility · Erosivity · Erosive force · Abrasion · RUSLE · Soil · Saltation · Creeping · Suspension

S. O. Nyawacha (✉) · V. K. Meta
The Technical University of Kenya, Jomo Kenyatta University of Agriculture and Technology, Space Generation Advisory Council, Nairobi, Kenya
e-mail: Vivianne.meta@locateit.co.ke

S. Adelabu et al. (eds.), *Remote Sensing of African Mountains*,
https://doi.org/10.1007/978-3-031-04855-5_6

6.1 Introduction

Rainfall erosivity is a force that acts on soil particles to cause soil particle movement through either creeping, saltation, or suspension, while soil erosion is the movement or abrasion of soil particles influenced by factors such as the physical properties of the soil particles including the weight and the chemical composition. External forces including wind and water as the major causes of soil particle movement (Fenta et al., 2020). Notably, the movements of large herds of cattle causing a cloud of fine particle suspension in the air acts as soil-crust busters, thus this activity cannot be directly associated as a cause to soil erosion.

Soil particles abrasion is dependent on the external forces, which combines with physical soil characteristics to cause motion in the direction of the force. The external forces, i.e. wind and water, need to surpass the minimum threshold force to initiate particle motion, while on the other hand, the soil particle has to be light enough, devoid of air spaces that causes floating tube effect, and the particles location be devoid of barriers such as vegetation and artificial blockages(Fryrear et al., 1994). Soil particles properties are a result of soil forming processes including weathering and tectonic movements influenced by anthropogenic factors. Anthropogenic factors influences the properties of soil over time, and as a result, affect soil particle strength to resist motion and infiltration (Djukem et al., 2020). Over time, the soil particle losses the resilience and coping mechanism to resist abrasion by the agents of erosion.

The East African Mountains represent the most arable areas of the continent with approximately 40% of the arable land between the tropics located on the mountainous regions. These areas are prone to high amounts of rainfall characterized by bimodal rainfall patterns. The rainfall patterns experienced in these areas advance intensive agricultural activities with little or no soil care practices. Instead, the agricultural areas have high levels of fertilization over time, increasing the acidity of the soil leading to loss of organic carbon content in the soil. This increases the carbon emission to the atmosphere, becoming one of the major contributors to climate change.

Agricultural practices have increased soil erosion and leaching in the mountainous areas than in undulating terrains (Kadomura and Yamamoto, 1978). There is, however, an alarming concern for soil conservation in highland areas due to its dwindling ability of food production. The loss of soil fertility has affected the crop productivity over time with the world glaring at a possible global food shortage by 2050 as soil productivity and arable lands continue to shrink (Kirui & Mirzabaev, 2014; Tilahun, M. (2015)). (Developing countries lack deliberate focus in assessing the degradation extent and putting in place conservation measures or building resilience that will exponentially reduce the adverse effects and reverse long-term soil leaching (Haregeweyn et al., 2015; Hurni et al., 2015).

Generally, forces that propagate soil erosion are influenced by different factors including climatic conditions, and in the case of the Eastern Africa Mountains, the amount of runoff water as well as the steep slope and terrain greatly influences soil

erosion. Other factors such as temperature, soil type as those endowed with organic matter are easily eroded downstream (Fenta et al., 2020). Other factors may also include the availability of opposing forces such as vegetation cover, artificial barriers, and the soil crusting effect believed to be the coping mechanism of the soil particles to resist erosion, majorly affecting the arid and semi-arid areas, among others (Fryrear et al., 1994).

6.2 Materials and Methods

6.2.1 Data

The increased need for open and validated data is leading to the development and deployment of the various data cubes across the geospatial space; since Geospatial data is expensive to produce and maintain, there is a concerted effort among layers to develop data hub that simplifies the data access for retrieval and analysis (Fryrear et al., 1994). Analyzing and studying phenomenon such as land degradation and the effect of water on soil erosion was a costly venture, the application and use of Earth Observation techniques and Geographic Information Science (GIS) is gaining traction. The data access from platforms such as Google earth engine is easing complex environmental modelling.

Climaticdatasets was sourced from Terra Climatology using a direct Application Programming Interface, from Google earth engine (GEE) (http://www.climatologylab.org/terraclimate.ht ml) (Abatzoglou et al. 2018). Soil datasets, International Soil Reference Information Centre (ISRIC) produced the prerequisite soil texture datasets (https://www.isric.org/). With GEE developed, it is easier to acquire and process dataset in the java script coding environment compared to initial raw soil data download and processing.

Harmonized World Soil Database (HWSD) complimented the no data values, especially in the desert areas that are not recorded by the satellite sensors. The HWSD database is a database with over 15, 000 different soil mapping units that combines existing regional and national updates of soil information worldwide (SOTER, ESD, Soil Map of China, WISE) with the information contained within the 1:5 000,000 scale FAO-UNESCO Soil Map of the World (FAO/UNESCO Soil Map of the World | FAO SOILS PORTAL | Food and Agriculture Organization of the United Nations, 2022). The land cover dataset originated from the Climate Change Initiative (CCI) a sentinel 2-100 meter resolution product, with the most current available datasets of 2019, reclassified using *C* factor values (Fryrear et al., 1994), also applied by (Fenta et al., 2020).

United Nations Convention to Combating Desertification (UNCCD) (https://www.unccd.int/) provided the user manual to interpret the land-use land cover product. The fractional cover data is product of ESA Proba V 100 meter resolution sensor.

6.2.2 Study Area

The Eastern Africa highlands exist within the Inter Convergence Tropical Zone, experiencing warm and temperate climatic condition. The higher altitude areas, however, also experience snowing. The higher the altitude of the mountains with constant change/variation in temperature, the snowy it becomes.

The Eastern Africa highlands have various volcanic mountains formed due to tectonic movements forming a complex structure at the intersection of fault lines in the Rift Valley. Some of these mountains are active volcanoes such as Mount Kilimanjaro, while others present a more dormant nature, e.g. mount Kenya, with Mount Ruwenzori's peculiarity of not being a volcanic mountain standing out.

The Eastern Africa region is located between 21° west, 52° east, 12.5° south, and 23° north of equator (Fig. 6.1). It is estimated to have between 350 million to 365 million people (United Nation, 2019), with expectation of the population doubling by 2050, which is also consistent with the global population projection of 2050.

The impact of soil erosion due to water in these areas is under researched; thereby assessing the accurate amounts of soil loss due to water erosion is accurately not attainable but precisely computed.

However, studies have shown that the high precipitation levels, the slope distance, and degree immensely contribute to mass movement of soil by water downhill. This phenomenon has exposed the area to loss of nutrient-rich soil affecting the general productivity of the soils upstream.

This area exists within the Great Rift Valley belt, with a complex geomorphological structure and very high elevated areas such as Mt. Kenya and Mt. Kilimanjaro, as well as with steep valleys and extensive plains caused by the complex geomorphological processes such as tectonic plate movements (Freund & Merzer, 1976).

6.3 Assessment of Soil Abrasion as a Result of Rainfall Erosivity

Soil erosion by water is dependent on several regional scales. The contemporary mode of assessing soil erosion by water and wind entails a process-based methodology that assesses at field level (Morgan et al., 1998).

The ability to compute rasters in Geographic Information Systems has ensured successful modelling of the susceptible areas of soil loss by water using different models, among them being the GIS-based Revised Universal Soil Loss Equation (RUSLE).

The Revised Universal Soil Loss Equation (RUSLE) simplifies the process-based models, while maintaining the authenticity and integrity of predicting vulnerable areas to soil loss (Fenta et al., 2020)

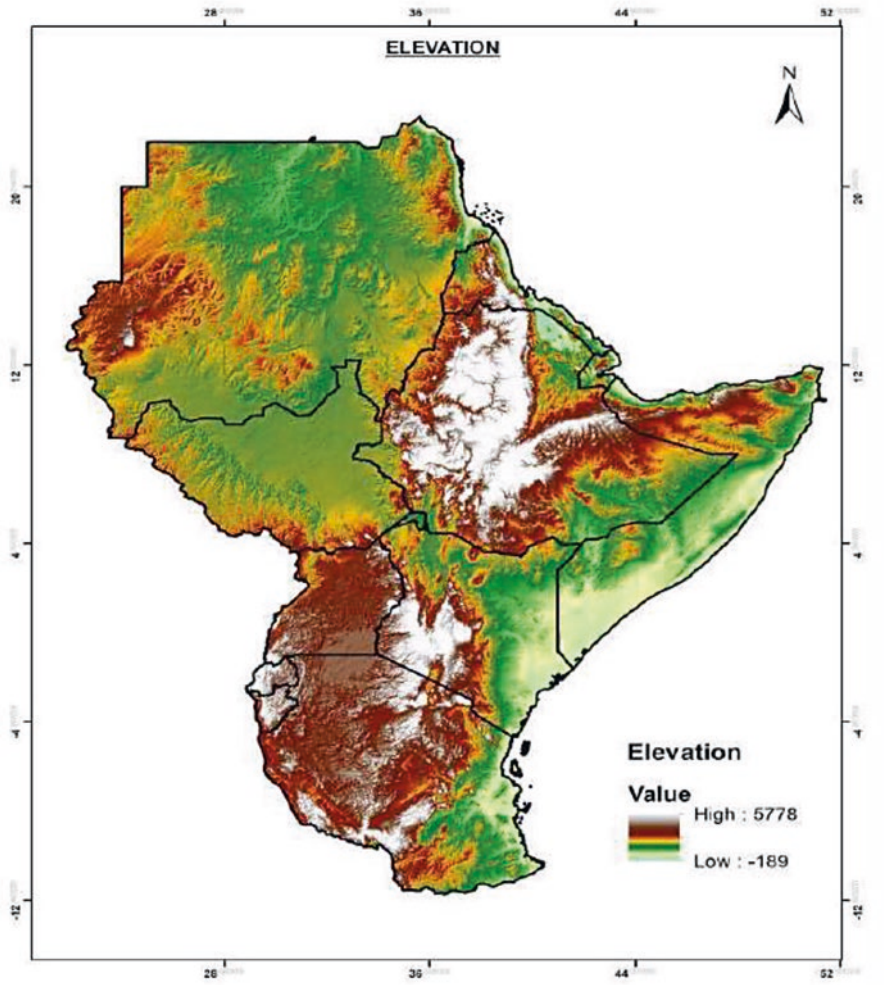

Fig. 6.1 Altitude map of the eastern Africa region, with an emphasis on the areas with high elevation

The RUSLE model ingest five factors including the rainfall erosivity, soil erodibility factor, slope, and steepness of the surface, anthropogenic factors influenced by land use and the conservation management practices (Fenta et al., 2020) (Eq. 6.1).

$$RE = R * K * LS * C * P \tag{6.1}$$

R is the rainfall amount in millimeters, the influencing force to causing soil abrasion, *K* is the Soil Erodibility factor or the tendencies of soil to movement by a force of a certain magnitude, *and* LS is the slope length, while *C* and *P* are the surface cover factor and conservation management practices, respectively. However, it is

evidently difficult to assess the effect of management practices, as those practices are not documented. Assessing management practices *P* requires a rigorous field assessment and calibration for parameterizing the management practices in the field. This technicality led to most scholars applying proxy data such as vegetation cover, while developing a linear correlation management practice and its impact on soil conservation (Ligdi & Morgan, 1995).

For rainfall, it is more relevant when presented in millimeters, and the characterization of its intensity is possible. However, rainfall intensity is normalized through a transformation, and values rescaled between the values of one and two. With the latter representing the highest rainfall erosivity as shown in Fig. 6.2, soil erodibility factor, on the other hand, is directly proportional to the organic matter content and calcium carbonate content.

Soil movement by water is dependent on various properties including the soil moisture content, which influences the weight of the particle, with most mountainous soil particles endowed with loam and sandy loam, with an approximate size of 0.063–0.250 mm (M et al., 2004). The hydraulic conductivity properties of soils also affect the soil particle abrasion as well as the infiltration ability of a soil particle, with the clay soil having the lowest soil infiltration strength.

Soil erodibility in the mountainous region is modelled using the Eq. 6.2. The model takes into account organic matter content in soil, *s* and *p* values based on the size of soil particle, where in Eastern Africa 2.5 diameter is used to develop the soil erodibility model (Fig. 6.3).

Equation 6.2: Soil Erodibility model.1

$$K = \left(\frac{2.1 * 10^{-4} M^{2.14} \left(12 - OM\right) + 3.25\left(s - 2\right) + 2.5\left(p - 3\right)}{100} \right) * 0.1317 \quad (6.2)$$

It is worth noting that soil erodibility factor was also modelled based on soil color and soil types as highlighted by (Meshesha et al., 2012). The other modelling was based on geometric mean particle as demonstrated by Dangler and El-Swaify (1976). The cover management factor interrogates the effect of plant cover either crops or non-crops, while giving each category a cover factor (*c*-factor). The *C* factor values are different depending on the vegetation density. For instance, cereal grains have between 0.20 and 0.38 depending on the density of either maize, rice, or other cereal crops available. Leguminous crops have a *c* factor value of 0.32, while oil seed crops vary from 0.28 to 0.50. The tree cover crops such as tea and sugarcane have a value from 0.15 to 0.20 (Panagos et al., 2015).

(Ligdi & Morgan, 1995) generated a linear correlation between the cover management factor and Normalized Difference Vegetation Index (NDVI), developing an equation of the form as highlighted in Eq.6.3. The equation acknowledges the role that vegetation plays in curbing or promoting any form of soil abrasion.

$$C = 1.02 - 1.21 * \mathrm{NDVI} \quad (6.3)$$

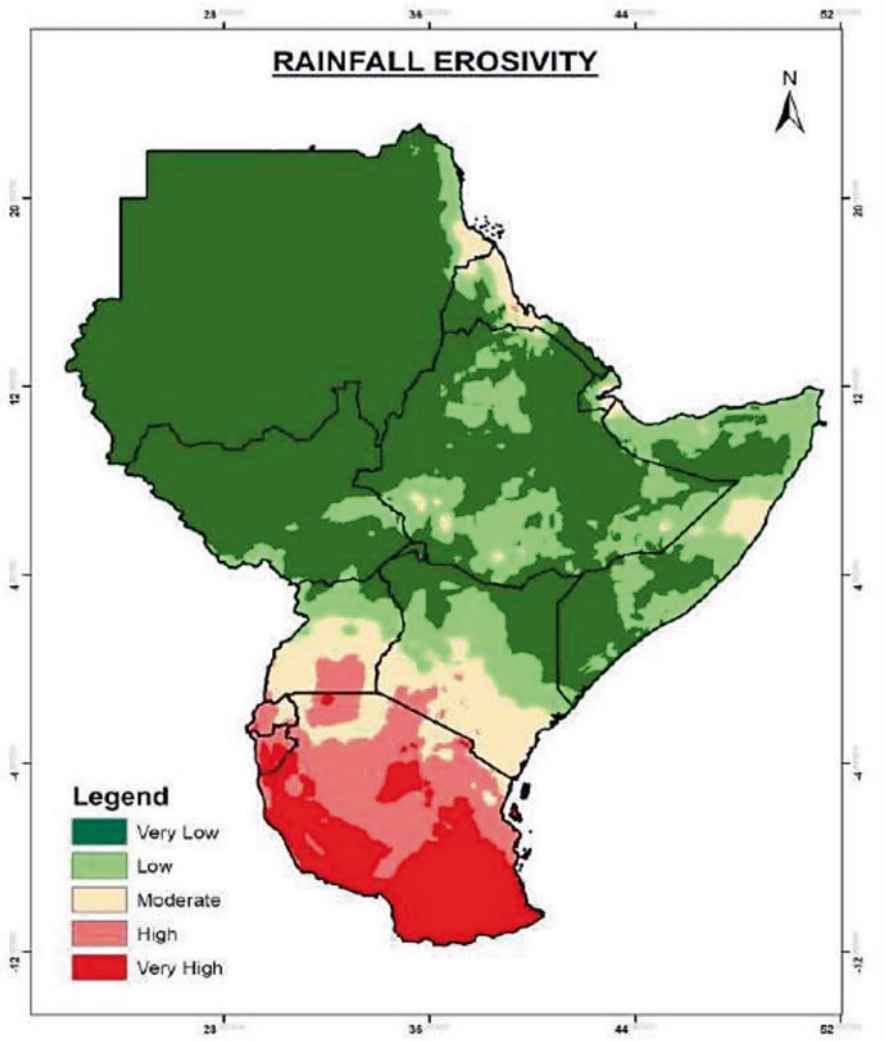

Fig. 6.2 Rainfall erosivity in the Eastern Africa

The above model is used in assessing the cover management factor in Eastern Africa as shown in Fig. 6.4

The *P* factor, which represents various soil erosion management for conservation purposes, has a high correlation with the Slope length (LS) and aspect. The various LS percentages are reclassified to a *P* factor value representing the management practices.

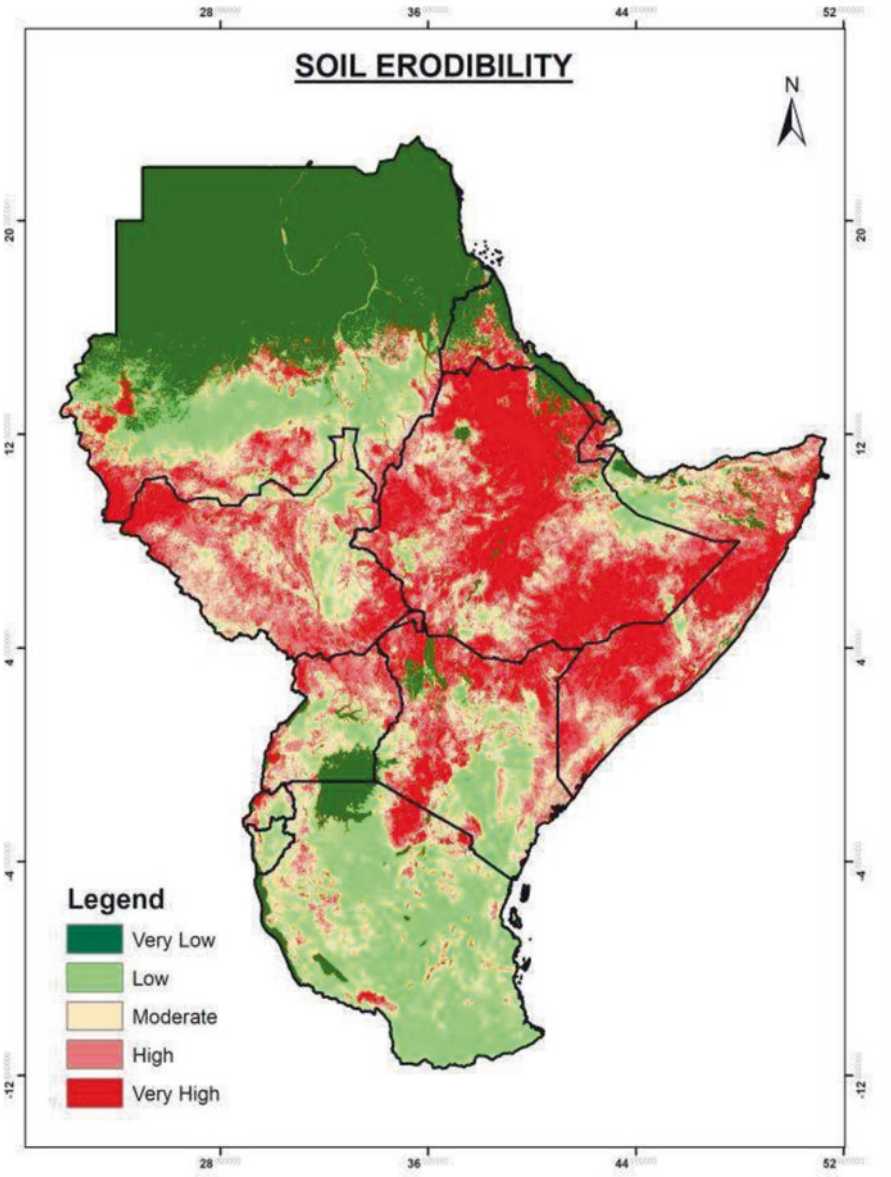

Fig. 6.3 Soil erodibility in the Eastern Africa Area in 2020

(Lufafa et al., 2003) developed a linear correlation model that relates the conservation practices to percentage slope as is highlighted in Eq. 6.4. *Conservation management practice linear correlation eq.* 6.4.

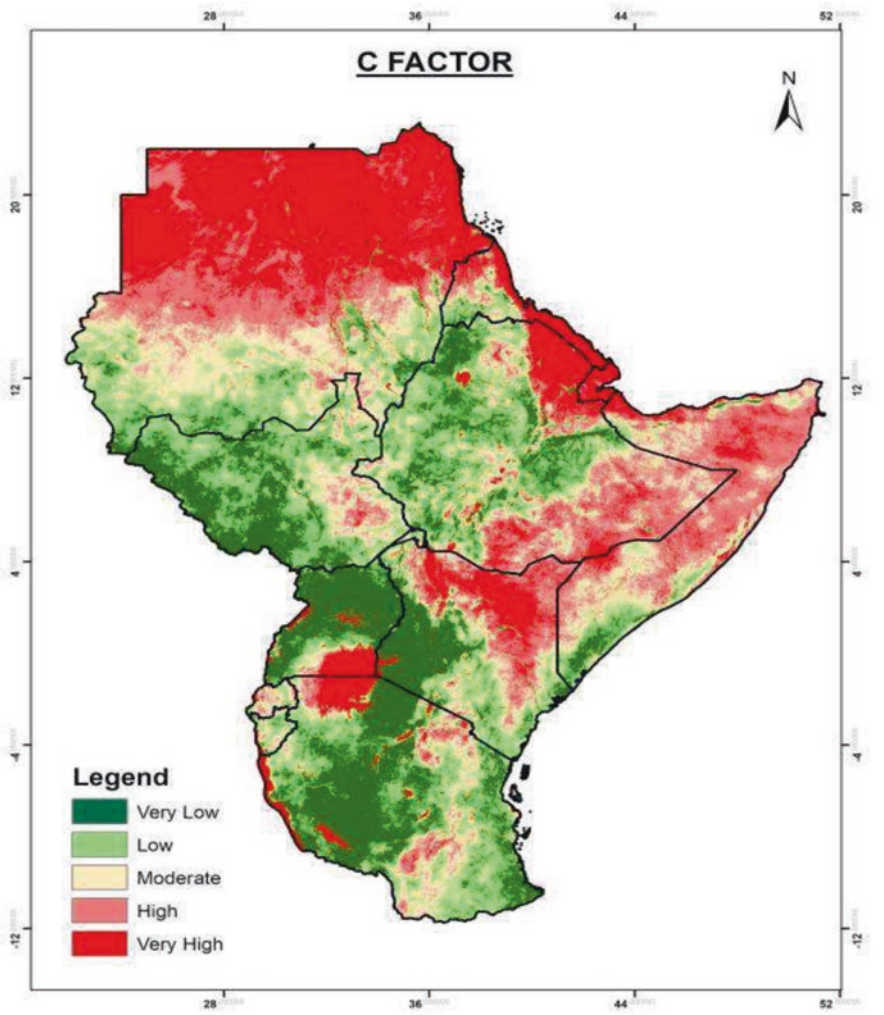

Fig. 6.4 *C* factor in the Eastern Africa region

$$P = 0.2 - 0.03 * \text{Percent Slope} \tag{6.4}$$

The management factor is high in areas surrounding the highland regions (Fig. 6.5). These areas experiences intensive agricultural practices and depict an inverse correlation to the *C* factor. The areas of high *C* factor are characterized with low agricultural practices, with desert-like climatic condition.

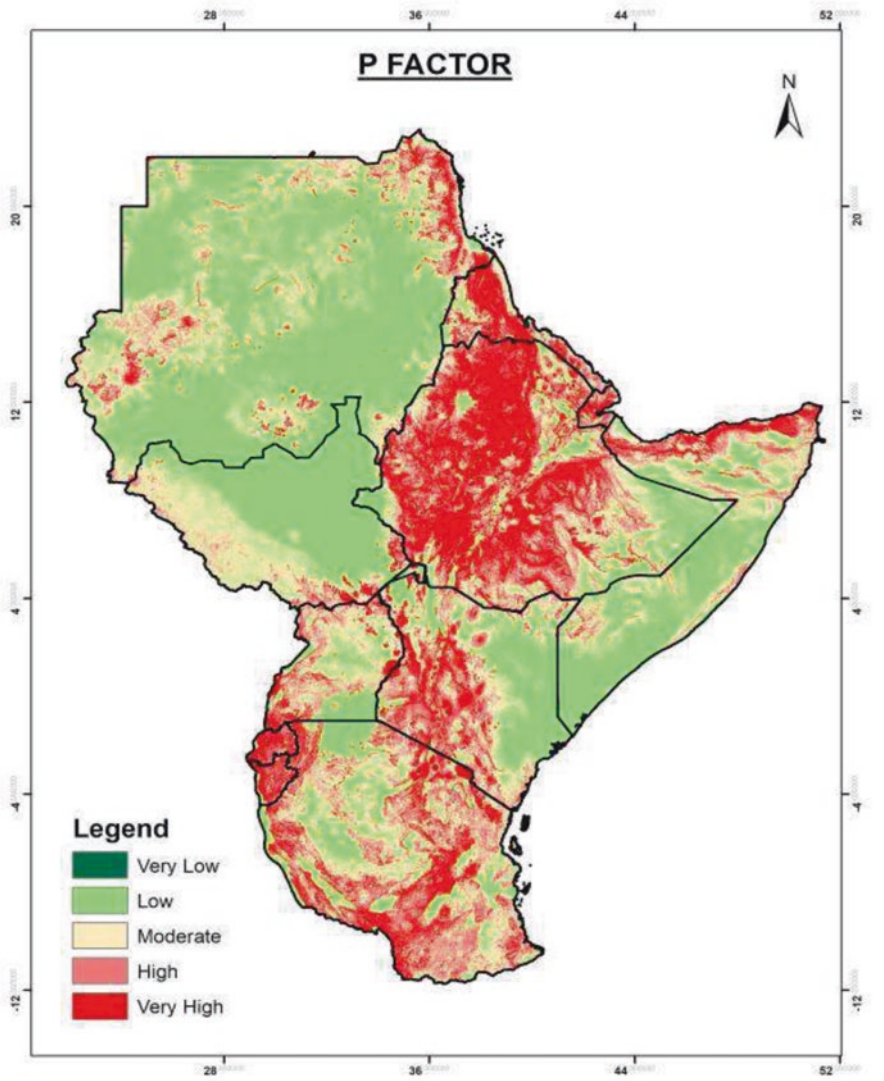

Fig. 6.5 The management conservation practices in the Eastern Africa region

6.4 Results and Discussion

6.4.1 Spatial Distribution of Rainfall Erosivity Risk Areas

The attribution of soil erosion to water is mainly visible in the high-elevated areas of the region, with rainfall intensity, slope length, and aspect being the major driving factors to soil particle movement (Fig. 6.6).

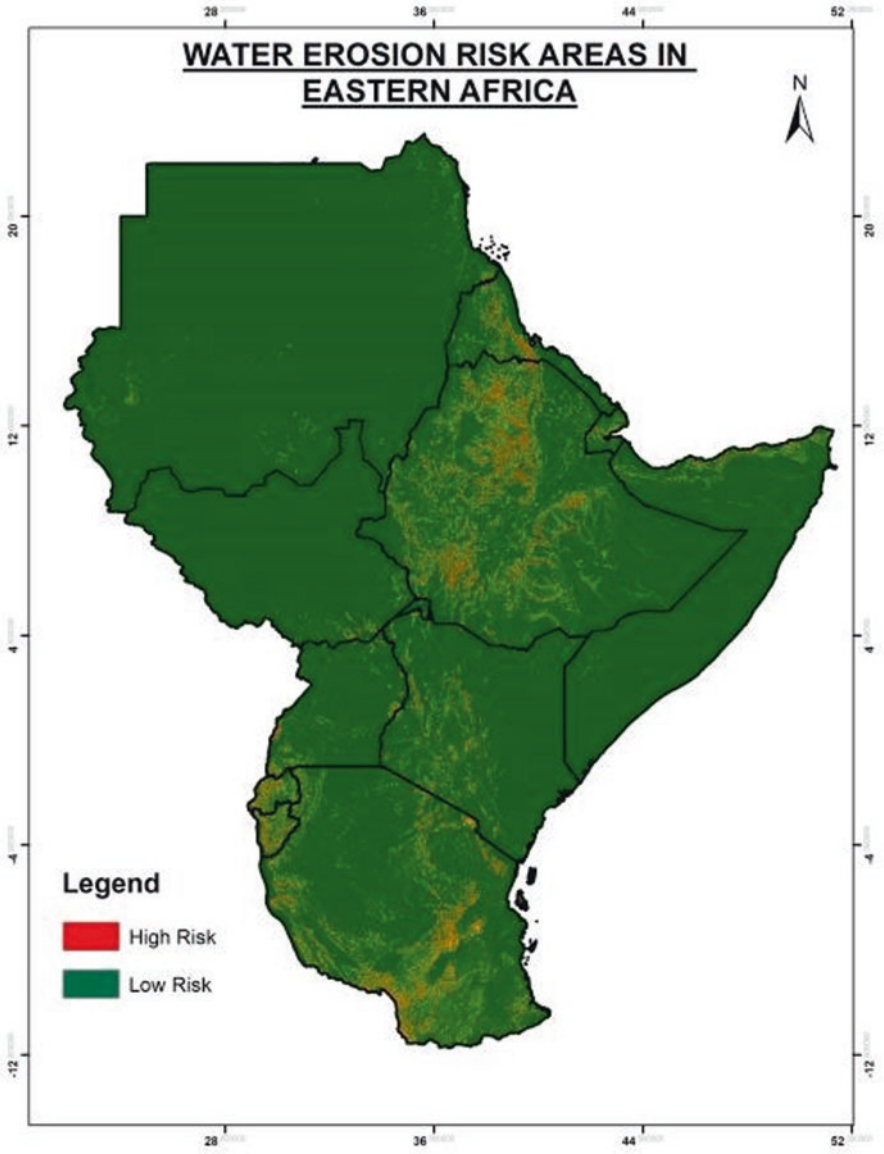

Fig. 6.6 Water erosion risk areas in the Eastern Africa in 2020

The spatial distribution is concentrated around the rift valley and the highland areas.

The results of areas depicting high rainfall erosivity coincide with high altitude areas, with part of Ethiopian highlands, Kenyan Rift Valley highlands, Rwanda and Burundi Hills showing high rainfall sensitivity. Countries like Burundi show sensitivity of above 80% of susceptibility. The combination of the factors to model

rainfall sensitivity depicts areas that are not only affected by the surface ruggedness and steep slope, but also factors such as soil physical and chemical properties.

Rainfall erosivity high sensitive areas are around the highlands and mountainous regions, confirming the hypothesis that the Eastern African Mountains are vulnerable to soil erosion and mass wasting caused by erosive force of water.

The Ethiopian highlands, where agriculture is practiced, presented approximately 15% of areas susceptible to water erosion. However, from the management practice modelled, the areas showed high conservation practices such as contour farming, which is attributed to high level of agricultural activities in the highly elevated areas (Fig. 6.5).

The South Eastern Tanzanian Highlands, with fairly a high elevation value, has approximately 5% of the areas susceptible to water erosion. This is influenced by the nature of agricultural practices (unsafe practices) or pure management practices. However, these areas also present the highest level of rainfall erosivity (Fig. 6.2).

Generally, around Eritrea and Djibouti, the soil particle and the climatic conditions contribute to the susceptibility to water erosion. These areas do have high-elevated areas, although rainfall annual average is low, the areas have soil particle that are susceptible to abrasion (Fig. 6.7).

Rwanda, with more than 85% of the areas susceptible to water erosion, is endowed with rugged terrain and high rainfall amount annually. The surface steepness and the slope length factor plays a major role in contributing to the high and runoff erosivity in the areas.

Kenya has approximately 5% pockets of susceptible areas around the Rift Valley Highlands and the Central highlands region, areas that practice intensive agriculture. The high rainfall capacity received as well as the slope length and aspect contributes immensely to the susceptibility of these areas to water erosion.

The other areas such as South Sudan and Sudan are generally flat and may not be subject to highland type of climatic and topographical conditions. The area west and south of Sudan, with a pocket of high-elevated areas, shows a 2% susceptibility to water erosion confirming the hypothesis that high areas are under constant threat to land degradation by water.

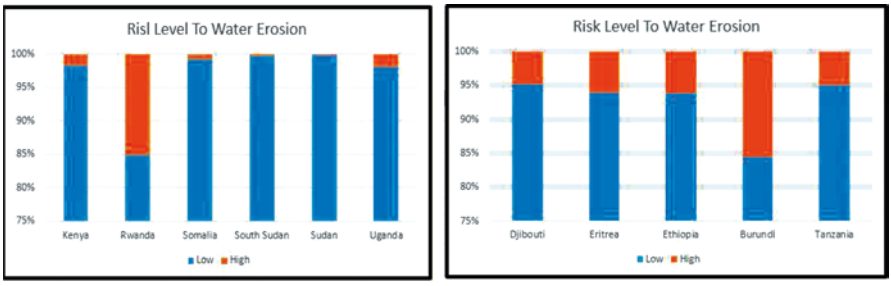

Fig. 6.7 Graph showing the statistics distribution of risk areas to water erosion in Eastern Africa

6.5 Conclusion and Recommendations

This study has asserted the hypothesis that the Eastern Africa Mountains experiences high risk to soil erosion and mass wasting as a result of high rainfall amount and other factors such as soil structure, soil texture, vegetation cover, and management practices.

It is the study's recommendation that more conservation measures and management practices be initiated in order to conserve the soil nutrients for a fortunate agricultural practice in the Eastern African Mountains.

References

Abatzoglou, J. T., Dobrowski, S. Z., Parks, S. A., Hegewisch, K. C. (2018). Terraclimate, a high-resolution global dataset of monthly climate and climatic water balance from 1958–2015, Scientific Data.

Borrelli, P., Lugato, E., Montanarella, L., & Panagos, P. (2016). A New Assessment of Soil Loss Due to Wind Erosion in European Agricultural Soils Using a Quantitative Spatially Distributed Modelling Approach. *Land Degradation & Development, 28*(1), 335–344. https://doi.org/10.1002/ldr.2588

Dangler, E. W., & El-Swaify, S. A. (1976). Erosion of Selected Hawaii Soils By Simulated Rainfall. *Soil Science Society of America Journal, 40*(5), 769–773. https://doi.org/10.2136/sssaj1976.03615995004000050040x

Djukem, W. D. L., Braun, A., Wouatong, A. S. L., Guedjeo, C., Dohmen, K., Wotchoko, P., Fernandez-Steeger, T. M., & Havenith, H. -B. (2020). Effect of Soil Geomechanical Properties and Geo-Environmental Factors on Landslide Predisposition at Mount Oku, Cameroon. *International Journal of Environmental Research and Public Health, 17*(18), 6795. https://doi.org/10.3390/ijerph17186795

FAO/UNESCO Soil Map of the World | FAO SOILS PORTAL | Food and Agriculture Organization of the United Nations. (2022). Fao.org. https://www.fao.org/soils-portal/data-hub/soil-maps-and-databases/faounesco-soil-map-of-the-world/en/

Fryrear, D. W., Krammes, C. A., Williamson, D. L., & Zobeck, T. M. (1994). Computing the wind erodible fraction of soils. *Journal of Soil and Water Conservation, 49*(2), 183–188. https://www.jswconline.org/content/49/2/183.short

Fenta, A. A., Tsunekawa, A., Haregeweyn, N., Poesen, J., Tsubo, M., Borrelli, P., Panagos, P., Vanmaercke, M., Broeckx, J., Yasuda, H., Kawai, T., & Kurosaki, Y. (2020). Land susceptibility to water and wind erosion risks in the East Africa region. *Science of the Total Environment, 703*, 135016. https://doi.org/10.1016/j.scitotenv.2019.135016

Freund, R., & Merzer, M. (1976). The formation of rift valleys and their zigzag fault patterns. *Geological Magazine, 113*(6), 561–568. https://doi.org/10.1017/s0016756800041315

Haregeweyn, N., Tsunekawa, A., Nyssen, J., Poesen, J., Tsubo, M., Tsegaye Meshesha, D., Schütt, B., Adgo, E., & Tegegne, F. (2015). Soil erosion and conservation in Ethiopia. *Progress in Physical Geography: Earth and Environment, 39*(6), 750–774. https://doi.org/10.1177/0309133315598725

Hurni, H., Giger, M., Liniger, H., Mekdaschi Studer, R., Messerli, P., Portner, B., Schwilch, G., Wolfgramm, B., & Breu, T. (2015). Soils, agriculture and food security: the interplay between ecosystem functioning and human well-being. *Current Opinion in Environmental Sustainability, 15*, 25–34. https://doi.org/10.1016/j.cosust.2015.07.009

Kadomura, H., & Yamamoto, H. (1978). Man-induced erosion: the rate of erosion and an example from Okinawa Island, Southern Japan. *Journal of Geography (Chigaku Zasshi), 87*(1), 1–15.

Kirui, O. K., & Mirzabaev, A. (2014). Economics of land degradation in Eastern Africa. Econstor. eu. https://doi.org/http://hdl.handle.net/10419/99988

Ligdi, E. E., & Morgan, R. P. C. (1995). Contour grass strips: a laboratory simulation of their role in soil erosion control. *Soil Technology, 8*(2), 109–117. https://doi.org/10.1016/0933-3630(95)00011-0

Lufafa, A., Tenywa, M. M., Isabirye, M., Majaliwa, M. J. G., & Woomer, P. L. (2003). Prediction of soil erosion in a Lake Victoria basin catchment using a GIS-based Universal Soil Loss model. *Agricultural Systems, 76*(3), 883–894. https://doi.org/10.1016/s0308-521x(02)00012-4

Lujan, D. L. (2006). Soil physical properties affecting soil erosion in tropical soils. Invited presentations, college on soil physics, 232–245.

M, G. D., Ghirardi, G., R, N. D., Pla Sentis, I, & L, S. E. (2004). Invited presentations. College on soil physics 2003. Osti.gov. https://www.osti.gov/etdeweb/biblio/20946943

Meshesha, D. T., Tsunekawa, A., Tsubo, M., & Haregeweyn, N. (2012). Dynamics and hotspots of soil erosion and management scenarios of the Central Rift Valley of Ethiopia. *International Journal of Sediment Research, 27*(1), 84–99. https://doi.org/10.1016/s1001-6279(12)60018-3

Morgan, R. P. C., Quinton, J. N., Smith, R. E., Govers, G., Poesen, J. W. A., Auerswald, K., Chisci, G., Torri, D., & Styczen, M. E. (1998). The European Soil Erosion Model (EUROSEM): a dynamic approach for predicting sediment transport from fields and small catchments. *Earth Surface Processes and Landforms, 23*(6), 527–544. https://doi.org/3.0.co;2-5">10.1002/(sici)1096-9837(199806)23:63.0.co;2-5

Panagos, P., Borrelli, P., Meusburger, K., Alewell, C., Lugato, E., & Montanarella, L. (2015). Estimating the soil erosion cover-management factor at the European scale. *Land use policy, 48*, 38–50.

Tilahun, M. (2015). The Economics of Land Degradation in Africa_Benefits of Action Outweigh the Costs_A complementary report to the ELD Initiative. Cgiar.org. https://doi.org/http://www.eld-initiative.org/

Chapter 7
Development of Lightning Hazard Map for Fire Danger Assessment Over Mountainous Protected Area Using Geospatial Technology

Dipuo Olga Mofokeng, Adeyemi Olusola, and Samuel Adelabu

Abstract Lightning is regarded as a leading cause of fatalities, injuries, property damages, and interruptions to businesses. As against some other tropical countries, especially around the equator in Africa and South America, South Africa does not experience as much lightning activity; however, it is still considered a lightning-prone country. With the advent of remote-sensing technology and its capabilities, the world can detect nearly all lightning strikes in real-time with the ability to also geolocate the strike with high temporal and spatial accuracy. This study aims to advance the understanding of the geography of CG lightning activity in South Africa through the application of geospatial technology. Using spatial analysis techniques, this research evaluated 11-year lightning data (2007–2017) to develop a lightning hazard map for Golden Gate Highlands National Park. The monthly strike count of lightning increases from the minimum value in July (0.08%) and displays a peak in December (23.80%). The average diurnal variation (2007–2017) suggests that lightning is more prevalent in terms of occurrence from 14:00 to 18:00 SAST with two clear maxima at 15:00 SAST and 17:00 SAST. The lowest lightning activity is during the morning hours at 05:00 and 06:00 SAST, and yet again at hour 08:00 SAST. The average diurnal variation (2007–2017) suggests that lightning is more prevalent in terms of occurrence from 14:00 to 18:00 SAST with two clear maxima at 15:00 SAST and 17:00 SAST. The lowest lightning activity is during the morning hours at 05:00 and 06:00 SAST, and yet again at hour 08:00 SAST.

D. O. Mofokeng (✉)
Department of Geography, Afromontane Research Units (ARU), University of the Free State, Phuthaditjhaba, Free State, South Africa

A. Olusola · S. Adelabu
Department of Geography, University of the Free State, Bloemfontein Campus, South Africa

S. Adelabu et al. (eds.), *Remote Sensing of African Mountains*,
https://doi.org/10.1007/978-3-031-04855-5_7

Spatial autocorrelation analysis revealed that the clustering of lightning strikes at the park is at the distance of about 1.2 km. This connotes that strikes clustered with other strikes are not likely to strike an individual specific location from centre of cluster of strikes much beyond a circle with a radius of 1.2 km.

Keywords Lightning · Spatial Statistics techniques · Remote Sensing · Fire Danger Assessment

7.1 Introduction

Lightning as an activity most likely predates human existence (Gijben, 2012, Rakov and Uman, 2003) and even a critical meteorological phenomenon. Lightning is regarded as a leading cause of fatalities, injuries, property damages, and interruptions to businesses (Cha et al., 2017, Gijben et al., 2017). By definition, lightning can be described as the release of static electricity in the sky or between the clouds and the ground (Gijben, 2012, Rakov and Uman, 2003). On a global scale, lightning is responsible for not more than 24,000 deaths and 240,000 injuries on an annual basis (Blumenthal et al., 2012). From Earth Observation Satellites (EOS), about 39–49 lightning flashes are captured around the globe per second. This is translated to about 1.4billion flashes per day on a Cloud-to-Ground (CG) scenario (Christian et al., 2003, Gijben et al., 2017).

As against some other tropical countries, especially around the equator in Africa and South America, South Africa does not experience as much lightning activity; however, it is still considered a lightning-prone country (Bhavika, 2007, Gijben, 2012). Yearly death rates from lightning in South Africa is 6.3 per million of the population, which is 15 times more than the global average (Gill, 2009). This figure is presumed to be underestimated per actual mortality rate. This underestimation is likely to be because lightning deaths are not rigidly reported in rural areas (Gijben et al., 2017). As a natural ignition source for global fire, lightning activities were recently operationalized as one of the driving factors in fire danger or risk modelling (Chuvieco et al., 2014, 2010, Eskandari and Chuvieco, 2015, Huang et al., 2015). According to Cha et al. (2017), an average of 816 fires were ignited by lightning each year globally.

During 2005, lightning fire burnt a large area of fynbos and commercial timber plantation in Tsitsikamma, Western Cape Province of South Africa (Durrheim, 2010). According to the Council for Scientific and Industrial Research (CSIR) report on the Elandskraal fire that ravaged approximately 9440 hectares, it was revealed that the positive lightning strike observed on the 22 March 2017 was responsible for the fire which started on the 07 June 2017 (Frost et al., 2018).

With the advent of remote-sensing technology and its capabilities, the world can detect nearly all lightning strikes in real-time with the ability to also geolocate the strike with high temporal and spatial accuracy. Numerous studies have focused on understanding lightning activities in many countries using different lightning

location systems (Christian et al., 2003; Rakov and Uman, 2003; Kigotsi et al., 2018). Most of the lightning systems detect electromagnetic reading using Time of Arrival (ToA) and Magnetic Direction Findings (MDF) methods or a combination of ToA and MDF. A summary of literature relating to the methods can be found in (Gill, 2009). These systems are either ground-based or satellite lightning sensors. The latter detects lightning from space through the earth-orbiting satellite which either detects light or electromagnetic waves from lightning discharge (Rakov and Uman, 2003). The well-known satellite-lightning sensors include National Aeronautical & Space Administration (NASA) Optical Transient Detector (OTD) and Lightning Imaging Sensors (LIS) on-board the Tropical Rainfall Measuring Mission (TRMM) (1997–2014) (Christian et al., 2003, Kigotsi et al., 2018). Formerly, sensors which detect electromagnetic pulse in very low frequency (VLF) or low frequency (LF) include regional Lightning Detection Network (LDN) such as United States of America National Lightning Detection Network (USA NLDN) and Southern African Lightning Detection Network (SALDN) in South Africa. Global LDN includes World Wide Lightning Location Network (WWLLN) and the Global Lightning datasets (Kigotsi et al., 2018).

The spatio-temporal lightning flash density and occurrence have been investigated in the United States (Bentley and Stallins, 2005); Canada (Cha et al., 2017), Europe (Anderson and Klugmann, 2014), Mediterranean (Price and Federmesser, 2006), India (Dewan et al., 2018), Africa (Kigotsi et al., 2018, Mayet et al., 2016) at the global scale (Cecil et al., 2014, Christian et al., 2003). According to Evert and Schulze (2005), studies on lightning have been in existence for about eight decades. However, in the past couple of years, there has been tremendous growth in South Africa as a result of the introduction of the National System (see Gill, 2009). Gill (2009) was the first to utilize the 2006 SALDN data in the development of the climatology of South Africa. This was later updated by Gijben (2012) using the 2006–2010 dataset. Recently, Evert and Gijben (2017) utilized the 2006–2017 SALDN data to update the national lightning flash density map over South Africa. In their study, Evert and Gijben (2017) observed that the highest flash density occurs along the eastern escarpment of the country with values exceeding 15 flashes km^{-2} $yr.^{-1}$.

Despite the availability of geo-coordinated lightning data, most CG lightning studies found within the country (South Africa) typically only focus on visualizing the distribution of CG lightning activity as a flash density for the simple purpose of identifying areas of high flash density rate. These forms of studies often do little in explaining the observed spatial patterns of flash density. Furthermore, based on the uniqueness of the country's physiography, there are landscapes across the country that are unique to lightning activities, such as montane environments. Montane environments within South Africa are unique, in that they serve as places of water towers for South Africa and some neighbouring countries, also these areas preserve very unique grasslands that are endemic to South Africa and of global interest. Also, montane environments in South Africa are witnessing the impact of the changing climate through the emergence of invasive species and incessant lightning strikes. Therefore, this study aims to advance the understanding of the geography of CG

lightning activity in South Africa through the application of geospatial technology. Using spatial analysis techniques, this research evaluated 11-year lightning data (2007–2017) to develop a lightning hazard map for Golden Gate Highlands National Park by examining the statistical spatial and temporal patterns of lightning activity of Golden Gate Highlands National Park and their relationship with environmental characteristics, namely, elevation, slope, aspect, fire scars, and the vegetation type.

7.2 Material and Methods

7.2.1 Study Area

As a protected montane area, the Golden Gate Highland National Park (GGHNP) lies between 1657 m and 2797 m above sea level north-eastern of the Free State Province in South Africa (South African National Parks, 2013) (Fig. 7.1). The park is a unique Grassland Biome in South Africa and is situated in the summer rainfall region. The rainfall here is characterized by seasonal stretching from September to April with a mean annual value between 1800 mm and 2000 mm. The area is categorized as a dry sub-humid region. Summers are temperate with mean temperature (13 °C–26 °C) and winters are cold with mean temperature (1 °C–15 °C). In essence,

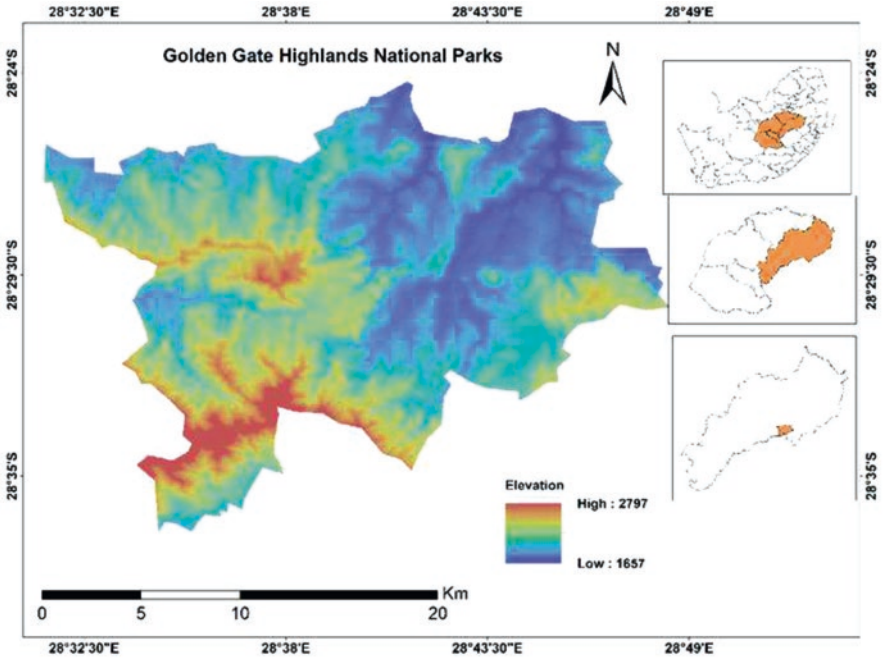

Fig. 7.1 Location of the study area (GGHNP)

the fire season starts in May and lasts till September. Despite numerous fire mitigation and management strategies (Strydom and Savage, 2016), this region is still highly vulnerable to wildfire which is in part due to its rugged terrain. On average, the park has lost 6809 ha of vegetation to fire accounting for 20% of the area (Govender, 2011).

7.2.2 Material

7.2.2.1 CG Lightning Data

CG lightning data was acquired from the Southern African Lightning Detection Network (SALDN) of the South African Weather Services (SAWS). The SALDN became operational in 2005 and underwent a series of upgrades. From 2015, the network consisted of 25 Vaisala CG lightning sensors that can detect all cloud-to-ground lightning discharges with a 90% efficiency measure (Evert and Gijben, 2017). The SALDN is capable of detecting lightning with a location accuracy of ~0.5 km (500 m) covering all of South Africa, Lesotho, and Swaziland (Bhavika, 2007, Evert and Gijben, 2017, Gijben et al., 2017). The network records lightning events chronologically. The attribute information of each lightning strike is recorded including date and time, latitude, longitude, peak current with negative(−) or positive (+) polarity, major and minor ellipsoid angle, and the number of direction finders that sensed the event (Bhavika, 2007). As recommended by International Electrotechnical Commission Standards (IEC 62858), lightning data for at least 10 years is required to ensure that short-term scale variation in lightning parameters due to a variety of meteorological oscillations are accounted for (Javor et al., 2018). Therefore, in this study, lightning strike data for 11 years from January 2007 to December 2017 was utilized.

7.2.2.2 Terrain Elevation, Slope, and Aspect

Advanced Spaceborne Thermal Emission and Reflection Radiometer-Digital Elevation Model (ASTER-DEM) data at 30 meters freely obtained from USGS EarthExplorer (http://earthexplorer.usg.gov) was used for retrieval of elevation, aspect, and slope values. These values were selected due to its known role of orographic lifting to the enhancement of convection and consequently to lightning (Kotroni & Lagouvardos, 2008).

7.2.2.3 Vegetation Type

Vegetation plays a pivot role in the universal climatic variation together with the convective growth and lightning activity (Dissing and Verbyla, 2003; Mushtaq et al., 2018). Vegetation type of GGHNP was attained from Fire Ecology Department, South Africa National Park, in the polygon shapefile providing GIS coverage that shows vegetation types in community and habitat.

7.2.2.4 Historical Fire

Historical fire scar/spot data was received from the Fire Ecology and Biogeochemistry Department, South Africa National Parks, with their geographical coordinates in polygon shapefile format. The significance of these data in lightning activity is that a possible-induced thunderstorm can be conceived from all sides of fire scars (Kilinc and Beringer, 2007).

7.2.3 Methods

Lightning data was provided in a formatted text (.cvs) that was first parsed and saved in a spreadsheet and then converted into a point vector layer in a GIS environment using Microsoft Excel and ArcMap 10.2. software, respectively. The georeference UTM Zone 35S was used as the projection. A Clip Tool was employed to extract the study area. Databases of lightning activity by year, monthly, and hourly were then created by using the Select by Attributes tool.

7.2.3.1 Temporal Distribution of Lightning Strikes Activity

Lightning strikes counts were analysed to explore temporal patterns of lightning activities over GGHNP. Annually, monthly, seasonal, and diurnal distributions were calculated with the summation of counts for respective periods. To evaluate the influence of season on lightning activity, monthly data was summarized according to four seasons: summer (Dec, Jan, Feb), autumn (March, April, May), winter (June, July & August), and spring (Sept, Oct, Nov). For diurnal, a series of graphs and tables were created using Excel to visualize the temporal distribution of lightning activity of the park.

7.2.3.2 Spatial Distribution of Lightning Strikes Activity

To capture the spatio-temporal distribution of lightning activity, maps for visualization showing the individual CG lightning strikes as points and density were created. In this study, the Hex binning analysis was employed. This analysis helps in aggregating spatially lightning strike data. The reason here is that the Hex binning as used in this study will help to spatially aggregate the dataset (lightning strike) in a hexagonal manner. The assumption stems from studies (Carr et al., 1992; Genton et al., 2006) that have posited that hexagons are visually appealing and have better symmetry of nearest neighbour than square or rectangular bins. The hex grid (100 m) for each of the dataset (lightning) were created using MMQGIS plugin version 2018.1.2 and the lightning data was spatially joined to the hex grid using the join by location attribute in QGIS 2.18.5. The lightning flash density attribute was added to the new feature table and calculated using the Field Calculator tool by dividing the 'count' by cell area and then by the number of years spanning the dataset resulting in a count per km^2 per year *(Ng)*.

Hot Spot Analysis was employed to determine whether or not there is clustering and also to measure the degree of spatial autocorrelation of CG lightning in the study area. Hot Spot Analysis was performed using lightning strikes density data as an input. Several analyses or processes precede hotspot analysis. First, we determined the specific threshold distance or distance band for neighbouring feature, which is called neighbourhood. The neighbourhood consists of features that are analysed together to assess local clustering and this is made possible through the use of a threshold distant band (TDB). To determine the TDB, the Incremental Spatial Autocorrelation (ISA) tool in ArcGIS was conducted.

ISA is a measure of spatial autocorrelation. The Z-score here depicts the spatial clustering intensity and statistically significant peak z-score indicates where spatial processes promoting clustering are most pronounced. These peak distances were used to determine a distance band or threshold distance band for hot spot analysis using Getis–Ord G_i^* (ArcGIS, 2013, Cha et al., 2017).

Furthermore, Incremental Spatial Autocorrelation calculates Global Moran I. Moran's I is a measure of the correlation where negative correlation indicates the dispersion of similar values, positive correlation indicates clustering of similar values (either high or low), and zero correlation indicates complete spatial randomness. It informs us whether a set of features is clustered, dispersed, or random. It is based on spatial covariation divided by total variation as shown in Eq. 7.1 (Amrhein, 2017, Moran, 1950).

$$I = \frac{n\sum_{j=1}^{n}\sum_{j=1}^{n} W_{ij}\left(y_i - y\right)\left(y_j - y\right)}{\left(\sum_{i=1} n\left(y_i - y\right)^2\left(\sum_{i=1} n\sum_{j=1}^{n} w_{ij}\right)\right)} \tag{7.1}$$

From Eq. (7.1), n is the total number of features, w_{ij} is the spatial weight matrix between feature i and j, the variable y is the features attribute value.

Values for Moran's I range from −1 (dispersion) to +1 (clustered). A Z-score and p-value are also calculated for Moran's I statistic. For statistically significant positive Z-scores, the null hypothesis of spatial randomness is rejected, and the high and low values in the dataset are considered to be more clustered than expected. For statistically significant negative Z-score, the spatial distribution of high and low values is considered dispersed and the null hypothesis is rejected (Amrhein, 2017, Moran, 1950). Results were represented in the form of line graphs of Moran I and Z-score vs distance.

To explain a spatial pattern of the CG lightning strike density, hotspot analysis was eventually performed using Hot Spot Analysis *Getis–Ord* G_i* Tool of ArcMap. Getis–Ord G_i* evaluates the spatial correlation from a local scale perspective. The G_i* as a statistic helps in determining areas of high and low clusters by looking at local averages to global averages. The G_i*statistic ranges in values from −3 to +3 and is calculated for each feature and produces a Z-score indicating the intensity of the high or low clustering with respect to its neighbourhood depending on the sign of Z-score. A statistically significant 'hot spot' is one where a feature with high value is surrounded by other features with high values (positive Z-score). Likewise, a 'cold spot' is one where a feature with low value is surrounded by other features with low values (ArcGIS, 2013, Cha et al., 2017, Getis and Ord, 1992). The G_i* is calculated using Eq. 7.2.

$$G_i^* = \frac{\sum_{j=1}^{n} \mathrm{w}_{i,j},, x_j - X\sum_{j=1}^{n} \mathrm{w}_{\mathrm{i,j}}}{S\sqrt{\sum_{j=i}^{n} xj^2 - \left(X\right)^2}} \tag{7.2}$$

where x_j is the attribute value for feature j, $w_{i,j}$, is the spatial weight between i and j, and n is equal to the total number of features. Also, X and S are shown in Eqs. 7.3 and 7.4, respectively.

$$X = \sum_{j=1}^{n} x_j \tag{7.3}$$

$$S = \sum_{j=1}^{n} x^2 j - \left(X\right)^2 \tag{7.4}$$

7.3 Development of Lightning Hazard Map

For the spatial distribution of Lightning Hazard Map (LHM), the Inverse Distance Weighted (IDW) technique of ArcMap 10.2 was employed. LHM was developed from the Z-score of the Hot Spot Analysis. The output of the IDW was normalized to range between 0 and 1 using the Raster normalization tool (ArcGIS), while the Reclass tool was used to stratify the entire data layer into five classes based on lightning potential risk of lightning activities guided by previous researches. These classes are categorized as follows: almost danger-free (0–0.2), minimal danger (0.2–0.35); moderate danger (0.35–0.50); severe danger (0.50–0.75); and extreme Danger (0.75–1).

7.3.1 Relationship of Lightning Hazard Map with Topography (Elevation, Slope, Aspects, Vegetation Types, and Fire Scar)

Regression analysis was undertaken to explore the relationship of LHM with terrain parameters, (elevation, slope, and aspect), vegetation types, and fire scars. Statistical analysis of the data, namely, Coefficient, Probability or Robust Probability, and Variance Inflation Factor (VIF), as well as t-test were used to assess each variable. In preparing the data for statistical analysis, the study area elevation data was prepared using methods by Adelabu et al. (2018). Slope and aspect were calculated using the Surface Tool. All raster layers were converted into vector layers (polygons) to align with vegetation types and fire scar layers and resampled to 1000 m. All six (6) layers were overlaid using the Spatial Join Tool of ArcMap. Regression analysis was performed using Ordinary Least Squares (OLS) Modelling spatial relationship Tool of ArcMap 10.2 software. The diagnostic results were displayed in the form of a table.

7.4 Results

7.4.1 CG Lightning Strike Events and Density Maps

Within the GGHNP, a total of 114,720 lightning strikes were recorded between January 2007 and December 2017. About 94.86% were of negative polarity and 5.14% of positive polarity. In general, most of the previous studies showed a similar pattern of positive polarity accounting for less than 10% of total CG activities (Dewan et al., 2018). Since the CG lightning point event map is difficult to visually interpret, a lightning flash density map on the hexagon polygon grid for the entire 11-year period is displayed in Fig. 7.2. The map showed that the density of lightning

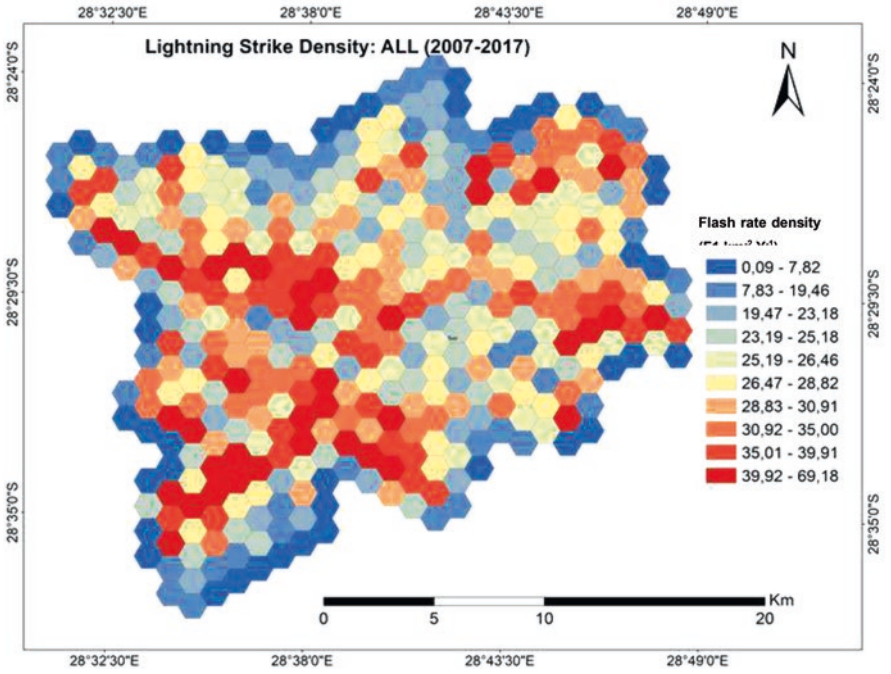

Fig. 7.2 Map depicting the spatial density of CG lightning flashes within GGHNP between 2007 and 2018. Lightning density (Ng) displayed the number of CG lightning events per km^2 per year

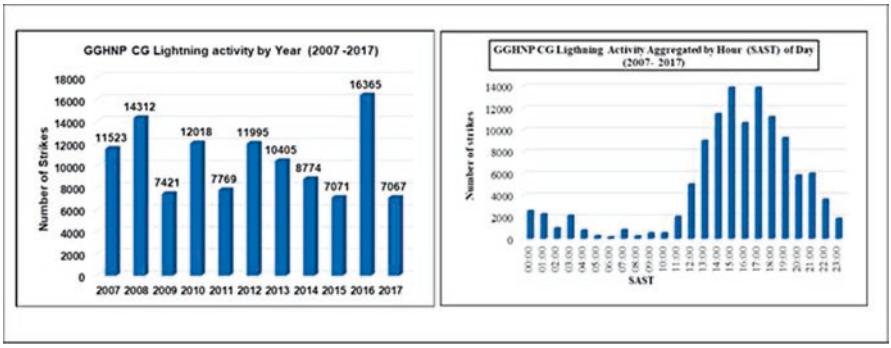

Fig. 7.3 Graph of lightning events by year and hour

strikes is not uniform throughout the park. Areas of high density (in red) can be seen throughout the park. These observed variations in the CG lightning pattern follow the topography of GGHNP. The highest density was prominent at a highly elevated area within the park.

7.4.2 Temporal Analysis

From Fig. 7.3, it can be observed that the GGHNP experienced the highest number of lightning events during 2016 (16,365). The distribution shows that the years 2015 (7071 events) and 2017 (7067 events) witnessed the lowest number of individual lightning strikes in the park. Based on the inter-annual variability (Fig. 7.3 and Table 7.1), there is a possibility that the occurrence of these strikes is related to a large-scale climate phenomenon, such as the ElNino Southern Oscillation (ENSO) and the Southern Annular Mode (SAM) (Dowdy, 2016, Guha et al., 2017, Mariani et al., 2016). However, there is still the need to carefully unravel this relationship using standard climatic procedures.

Fig. 7.4 shows the seasonal variation of lightning strikes over the GGHNP for the period between 2007 and 2018. It was evident that maximum lightning strikes were observed in summer. The decrease of lightning activity observed on the onset of autumn to the winter season is consistent with the results of (Gill, 2009). Gill (2009) also observed a shift in lightning activity with the change in season in South Africa. Regularly in summer, a surface trough (an elongated area with relatively low pressure values when reduced to sea level) associated with the deep intrusion of well-defined easterly wave that will result in the development of a line of convection extending from northwest towards the southeast over the country. Such line thunderstorms are well organized and moved from west to east bringing rain and accompanied lightning to the most of the Free State province (Gill, 2009). Low lightning activity in the winter season could be attributed to the less vegetation cover and more bare-ground. The study by Kotroni and Lagouvardos (2008) revealed that over a bare ground, the lightning yield is low. Changes in the surface temperature from minimum in winter followed by maximum on the onset of springs may lead to fluctuation of lightning activity. Moreover, high lightning activity in summer could be attributed to cloud cover during late springs.

Table 7.1 Percentage of lightning strikes count by month and season between 2007 and 2017

Month	Percentage	Season	Percentage
Dec	23.80%	Summer	56.26%
Jan	17.57%		
Feb	14.89%		
Mar	10.71%	Autumn	14.22%
Apr	2.82%		
May	0.69%		
Jun	0.47%	Winter	0.68%
Jul	0.08%		
Aug	0.13%		
Sep	1.90%	Spring	28.84%
Oct	13.38%		
Nov	13,56%		

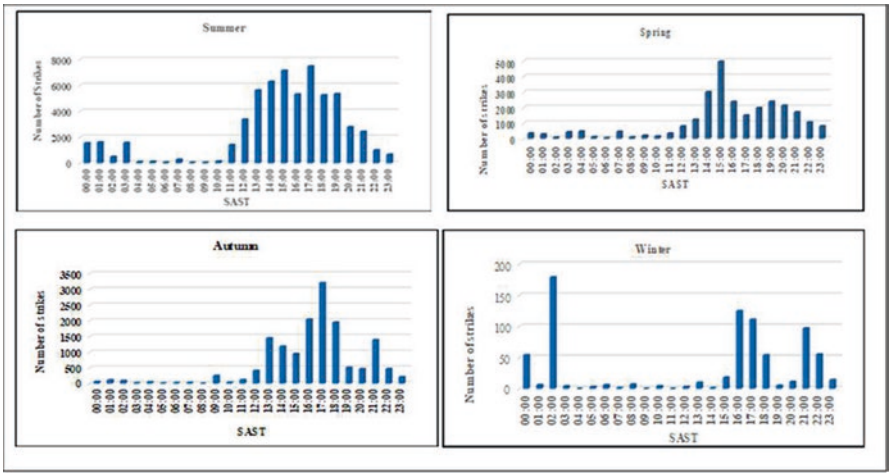

Fig. 7.4 Seasonal variation lightning strikes over GGHNP

In addition, Fig. 7.4 illustrates the diurnal variation of lightning activity on a seasonal basis. It revealed that majority of lightning activity occurred in the afternoon to the early evening across all four seasons. The diurnal pattern described the influence of solar radiation on the development of thunderstorms. The observed afternoon peak in lightning activity correlates to the peak in solar radiation and subsequently high energy levels during this time of the day (Bhavika, 2007). Gill (2009) demonstrated that heat-generated, isolated, or scattered thunderstorm activity is also common in the late afternoon. However, an abnormal observation was made during winter season with peak in early hours of the morning (02:00). This diurnal pattern indicated that winter lightning is not sensitive to solar heating, and thus frontal activity is the dominant factor influencing thunderstorm development in this season (Bhavika, 2007).

7.5 Spatial Pattern Analysis

7.5.1 Global Moran 1

Output from Moran I analysis on the monthly scale, as depicted in Fig. 7.5a, revealed that the Moran I values are greater than 0 ranging from 0.01 to 0.49 throughout the year, with the exception of July. This indicates positive spatial autocorrelation of clustering of either high or low values of CG lightning density. However, the Moran I value of July is smaller than 1 indicating that the spatial pattern is randomly distributed. In winter months (June, August, and September), Moran I values range from 0.01 to 0.07, which reveals that spatial pattern is close to the random distribution pattern of CG lightning density. The z-score values are above zero (see

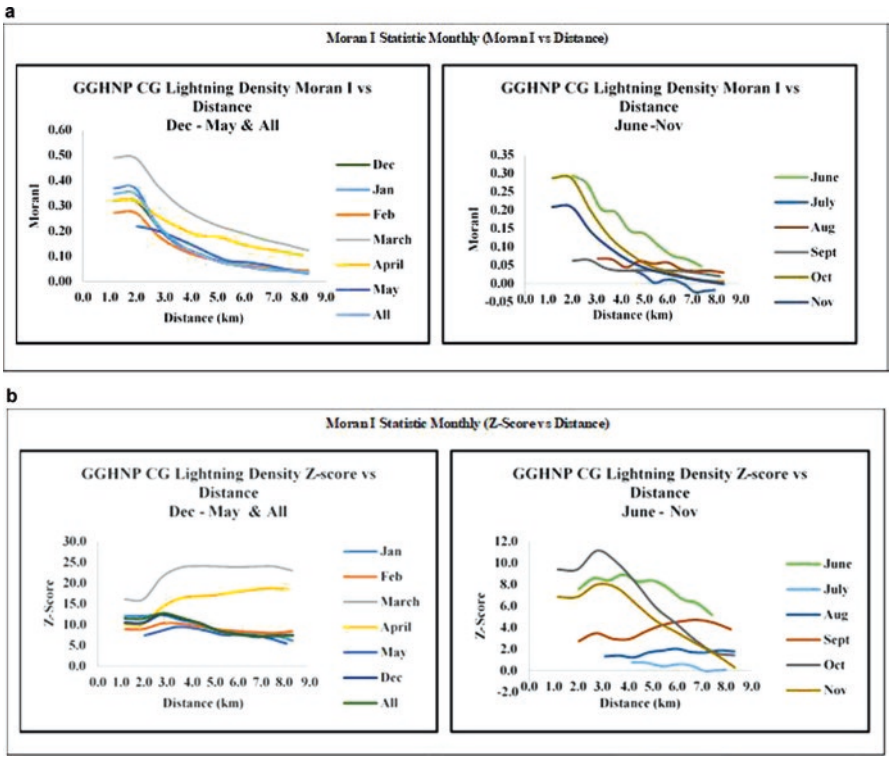

Fig. 7.5 Global Moran I statistic results for monthly data (**a**) Moran I vs Distance, (**b**) Z-score vs Distance

Fig. 7.5b) and observed p-values are low, therefore, the spatial pattern is statistically significant and rejected the null hypothesis that lightning density is randomly distributed except in the month of July. The CG lightning density and the Moran I curves show the bias of lightning density with distance. From Fig. 7.5a, b, the CG lightning density shows a persistent decrease with distance for afternoon and evening hours ranging from 0.00 to 0.48 at 1.2 km to values less than 0.0 at 8.3 km. From Fig. 7.5, it can be posited that the spatial distribution of lightning density within the protected area is clustered at a distance of about 1.2 km which becomes closer to random as the neighbourhood distance increases. On the other hand, the Moran I curve for late morning hours suggests a random pattern since the morning hours is less than zero and negative for 06:00 SAST and 09:00 SAST (Fig. 7.6a).

From Fig. 7.6b, the observed Z-score ($Z > 0$ and positive) curves for early morning, afternoon, and evening hours are above zero and are positive signalling a positive spatial auto-correlation and an indication of a significant clustered pattern ($p < 0.5$). Based on Fig. 7.6b, the Z-score ($Z < 0$ and negative) for late morning hours 06:00 and 08:00 SAST suggests a negative non-significant spatial correlation, hence, lightning activities within GGHNP during 06:00 and 08:00 are likely to be random.

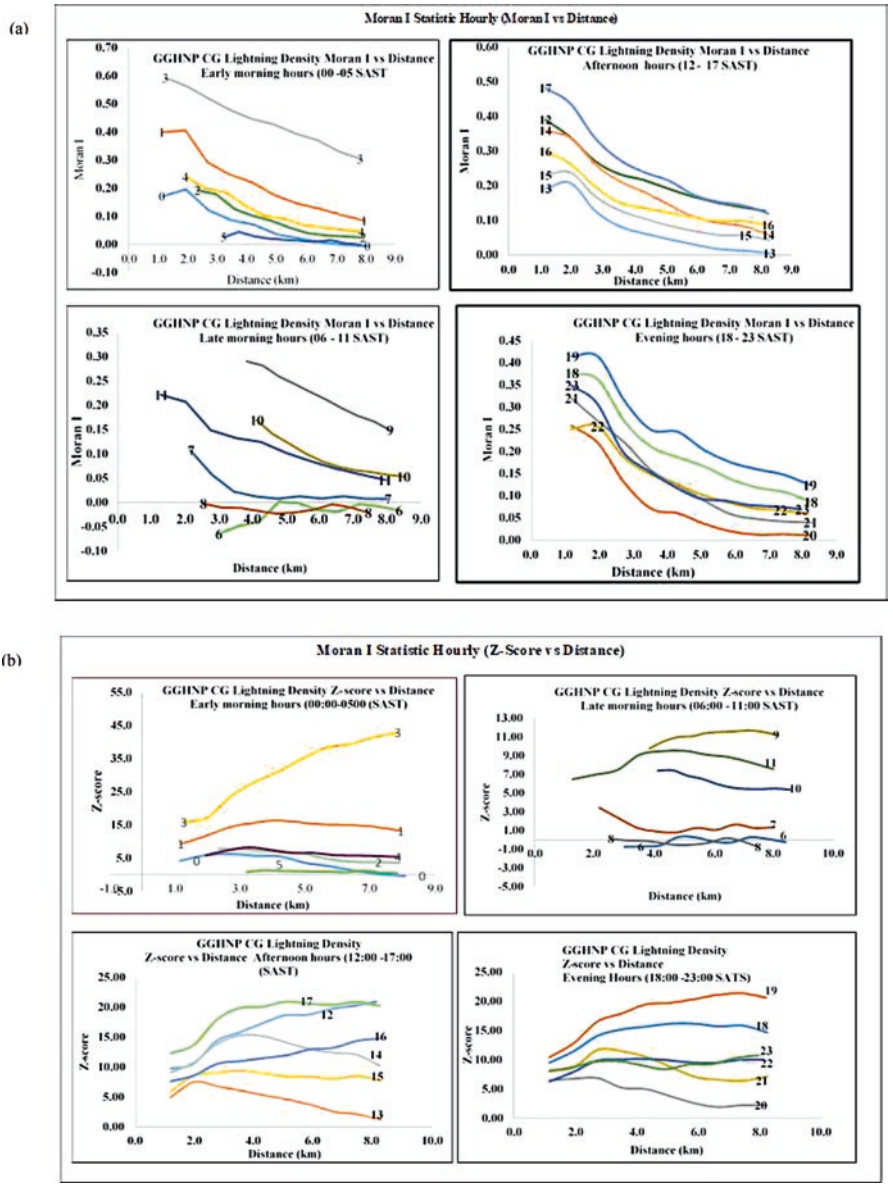

Fig. 7.6 Global Moran I statistic diurnal data (**a**) Moran I vs Distance, (**b**) Z-score vs Distance

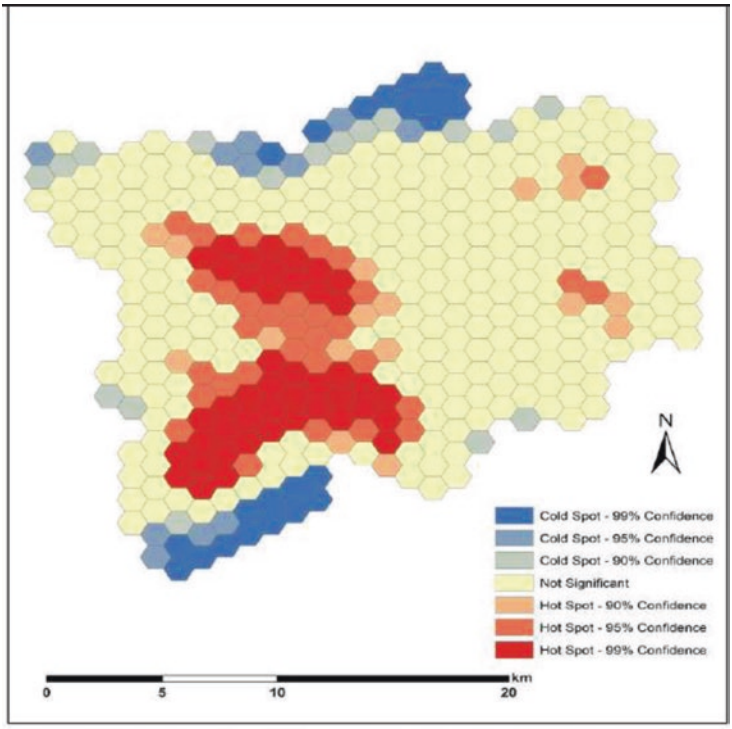

Fig. 7.7 GGHNP lightning strike density showing hot and cold spots

7.5.2 Hotspot Analysis Getis–Ord $\mathbf{G}_i^*$

The map of Hotspot Analysis Getis–Ord G_i^*statistic using the 11-year lightning activity is presented in Fig. 7.7. It illustrates the regions of a statistically significant cluster of high and low values (hot and cold spots) presented in shades of red and blue based on the calculated Z-score and p-values. From Fig. 7.7, the main clusters are large and are identified as hot spots. These are at a higher elevation within the park such as in the south-western through the north-western and eastern part of the park. These hotspot areas cover 23.76% of the study area. Clusters of statistically significant low values or cold spots are mainly located in the northern part of the park. While 13.43% was found as statistically significant and identified as a cluster of low values (cold spot).

The results of the Getis–Ord G_i^*statistic for aggregated monthly data are revealed in Fig. 7.8. It showed that July and August (winter months) have a smaller area of coverage of high values of clustering and non-existing low values of clustering. Large coverage is identified as clusters of high values for all months between September and June. Table 7.2 showed the percentage of the area identified as clusters of high values (hotspot) and low values (cold spot), as well as non-significant

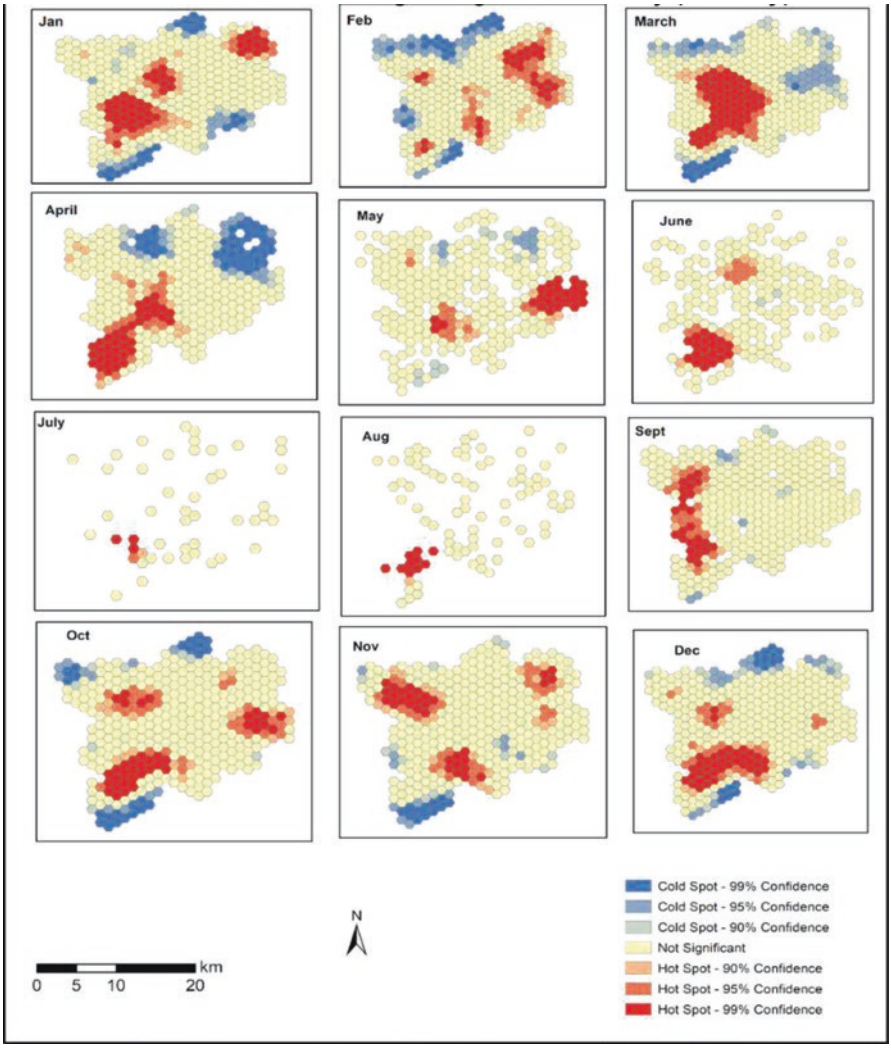

Fig. 7.8 GGHNP monthly lightning strike density showing hot and cold spots

for the monthly dataset. February and March have the largest coverage identified as clusters of high values (hotspot). During winter months when the lightning activity is at least, the largest area of coverage of hotspot is located in June (18.27%) followed by August (12.38%) and July (10.36%) and located in the south-western part of the park and a small portion at the centre of the park.

During summer months when lightning activity is at its peak, the largest areas of coverage of hotspots are observed in February (23.70%) located in north-east and eastern parts of the park, followed by January (23.21%) and December showing the least (19.36%) and concentrated more in the south-west part of the park. During the autumn season, March (23.70%) contributed the highest area of coverage of hotspot

Table 7.2 Summary of monthly Getis–Ord G_i^*result showing the percentage of area identified as clusters of high values (hotspot), low values (cold spot), and non-significant

Month	High	Low	Non-Significant	Month	High	Low	Non-significant
Jan	23.21	13.03	63.76	**Jul**	10.36	0	89.64
Feb	23.7	18.86	57.44	**Aug**	12.38	0	87.62
Mar	23.7	23.25	53.05	**Sept**	14.75	3.64	81.62
Apr	19.32	19.91	60.77	**Oct**	21.6	10.99	67.41
May	15.43	7.12	77.44	**Nov**	21.4	9.24	69.62
Jun	18.27	0.96	80.77	**Dec**	19.36	13.43	67.21
All	23.76	12.85	63.4				

located extremely at the central part followed by April (19.32%) located in south-western and May (15.43%) located in the eastern part of the park. The high values of the cluster during the spring season are high in October (21.60%) concentrated mostly in the south-western region and less in the eastern part of the park and followed by November (21.14%) located in the north-west portion, September with the least (14.75%) in north and south-western part of the park. The cold spots of lightning strike density are large in coverage during April and non-exist in July and August.

The hotspot coverage appears to be at its greatest during 22:00 SAST (30.08%), 03:00 SAST (26.19%) and 17:00 SAST (25.75%) as shown in Fig. 7.9 and Table 7.3. The north-western, south-western, and central mountains have a consistently high level of hotspot during these time periods and through 06:00 SAST (3.33%) where it is almost non-existence. In the mountains of north-eastern and eastern GGHNP, the hotspot coverage in this region of the park is consistent but relatively smaller in coverage expect during 01:00, 04:00, 12:00, 16:00, and 19:00 SAST. Cold spot coverage appears to be at its greatest during 03:00 SAST (38.11%) and occurs mostly over the north-eastern flat terrain region of GGHNP. Therefore, the results of the Getis–Ord G_i^* test reveal localized hot and cold spots of CG lightning activity within GGHNP and vary with the seasons on the monthly time scale as well as diurnally hour of the day. The hot spots are generally located in or near the mountains while most of the cold spots are located in the flat terrain of GGHNP.

7.5.3 Development of Lightning Hazard Map

The development of LHM was drawn from the Z-score of Hotspot analysis, interpolated, normalized, and classified according to the potential of lightning hazard. The map showing coverage extent of hazard severity is illustrated in Fig. 7.10. It revealed that 48.76% of the entire landmass of the GGHNP falls under the severe danger zone. Two patches of the extreme danger zone are seen on the map towards the southwestern part and north-central portion of the map. Only very few portions of the entire landmass fall under almost danger-free zone, suggesting that the entire landmass of the GGHNP is largely prone to lightning hazard (Fig. 7.11).

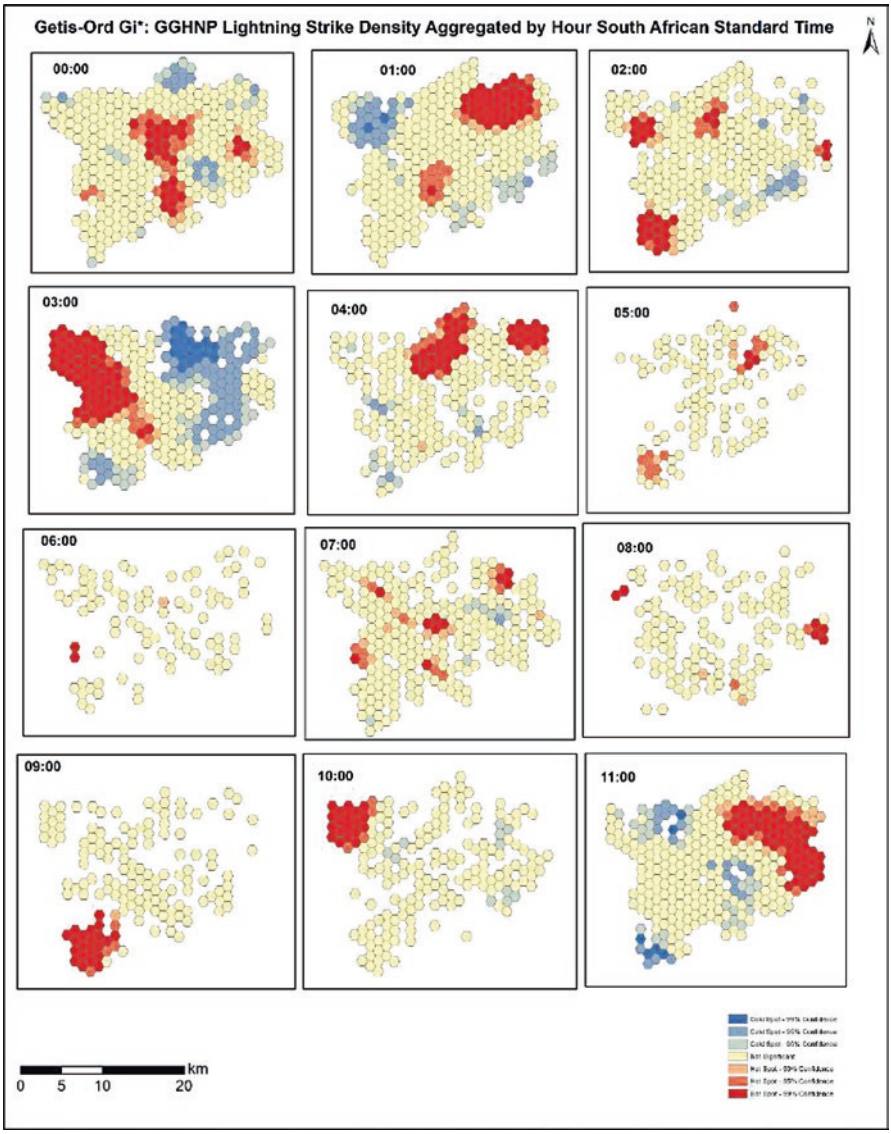

Fig. 7.9 GGHNP average hourly lightning strike density showing hot and cold spots

7.5.4 Regression Analysis

In order to explore the relationship between the developed LHM and the terrain parameters (aspect, slope, and elevation), vegetation type, and fire scars, the regression analysis was executed. OLS regression (Table 7.4) yielded a model that explained 77% of the variation in lightning hazard map as explained by R^2 value of

Table 7.3 Summary of hourly Getis–Ord G_i^*result showing the percentage of area identified as clusters of high values (hotspot), low values (cold spot), and non-significant

Hour	High	Low	Non-significant	Hour	High	Low	Non-significant
00	18	10.25	71.75	12	22.14	22.43	55.47
01	18.14	15.61	66.25	13	12.51	9.26	78.22
02	16.03	7.77	76.2	14	24.46	20	55.54
03	26.19	38.11	35.69	15	22.25	8.33	69.4
04	21.32	5.98	72.7	16	23.03	18.9	58.06
05	16.39	0	83.61	17	25.75	21.24	53.75
06	3.33	0	96.6	18	20.86	14.98	64.16
07	13.56	3.71	82.73	19	18	15.99	66.01
08	7.8	0	92.2	20	16.17	8.55	75.28
09	17.61	0	82.39	21	22.25	14.09	63.77
10	12.6	6	81.4	22	30.08	13.29	56.63
11	23.4	17.08	59.52	23	19.1	12.62	68.28

0.77. The coefficient statistic which explains the type and strength of co-relationship showed negative relationship between LHM and aspect (−0.0424). However, positive and statistically significant relationship was found on fire scars (4.5668), slope (0.683), vegetation (0.021), and elevation (0.0029). These results are in agreement with the study conducted in Yellowstone National Park (Amrhein, 2017), whereby there was no relation of any aspect with lightning activity. The predictor variables used to predict spatial clustering all have variable inflation factor (VIF) less than 7.5 (Table 7.4) indicating little redundancy amongst variables except fire scars. However, fire scars have a robust relation with LHM.

The model was identified as statistically significant owing to the very low value of Joint F- and Wald-Statistic that is smaller than 0.05. With the Koenker (BP) statistics showing no statistical significance indicate that the model is consistent in data space, the variation in the relationship between predicted lightning strike density and explanatory variables does not change within explanatory variable magnitude. Therefore, there is no heteroscedasticity (non-constant variable or non-stationary) in the model. The Jarque–Bera Statistic test was also not statistically significant indicating that the regression residuals are normally distributed with a p-value higher than 0.05, therefore the model is unbiased. The adjusted R^2 and AICs values of the model are 0.63 and 73.66, respectively, validating the sound performance of the predicted model.

7.6 Discussion

The study revealed the outcomes in assessing the spatio-temporal patterns of CG lightning activity over the GGHNP. The application of statistical spatial autocorrelation and clustering techniques such as Global Moran I and Getis–Ord G_i^* was

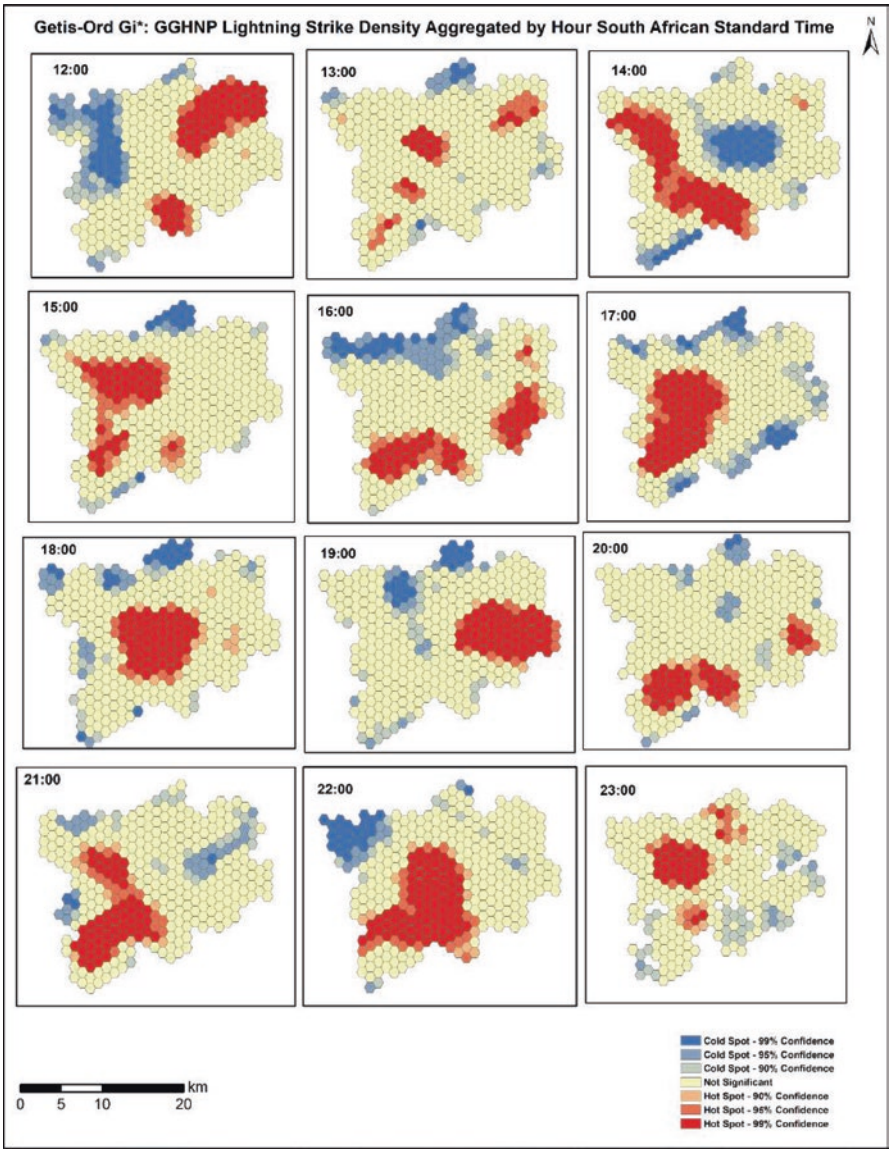

Fig. 7.10 GGHNP average hourly lightning strike density showing hot and cold spots (contd)

effective in delineating the LHM, identifying what areas of the park experience clusters of lightning activity. The regression analysis was performed testing the relationship between the developed LHM and physical properties of GGHNP terrain.

The monthly strike count increases from the minimum value in July (0.08%) and displays a peak in December (23.80%) as shown in Table 7.1. It is observed that the maximum lightning strikes count occurred in the summer months (DJF), accounting

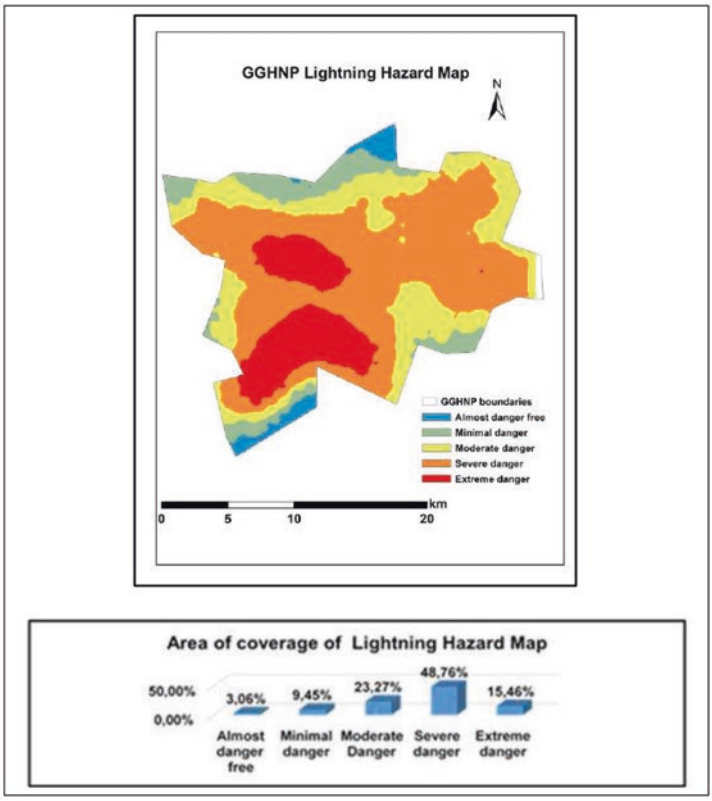

Fig. 7.11 Lightning hazard map for GGHNP (2007–2017) showing coverage extent of hazard severity

Table 7.4 OLS regression diagnostic for the entire dataset

Dependent variable	Lightning hazard map					
Variables	Coefficient	Std. error	t-Statistic	Probability	Robust_Pr	VIF
Aspect	−0.0424	0.0606	−0.6949	0.4970	0.4884	1.41
Elevation	0.0029	0.0008	3.5989	0.0024*	0.0003*	2.14
Slope	0.0683	0.0699	0.9773	0.3429	0.2706	1.72
Vegetation	0.0211	0.0676	0.3125	0.7586	0.6393	1.35
Fire	4.5668	6.1007	0.74857	0.4649	0.008631*	37.164
R-Squared	0.770884	**Wald-Statistic**	0.000000*			
Adjusted R-Squared	0.670646	**Koenker (BP)**	0.415350			
(AICc)	73.663751	**Jarque–Bera**	0.789538			
F-Statistic	0.000382*					

for 56.26% of the total lightning strikes. This is followed at a distance by the spring (SON) and autumn (MAM) months. SON and MAN accounted for 28.84% and (14.22%), respectively, with the lowest count in the winter (JJF) months (0.68%). Also, we observed that as the winter season progresses, that is April upwards, lightning strikes count showed a decreasing trend. This decreasing trend during the autumn season moving into the winter season is constituent with Dewan et al. (2018) who reported a shift in lightning strikes count with the change in season in Bangladesh. The summer peaks and the consistent monthly variability are consistent with Bhavika (2007) and Mayet et al. (2016). The lightning strikes observed during summer months are associated with the nature of the terrain leading to orographic forcing; the increase in the total precipitable water column as a result of abundant moisture in the atmosphere; an increased surface temperature due to intense solar heating leading. The persistent heating of the land atmosphere creates instability in the atmosphere, by enhancing convection activities leading to severe storms heralded by lightning.

The average diurnal variation (2007–2017) as depicted in Fig. 7.3 suggests that lightning is more prevalent in terms of occurrence from 14:00 to 18:00 SAST with two clear maxima at 15:00 SAST and 17:00 SAST. The lowest lightning activity is during the morning hours at 05:00 and 06:00 SAST, and yet again at hour 08:00 SAST. A 24-h distribution of lightning activity was divided by 6-h periods revealed the following pattern: early mornings (00–05:59) 7.82%, late morning (06:00–11:59) 3.72%, afternoon (12:00–17:59) 55.60%, and evening (18:00–23:59) 32%. From the foregoing, within the GGHNP, the lightning activity follows an afternoon–evening maxima. A comparison of diurnal variation across the seasons reveals that lightning activity is predominantly late afternoon-type, although it is not evident in the winter season. Both summer and autumn have prominent peak at 17:00 SAST and spring at 15:00 SAST. During winter, lightning activity is greatly diminished, however, there is a prominent peak at 02:00 SAST. The diurnal variability and interseasonal diurnal variability observed in Figs. 7.3 and 7.4 are in agreement with the study by Dewan et al. (2018), which found that peak lightning activity usually occurs during the afternoon-evening hour.

Number of factors may be related to this type of diurnal variation; these include diurnal solar cycle leading to destabilisation of the atmosphere and development of convective particular in springs and summer seasons (Williams, 1994). In southwestern and north-central part of GGHNP, topography forcing the Thaba Bosiu Plateau and the foothills of Maluti Mountains allow convection and associate lightning to develop. Thus, topography in conjunction with synoptic system may lead to convective development (Qie et al., 2003) subsequently to the development of thunderstorm and lightning. Early morning peaks observed in winter season might be attributed to land and sea breezes circulation, nocturnal valley wind which promotes convection to early mornings and vertical wind shear for local convection (Dewan et al., 2018).

Regional road that passes through the GGHNP may enhance aerosol in atmosphere caused by increased anthropogenic activities within and adjacent to the park. The study by Mushtaq et al. (2018) showed that presence of aerosol in the

atmosphere may affect the lightning activity. South-western and northern central part of GGHNP support the notion that mesoscale convective is higher in the mountainous area. Qie et al. (2003) articulated three trigger mechanisms of such concept as orographic and terrain effects, presence of wind discontinuity line or dry line, and availability of vegetation moisture. Since these areas of the park are dominated by moderate height terrain, orographic lifting with respect to complex terrain could initiate conditional instability of atmosphere which favours the development of thunderstorm – facilitated lightning. Therefore, these mechanisms influence the spatial clustering of lightning activity over the study area.

Spatial autocorrelation analysis revealed that the clustering of lightning strikes at the park is at a distance of about 1.2 km. This connotes that strikes clustered with other strikes are not likely to strike an individual specific location from centre of cluster of strikes much beyond a circle with radius of 1.2 km. Spatial regression analysis (OLS) identified that elevation, slope, vegetation type, and fire scars are as statistically significant and positive in predicting the development of LHR. The vegetation-type variable was statistically significant showing a positive relation with LHM. This relation of vegetation type with LHM could be viewed in light of the vegetation of the study area. GGHNP is predominantly an Afromontane grassland park. There is a conjecture that grassland has much higher sensible heat flux because they have senesced during dry season, and an increased sensible heat flux may drive thermal convection and increase lightning activity. Although fire scars were found to be the only variable with the highest IVF values, which is responsible for multicollinearity and the most variables with the robust correlationship with the LHM. This multicollinearity is due to the fact that the short-period dataset (I year dataset) was used for this variable; therefore, increasing the sample size or long-period dataset could be a solution (ArcGIS, 2013). A small fire scar will show an increase in heating, but its impact on the heating of the boundary layer will be minimal (Kilinc and Beringer, 2007).

7.7 Conclusion

To the best of our knowledge, this is the first study of its kind to make use of SALDN data over the mountainous protected area to explore the statistical spatial and temporal patterns of lightning activity: the first to employ spatial analysis techniques to determine the clustering of CG lightning within the GGHNP. Global clustering spatial pattern was calculated using Global Moran*I*employed on lightning-strike for the entire dataset (2007–2017), and monthly and hourly data revealed that there is strong evidence of global clustering and spatial patterns are statistical spatially significant and appear to be clustered except in July, late morning hour of 06:00, 08:00, and 09:00 SAST. The study demonstrated that the overall spatial pattern of CG lightning activity varies with time due to regional and local weather patterns as influenced by a large scale of climatic nodes (ENSO and SAM). This relationship still needs to be explored. Monthly variation revealed that lightning activities are at

peak during summer, in December, while diurnal variation revealed afternoon-evening maxima attributed to orographic effect, availability of abundant moisture, and diurnal solar heating cycle. The developed LHM revealed that almost 16% of the study area is at risk of lightning. OLS helped to identify the key factors contributing to the lightning threat being elevation. The study is a step towards new information regarding the spatio-temporal distribution of CG lightning. The data derived from this study would be of significance for wildfire models used to predict, monitor, and assess the lightning-induced wildfire. Knowing where and when lightning is mostly to cluster will allow managers to preposition suppression, plan for fuel treatment, and prepare fire prevention and public safety (Van Wagtendonk and Cayan, 2008). Although this study furnished some initial results, incorporating strikes characteristics (polarity, multiplicity, and strength), regional climate conditions and local weather patterns that result from physical geography of GGHNP would advance the understanding of spatio-temporal distribution of CG lightning activity. Knowledge of why positive or negative clusters occur in the study area can be used to improve lightning-induced wildfire models.

References

Adelabu, S. A., Adepoju, K. A., & Mofokeng, O. D. (2018). Estimation of fire potential index in mountainous protected region using remote sensing. *Geocarto International, 35*, 29–46.

Amrhein, E. (2017). *The geography of cloud-to-ground lightning in Yellowstone National Park*.

Anderson, G., & Klugmann, D. (2014). A European lightning density analysis using 5 years of ATDnet data. *Natural Hazards and Earth System Sciences, 14*, 815–829.

ArcGIS, Environmental Systems Research Institute (ESRI). (2013). *10.2 Desktop Help*. ESRI, Inc. Redlands, CA.

Bentley, M. L., & Stallins, J. (2005). Climatology of cloud-to-ground lightning in Georgia, USA, 1992–2003. *International Journal of Climatology: A Journal of the Royal Meteorological Society, 25*, 1979–1996.

Bhavika, B. (2007). *The influence of terrain elevation on lightning density in South Africa*. University of Johannesburg.

Blumenthal, R., Trengrove, E., Jandrell, I. R. & Saayman, G. (2012). *Lightning medicine in South Africa*.

Carr, D. B., Olsen, A. R., & White, D. (1992). Hexagon mosaic maps for display of univariate and bivariate geographical data. *Cartography and Geographic Information Systems, 19*, 228–236.

Cecil, D. J., Buechler, D. E., & Blakeslee, R. J. (2014). Gridded lightning climatology from TRMM-LIS and OTD: Dataset description. *Atmospheric Research, 135*, 404–414.

Cha, D., Wang, X., & Kim, J. W. (2017). Assessing lightning and wildfire hazard by land properties and cloud to ground lightning data with association rule mining in Alberta, Canada. *Sensors, 17*, 2413.

Christian, H. J., Blakeslee, R. J., Boccippio, D. J., Boeck, W. L., Buechler, D. E., Driscoll, K. T., Goodman, S. J., Hall, J. M., Koshak, W. J., & Mach, D. M. (2003). Global frequency and distribution of lightning as observed from space by the Optical Transient Detector. *Journal of Geophysical Research: Atmospheres, 108*, ACL 4-1–ACL 4-15.

Chuvieco, E., Aguado, I., Jurdao, S., Pettinari, M., Yebra, M., Salas, J., Hantson, S., De La Riva, J., Ibarra, P., & Rodrigues, M. (2014). Integrating geospatial information into fire risk assessment. *International Journal of Wildland Fire, 23*, 606–619.

Chuvieco, E., Aguado, I., Yebra, M., Nieto, H., Salas, J., Martín, M. P., Vilar, L., Martínez, J., Martín, S. P. I., De La Riva, J., Baeza, J., Rodríguez, F., Molina, J. R., Herrera, M. A., & Zamora, R. (2010). Development of framework for fire risk assessment using remote sensing and geographic information system technologies. *Ecological Modelling, 1*, 46–58.

Dewan, A., Ongee, E. T., Rahman, M. M., Mahmood, R., & Yamane, Y. (2018). Spatial and temporal analysis of a 17-year lightning climatology over Bangladesh with LIS data. *Theoretical and Applied Climatology, 134*, 347–362.

Dissing, D., & Verbyla, D. L. (2003). Spatial patterns of lightning strikes in interior Alaska and their relations to elevation and vegetation. *Canadian Journal of Forest Research, 33*(5), 770.

Dowdy, A. J. (2016). Seasonal forecasting of lightning and thunderstorm activity in tropical and temperate regions of the world. *Scientific Reports, 6*, 20874.

Durrheim, G. (2010). *Monitoring for sustainable indigenous forest management in the Garden Route National Park*. Scientific Services, South African National Parks.

Eskandari, S., & Chuvieco, E. (2015). Fire danger assessment in Iran based on geospatial information. *International Journal of Applied Earth Observation and Geoinformation, 42*, 57–64.

Evert, C. & Gijben, M. (2017). Official South African Lightning Ground Flash Density Map 2006 to 2017. Inaugural Earthing Africa Symposium and Exhibition, Thaba Eco Hotel, Johannesburg, 5-9.

Evert, R., & Schulze, G. (2005). Impact of a new lightning detection and location system in South Africa. *2005 IEEE Power Engineering Society Inaugural Conference and Exposition in Africa*, 356–363.

Frost, P., Kleyn, L., van den Dool, R., Burgess, M., Vhengani, L., Steenkamp, K. & Wessels, K. (2018). *The Elandskraal Fire, Knysna*. CSIR Report, (271960-1).

Genton, M. G., Butry, D. T., Gumpertz, M. L., & Prestemon, J. P. (2006). Spatio-temporal analysis of wildfire ignitions in the St Johns River water management district, Florida. *International Journal of Wildland Fire, 15*(1), 87–97.

Getis, A., & Ord, J. K. (1992). The analysis of spatial association by use of distance statistics. *Geographical Analysis, 24*, 189–206.

Gijben, M. (2012). The lightning climatology of South Africa. *South African Journal of Science, 108*, 44–53.

Gijben, M., Dyson, L. L., & Loots, M. T. (2017). A Statistical scheme to forecast the Daily Lightning threat over Southern Africa using the unified model. *Atmospheric Research, 194*, 78–88.

Gill, T. (2009). *Initial steps in the development of a comprehensive lightning climatology of South Africa*. Doctoral dissertation, University of the Witwatersrand.

Govender, N. (2011). *Proposed changes to the fire management policy of Golden Gate Highlands National Park*. South African National Parks. (SANP), Pretoria, RSA.

Guha, A., Banik, T., Roy, R., & de Kumar, B. (2017). The effect of El Nino and La Nina on lightning activity: Its relation with meteorological and cloud microphysical parameters. *Natural Hazards, 85*, 403–424.

Huang, Y., Wu, S., & Kaplan, J. O. (2015). Sensitivity of global wildfire occurrences to various factors in the context of global change. *Atmospheric Environment, 121*, 86–92.

Javor, V., Stoimenov, L., Džaković, N., Dinkić, N., Javor, D., & Betz, H.-D. (2018). LINETGIS analysis of lightning flash density in Serbia based on ten years data. *Serbian Journal of Electrical Engineering, 15*, 201–211.

Kigotsi, J. K., Soula, S., & Georgis, J.-F. (2018). Comparison of lightning activity in the two most active areas of the Congo Basin. *Natural Hazards and Earth System Sciences, 18*, 479–489.

Kilinc, M., & Beringer, J. (2007). The spatial and temporal distribution of lightning strikes and their relationship with vegetation type, elevation, and fire scars in the Northern Territory. *Journal of Climate, 20*, 1161–1173.

Kotroni, V., & Lagouvardos, K. (2008). Lightning occurrence in relation with elevation, terrain slope, and vegetation cover in the Mediterranean. *Journal of Geophysical Research: Atmospheres, 113*.

Mariani, M., Fletcher, M. S., Holz, A., & Nyman, P. (2016). ENSO controls interannual fire activity in southeast Australia. *Geophysical Research Letters, 43*, 10,891.

Mayet, N., Knight, J., & Grab, S. W. (2016). Spatial and temporal patterns of lightning strikes in the eastern Lesotho Highlands, southern Africa. *South African Geographical Journal, 98*, 321–336.

Moran, P. A. (1950). Notes on continuous stochastic phenomena. *Biometrika, 37*, 17–23.

Mushtaq, F., Lala, M. G. N., & Anand, A. (2018). Spatio-temporal variability of lightning activity over J&K region and its relationship with topography, vegetation cover, and absorbing aerosol index (AAI). *Journal of Atmospheric and Solar-Terrestrial Physics, 179*, 281–292.

Price, C., & Federmesser, B. (2006). Lightning-rainfall relationships in Mediterranean winter thunderstorms. *Geophysical Research Letters, 33*, L07813.

Qie, X., Toumi, R., & Yuan, T. (2003). Lightning activities on the Tibetan Plateau as observed by the lightning imaging sensor. *Journal of Geophysical Research: Atmospheres*, *108*.

Rakov, V. A., & Uman, M. A. (2003). *Lightning: Physics and effects*. Cambridge University Press.

South African National Parks, S. (2013). *Golden Gate Highland National Park Management Plan 2013–2023*. Access on 01 February 2018. https://www.sanparks.org/assets/docs/conservation/park_man/golden-gate-draft-plan.pdf

Strydom, S., & Savage, M. J. (2016). A spatio-temporal analysis of fires in South Africa. *South African Journal of Science, 112*, 1–8.

Van Wagtendonk, J. W., & Cayan, D. R. (2008). Temporal and spatial distribution of lightning strikes in California in relation to large-scale weather patterns. *Fire Ecology, 4*, 34–56.

Williams, E. R. (1994). Global circuit response to seasonal variations in global surface air temperature. *Monthly Weather Review, 122*, 1917–1929.

Chapter 8
Water Resources Monitoring Over the Atlas Mountains in Morocco Using Satellite Observations and Reanalysis Data

Abdelghani Boudhar, Wassim Mohamed Baba, Ahmed Marchane, Hamza Ouatiki, Hafsa Bouamri, Lahoucine Hanich, and Abdelghani Chehbouni

Abstract The Atlas Mountains cover a large area in the Moroccan territory, with an extent of about 800 km in length and 60 km in large, including various summits above 3000 m of altitude. From these high areas originate the main rivers that supply an important amount of surface water for domestic, agricultural, and industrial use, and it also significantly contributes to groundwater recharge. Due to its complex topography, the observation network in the high mountains is very sparse and

A. Boudhar (✉) · H. Ouatiki
Data Science for Sustainable Earth Laboratory (Data4Earth), Sultan Moulay Slimane University, Beni Mellal, Morocco

Center for Remote Sensing Application (CRSA), Mohammed VI Polytechnic University, Ben Guerir, Morocco
e-mail: ab.boudhar@usms.ma

W. M. Baba · A. Marchane
Center for Remote Sensing Application (CRSA), Mohammed VI Polytechnic University, Ben Guerir, Morocco

H. Bouamri
Data Science for Sustainable Earth Laboratory (Data4Earth), Sultan Moulay Slimane University, Beni Mellal, Morocco

L. Hanich
Center for Remote Sensing Application (CRSA), Mohammed VI Polytechnic University, Ben Guerir, Morocco

Faculty of Sciences and Techniques, Cadi Ayyad University, Marrakech, Morocco

A. Chehbouni
Center for Remote Sensing Application (CRSA), Mohammed VI Polytechnic University, Ben Guerir, Morocco

Centre d'Études Spatiales de la Biosphère (CESBIO), University of Toulouse, CNRS/CNES/IRD/UPS, Toulouse, France

S. Adelabu et al. (eds.), *Remote Sensing of African Mountains*,
https://doi.org/10.1007/978-3-031-04855-5_8

most of the streams are ungauged or in the best of cases have a short time series of data records. Moreover, climatic conditions in this scarcely gauged environment show a considerable spatial variation (e.g., altitude, exposition, ocean and desert effects) and temporal variability (e.g., interannual and seasonal). This spatio-temporal dynamic is currently not well studied and understood.

Geospatial technics could offer an opportunity to better understand the water cycle components over a large zone, and therefore lead to an efficient management of water resources. In this perspective, the present chapter gives an overview of the spatio-temporal dynamics of the main water resources indicators across the Atlas ranges. To this end, multi-source datasets (MODIS, ERA5, PERSIANN-CDR, GPM IMERG v6, SRTM-DEM) are used and combined through different workflows to produce long time series to analyse the behaviour of snow, precipitation, and temperature patterns at various time steps. Such information is of crucial importance for basin-scale modelling to assess hydrological response to snow dynamics and thus water resources along the Atlas.

Keywords Atlas Mountains · Water · Climate · Remote sensing · Re-analysis data

8.1 Introduction

The Atlas Mountains in Morocco represents an important water reservoir for populations living downstream lands and surrounding arid plains. The major rivers in the country originate from these mountains and their flows, used directly or from reservoirs, are mainly associated to precipitations amount that fall in the high altitudes. In addition, the principal aquifers adjacent to the mountain chains are generally recharged by streamflow, via wadis or underground dugouts, produced from the headwater basins in high altitudinal zones (N'da et al., 2016; Hssaisoune et al., 2020).

Due to the orographic effect, head watersheds with elevations above 1400 m are seasonally covered by snow (Boudhar et al., 2010; Marchane et al., 2015). They receive an enhanced rate of precipitation in the form of snowfall during the cold season (Baba et al., 2019). Moreover, they have lower temperatures, generally negative or nearing the zero Celsius, which permits to preserve the snowfall in a snowpack form during the winter, and early spring for the high elevated areas. As measured on the southern (Mgoun sub-catchment) and the northern (Ourika sub-catchment) slopes of the High Atlas range, snowfall represents between 20% and 80% of total precipitation depending on elevations and season (Schulz, 2006; Boudhar et al., 2016). Across the Tensift headwater basin, meltwater from snow constitutes approximately a rate between 25% and 50% of the total annual runoff volume (Boudhar et al., 2009).

Furthermore, it is worldwide known that topography, particularly elevation, strongly affects the spatial distribution of rainfall (Duckstein et al., 1973; Liao et al., 2007; Qing et al., 2011). It acts by disturbing the local wind patterns and enhancing the condensation process through the orographic uplift (Bonacina, 1945; Qing et al.,

2011). The latter can be responsible for more than 30% of the spatial variability of annual and seasonal rainfall totals (Spreen, 1947; Sevruk, 1997; Qing et al., 2011). This variability is often translated by an increase in rainfall with elevation, which can be in terms of the number of events, the magnitude of the events, or the combination of both (Pedgley, 1970; Duckstein et al., 1973; Salles et al., 2001). However, the rainfall–elevation relationship, more apparent for coarse time scales (monthly onwards) (Salles et al., 2001; Song et al., 2019), can be inverted in some contexts exhibiting strong negative correlations (Lu et al., 2008). For these reasons, water resources availability in mountain part is vital for various socio-economic activities in lowlands. This dependency on the upstream surface water and snowpack storage is becoming more important during last decades as a result of climate change and anthropic effects.

Climatic regional studies in Morocco project an increase in dry periods by 2050 that could dramatically impact water resources availability (Driouech et al., 2010; Jaw et al., 2015; Khomsi et al., 2015; Driouech et al., 2020). Future climate scenarios in the Mediterranean context, including the Atlas Mountains, indicate an increase in temperature, and driers conditions will induce a decline in snow accumulation and duration (Fayad et al., 2017; López-Moreno et al., 2017; Polo et al., 2019). As such, changes in precipitation's amount and phases will significantly affect basin's hydrological response and seasonal rivers regimes. It could also influence water balance and other physical processes that control fluxes exchanges between streamflow, reservoirs storages, groundwater table, and soil moisture.

In this context of water shortage and climate change constraints, a good understanding of the hydrological functioning in mountain basins, to quantify water redistribution at the catchment scale, is of a significant importance for water management purpose. To this end, field measurements are the optimal manner to obtain real information on water and climate parameters, which are very scarce in the Atlasic basins due to the rugged terrain and inaccessibility. To overcome this limitation, datasets from Earth Observations and climate models are useful for retrieving information related to water cycle. The aim of this chapter is to monitor and characterize the spatio-temporal behaviour of the main water and climate-related parameters over the whole Atlasic Mountains using large-scale satellite products and Reanalysis models.

8.2 The Atlas Mountains Context

This study focuses on the Atlas Mountains range located in central Morocco, northwestern part of Africa, over an extent of about 800 km in length and 60 km in large (Fig. 8.1). This area is distributed from south to north into three broadly parallel ranges: The Middle Atlas, the High Atlas, and the Anti-Atlas. Altitudes for these chains range from 1000 m to a culminating point on the Jbel Toubkal, the highest summit of North Africa at 4167 m, followed by the Megoun massif at 4068 m, both located in the High Atlas. As illustrated in Fig. 8.1, the Atlas Mountains host the

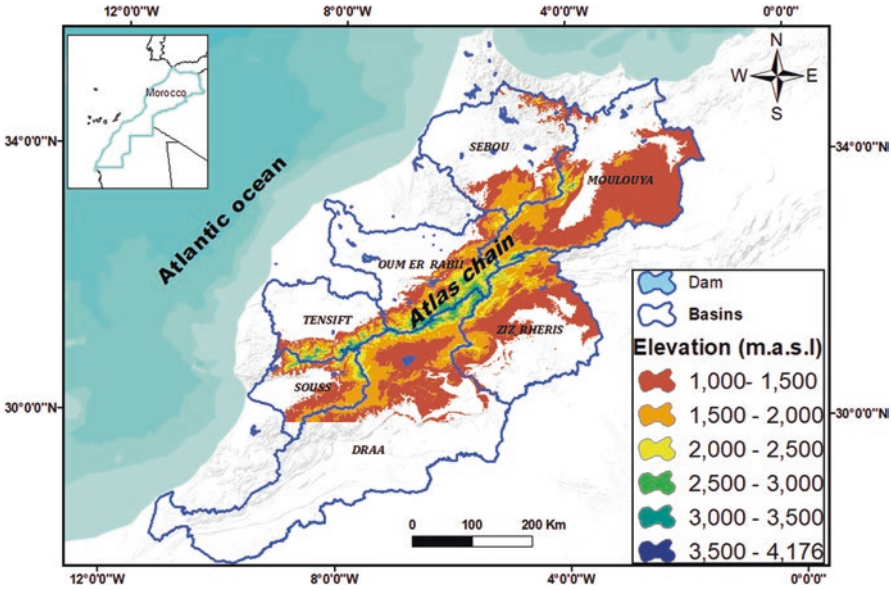

Fig. 8.1 Localization of the Atlas chain and the main supplied river basins in Morocco

headwater part of the main river basins of Morocco: Moulouya, Oum Er-Rbia, Sebou, Tensift, Draa, Ziz-Rheris, and Souss.

In term of topography, physiographic parameters are extracted from an SRTM (The Shuttle Radar Topography Mission) digital elevation model (DEM), considering pixels above 1000 m for the followed analysis (Fig. 8.2). Overall, the lower elevations ($Z < 1400$ m) represent a large portion (up to 50%) of the total area, with an overall mean of 1500 m. Slope distribution varied largely with a mean of ~20°. Generally, the Atlas features take a mean direction of (NW-SE) and 70% of total surface is covered by north and east aspects.

Regarding climate, the Atlas region is under the combined influence of the Atlantic Ocean to the west, the Mediterranean Sea to the north and the desert Sahara to the south (Knippertz et al., 2003). It presents a great climatic barrier between the north of the country and the desert in the south. We can therefore find a wide variety of climates going from moderate humid and sub-humid climates at the northern slope of the High Atlas to semi-arid and arid climates in south of the Atlas.

8.3 Snow Cover Duration from MODIS Snow Product

Seasonal and interannual variations of snow cover across the Atlas chain have been previously derived from various spatial satellite data (e.g. SPOT-VEGETATION, MODIS, Landsat, Formosat, Sentinel-2A) through numerous works (Baba, 2018; Boudhar et al. 2009; Chaponnière, 2005; Ahmed Marchane et al., 2015). They were

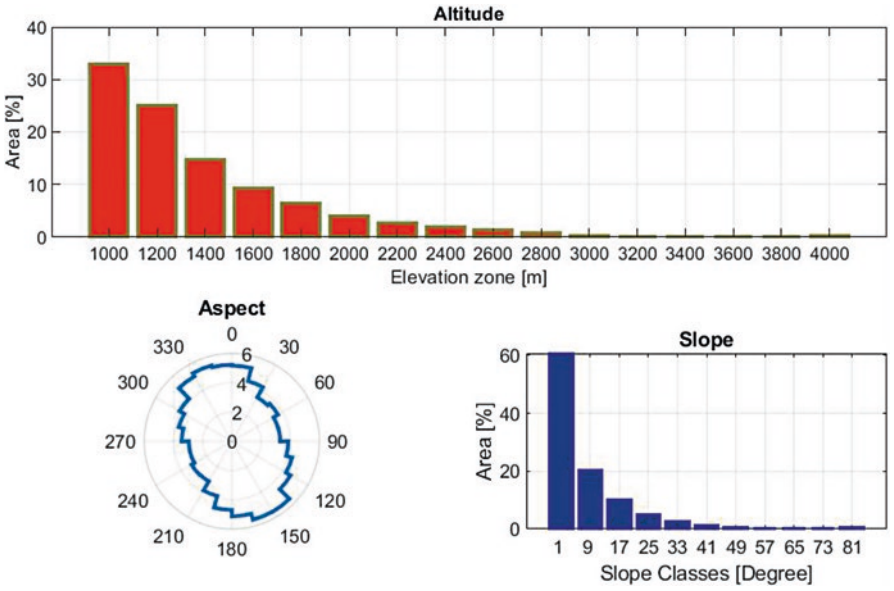

Fig. 8.2 Hypsometric curve, aspect rose diagram, and percentages of slope band's area of the Atlas Mountain (elevation > 1000 m)

interested on mapping and monitoring the basic characteristics of snow cover area (SCA) at various scales over the Atlas in Morocco (Boudhar et al., 2010; Boudhar et al., 2007; Marchane et al., 2013, Marchane et al., 2015).

The signal of SCA dynamic exhibits a high spatio-temporal heterogeneity, especially from year to year based on the topographic effect. An example of the temporal variability over a pilot sub-catchment in the Tensift river basin is shown in Fig. 8.3, where the time series of daily fractional snow cover (fSCA) shows significant intra- and inter-annual variability over the period 2003–2016. In other investigations, SCA chronological series were used as input to evaluate snowmelt contribution to streamflow even if empirically (Boudhar et al., 2020) or through hydrological models (Boudhar et al., 2009; Ouatiki et al., 2020). Also, this information was served to calibrate, assess, and improve snow models and thus quantify snow water equivalent (SWE) at local and basin scales (Boudhar et al., 2016; Bouamri et al., 2018; Baba et al., 2019).

Long-term SCA series over 17 years period, obtained from Moderate Resolution Imaging Spectroradiometer (MODIS) snow products, and pre-processed for cloud filtering by (Marchane et al., 2015), were used to analyse snow cover duration (SCD) variability. Figure 8.4 (top) shows the annual changes of the median SCD for the entire Atlas area that varies from 18 days per season in 2016 to 73 days in 2009 with an average of 46 days. This SCD rate is strongly associated to the topographic features, principally the altitude, and varies from 20 days to 140 days for low and high elevation zones, respectively (Fig. 8.4, bottom left). The relationship between SCD median for each altitudinal zone (step of 200 m), during 2000–2016 period,

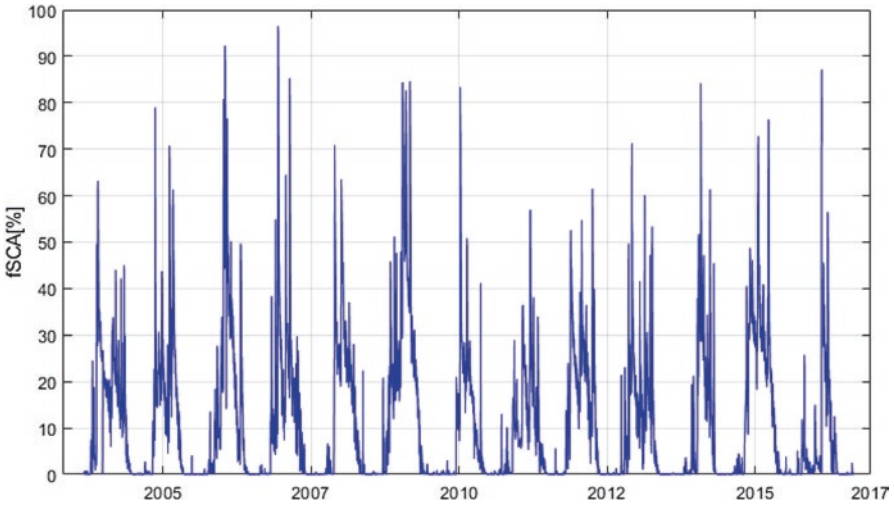

Fig. 8.3 Time series of mean SCA (fractional snow cover area: fSCA) MODIS over the entire period 2003–2016 in the Rheraya sub-catchment

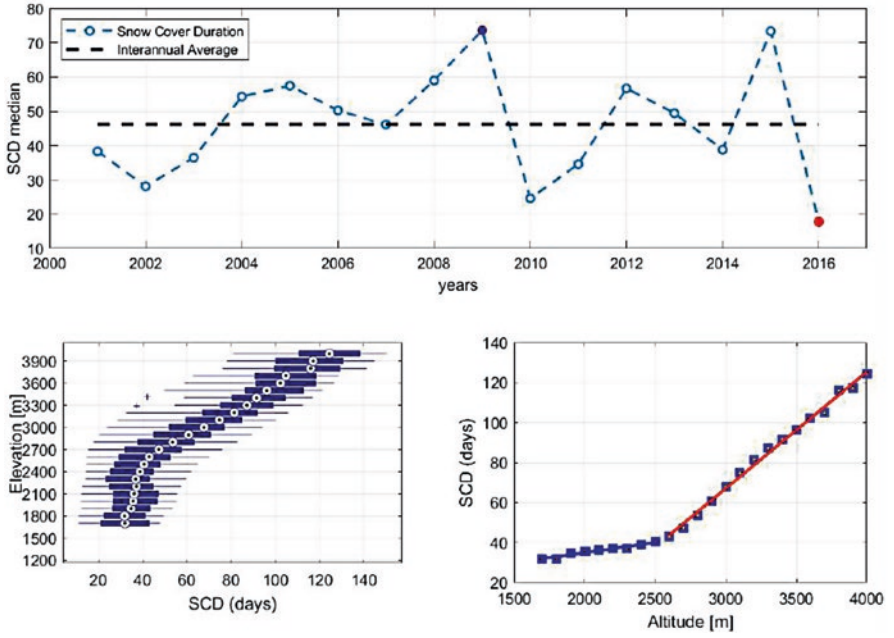

Fig. 8.4 Annual average of snow cover duration (SCD) (median value over whole Atlas area per season) variability (Top), boxplot of SCD by altitudinal band (period: 2000–2016), (Bottom Left) SCD median (2000–2016 mean) vs elevation (Bottom Right)

and elevation are significantly correlated with a mean Pearson coefficient ($r = 0.97$) (Fig. 8.4, bottom right). It is revealed that the topographic gradient of SCD is about 1 day/100 m for elevation under 2500 m and 5 days/100 m for the part upper to 2500 m.

8.4 Precipitation Variability Over the Atlas as Seen from Space

In this section, we discuss the spatial variability of rainfall over the seven Atlasic river basins. To do so, we employed rainfall estimates from PERSIANN-CDR and IMERG-v6 gridded satellite products. While PERSIANN-CDR is a model developed by the CHRS at the University of California Irvine, GPM is a space mission fully dedicated to precipitation monitoring under the joint control of NASA and JAXA (Ashouri et al., 2015; Huffman et al., 2019). The first uses Geostationary Infrared (IR) observations, and the second combines IR, Passive Microwave (PMW), and Radar data to produce near-global gridded rainfall products. These are freely provided as sub-daily estimates at 0.25° (PERSIANN-CDR) and 0.1° (GPM IMERG) spatial resolutions. The two products were chosen based on the findings from an unpublished study conducted over the Oum Er-Rbia river basin. In the study, eight rainfall gridded datasets (ARC, CHIRPS at a 25 km resolution, CHIRPS at a 5 km resolution, CMORPH-CRT; IMERG v6, PERSIANN-CDR, RFE, and TRMM 3B42 v7) were evaluated against in situ measurements at different time scales. IMERG and PERSIANN were found to provide the best performance compared to all of the considered products, in terms of both correlation and bias. In particular, IMERG significantly outperformed its predecessor TRMM and showed great potential for rainfall monitoring at regional scales.

Figure 8.5 displays the mean interannual rainfall calculated based on PERSIANN and IMERG estimates for the seven Atlasic river basins. It can be clearly seen that both products capture the north-to-south gradient that characterizes the spatial distribution of rainfall over the Moroccan territory (Filahi et al., 2016). The Sbou river basin, which is subject to strong influences from the Mediterranean sea and the Atlantic ocean (Knippertz et al., 2003), appears to receive the highest amounts of rainfall with a regional average of 481 $mm.y^{-1}$ (PERSIANN) and 603 $mm.y^{-1}$ (IMERG). The Daraa river basin, on the other hand, is the driest with a regional rainfall average of 125 $mm.y^{-1}$ (IMERG) and 150 $mm.y^{-1}$ (PERSIANN). Moreover, the effect of the atlas mountain on the spatial distribution of rainfall over northern Morocco is obvious, particularly in the IMERG estimates. The latter shows more zonal contrast compared to PERSIANN, which can be relative to its finer spatial resolution in conjunction with the high sensitivity of its radar system to a wider range of water droplet sizes. Overall, the Atlas Mountains play the role of an obstacle that holds most of the western advections, the main source of humid air masses for the majority of the studied region (Knippertz et al., 2003). It stimulates the generation of rainfall on its western slope more often than on the eastern one. Hence,

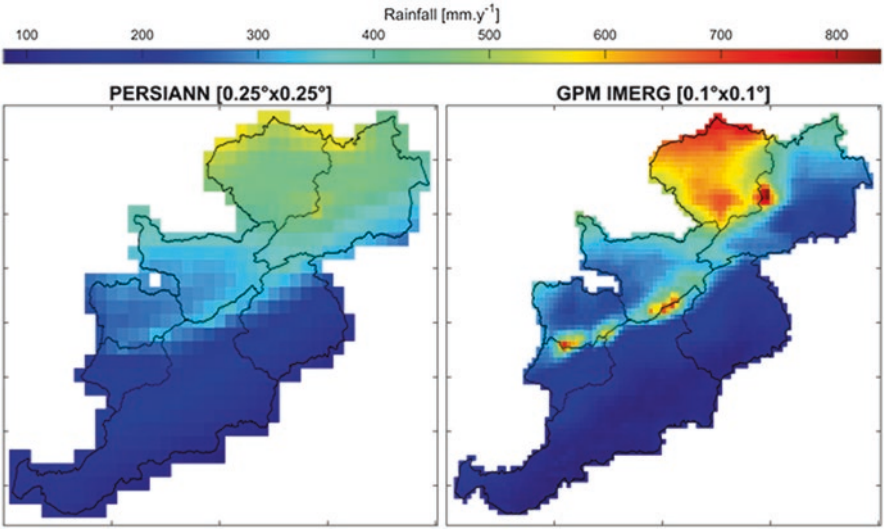

Fig. 8.5 Mean interannual rainfall calculated using PERSIANN and IMERG estimates for the period 2000–2019. The solid black lines represent the limits of the Atlasic river basins

the Sbou, Oum Er-Rbia, Tensift river basins appear to be wetter than the others. In particular, we note that the wetness of the western river basins, at the regional scale, can be largely attributed to the grid cells of high elevations, which tend to accumulate more rainfall than those covering the lowlands. This holds true for all the studied river basins, except for Sbou where the rainfall totals are relatively and evenly distributed.

Generally, it is widely known that the rainfall occurrence and magnitude tend to increase with elevation. However, the nature of this relationship may differ with regions, depending on their climatic regimes and geomorphologic characteristics. Thus, in the following, we investigate the spatial variability of rainfall with respect to the changes in elevation, over the seven Atlasic river basins individually. Figures 8.6 and 8.7 display the scatter points of the mean interannual rainfall versus median elevation of the grid cells situated within each of the river basins for PERSIANN and IMERG, respectively. The scattered points are classified according to the latitudes representing the centre of the grid cells. In each subplot, the red and the blue points refer to the grid cells located near the northern and southern limits of the corresponding basin, respectively. By comparing Figs. 8.6 and 8.7, we can see that PERSIANN is unable to clearly describe the dual between rainfall and elevation compared to IMERG. This can be due to the features that characterize the algorithms of each of the two products, including the used data sources and the adopted spatial resolutions. For instance, the combination between IR, PMW, and Radar data sources, in IMERG, allows more realistic, and thus less biased, estimates of rainfall compared to the IR-only process involved in PERSIANN. This can explain the strongly dampened estimates in PERSIANN relative to IMERG. Additionally, the finer spatial resolution in IMERG allows better sampling of studied basins, with

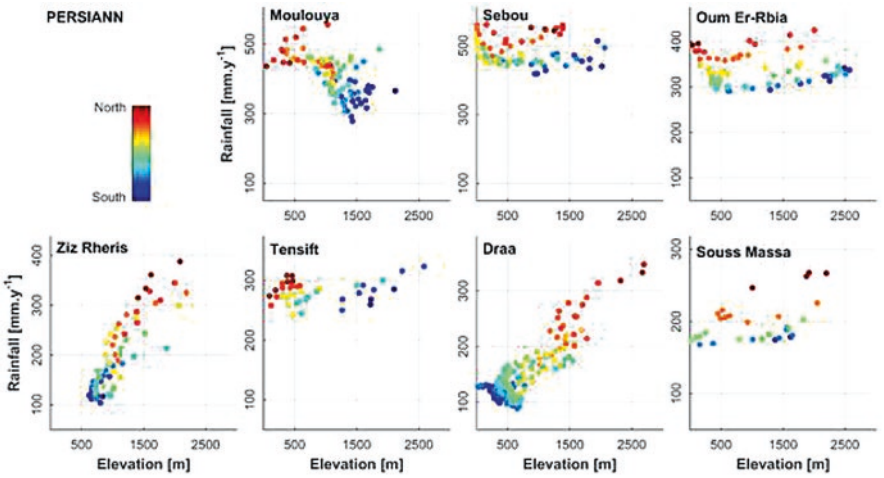

Fig. 8.6 Scatter plots of the mean interannual rainfall versus elevation using the PERSIANN estimates. Each subplot refers to an Atlasic river basin

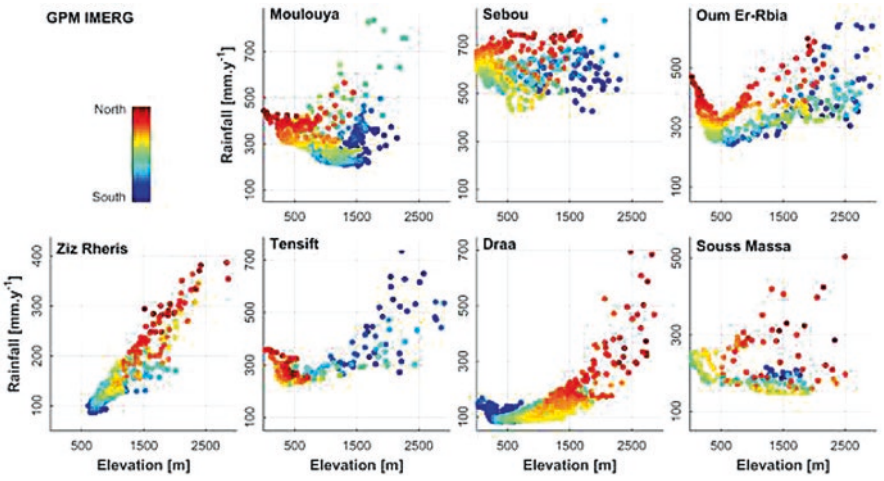

Fig. 8.7 Scatter plots of the mean interannual rainfall versus elevation using the IMERG estimates. Each subplot refers to an Atlasic river basin

more grid cells per unit than what PERSIANN provides. According to Fig. 8.3, different behaviours can be depicted. While no clear tendency can be concluded from the scattered point of the Sbou, the rainfall in the large majority of the grid cells that cover Moulouya and Souss-Massa seem to decrease with elevation. The mean interannual rainfall ranges from around 440 mm.y^{-1} (250 mm.y^{-1}) for Moulouya (Souss-Massa) at low elevations, near the coastal line of the Mediterranean Sea, to around 210 mm.y^{-1} (150 mm.y^{-1}) at regions of 1500 m a.s.l. Still, some high elevated grid cells show rainfall magnitudes larger than those of the coastal regions. They are

mainly located in the middle of Moulouya, near its limit with Sbou, and in the north of Souss-Massa, near its limit with Tensift (Fig. 8.5). In Daraa, Tensift, and Oum Er-Rbia, there are two different tendencies with elevation. We observe a decreasing tendency for the grid cells lying between the outlet, at the shore of the Atlantic Ocean and the regions of 500 m a.s.l. or less. An increasing tendency takes place starting from 500 m a.s.l., as the rainfall magnitudes correlate positively with elevation and become relatively more consistent above 1000 m a.s.l. Furthermore, basins such as the Oum Er-Rbia can be divided into two sub-regions with even two different increasing trend lines (regression lines) that can be drawn. A northern region with wetter conditions (represented with the red points) and a southern region that is relatively drier (represented with the blue points).

8.5 ERA5 Temperature Reanalysis Data

Due to the lack or the absence of meteorological stations and in-situ measurements in most of the Atlas basins, different studies were based on meteorological reanalysis data to monitor the snowpack state in the Mediterranean mountains (Fayad et al., 2017; Baba et al., 2018, 2019). ERA5 reanalysis data are the one of the reanalyses of the highest spatio-temporal resolution (hourly temporal resolution and ~30 Km of spatial resolution). For these reasons, we distribute ERA5 temperature by using SRTM (The Shuttle Radar Topography Mission) digital elevation model (DEM) over the mountainous areas. This enables us to study and analyse the air temperature evolution spatially and temporally. The distribution has been carried out by using the Barnes objective analysis scheme, which applies a Gaussian distance-dependent weighting function to interpolate the station data to the model grid resolution. This method is integrated in MicroMet (Liston & Elder, 2006). MicroMet outputs are daily rasters, with each pixel (200 m × 200 m) representing the temperature at given location. The distribution was performed from 1st January 1981 to 31st December 2019. A quantitative assessment of ERA-5 parameters against ground measurement over a pilot basin in Moroccan High Atlas (Rheraya) showed a good correlation, especially for air temperature (Baba et al., 2021). Following this approach, air temperature maps were produced over the whole Atlas, which cover the mountainous regions over 1500.m.a.s.l.

Different products were derived from these daily temperature maps, namely, the winter mean temperatures from 1981 to 2019 (Fig. 8.8) which show that a big part of the mountains is characterized by a freezing winter (<5 °C). This increases the potential for getting snow when it rains. Moreover, these low ambient temperatures, especially in the high elevated regions, are an important element to preserve the snow cover and delay its melting until spring.

Figure 8.9 shows that the mean temperatures in the mountainous region have a positive growing trend. More specifically, the two warmest winters during the last four decades are observed during the last 10 years. This growth in temperature has a significant impact on the evolution of the snowpack and the extension of the snow

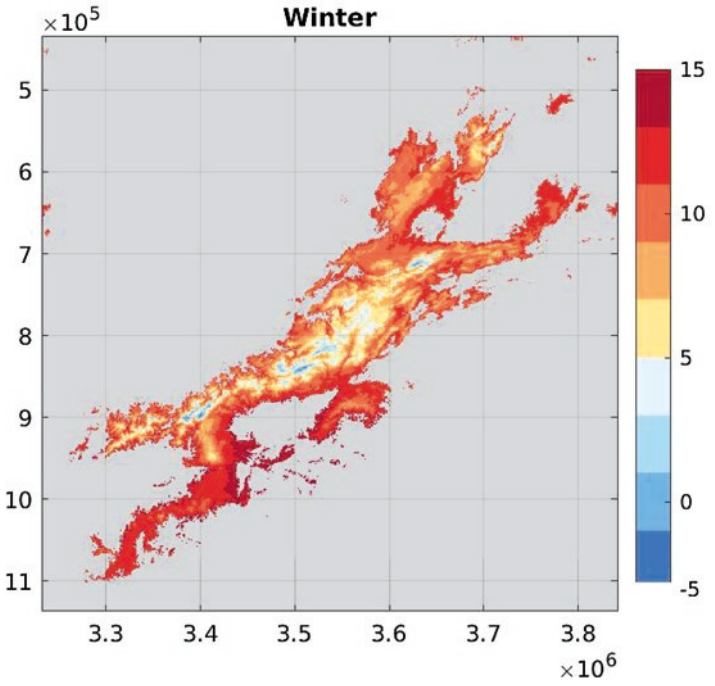

Fig. 8.8 Mean winter temperatures (°C) over the Moroccan mountains from 1981 to 2019. Regions below 1500.m.a.s.l were masked. Projection: UTM-29 N

cover. As an example, it is very clear that 2008–2009 is the coldest winter during the last four decades (Fig. 8.9), and similarly, from remote-sensing data we can observe that 2009 year had the largest snow cover durations during the last two decades (Fig. 8.9). Otherwise, 2009–2010 winter is one of the warmest winters with 0.2 °C over the mean of temperature during last four decades (Fig. 8.9). This is also expressed in term of snow cover duration: 2010 is the second lowest year (Fig. 8.9).

8.6 Conclusion

In this chapter, we have examined the usefulness of remote sensing and global reanalysis data to characterize water and climate parameters over the whole Atlas Mountains where ground observations are scarce. These chains play a vital role by supplying fresh water for agriculture, domestic, hydroelectric production, and industrial uses and also for eco-hydrological systems control.

Interannual fluctuations of all analysed parameters (Snow Cover Duration, Precipitation, and Air temperature) are marked by a strong variation, whether in temporal or spatial scale, that characterizes the Mediterranean climate and associated with a high dependency to elevation.

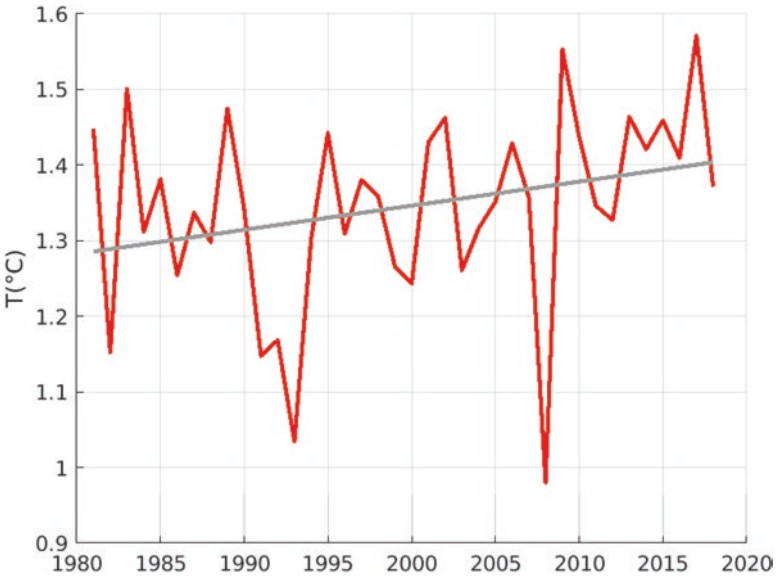

Fig. 8.9 Evolution of mean temperature (°C) during the winter in the Atlas Mountain from 1981 to 2019 (red fit). The grey line represents the trend line during the same period

Both remote sensing and reanalysis datasets show that the Atlas Mountains are increasingly warmer, and their snow cover decreases in term of duration. Therefore, we believe that it is necessary to seek with care the climate projections in the mountainous areas. This will allow us to have a wide view on the impact of climatic changes in the future on snowpack and therefore snowmelt distribution spatially and temporally.

This summarizing work is essential for understanding the global situation of water and climate associated parameters over the Atlas Mountains. Taking advantage of both geospatial and the existing in situ data, results and approaches here could be used for multiple applications. Regarding the freely access and quasi real-time availability of these data, the operational character could be developed over each river basin to support water resource management strategies.

References

Ashouri, H., Hsu, K. L., Sorooshian, S., Braithwaite, D. K., Knapp, K. R., Cecil, L. D., Nelson, B. R., & Prat, O. P. (2015). PERSIANN-CDR: Daily precipitation climate data record from multisatellite observations for hydrological and climate studies. *Bulletin of the American Meteorological Society, 96*(1), 69–83.

Baba, M. W., Boudhar, A., Gascoin, S., Hanich, L., Marchane, A., & Chehbouni, A. (2021). Assessment of MERRA-2 and ERA5 to model the snow water equivalent in the high atlas (1981–2019). *Water, 13*(7), 1–14. https://doi.org/10.3390/w13070890.

Baba, M. W., Gascoin, S., & Hanich, L. (2018). Assimilation of Sentinel-2 data into a snowpack model in the High Atlas of Morocco. *Published Online*, 1–23. https://doi.org/10.3390/rs10121982.

Baba, M. W., Gascoin, S., Jarlan, L., Simonneaux, V., & Hanich, L. (2018). Variations of the snow water equivalent in the Ourika catchment (Morocco) over 2000–2018 using downscaled MERRA-2 data. *Water, 10*(9), 1120.

Baba, M. W., Gascoin, S., Kinnard, C., Marchane, A., & Hanich, L. (2019). Effect of digital elevation model resolution on the simulation of the snow cover evolution in the high atlas. *Water Resources Research, 55*(7), 5360–5378.

Bonacina, L. C. W. (1945). Orographic rainfall and its place in the hydrology of the globe. *Quarterly Journal of the Royal Meteorological Society, 71*, 44–55.

Bouamri, H., Boudhar, A., Gascoin, S., & Kinnard, C. (2018). Performance of temperature and radiation index models for point-scale snow water equivalent (SWE) simulations in the Moroccan High Atlas Mountains. *Hydrological Sciences Journal, 63*(12), 1844–1862.

Boudhar, A., Boulet, G., Hanich, L., Sicart, J. E., & Chehbouni, A. (2016). Energy fluxes and melt rate of a seasonal snow cover in the Moroccan High Atlas. *Hydrological Sciences Journal, 61*, 931–943.

Boudhar, A., Duchemin, B., Hanich, L., Jarlan, L., Chaponnière, A., Maisongrande, P., Boulet, G., & Chehbouni, A. (2010). Long-term analysis of snow-covered area in the Moroccan High-Atlas through remote sensing. *International Journal of Applied Earth Observation and Geoinformation, 12*, S109–S115.

Boudhar, A., Duchemin, B., Hanich, L., Chehbouni, A. (2007). Analyse de la dynamique des surfaces enneigées du Haut Atlas marocain à partir des données SPOTVEGETATION. *Secheresse, 18*(4), 278–288. https://doi.org/10.1016/j.jag.2009.09.008.

Boudhar, A., Hanich, L., Boulet, G., Duchemin, B., Berjamy, B., & Chehbouni, A. (2009). Evaluation of the Snowmelt Runoff Model in the Moroccan High Atlas Mountains using two snow-cover estimates. *Hydrological Sciences Journal, 54*(6). 1094–1113. https://doi.org/10.1623/hysj.54.6.1094.

Boudhar, A., Ouatiki, H., Bouamri, H., Lebrini, Y., Karaoui, I., Hssaisoune, M., Arioua, A., & Benabdelouahab, T. (2020). Hydrological response to snow cover changes using remote sensing over the Oum Er Rbia Upstream Basin, Morocco. In *Mapping and spatial analysis of socio-economic and environmental indicators for sustainable development* (pp. 95–102). Springer.

Chaponnière, A., Maisongrande, P., Duchemin, B., et al. (2005). A combined high and low spatial resolution approach for mapping snow covered areas in the Atlas mountains. *International Journal of Remote Sensing, 26*(13), 2755–2777. https://doi.org/10.1080/01431160500117758.

Driouech, F., Déqué, M., & Sánchez-Gómez, E. (2010). Weather regimes—Moroccan precipitation link in a regional climate change simulation. *Global and Planetary Change, 72*(1), 1–10.

Driouech, F., ElRhaz, K., Moufouma-Okia, W., Arjdal, K., & Balhane, S. (2020). Assessing future changes of climate extreme events in the CORDEX-MENA region using regional climate model ALADIN-climate. *Earth Systems and Environment, 4*(3), 477–492.

Duckstein, L., Fogel, M. M., & Thames, J. L. (1973). Elevation effects on rainfall: A stochastic model. *Journal of Hydrology, 18*(1), 21–35.

Fayad, A., Gascoin, S., Faour, G., López-Moreno, J. I., Drapeau, L., Le Page, M., & Escadafal, R. (2017). Snow hydrology in Mediterranean mountain regions: A review. *Journal of Hydrology, 551*, 374–396.

Filahi, S., Tanarhte, M., Mouhir, L., El Morhit, M., & Tramblay, Y. (2016). Trends in indices of daily temperature and precipitations extremes in Morocco. *Theoretical and Applied Climatology, 124*(3–4), 959–972.

Hssaisoune, M., Bouchaou, L., & Sifeddine, A. (2020). Moroccan groundwater resources and evolution with global climate changes. *Geoscience, 10*(2), 81. https://doi.org/10.3390/geosciences10020081.

Huffman, G. J., Bolvin, D. T., Braithwaite, D., Hsu, K.-L., Joyce, R. J., Kidd, C., Nelkin, E. J., Sorooshian, S., Stocker, E. F., Tan, J., Wolff, D. B., & Xie, P. (2019). *NASA global precipitation measurement (GPM) integrated multi-satellitE retrievals for GPM (IMERG)* (pp. 343–353). Greenbelt.

Jaw, T., Li, J., Hsu, K.-I., Sorooshian, S., & Driouech, F. (2015). Evaluation for Moroccan dynamically downscaled precipitation from GCM CHAM5 and its regional hydrologic response. *Journal of Hydrology: Regional Studies, 3*, 359–378.

Khomsi, K., Mahe, G., Tramblay, Y., Sinan, M., & Snoussi, M. (2015). Trends in rainfall and temperature extremes in Morocco. *Natural Hazards and Earth System Sciences, 3*, 1175–1201. https://doi.org/10.5194/nhessd-3-1175-2015.

Knippertz, P., Christoph, M., & Speth, P. (2003). Long-term precipitation variability in Morocco and the link to the large-scale circulation in recent and future climates. *Meteorology and Atmospheric Physics, 83*(1–2), 67–88.

Liao, F., Hong, Y. C., & Zheng, G. G. (2007). Review of orographic influences on surface precipitation. *Meteorological Science and Technology, 35*(4), 309–316.

Liston, G. E., & Elder, K. (2006). A meteorological distribution system for high-resolution terrestrial modeling (MicroMet). *Journal of Hydrometeorology, 7*(2), 217–234.

López-Moreno, J. I., Gascoin, S., Herrero, J., Sproles, E. A., Pons, M., Alonso-González, E., Hanich, L., Boudhar, A., Musselman, K. N., Molotch, N. P., Sickman, J., & Pomeroy, J. (2017). Different sensitivities of snowpacks to warming in Mediterranean climate mountain areas. *Environmental Research Letters, 12*.

Lu, A., Kang, S., Pang, D., Wang, T., & Ge, J. (2008). Altitude effect of precipitation and the influence of global warming on it in China. *Ecology and Environment, 17*(5), 1875–1878.

Marchane, A., Jarlan, L., & Hanich, L. et al. (2015). Assessment of daily MODIS snow cover products to monitor snow cover dynamics over the Moroccan Atlas mountain range. *Remote Sensing of Environment, 160*, 72–86. https://doi.org/10.1016/j.rse.2015.01.002.

Marchane, A., Jarlan, L., Hanich, L., & Boudhar, A. (2013). Caractérisation de l'enneigement sur l'atlas marocain par le capteur MODIS et relation avec le climat (période 2000–2011). *Rev Française Photogrammétrie Télédétection, 204*, 13–22.

N'da, A. B., Bouchaou, L., & Reichert, B. et al. (2016). Isotopic signatures for the assessment of snow water resources in the Moroccan high Atlas mountains: contribution to surface and groundwater recharge. *Environment and Earth Science, 75*(9). https://doi.org/10.1007/s12665-016-5566-9.

Ouatiki, H., Boudhar, A., Ouhinou, A., Beljadid, A., Leblanc, M., & Chehbouni, A. (2020). Sensitivity and interdependency analysis of the HBV conceptual model parameters in a semi-arid mountainous watershed. *Water (Switzerland), 12*(9). https://doi.org/10.3390/w12092440.

Pedgley, D. E. (1970). Heavy rainfalls over Snowdonia. *Weather, 25*(8), 340–350.

Polo, M. J., Herrero, J., Pimentel, R., & Pérez-Palazón, M. J. (2019). The Guadalfeo Monitoring Network (Sierra Nevada, Spain): 14 years of measurements to understand the complexity of snow dynamics in semiarid regions. *Earth System Science Data, 11*(1), 393–407.

Qing, Y., Zhu-Guo, M., & Liang, C. (2011). A preliminary analysis of the relationship between precipitation variation trends and altitude in China. *Atmospheric and Oceanic Science Letters, 4*(1), 41–46.

Salles, M. A., Canziani, P. O., & Compagnucci, R. H. (2001). Spatial variations in the average rainfall-altitude relationship in Great Britain: An approach using geographically weighted regression. *International Journal of Climatology, 21*(4), 455–466.

Schulz, O. (2006). Modélisation de la fonte de neige dans les montagnes du Haut Atlas Central.

Sevruk, B. (1997). Regional dependency of precipitation-altitude relationship in the Swiss Alps. In *Climatic change at high elevation sites* (pp. 123–137). Springer.

Song, L., Chen, M., Gao, F., Cheng, C., Chen, M., Yang, L., & Wang, Y. (2019). Elevation influence on rainfall and a parameterization algorithm in the Beijing area. *Journal of Meteorological Research, 33*(6), 1143–1156.

Spreen, W. C. (1947). A determination of'the effect of topography upon precipitation. *Transactions. American Geophysical Union, 28*(2), 285–290.

Chapter 9
Evaluating Settlement Development Change, Pre, and Post-1994 in the Drakensberg Mountains of Afromontane Region, South Africa

T. F. Onaolapo, T. W. Okello, and S. A. Adelabu

Abstract Human settlement development is a predominant form of land cover change in any part of South Africa. This chapter provides an outline of the development pattern changes in three settlements of Thabo Mofutsanyana municipality in Drakensberg mountains, South Africa, for the past 30 years (1989–2019), with emphasis on 1994, the year when governance changed from minority to majority rule in South Africa. This research aims at understanding settlement pattern change in the selected settlement. Landsat images of 1989, 1999, 2009, and 2019 were downloaded from satellite images through remote-sensing method from Thematic Mapper. Classification and Regression Tree algorithm was used in classifying the land-use land cover, and the results of the study revealed that the settlements (built-up) Harrismith, Ladybrand, and Vrede experienced increase in all the years under study. The built-up area of Harrismith increased from 3.82% to 9.06% from 1989 to 1999, and also from 11.15% to 19 68% from 2009 to 2019. Also, Ladybrand's built-up increased from 5.03% to 12.53% in 1989 and 1999 and from 13.0% to 17.35% from 2009 to 2019, while Vrede's built-up increased from 1.06% to 3.37% in 1989 to 1999 and from 3.39% to 10.17% from 2009 to 2019. The spatial pattern of development that was observed in the study areas as revealed in the transition maps helped in establishing development trends. The main findings of the study reveal that the land area for settlement development (built-up) in the selected settlements of the study area has increased rapidly with the proportional loss of other land uses from 1989, 5 years before the change in government to 1999, 5 years after the change. This is related to various policies such as the Development Facilitation Act

T. F. Onaolapo (✉)
Department of Geography, University of the Free State, Qwaqwa, South Africa

T. W. Okello
Department of Biological and Environmental Sciences, Walter Sisulu University, Mthatha Campus, South Africa
e-mail: okellotw@ufs.ac.za

S. A. Adelabu
Department of Geography, University of the Free State, Bloemfontein, South Africa

S. Adelabu et al. (eds.), *Remote Sensing of African Mountains*,
https://doi.org/10.1007/978-3-031-04855-5_9

of 1995 and Housing Acts 107 of 1997, which enabled land and homeownership by all South Africans. Statistics South Africa's (Statistics SA) demographic data that was available also confirmed a population increase for the study area for the years under study. The research serves as a basis for sustainable settlement development in mountainous areas.

Keywords Settlement development · Remote sensing · Apartheid · Spatial pattern · Sustainable development

9.1 Introduction

Recent changes in human settlement development and their effects on the environment call for serious environmental concerns by experts and the human population (Li et al., 2020). The effects include climate change, land degradation, loss of biodiversity, air and water pollution. Loss of agricultural land to human settlement development was noted as the highest form of land cover change in South Africa (Musakwa & Van Niekerk, 2013). The topography of the area is characterized by low/high mountain and irregular land, which occurs above 1500 m elevation near the equator (Brand et al., 2008). Although there is no universally accepted definition for mountains, continuity, positioning, relief, altitude, slope, and size are criteria that have been used to define mountains. A mountain is defined in Ireland and the United Kingdom as any peak equal or above 610 m high (Nuttall & Nuttall, 2008; Wilson, 2001). The United Nations Environmental Programme's definition of a mountain includes elevation of at least 300 m and could even be as high as 2500 m or above (Blyth et al., 2002). However, this study defines the Afromontane region according to UNEP's definition as a region of high lands which occur above 300 m elevations.

Human settlements refer to 'the totality of the human community, whether city, town or village with the social, material, organizational, spiritual and cultural element to sustain it' (Habitat, 1976). Settlement development change, as well as urbanization, are global phenomena that are important developmental procedures impacting the physical environment via numerous socioeconomic and ecological procedures (Basiago, 1998). Settlement can be divided into two types: urban and rural settlement. Urban settlements such as towns, cities, informal settlements, and peri-urban areas are usually characterized by high populations. In contrast, rural settlements are areas in which people depend directly on their immediate environments through agriculture, fishing, and the collection of resources for their daily needs and are usually characterized by a low population (Habitat, 1976). Settlement patterns all over the world differ from one place to another at different times (Hui & Moyse, 2018). Thus, the study of spatial analysis is of great importance to human beings and environmental sustainability. The spatial relationships between and amongst settlements are shaped by commerce, people's ideas, government policies, and the processing of raw materials into finished products (Cannon, 1990; Owusu, 2005). Thus, settlement patterns influence the environment, population distributions, the use of natural resources, which can generate economic prosperity (Sarkar,

2010). Settlement development (built-up area) is an apparent land cover change in the area as compared with other land uses in the study areas; this implies that the environment is much affected by human activities in settlement expansion. Few works of literature have highlighted physical factors like geographical location, topography, and water bodies, or economic, political, and social reasons as forces behind settlement development patterns and forms (Berry, 2015).

The history of socio-political change in the South African government is greatly connected with urbanization, which is a major force in settlement development. The change from the minority rule of government to the majority is perceived to have brought up a different situation that poses challenges before key players in the environment (Madlingozi, 2007). The change in governance informs the pattern of development in most communities in South Africa (Pallister-Wilkins, 2011; Turok, 2014). Some of the effects of the changes are haphazard development in the form of shacks and other informal settlements in and around cities (Onaolapo et al., 2020), and one of the major ways to monitor such land cover changes is through the use of satellite data from remote sensing (Coppin et al., 2004; Kleynhans et al., 2012; Lu et al., 2004).

The use of GIS and remote sensing to monitor land-use patterns and developmental change requires downloading two or several images with different resolutions (high, medium, or low) at different times, compilation and arrangement of the images, and grouping of each pixel, which enables to put into different classes (Moser et al., 2007; Radke et al., 2005). Land-use patterns and developmental changes in small and large settlements have been successfully monitored using different geospatial techniques, such as Change Detection, Moderate Resolution Imagine Spectrometer (MODRIS), (Wang et al., 2021; Wulder et al., 2018, Coops et al., 2009; Hansen et al., 2003, 2000; Mildrexler et al., 2007, 2009). These methods of geospatial techniques data collection have less human involvement and also enable the processing of large datasets in less time.

Mapping land use changes through remote sensing are time-saving, cost-saving, and resource-effective (Mahabir et al., 2018). High, medium, or low-spectral help in mapping out of old or new settlements, comparison of images taken at different periods helps in determining the changes over time as well as the emergence of new settlements (AbuHafeetha, 2014). Lloryd et al. (2016) emphasized the need for GIS tools to monitor and plan for land-use development of Monrovia in Liberia after the civil war in 2003. They discovered that haphazard development, which happened during the war, created a problem of development control in which 1.2 million people spread over a large space of land without any restriction (Lloyd et al., 2016). Sang et al. (2019) in Tianjin, northern China, studied and analysed the intensity and stationarity of land-use change; they used thematic mapper images of 1995, 2000, 2005, and Operation Land Imager (OLI) image 2015. They classified the land-use land cover using Classification and Regression Tree Table Algorithm. Their results showed that the increase of 7.5% in land-use change during 1995 to 2015 was due to rapid urban development (Sang et al., 2019).

Drastic land use and socioeconomic changes have led to urbanization and environmental concerns (Dadashpoor et al., 2019). Such a change in population and

environment coupled with less functional land-use planning and lack of development control results in environmental decline, indiscriminate landscape development, misuse of land, and strain on the ecosystem structure (Güneralp et al., 2017). Consequently, more forest areas and farmland have changed to built-up areas and other urban development in recent years (Coppin et al., 2002). This is also the case of Thabo Mofutsanyana municipality in the Afromontane region (Krannich et al., 2011; McGranahan, 1999; Urban et al., 2016). Mountainous areas received little or no attention when it came to spatial planning. Its unique nature demands adequate monitoring and planning, hence, the need for an in-depth study of the land-use patterns and assessing developmental trends over the period of time, which is important for future development and management. This study determines the changes in human settlement developments in the three selected settlements, Harrismith, Ladybrand, and Vrede, in Thabo Mofutsanyana municipality of Drakensberg mountain, Free State province using remote sensing and GIS. This study is important because of its peculiarity of settlement development in the mountainous area of Drakensberg mountain of the Afromontane region.

9.2 Description of the Study Area

Thabo Mofutsanyana municipality is within Drakensberg mountain, the Free State province of South Africa (Fig. 9.1). It is one of the five municipalities that exist within the province. The municipality has a total population of 769,761 people with a population density of 28.9 people per $km^{2;}$ the majority of its people speak Sesotho and a land surface area of 33,269 km^2 (Statistics, 2012). The primary function of the municipality is agriculture, with an administrative office at Phuthaditjhaba (Denoon-Stevens & Mocwagae, 2019). The municipality is bounded by Maluti, Drakensberg, and Eastern Free State mountains and by the Eastern Cape, KwaZulu-Natal, and Lesotho, which project a charming and beautiful scenery for tourism in the region (Statistics, 2012). The municipality makes the second smallest contribution to the GDP of the Free State, with trade, retail, wholesale, financial, and community services being the core contributing sectors (Kalane, 2015). Furthermore, its annual importing and exporting value is the second smallest amongst the five municipalities (Statistics, 2012).

The municipality is situated in a rural area in the eastern Free State, and it includes the former homeland of Qwaqwa (Mangope, 2015). It was also declared a Presidential Node in the early 2000s. The topography of the study area is a low mountain and irregular shapes. It has six local municipalities: Maluti-A-Phofung, Phumelela, Nketoana, Dihlabeng, Setsoto, and Mantsopa. Maluti-A-Phofung contains 55.5% of the municipality's total population and is the most populated. Three settlements were selected from three local municipalities For this research, three settlements, Harrismith, Ladybrand and Vrede, were selected from three local

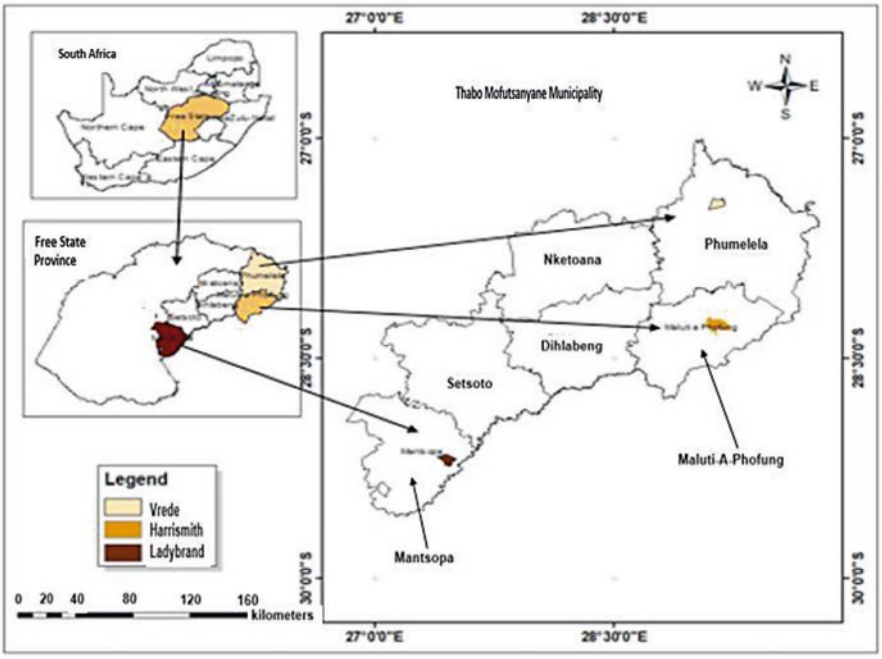

Fig. 9.1 Map of South Africa showing Free State Province and Thabo Mofuntsanyane municipality

municipalities, Maluti-A-Phofung, Mantsopa, and Phumelela, respectively. Maluti-A-Phofung local municipality – Highest population/almost the lowest land area in the municipality; and Harrismith, which is strategically placed between two prominent cities of South Africa, which are Johannesburg and Durban, it represents the urban settlement out of the three settlements understudy, it has a population of 27,869 (Statistics, 2012). Phumelela local municipality has the lowest population and largest land area, Vrede has a small population below 2000 people with a large area for farming; it represents the least in the hierarchy of the three settlements under study (Statistics, 2012). Mantsopa has the average land extent and population, it is located at the southern part of the municipality and Ladybrand is a close town to the Lesotho border, Maseru, this is very significant to the town's development pattern, and it represents an average town between the three settlements under study. It had a population of 4218 in 2011 (Statistics, 2012). Years were chosen at an interval of 10 years. (i.e. 1989, 1999, 2009, & 2019) for even monitoring; the first year represents 5 years before the change, while the second year represents 5 years after the change of government from minority to majority rule.

9.3 Methodology

In this research, temporal changes in the patterns of the landscape were identified using 30 m resolution LANDSAT TM and OLI. Table 9.1 contains a list of data employed for this research.

A preliminary survey was done to gather data for the classification of scheme's development and to serve as physical data validation for the classification and assessment of the images that were classified. Four scenes of Landsat4–5 Thematic mapper (TM) for 1989, 1999, and 2009 images and Landsat-8 Operational Land Imager (OLI) images for 2019 (Table 9.1) were used. The land-use maps for the research covered the years before and after the major event of a change in the political system of the country, and the images were downloaded based on the clearest visibility (free from being blurred by cloud) as they appeared on the satellite within the same season of the same year. Imageries were pre-processed; six image bands used for this study were geometrically rectified to Geographic Coordinate System.

Landsat images of 1989, 1999, 2009, and 2019, an interval of a decade was chosen to monitor a continuous change in the human settlement; also the first 2 years represented 5 years before and 5 years after 1994, the eventful year of transitioning from minority to majority rule (i.e. 1989 and 1999), respectively. These periods of interval enabled balance means of measuring changes, as 1999 was the end of the first term of office of elected politicians.

9.3.1 Image Pre-processing, Processing, and Classification

The images appear in distinct datasets as tiles for the same coverage of the same year and therefore mosaicked together with others to form a unified dataset that was assessed to detect the changes. The study was located on path 170, row 081 in the worldwide reference system type 2. These scenes were already georeferenced in the UTM (Universal Transverse Mercator) image projection Zone 35S with Datum WGS84 (Khan & Aaqib, 2017).

After pre-processing, every mosaicked image was classified into four land cover and land-use classes, which are built-up vegetation, bare surface, and water. Several

Table 9.1 Sources of study data downloaded from the United States Geological Survey (USGS) Glovis website

Date of Acquisition	Source/Sensors	Resolution
03/1989	Landsat 4–5TM	30 m
03/1999	Landsat 4–5TM	30 m
02/2009	Landsat 4–5TM	30 m
02/2019	Landsat 8 OLI	30 m

researchers have used the application of remote sensing to settlement studies, and many studies have been done using different image classification algorithms such as Classification and Tree Table Algorithm and Random Forest (Blaschke et al., 2008; Lu et al., 2006; Sinha et al., 2015). Both unsupervised and supervised methods of land-use classification were used for this research. The unsupervised classification was done for the years 1989, 1999, 2009, and 2019 using visual interpretations on Landsat images. For an improvement in the visual interpretation, the images were enhanced, their contrasts stretched, and false-colour composites were generated to increase the distinctions between their features. Initially, association analysis, texture, and knowledge-based visual interpretation were performed, followed by a careful analysis of the Landsat and OLI images while working on the land-use classes. The visual interpretation is able to identify real land use to a large extent but to further increase the accuracy of what was identified visually; reference data points were created randomly to identify the true land use of the points created based on visual interpretation on the satellite images. Create Random Point Pool of ArcGIS was used to establish 100 random points.

For supervised classification, the CART (Classification and Regression Tree) classifier, which is a non-parametric method, was used for the classification with 70% training data and 30% test data. CART describes how one can predict a target variable based on other values. The accuracy assessment was calculated for each settlement using a cross-tabulation matrix (Foody, 2002). This type of supervised classification was used because of the issue of mixed pixel (different land-use classes within the 30/ 30 m resolution); for example, Harrismith has some built-up and vegetation together. In order to avoid the issue of abnormal training data, the CART classifier was used because it is the most appropriate in situations where there are mixed pixels and gives better accuracy (Hong Wang et al., 2020). Lawrence and Wright (2001), in their study of land-use classification in rocky mountain provinces of Idaho, Montana, and Wyoming in the United States of America, used CART analysis to classify two TM scenes from 1994 images. They highlighted that CART analysis was easy to be implemented using commonly available image processing and statistical software because of its ability to resolve class overlap with the spectral and GIS layers. They emphasized the importance of the CART classifier, which is the ability to automatically pick the useful layers from and also its sensitivity to huge inconsistencies in the training samples within the classes, as well as the ability to avoid misclassification of training dataset (Lawrence & Wright, 2001). CART analysis can provide a low-cost and high-quality alternative result with less stress (Herold et al., 2003). Chen et al. (2017) recognized CART in their study at Long Country, China, as one of the models that is useful for spatial analysis and prediction of landslide susceptibility where they randomly selected 171 landslide locations and divided them into two groups of 70/30 training and test dataset and validation purpose (Chen et al., 2017).

Using CART involves the selection of input variables and split points on the variables until a suitable tree is created. This is done using a predefined stopping criterion, such as a minimum number of training instances assigned to the leaf model of the tree (Jena & Dehuri, 2020). The CART classifier method was used to

Table 9.2 Error matrix of accuracy assessments for Harrismith, Ladybrand, and Vrede

Classified Data		Reference Data					
	Settlement		**Built-up**	**Vegetation**	**Bare Surface**	**Water**	**Total**
	Harrismith	Built up	24.00	0	1.00	0	25.00
		Vegetation	0	11.00	0	0	11.00
		Bare surface	4.00	1.00	4.00	0	9.00
		Water	1.00	0	0	5.00	6.00
		Total	29.00	12.00	5.00	5.00	44.00
		Omission	0.17	0.083	0.20	0	51.00
		Commission	0.040	0	0.56	0.17	
		Producer accuracy	0.83	0.92	0.80	1.	
		User accuracy	0.96	1.00	0.45	0.83	
		Total accuracy	**86%**				
	Ladybrand	Built-up	11.00	1.00	1.00	0	13.00
		Vegetation	1.00	5.00	0	0	6.00
		Bare surface	2.00	0	5.00	0	7.00
		Water	0	0	0	2.00	2.00
		Total	14.00	6.00	6.00	2.00	23.00
		Omission	0.22	0.17	0.17	0	28.00
		Commission	0.15	0.17	0.29	0	
		Producer accuracy	0.79	0.83	0.83	1	
		User accuracy	0.85	0.83	0.72	1.00	
		Total accuracy	**82%**				
	Vrede	Built up	4.00	0	1.00	0	5.00
		Vegetation	0	12.00	0	0	12.00
		Bare surface	1.00	0	3.00	0	4.00
		Water	0	0	0	1.00	1.00
		Total	5.00.	12.00	4.00	1.00	20.00
		Omission	0	0	0.25	0	22.00
		Commission	0.20	0	0.25	0	
		Producer accuracy	0.80	1.	0.75	1.	
		User accuracy	0.80	1.00	0.75	1.00	
		Total accuracy	**91%**				

minimize errors that may come up because of heterogeneous land use during classification. Error matrix results were obtained using 100 training pixels (25 pixels per class) after cross-validation; this is generally accepted as a tool for land-use classification accuracy (Li & Song, 2019). Table 9.2 shows the results of the error matrix of accuracy assessments using the OLI image of 2019.

Accuracy assessment was done so as to validate the result of the classification; the first assessment was done through the historical information gathered from the

community leaders at the study areas who have been residing in the areas for over four decades. These leaders were able to attach some of the major events that happened, which led to settlements development and landmark transformation. These pieces of information helped in the establishment of majority results of the research. The other assessment was done through the quantitative method; the area ratio of the produced map was compared with the area ratio of the reference data; this validation method could only be done on the current image with the collected field data. The research assumption made here was that the previous years were correct based on the accuracy of the recent image. The quantitative accuracy involves the classification of all reference sites, which provide basic information about assessment of the map user and producer. The accuracy assessment done is hereby presented in Table 9.2.

The results of supervised classification, when compared with the unsupervised classification, give an accuracy of between 82% and 92% of the computed sample size after performing an accuracy assessment. Generally, an accuracy of between 80 and 85% is acceptable for land cover maps (Foody, 2002). The overall accuracy of classification was 86% for Harrismith, 91% for Vrede, and 82% for Ladybrand.

9.4 Results

Each of the classified images produced a noticeable land-use land cover change in Harrismith with various increases and decreases for all the years (Fig. 9.2). The built-up areas proliferated progressively in those years with a consistent increase from 3.82% to 9.06% and to 11.15%, then to 19.68% in the years 1989, 1999, 2009, and 2019. There was a little increase in vegetation area coverage from 44.83% in 1989 to 47.79% in 1999 but later decreased drastically by 2009 to 32.40% and later to 16.88% in 2019. The bare surface varies with decreases and increases from 50.47% to 41.65% and to 54.29%, then to 60.97% in 1989, 1999, 2009, and 2019, respectively. Water bodies increased slightly in the first 3 years under study, i.e. 1989, 1999, and 2009 with 0.88%, 1.47%, and 2.59% but later decreased to 2.48% in 2019; the level of increase or decrease in the level of water bodies at any given time usually depends on climate elements such as temperature, rainfall, humidity. Free State is often associated with low precipitation areas and, therefore, usually prone to drought (Hlalele, 2019). Accuracy assessment of Harrismith maps was 86%. The map of Harrismith showing land-use land cover classifications is presented in Fig. 9.2.

The classified images produced a noticeable land-use land cover change in Ladybrand with various increases and decreases for all the years (Fig. 9.3). The built-up areas proliferated progressively from 5.03%, 12.53%, 13.0%, and 17.35% in those years, with a stable and rapid increase in vegetation area coverage from 41.13%, 44.87%, 66.51%, and 69% in the years 1989, 1999, 2009, and 2019, respectively. Bare surface constantly decreases from 53.42%, 42.51%, 20.45%, and 13.62% in the years, respectively, while water bodies decreased drastically from

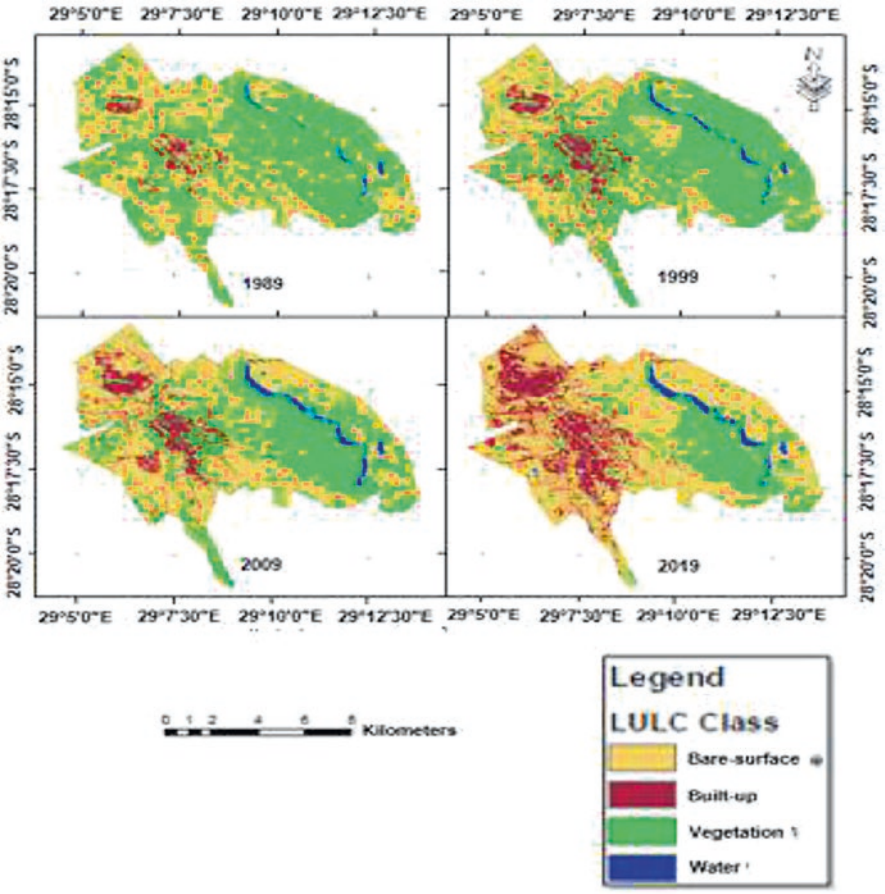

Fig. 9.2 The map of Harrismith showing the land-use land cover classifications

0.42%, 0.092%, 0.092%, and later 0.074%; this might have indicated a period of drought during the years (Ngaka, 2012). The accuracy assessment of Ladybrand maps was 82%. The analysis of the images for the Ladybrand map is presented in Fig. 9.3.

The built-up areas proliferated progressively in those years with percentages of 1.06%, 3.37%, 3.39%, and 10.17%, respectively. There was also a decrease in vegetation area coverage from 48.46% to 35.79% in 1989 to 1999 but later increased greatly to 47.80% in 1999 and later to 74.03% in 2019. Bare surface fluctuated as it increased initially from 49.50% in 1989 to 60.16% in 1999 but gradually decreased to 48.20% in 1999 and 14.88% in 2019 while water bodies decreased drastically from 0.98% in 1989 to 0.68% in 1999 and further decreased slightly to 0.62% in 2009 but later increased to 0.92% afterward. The accuracy assessment for Vrede maps was 91%. The analysis of the images for the Vrede map is presented in Fig. 9.4.

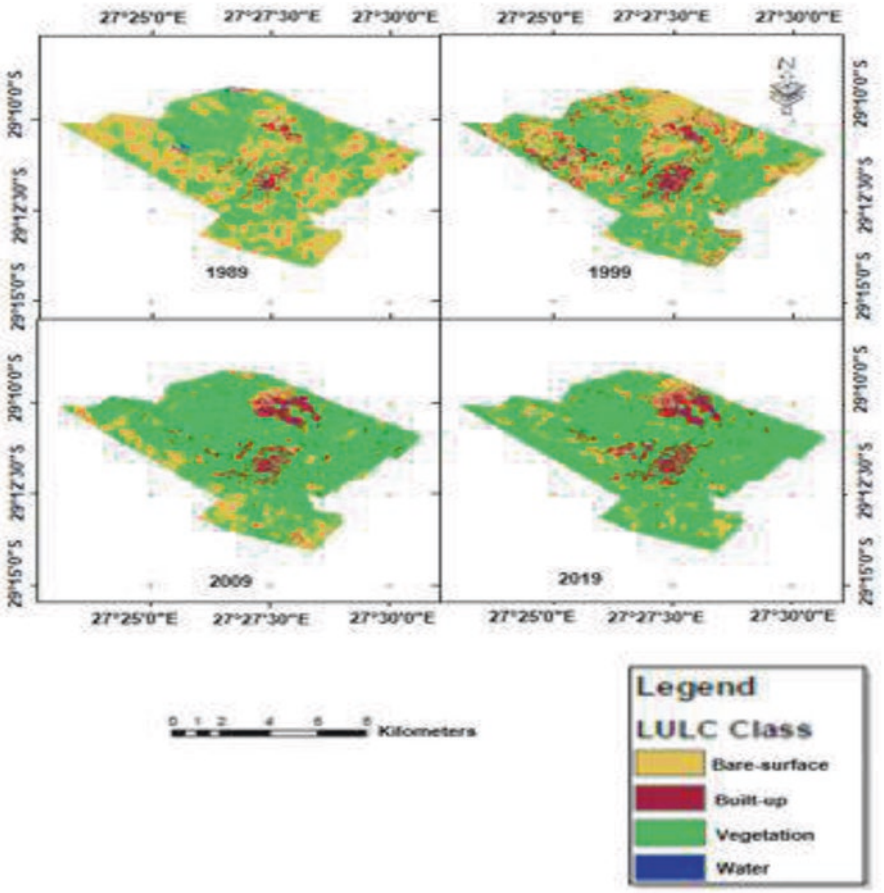

Fig. 9.3 The map of Ladybrand showing the land-use land cover classifications

Table 9.3 shows the coverage for each land cover/land-use class on Harrismith, Ladybrand, and Vrede. In Harrismith, it presented a constant increase in settlement development from the year 1989 to the year 2019; bare surface and vegetation reveal fluctuating changes in those years. While in Ladybrand, it displayed a constant increase in settlement development from the year 1989 to the year 2019; bare surface constantly declined while vegetation proliferated steadily, also water bodies constantly decreased. In Vrede, the table displayed a constant increase in settlement development from the year 1989 to the year 2019, bare surface and vegetation revealed a matching change, fluctuating over the years, and also water bodies decreased at first but later slightly increased in the year 2019.

Classification of every image generated an obvious change in land cover and land use, as shown in Figs. 9.2, 9.3, and 9.4, with their respective Tables 9.3 for the years under study. A noticeable increase of 163.5%, 149.45%, and 218.87% for built-up areas in Harrismith, Ladybrand, and Vrede, respectively, were observed

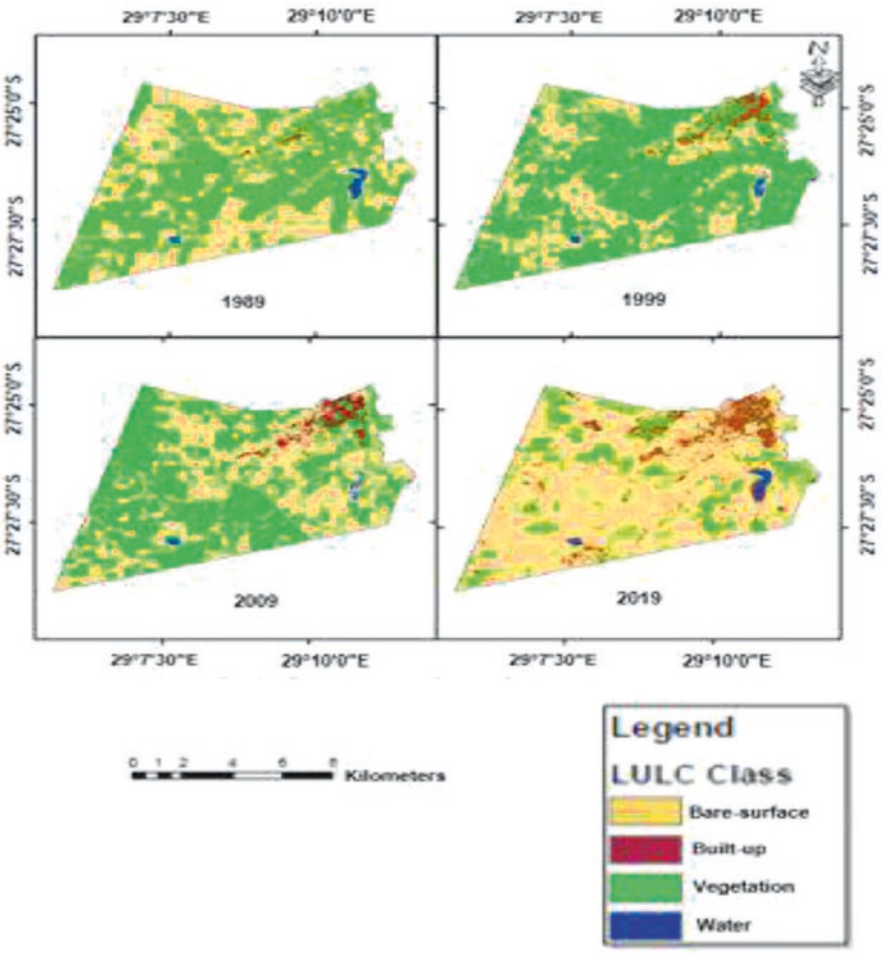

Fig. 9.4 The map of Vrede showing the land-use land cover classifications

from 1989 to 1999. On the other hand, between 1999 and 2009, Harrismith experienced a moderate increase, Ladybrand experienced a relatively low increase, while Vrede had the lowest increase. In the years between 2009 and 2019, there was an average increase of 67.78% in the built-up area of Harrismith. Ladybrand had an increase of 24.43%, which is relatively low compared to the 1989–1999 increment and also amongst the three settlements under study. On the other hand, Vrede experienced an increase of 182.35%, which is considered most rapid out of the three settlements for the period between 2009 and 2019.

Table 9.4 shows the figures of the built-up area and their percentages in relation to the total area. It represents settlement development trend for the three settlements (Harrismith, Ladybrand, and Vrede) for the years under study (1989, 1999, 2009,

Table 9.3 Classification of the land-use land cover of Harrismith, Ladybrand, and Vrede in km sq. and percentages

Class	1989		1999		2009		2019	
	Area (km^2)	Percentage (%)	Area (km^2)	Percentage (%)	Area (km^2)	Percentage (%)	Area (km^2)	Percentage (%)
HARRISMITH								
Built up	3.9780	3.82	9.4545	9.06	11.6379	11.15	20.5482	19.68
Vegetation	46.8054	44.83	49.8859	47.79	33.3837	32.40	17.6246	16.88
Bare surface	52.6428	50.47	43.4745	41.65	56.6793	54.29	63.6573	60.97
Water	0.9216	0.88	1.5336	1.47	2.6469	2.59	2.5902	2.48
Total	104.4	100	104.4	100	104.4	100	104.4	100
LADYBRAND								
Built-up	2.73	5.03	6.81	12.53	7.06	13.00	9.41	17.35
Vegetation	22.35	41.13	24.38	44.87	36.13	66.51	37.49	69.00
Bare surface	29.03	53.42	23.10	42.51	11.10	20.45	7.40	13.62
Water	0.23	0.42	0.05	0.092	0.05	0.092	0.040	0.074
Total	54.34	100	54.34	100	54.34	100	54.34	100
VREDE								
Built up	0.53	1.06	1.69	3.37	1.70	3.39	5.10	10.17
Vegetation	24.29	48.46	17.94	35.79	23.96	47.80	37.11	74.03
Bare surface	24.81	49.50	30.16	60.16	24.16	48.20	7.46	14.88
Water	0.50	0.98	0.34	0.68	0.31	0.62	0.46	0.92
Total	50.13	100	50.13	100	50.13	**100**	50.13	100

Table 9.4 Classified settlement development between 1989 and 2019 (area in Km^2)

Settlements	1989		1999		2009		2019	
	(Km^2)	(%)	(Km^2)	(%)	(Km^2)	(%)	(Km^2)	(%)
Harrismith	4.0	3.82	9.46	9.06	11.64	11.15	20.55	19.68
Ladybrand	2.73	5.03	6.81	12.53	7.00	13.00	9.41	17.35
Vrede	0.53	1.06	1.69	3.37	1.70	3.39	5.10	10.17

and 2019). The figures showed an increase all along with the year intervals. (Here, values of the built up in the three settlements are put together to easily analyse the settlement development trend.)

Three built-up transition layer maps of the years' interval for 1989–1999, 1999–2009, and 2009–2019 are presented to show a detailed settlement development change pattern. Figures 9.5a–c show the maps of settlement development (built-up). The spatiotemporal maps revealed an expansion in the built-up area of the study area within the years of study; years 1989, 1999, 2009, and 2019 maps

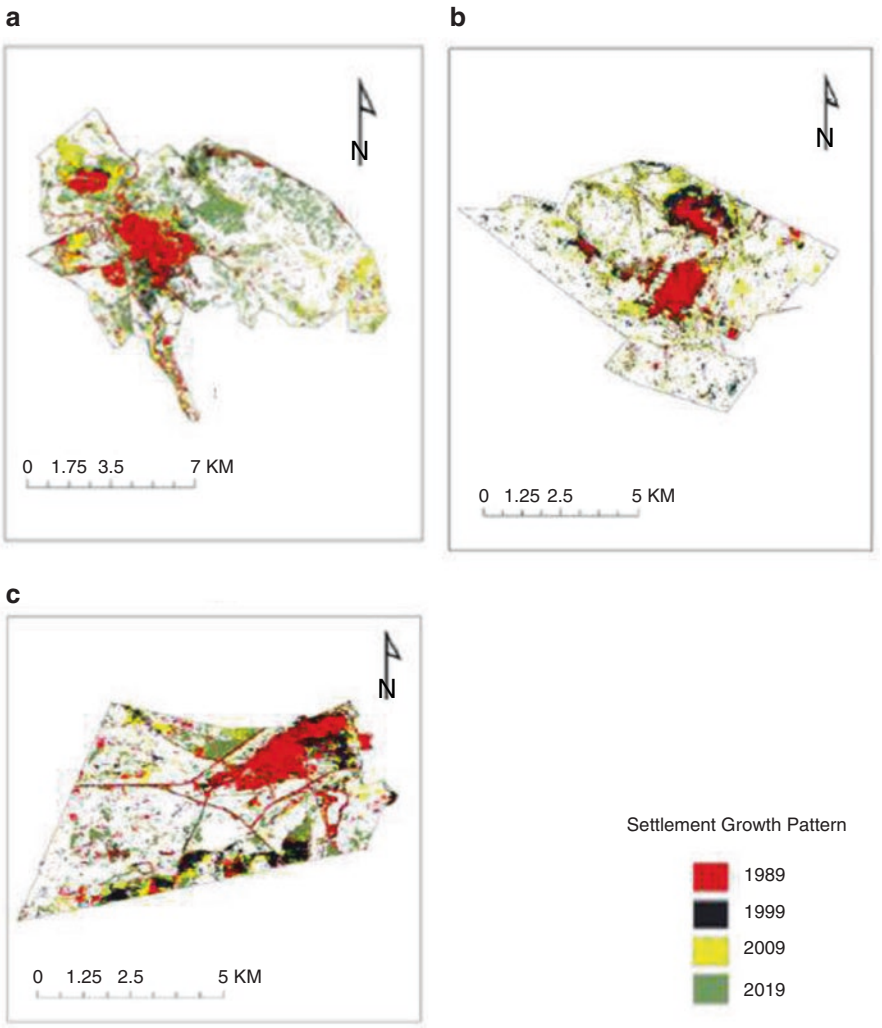

Fig. 9.5 (**a**) Spatial pattern of settlement development, Harrismith, (**b**) Spatial pattern of settlement development, Ladybrand, (**c**) Spatial pattern of settlement development, Vrede

were overlaid. Figure 9.6 illustrates the percentage increase in built-up in the years under study (1989, 1999, 2009, and 2019) for the three settlements. The figure shows a growth in the percentage changes in the built-up area of the study areas within the years under study (i.e. years 1989, 1999, 2009, and 2019).

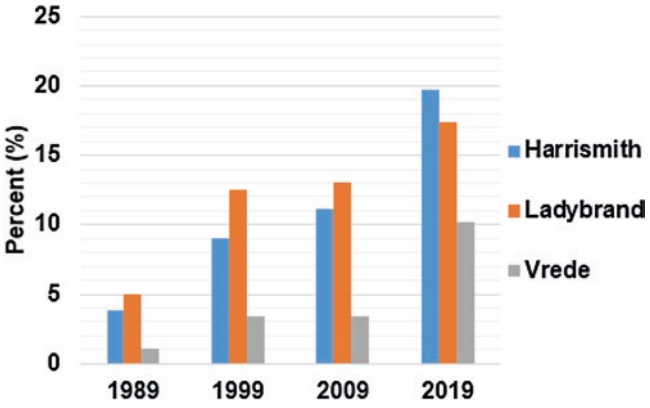

Fig. 9.6 Percentage increase in built-up years under study

9.5 Discussion

The post-classification change detection shown in Figs. 9.2, 9.3, and 9.4, with their respective Tables 9.3, established an increase for human settlements as coverage for the built-up areas as revealed from the analysed results showing a constant growth for the years under study. This estimated result from 1989 to 1999 showed the highest increment in built-up areas amongst the range of years considered. The built-up area of Harrismith, which occupied 3.82% of the total land area, increased to 9.06% in 1999, while Ladybrand increased from 5.03% in 1989 to 12.53% in 1999. Also, Vrede's built-up area proliferated from 1.06% in 1989 to 3.37% of the total land area in 1999.

This analysis reveals the situation of settlement development 5 years before and after the 1994 transformation of government from minority to majority rule. After 1994, various policies on human settlement development were put in place. Two such policies, which are very prominent, are the Development Facilitation Act of 1995 and Housing Acts 107 of 1997. These two acts enabled land and house ownership by any eligible citizen, to get debt relief and discount benefits, and also to register such property at the same time. Another important factor for the settlement expansion is that the African National Congress (ANC), the ruling political party in South Africa, proposed the construction of one million housing units all over the country every year since their resumption in office in 1994 (Thring, 2003). There were 235,635 housing units built by the RDP (Reconstruction and Development Programme) between 1998 and 1999, which is the highest number of housing units built so far. The numbers have been decreasing ever since then until 2017, according to the available record (Stats, 2018).

Usually, major political events such as independence, expiration of war, or new policy formulations are important factors for settlement development. AbuHaffetha (2014) examined the urbanization's impact of the separation wall on the sustainability of agriculture in Palestine; he discovered that this government policy led to

the loss of agricultural land and a major increase in built-up areas (AbuHafeetha, 2014). Mansaray et al. (2016) used remote-sensing tools to map out urban expansion and the rate of deforestation in Freetown, Sierra Leone, pre- and post-war (which occurred between 1999 and 2002). He classified land cover change between 1986 and 2015 and discovered an increase in built-up at the loss of grassland; also, the rate of land cover change increased by 28.5% from 2001 to 2015 as against 20.9% of 1986–2001. This happened because of the increase in population, infrastructural development, and economic growth after the civil war in 2002 (Mansaray et al., 2016).

In the estimated result for the years 1999 to 2009, the increment experienced by the three settlements is the lowest as compared to other year ranges. Here Harrismith experienced a 23% increment, an increase in built-up areas from 9.46km^2 in 1999 to 11.64km^2 in 2009. This is followed by Ladybrand with a 9.53% increment; an increase in built-up areas from 6.82km^2 in 1999 to 7.17km^2 in 2009, and lastly, Vrede with a 0.59% increment; an increase in built-up areas from 1.69km^2 in 1999 to 1.70km^2 in 2009. Statistics reveal fluctuation in the number of housing units built by RDP between 1999 and 2009. The lowest number of houses built during this period (1999–2009) was between 2002 and 2003, which was 131,784. The number of houses built between 2009 and 2010 was 166,758 (Stats, 2012, 2018). This may be because there was less pressure on the political leaders as they had delivered and seemed to have improved on the minority government in delivering and meeting masses housing needs in the first 5 years of their rule. Then comes a time to relent and focus more on other aspects of the political campaign. There was also a case of HIV epidemics between 1999 and 2008 (Shisana et al., 2009), which claimed lots of lives and caused population decline. The government at this period needed to focus more on the health sector than housing. Therefore, the government diverted resources into curbing the HIV scourges, which was a pandemic at that period, and built fewer houses as a result.

The 2009–2019 built-up estimated results for the land-use area show average increment for the three settlements as compared to other year ranges. Vrede led in the increase with 200%, an increase in built-up areas from 1.70km^2 in 2009 to 5.10km^2 in 2019. The main economic activity in this area is agriculture; the majority of the farmers are pastoral farmers (Olubode-Awosola, 2006); the increase in built-up was evident in indiscriminate shacks around the settlement and grassland for cattle. This is followed by Harrismith with 76.55%, an increase in built-up areas from 11.64km^2 in 2009 to 20.55km^2 in 2019, and lastly, Ladybrand with 34.43%, an increase in built-up areas from 1.70km^2 in 2009 to 10.17km^2 in 2019. This was a pick-up period in the nation, and the battle of the epidemics seemed to have been won as 161,758 housing units were built in 2009; at this period, the housing activities were coming back to the public interest (Stats, 2018). Though it was noted from the Human Settlement Department's record after 2010, the rate at which houses were built has continued to drop, and about 85,000 units were built in 2017 (Stats, 2018).

Turok assumed that statistics from the historic population in South Africa are unreliable, believing that minority governments did not take trustworthy statistics of the black population before 1994. As a result, getting an exact population figure of years before 1994 is almost impossible (Turok, 2012). However, the available data of 2001 and 2011 show a minimum and average increase in population figures. Population figures in Thabo Mofutsanyana increased from 725,932 to 736,238 with a population density of 21.8/km^2 to 22km^2, respectively, from 2001 to 2011. The available population figures revealed that Harrismith and Vrede's figures increased by 6.82% and 32.68% from 2001 to 2011. The population figure from the Statistics SA shows different fluctuations that vary from year to year; this may be due to change in boundaries (administrative and political) from time to time and other factors.

A field survey was conducted which revealed that the rapid increase experienced by these three settlements is due to the new policies after 1994, which gave rights to both blacks and whites to own lands and have title deeds in any part of the country (James, 2007). This gave rise to tents dwellers before 1994 to register them by way of grants from Housing Acts 107 of 1997 (James, 2007). In developing countries, less attention has been given to settlement planning and development in and around the mountainous region, whereas mountains provide shelter, tourism, economy, energy source, water supply, and food (Romero-Lankao & Norton, 2018). The liberty created by the majority rule to own land and houses, which in a way is pro-poor, seemed to be taken for granted, especially in the less urban areas in the municipality; this made development around these places to be less controlled and rendering the important feature (the mountain) to be misused and degraded. Effective and functional planning and development schemes need to be put in place to curb this misuse and preserve the essential features. These, in a way, will improve the livelihood of the residents and help achieve sustainable mountain development, which is one of the United Nation's goals on sustainable development (De Los Andes, 2012). The majority of the population are farmers of livestock and crops at both subsistence and commercial scale. Though there is a notion that subsistence farmers are leaving farms for other low-cadre jobs like security works for lack of enough supports for farmers in terms of loans and training from the government (Myeni & Moeletsi, 2020; Hlongwane, 2015; Strydom et al., 2015). This accounts for the fluctuations in the green areas (agriculture, grassland, and vegetation) in the study area.

Another major issue worthy of note is that grassland and forest areas within Drakensberg mountains in South Africa are generally dispersed in a fire-predisposed area, unlike the lowland vegetation, and most of the species are low in fire resistance (Adie et al., 2017). The study area is also associated with low precipitation of rainfall between 800 and 1200 mm per annum and sometimes drought (Brand et al., 2008). These are responsible for the increase in the bare surface and fluctuation in land area for water bodies.

9.6 Conclusion and Recommendations

In this research, an evaluation of the importance of remote-sensing datasets as a tool in mapping land-use change, spatial changes in settlement development, land-use planning, and management have been demonstrated. The result of the accuracy assessment and information from the field showed a satisfactory classification. The present land-use results and the over-time changing patterns are essential in Thabo Mofutsanyana municipality, particularly for the spatial development, land distribution, management of resources, and future sustainable development plans. Furthermore, this study attached the change that occurred in land-use land cover of the nation to the transition of government from minority to majority rule, and this has in one way or the other affected the total landscape of the study area. Therefore, in this study, this phenomenon was confirmed using Harrismith, Ladybrand, and Vrede. Also, economic factors as a result of tourism attraction created by the mountains could also be responsible for settlement development in terms of temporary homes and camps. Harrismith is a middle town between two major cities of South Africa, which are Johannesburg and Durban; this location factor may somehow be responsible for some people's settling down. Ladybrand is a city that is very close to Maseru, which is the Lesotho border, migrants from Lesotho are likely going to settle at Ladybrand temporarily or permanently when they first get to South Africa. More research will be conducted on other possible reasons for settlement development in the study area.

Some of these factors are also likely to be responsible for the patterns and forms of the settlements understudy. This study endeavoured to create awareness in the area of mountain development, sustainable settlement planning, as well as an all-inclusive development control strategy to preserve the environment around the mountain.

Acknowledgments This research was funded in part by Afromontane Research Unit (ARU) and in part by the Risk and Vulnerability Science Center (RVSC-NRF) under the grant number 128386.

Competing Interests The author has declared that no competing interests exist.

Ethical Considerations This research discussed in this chapter followed all ethical standards for research without direct contact with human or animal subjects.

Data Availability Statement Data sharing is not applicable to this chapter as no new data were created or analysed in this study.

Disclaimer The views and opinions expressed in this chapter are those of the authors and do not necessarily reflect the official policy or position of any affiliated agency of the authors.

References

AbuHafeetha, M. (2014). *The impacts of urbanization on agricultural sustainability in Palestine after the construction of the Separation Wall: The case of the city of Tulkarem*. Ph.D. Thesis, University of Calgary, Canada.

Adie, H., Kotze, D. J., & Lawes, M. J. (2017). Small fire refugia in the grassy matrix and the persistence of Afrotemperate forest in the Drakensberg mountains. *Scientific Reports, 7*(1), 1–10.

Basiago, A. D. (1998). Economic, social, and environmental sustainability in development theory and urban planning practice. *Environmentalist, 19*(2), 145–161.

Berry, B. J. (2015). *The human consequences of urbanisation.* Macmillan International Higher Education, London.

Blaschke, T., Lang, S., & Hay, G. (2008). *Object-based image analysis: Spatial concepts for knowledge-driven remote sensing applications.* Springer Science & Business Media, Berlin/Heidelberg, Germany.

Blyth, S., Groombridge, B., Lysenko, I., Miles, L., & Newton, A. (2002). UNEP–WCMC (United Nations Environment Programme–World Conservation Monitoring Centre) Report, Mountain watch: environmental change and sustainable development in mountains. *UNEP World Conservation Monitoring Centre, Cambridge, UK*, 19.

Brand, R. F., Du Preez, P. J., & Brown, L. R. (2008). A floristic description of the Afromontane Fynbos communities on Platberg, Eastern Free State, South Africa. *Koedoe, 50*(1), 202–231.

Cannon, T. (1990). Regions: spatial inequality and regional policy. *The geography of contemporary China: The impact of Deng Xiaoping's Decade* (pp. 28–60), Taylor and Francis, London.

Chen, W., Xie, X., Wang, J., Pradhan, B., Hong, H., Bui, D. T., … Ma, J. (2017). A comparative study of logistic model tree, random forest, and classification and regression tree models for spatial prediction of landslide susceptibility. *Catena, 151*, 147–160.

Coops, N. C., Wulder, M. A., & Iwanicka, D. (2009). Large area monitoring with a MODIS-based Disturbance Index (DI) sensitive to annual and seasonal variations. *Remote Sensing of Environment., 113*(6), 1250–1261.

Coppin, P., Jonckheere, I., Nackaerts, K., Muys, B., & Lambin, E. (2004). Digital change detection methods in ecosystem monitoring: a review. *International Journal of Remote Sensing., 25*(9), 1565–1596.

Coppin, P., Lambin, E., Jonckheere, I., & Muys, B. (2002). Digital change detection methods in natural ecosystem monitoring: A review. In *Analysis of Multi-Temporal Remote Sensing Images* (pp. 3–36). World Scientific, Singapore.

Dadashpoor, H., Azizi, P., & Moghadasi, M. (2019). Land use change, urbanization, and change in landscape pattern in a metropolitan area. *Science of the Total Environment, 655*, 707–719.

De Los Andes, C. (2012). Mountains as the water towers of the world: A call for action on the sustainable development goals (SDGs). *Policy, 1*, 1–10.

Denoon-Stevens, S., & Mocwagae, K. (2019). The potential of the University of the Free State QwaQwa campus to enable growth of the economy of QwaQwa. *Town and Regional Planning, 74*, 1–11.

Foody, G. M. (2002). Status of land cover classification accuracy assessment. *Remote Sensing of Environment., 80*(1), 185–201.

Güneralp, B., Lwasa, S., Masundire, H., Parnell, S., & Seto, K. C. (2017). Urbanization in Africa: challenges and opportunities for conservation. *Environmental Research Letters, 13*(1), 015002.

Habitat, U. (1976). *The Vancouver declaration on human settlements*. UN Habitat.

Hansen, M., DeFries, R., Townshend, J., Carroll, M., Dimiceli, C., & Sohlberg, R. (2003). Global percent tree cover at a spatial resolution of 500 meters: First results of the MODIS vegetation continuous fields algorithm. *Earth Interactions, 7*(10), 1–15.

Hansen, M. C., DeFries, R. S., Townshend, J. R., & Sohlberg, R. (2000). Global land cover classification at 1 km spatial resolution using a classification tree approach. *International Journal of Remote Sensing., 21*(6-7), 1331–1364.

Herold, N., Koeln, G., & Cunnigham, D. (2003). *Mapping impervious surfaces and forest canopy using classification and regression tree (CART) analysis.* Paper presented at the ASPRS 2003 Annual Conference Proceedings.

Hlalele, B. M. (2019). *Bi-hazard assessment for timely and effective disaster management: Free State disaster area 2015*, EM International, India.

Hlongwane, N. (2015). *Breeding admixture of cattle populations kept in the Thabo Mofutsanyane District*. Central University of Technology, Free State.

Hui, E., & Moyse, J. (2018). Settlement patterns and competition for space. In *Barnacle biology* (pp. 363–376). Routledge, Oxfordshire, England, UK.

James, D. (2007). *Gaining ground?: Rights and property in South African land reform.* Routledge-Cavendish, Abingdon, Oxfordshire, United Kingdom

Jena, M., & Dehuri, S. (2020). DecisionTree for classification and regression: A state-of-the art review. *Informatica, 44*(4).

Kalane, L. (2015). *Reasons for failure of SMEs in the Free State*. University of the Free State.

Khan, S., & Aaqib, S. M. (2017). Empirical evaluation of ArcGIS with contemporary open source solutions-A study. *International Journal of Advance Research in Science and Engineering, 6*(1), 724–736.

Kleynhans, W., Salmon, B. P., Olivier, J. C., Van den Bergh, F., Wessels, K. J., Grobler, T. L., & Steenkamp, K. C. (2012). Land cover change detection using autocorrelation analysis on MODIS time-series data: Detection of new human settlements in the Gauteng province of South Africa. *IEEE Journal of Selected Topics in Applied Earth Observations and Remote Sensing, 5*(3), 777–783.

Krannich, R. S., Luloff, A. E., & Field, D. R. (2011). *People, places and landscapes: Social change in high amenity rural areas* (Vol. 14). Springer Science & Business Media, Berlin/Heidelberg, Germany.

Lawrence, R. L., & Wright, A. (2001). Rule-based classification systems using classification and regression tree (CART) analysis. *Photogrammetric engineering and remote sensing, 67*(10), 1137–1142.

Li, H., & Song, W. (2019). Expansion of rural settlements on high-quality arable land in Tongzhou District in Beijing, China. *Sustainability, 11*(19), 5153.

Li, X., Chen, D., Duan, Y., Ji, H., Zhang, L., Chai, Q., & Hu, X. (2020). Understanding Land use/Land cover dynamics and impacts of human activities in the Mekong Delta over the last 40 years. *Global Ecology and Conservation, 22*, e00991.

Lloyd, E. K., Bhatt, B. V., & Padhya, H. J. (2016). Urban land use planning scopes in post-war city of Monrovia, Republic of Liberia. *International Journal of Advanced Research in Engineering, Science & Management (IJARESM)*, *1*, 1–12.

Lu, D., Mausel, P., Brondizio, E., & Moran, E. (2004). Change detection techniques. *International Journal of Remote sensing, 25*(12), 2365–2401.

Lu, D., Weng, Q., & Li, G. (2006). Residential population estimation using a remote sensing derived impervious surface approach. *International Journal of Remote Sensing, 27*(16), 3553–3570.

Madlingozi, T. (2007). Post-apartheid social movements and the quest for the elusive 'new' South Africa. *Journal of Law and Society, 34*(1), 77–98.

Mahabir, R., Croitoru, A., Crooks, A. T., Agouris, P., & Stefanidis, A. (2018). A critical review of high and very high-resolution remote sensing approaches for detecting and mapping slums: Trends, challenges and emerging opportunities. *Urban Science, 2*(1), 8.

Mangope, D. (2015). *The Sustainability of Financial Investment in Community-based Tourism Projects in the Thabo Mofutsanyana District of the Free State Province*. Central University of Technology, Free State.

Mansaray, L. R., Huang, J., & Kamara, A. A. (2016). Mapping deforestation and urban expansion in Freetown, Sierra Leone, from pre-to post-war economic recovery. *Environmental Monitoring and Assessment, 188*(8), 470.

McGranahan, D. A. (1999). *Natural amenities drive rural population change* (Vol. 781). US Department of Agriculture, ERS, Washington, D.C., United States.

Mildrexler, D. J., Zhao, M., Heinsch, F. A., & Running, S. W. (2007). A new satellite-based methodology for continental-scale disturbance detection. *Ecological Applications, 17*(1), 235–250.
Mildrexler, D. J., Zhao, M., & Running, S. W. (2009). Testing a MODIS global disturbance index across North America. *Remote Sensing of Environment, 113*(10), 2103–2117.
Moser, G., Serpico, S., & Vernazza, G. (2007). Unsupervised change detection from multichannel SAR images. *IEEE Geoscience and Remote Sensing Letters, 4*(2), 278–282.
Musakwa, W., & Van Niekerk, A. (2013). Implications of land use change for the sustainability of urban areas: A case study of Stellenbosch, South Africa. *Cities, 32*, 143–156.
Myeni, L., & Moeletsi, M. E. (2020). Factors Determining the Adoption of Strategies Used by Smallholder Farmers to Cope with Climate Variability in the Eastern Free State, South Africa. *Agriculture, 10*(9), 410.
Ngaka, M. J. (2012). Drought preparedness, impact and response: A case of the Eastern Cape and Free State provinces of South Africa. *Jàmbá: Journal of Disaster Risk Studies, 4*(1), 1–10.
Nuttall, J., & Nuttall, A. (2008). *The mountains of England and Wales: Vol 2 England* (Vol. 2). Cicerone Press Limited, Kendal LA9 7RL, United Kingdom.
Olubode-Awosola, O. O. (2006). *Farm-level resource use and output supply response: a Free State case study*. University of the Free State.
Onaolapo, T. F., Okello, T. W., & Adelabu, S. A. (2020). Assessing spatiotemporal settlement patterns in Eastern Free State, South Africa, pre and post transition from apartheid to majority rule. *Transactions of the Royal Society of South Africa, 75*, 140–158.
Owusu, G. (2005). The role of district capitals in regional development: Linking small towns, rural–urban linkages and decentralisation in Ghana. *International Development Planning Review, 27*(1), 59–89.
Pallister-Wilkins, P. (2011). The separation wall: A symbol of power and a site of resistance? *Antipode, 43*(5), 1851–1882.
Radke, R. J., Andra, S., Al-Kofahi, O., & Roysam, B. (2005). Image change detection algorithms: a systematic survey. *IEEE Transactions on Image Processing., 14*(3), 294–307.
Romero-Lankao, P., & Norton, R. (2018). Interdependencies and risk to people and critical food, energy, and water systems: 2013 flood, Boulder, Colorado, USA. *Earth's Future, 6*(11), 1616–1629.
Sang, X., Guo, Q., Wu, X., Fu, Y., Xie, T., He, C., & Zang, J. (2019). Intensity and stationarity analysis of land use change based on CART algorithm. *Scientific Reports, 9*(1), 1–12.
Sarkar, A. (2010). Analysis of human settlement patterns using RS and GIS in the plains of West Bengal. *The On-Line Indian Journal of Spatial Science, 1*(1), 1.1–1.16.
Shisana, O., Rehle, T., Simbayi, L., Zuma, K., Jooste, S., Wyk, P.-V., . . ., & Zungu, N. (2009). South African national HIV prevalence, incidence, behaviour and communication survey, 2008: a turning tide among teenagers? *Human Sciences Research Council (HSRC)*, *1*, 1–195.
Sinha, S., Jeganathan, C., Sharma, L., & Nathawat, M. (2015). A review of radar remote sensing for biomass estimation. *International Journal of Environmental Science and Technology, 12*(5), 1779–1792.
Statistics. (2012). *Census 2011 release – P0301.4*. Statistics South Africa.
Stats, S. (2012). *Census 2011 statistical release*. Statistics South Africa.
Stats, S. (2018). *Statistical Publications, July 2018*.
Strydom, A. J., Mangope, D., & Henama, U. S. (2015). Economic sustainability guidelines for a Community Based Tourism Project: The Case of Thabo Mofutsanyane, Free State Province. *African Journal of Hospitality, Tourism and Leisure, 6*(3), 1–17.
Thring, P. (2003). *Housing policy and practice in post-apartheid South Africa*. Heinemann Educational Books, Portsmouth, New Hampshire.
Turok, I. (2012). *Urbanisation and development in South Africa: Economic imperatives, spatial distortions and strategic responses*: *United Nations Population Fund*. Human Settlements Group, International Institute for Environment, High Holborn London.
Turok, I. (2014). South Africa's tortured urbanisation and the complications of reconstruction. *Urban growth in emerging economies: Lessons from the BRICS*. *143*.

Urban, M. C., Bocedi, G., Hendry, A. P., Mihoub, J.-B., Pe'er, G., Singer, A., … Godsoe, W. (2016). Improving the forecast for biodiversity under climate change. *Science, 353*(6304), aad8466.

Wang, H., Liu, C., Zang, F., Yang, J., Li, N., Rong, Z., & Zhao, C. (2020). Impacts of topography on the land cover classification in the Qilian Mountains, Northwest China. *Canadian Journal of Remote Sensing, 46*(3), 344–359.

Wang, H., Xie, M., Li, H., Feng, Q., Zhang, C., & Bai, Z. (2021). Monitoring ecosystem restoration of multiple surface coal mine sites in China via LANDSAT images using the Google Earth Engine. *Land Degradation & Development, 32*, 2936.

Wilson, P. (2001). Listing the Irish hills and mountains. *Irish Geography, 34*(1), 89–95.

Wulder, M. A., Li, Z., Campbell, E. M., White, J. C., Hobart, G., Hermosilla, T., & Coops, N. C. (2018). A national assessment of wetland status and trends for Canada's forested ecosystems using 33 years of earth observation satellite data. *Remote Sensing, 10*(10), 1623.

Chapter 10
Digital Soil Mapping for Hydropedological Purposes of the Cathedral Peak Research Catchments, South Africa

Rowena Harrison and Johan van Tol

Abstract Conventional soil mapping in montane environments is often a difficult and laborious task, given access difficulties, the topography of the environment, and the time required to conduct the field investigation. Utilising a remote-sensing tool, such as the Arc Soil Inference Engine (ArcSIE), to map soils in these locations can add valuable information for land management. The ArcSIE tool was utilized in the Cathedral Peak research catchments, in KwaZulu-Natal, South Africa, with the aim of creating an understanding of the hydropedological behaviour of the soils of three research catchments. A rule-based approach was first undertaken, followed by a case-based validation. A fuzzy membership map of each soil group was produced which integrated all inputs. The overall Kappa coefficient for CP-III is 0.57, for CP-VI is 0.59, and for CP-IX is 0.74. The hydropedological soil group maps achieved an appropriate representation of the complex nature of the soil–landscape relationship, with changes between one soil group and the next being gradual and continuous. Accuracies and inaccuracies within the fuzzy membership maps can be quantified, allowing for a confidence rating in the use of these maps. These maps can therefore be used in further applications in water and land management for the area.

Keywords Digital soil mapping · Remote sensing · Hydropedology · Afromontane catchments · Soil science

R. Harrison (✉)
Department of Soil, Crop and Climate Sciences, University of the Free State, Bloemfontein, South Africa

J. van Tol
Department of Soil, Crop and Climate Sciences, University of the Free State, Bloemfontein, South Africa

Afromontane Research Unit, University of the Free State, QwaQwa, South Africa
e-mail: vanTolJJ@ufs.ac.za

S. Adelabu et al. (eds.), *Remote Sensing of African Mountains*,
https://doi.org/10.1007/978-3-031-04855-5_10

10.1 Introduction

Conventional soil mapping in montane environments is often a difficult and laborious task, given access difficulties, the topography of the environment, and the time required to conduct the field investigation (Ismail & Yacoub, 2012; Martín-López et al., 2019). In recent years, thematic mapping has undergone a revolution as the result of advances in geographic information and remote-sensing techniques (Ismail & Yacoub, 2012), and this has brought about the use of Digital Soil Mapping (DSM) as a key tool in reducing the time and financial aspects of conventional soil-based mapping. DSM is the interpretation of spatial and temporal soil property variations using mathematical models based on quantitative relationships between environmental information and soil measurements (Martín-López et al., 2019).

The use of DSM techniques is supported by the factors of soil formation, coupled with soil–landscape relationships (McBratney et al., 2003; Silva et al., 2019). Jenny (1941) used the well-known and widely accepted model as a mechanistic model for soil development; S = f (c, o, r, p, t), where S (soil) is a function of climate (c), organisms (o), relief (r), parent material (p), and time (t). However, since the late 1960s, there has been an emphasis on more geographic, topographic, and spatial approaches to interpreting the position of soils in relation to the landscape (McBratney et al., 2003). This more recent interest is driven by an increasing recognition of the ecological, economic, and societal benefits of understanding soil properties, their spatial distribution, and the value of this knowledge for use in the management objectives of a variety of industries and land uses (Kimsey, 2020).

The geographic and topographic nature of DSM makes it relevant to pedology and hydrology (Lin et al., 2006; Ma et al., 2019). Soil–water interactions across multiple scales control much of soil development, and this results in the spatial variability studied by pedologists. These interactions also control water quantity and quality in surface and groundwater systems, and thus are important to hydrologists (Lin et al., 2006). Combining pedologic and hydrologic expertise can be particularly powerful in addressing complex environmental issues (Bouma, 2006; European Confederation of Soil Science Societies, 2004; Lin et al., 2006; van Tol et al., 2018), and thus the introduction of utilising DSM in hydropedology is an important component in understanding and predicting soil variability within a landscape (Thompson et al., 2012).

A landscape can be divided into two hydrologic zones including the recharge zone and the discharge zone (Heath, 1980). A downward movement of water from the soil surface to the groundwater describes the recharge zone, while the opposite, a movement of water upwards from the groundwater towards the surface portrays the discharge zone. A lateral or flow through zone can also occur in certain landscapes with a shallow water table. Here the groundwater has reached the surface and runs parallel to the ground surface. Dissolved organic matter, sediment, and reduced Iron (Fe) and Manganese (Mn) are carried within this moving water (Lindbo & Richardson, 2000; Rhoton et al., 2002; Vepraskas & Lindbo, 2012).

Research into the dynamics of hydropedology, particularly within South Africa, has shown that the placement of soils within a landscape are not randomly distributed but can be grouped into four hydropedological soil types, namely, recharge soils, interflow soils, responsive soils, and stagnating soils. These groups of soils convey water differently, and thus have different hydropedological behaviour (van Tol & Le Roux, 2019).

Previous studies have highlighted the effect of the landscape on the flow dynamics of soils (Diek et al., 2014; Grayson et al., 1997; Mahmood & Vivoni, 2011; Penna et al., 2009; Teuling & Troch, 2005) with soil moisture varying with topography under wet conditions, whereas under drier conditions, soil moisture has been shown to be associated with local soil and vegetation controls. So, although topography, texture, and vegetation all influence soil moisture variability, the relative magnitude of these controls can vary strongly (Diek et al., 2014; Grayson et al., 1997; Mahmood & Vivoni, 2011; Penna et al., 2009; Teuling & Troch, 2005). This is due to the complex and varied characteristics of soils which influence their ability to store and transmit water (van Tol et al., 2020).

The spatial distribution of soils within a landscape can also be described utilising the soil catena concept. Described by Milne (1936) as the association of the distribution of soils with the topography of the hillslope, and later by Bushnell (1942) as the identification of the hydrosequence of soils along a hillslope from the ridgetop to the valley bottom or watercourse. The catchment's hydrological response is the sum of the hydrological responses of the individual hillslopes within a catchment (van Zijl et al., 2019). Thus, the importance of grouping soils according to their hydropedological characteristics plays an important part in understanding water fluxes and flow pathways in landscapes (Lin et al., 2006; van Tol, 2020), as well as creating hydrosequences within a catchment. The use of DSM in determining the hydropedological grouping of soils is therefore important in assessing such properties of a catchment including soil water retention, flooding potential, erosion hazard, and depth to the seasonal high-water table (Thompson et al., 2012).

One of the baseline inputs in DSM is identifying where the wetlands and watercourses are situated. Wetlands are a transitional ecosystem between terrestrial and open-water or aquatic environments (Mitsch & Gosselink, 2015). They therefore contain either open water bodies, dense vegetation, or a mixture of the two (Kaplan & Avdan, 2017). The use of satellite imagery has been successfully used in the past for open-water delineations, as well as for vegetation classification and change detection in wetland ecosystems. Several mapping studies have demonstrated the potential of applying remote-sensing methods to wetland identification (Berberoglu et al., 2004; Frohn et al., 2009; Klemas, 2005, 2011; Lunetta & Balogh, 1999; Phillips et al., 2005; Quinn & Epshtein, 2014). Further studies illustrate how vegetation characteristics such as density, vitality, and spatial extent serve as important ecohydrologic indicators (Kokaly et al., 2003; Lin & Liquan, 2006). Applying these indicators, one can use remote-sensing techniques such as Normalized Difference Vegetation Index (NDVI) analysis to gain an understanding of where the wetlands are situated within a catchment.

This baseline information can then be utilized with topographical indices to determine the distribution of soils or the properties of soils within a catchment. Several studies have highlighted the use of DSM programmes for these mapping exercises (Behrens et al., 2005; Lagacherie, 2008; McBratney et al., 2003). One such programme is ArcSIE (Soil Inference Engine) which has been utilized in a number of studies across the globe focusing on both soil classification mapping as well as soil properties mapping (Ashtekar et al., 2014, de Menezes et al., 2014a, b; Silva, 2014; Smith et al., 2010). ArcSIE supports a knowledge-based approach to establish relationships between soils and the environment in which the soils are formed (Shi, 2013). It is thus ideally suited to mapping the hydropedological behaviour of soils within a catchment area.

The aims of this chapter are therefore to use remote-sensing techniques and DSM for hydropedological purposes on a catchment scale in order to understand the various flow dynamics of these catchments. The information obtained from the mapping of the hydropedological soil groups and the interactions between these groups aims to further enhance land use and water management planning in these areas.

10.2 Methodology

10.2.1 Study Site

This study took place within the Cathedral Peak experimental research catchment site, which is situated in the northern part of the uKhahlamba-Drakensberg escarpment, KwaZulu-Natal, South Africa. The site is managed by Ezemvelo KZN Wildlife, while the South African National Environment Observatory Network (SAEON) undertakes the monitoring of the catchments. The catchments, of which there are 15, range in altitude from 1820 m.a.s.l to 2, 463 m.a.s.l. The geological formations of the Drakensberg are the Stormberg and Beaufort Series of the Karoo System. The basaltic lavas of the Stormberg Series overlie the cave sandstones and mudstones as well as the Beaufort Series sandstones, mudstones, and shales which make up the little berg in which the catchments are situated (Nanni, 1956; Toucher et al., 2016).

The research catchments are predominantly covered by grasslands of the uKhahlamba Basalt Grassland vegetation type interspersed with Northern Afrotemperate Forest patches and wetlands (Mucina et al., 2006). Three similar catchments were selected for this study and are named CP-III, CP-VI, and CP-IX (Fig. 10.1). These catchments have been managed differently both in a historical context as well as currently. The first catchment, CP-III, has an area of 138.9 ha and a mean annual rainfall of 1564 mm. The catchment was used for an afforested experiment, in which *Pinus patula* was grown throughout the catchment in the 1950s and 1960s. After an accidental fire, the trees were removed in 1981, and the

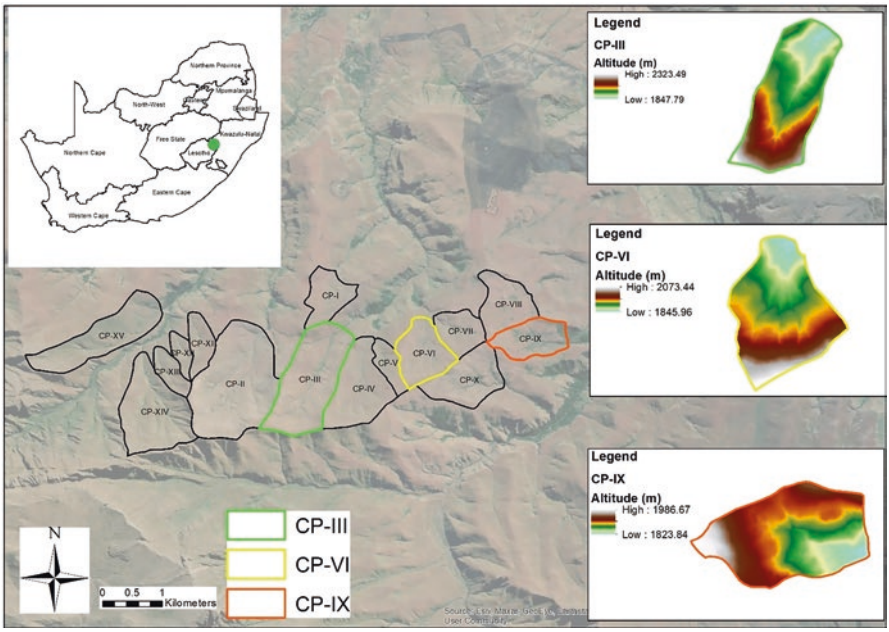

Fig. 10.1 Locality of the catchments selected for the study. (Adapted from Harrison et al. 2022)

catchment has become degraded over time. It is covered by *Pteridium* sp. (Bracken) and annually burned during spring. The second catchment, CP-VI, has an area of 67.7 ha and a mean annual rainfall of 1340 mm. It is covered by grassland which is burned biennially during spring. The third catchment, CP-IX, has an area of 64.5 ha and a mean annual rainfall of 1257 mm. It has been completely protected from fire since 1952 but has experienced accidental burns and wildfires in some years. As a result of fire exclusion, this catchment is dominated by woody scrub (*Leucasidea serica*) (Toucher et al., 2016; Harrison et al., 2022).

10.2.2 Classification of Hydropedological Soil Groups

The grouping of the hydropedological character of soils (based on the classifications from van Tol & Le Roux, 2019) were utilized in this study. The hydropedological soil groups are defined for this study as (Harrison et al. 2022):

1. Recharge Shallow Soils – these are freely drained and are shallow in nature (<500 mm). The freely drained B horizon merges with fractured rock or a lithic horizon. These soils occur on steeper convex slopes in the higher lying parts of the catchments.

2. Recharge Deep Soils – these are freely drained and are deeper than the Recharge Shallow Soils (>500 mm). The freely drained B horizon merges into fractured rock or a lithic horizon. These soils were identified throughout the catchments on gentler convex and concave slopes.
3. Interflow soils – these have a freely drained upper horizons which overlie relatively impermeable bedrock. Hydromorphic properties are identified at this interface and signify periodic saturation associated with a water table. These soils occur on gentler concave slopes in areas delineated as wetlands as well as adjacent to watercourses.
4. Responsive Saturated – these display indications of long-term saturation and were identified in permanently saturated wetlands in the valley bottom positions of the catchments as well on gentle concave slopes. As these soils are close to saturation all year round, the respond quickly to rainfall events and generate overland as any additional precipitation will flow overland due to saturation excess.

10.2.3 Normalized Difference Vegetation Index Analysis

The first aim of the DSM study was to broadly identify and map the watercourses and wetlands located within each of the three catchment sites. In order to achieve this, the use of satellite imagery and the analysis of this imagery was undertaken. Imagery from the Sentinel-2 satellite was utilized. Sentinel-2 is an Earth observation satellite operated by the European Space Agency. It was launched on the 23rd of June 2015 as part of the European Copernicus Programme to perform terrestrial observations in support of services such as forest monitoring, land cover changes detection, and natural disaster management. Sentinel-2 records 13 bands in the visible, near infrared, and short-wave infrared part of the spectrum, and its images have a resolution of 10–60 m (Drusch et al., 2012; Kaplan & Avdan, 2017). The images can be downloaded free from the Copernicus Open Access Hub (https://scihub.copernicus.eu/).

Sentinel-2 imagery from the 25th of June 2020 was used in this study to map the wetlands and watercourses within each of the catchments. This date was chosen as cloud cover over the selected catchments was 1.2%, and thus the area of study was clearly visible. Preprocessing of the data was undertaken utilising the semi-automatic classification plugin for QGIS version 3.10.9. This allowed forv the individual bands to be set according to their central wavelengths (Congedo, 2014).

After preprocessing, a Normalized Difference Vegetation Index (NDVI) analysis was conducted. The NDVI processing utilizes the following formula, for classifying different land covers within the catchments (Zhao et al., 2017).

$$\mathrm{NDVI} = \mathrm{Index}\left(\mathrm{NIR}, \mathrm{RED}\right) = \frac{NIR - \mathrm{RED}}{NIR + \mathrm{RED}}$$

Where NIR is the near infrared band and RED the red band, so for the Sentinel-2 images the following applies:

$$\text{Sentinel-2 images NDVI} = \text{Index}\left(\text{Band8, Band4}\right) = \frac{\text{Band8} - \text{Band4}}{\text{Band8} + \text{Band4}}$$

According to the Earth Resources and Observation Science (EROS) Centre, values of the NDVI analysis range from −1 to 1. Areas of bare soil and/or open water have a very low NDVI value (i.e., 0.1 or less). Sparse vegetation results in moderate NDVI values (approximately 0.2–0.5), while high NDVI values (0.6–0.9) correspond to dense vegetation.

Based on prior knowledge of the catchments, areas which are known to be wetlands and watercourses are associated with denser vegetation as compared to terrestrial areas. Therefore, initial classification of wetlands and watercourses within the catchments was taken as areas with NDVI values higher than 0.4.

10.2.4 Rule-Based Digital Soil Mapping Utilising the Arc Soil Inference Engine (ArcSIE)

The creation of the digital soil maps for the three catchment areas utilized the ArcSIE (Soil Inference Engine) version 10.2.105. ArcSIE is a toolbox that functions as an Extension of ArcMap and generates soil maps based on the soil-environment model:

$$S = f\left(E\right)$$

This model states that the information about soil (S) can be derived from the information about the soil formative environment (E), including topography, geology, climate, and vegetation (Zhu et al., 2010).

ArcSIE was designed for creating soil maps using fuzzy logic in which DSM is performed according to existing relationships between soil attributes and landforms (de Menezes et al., 2014a, b). The fuzzy logic model is based on the concept of fuzzy sets (Zadeh, 1965) and the complex nature of soils and landscapes which creates a more gradual and continuous change in soils and their properties. This forms an uncertainty in the allocation of boundaries between one soil group and another and should therefore not be represented by the abrupt lines depicted in polygon-based maps. Fuzzy logic therefore attempts to represent this uncertainty by predicting the soil groups as an alternative that is more adapted to the reality of the environment (Martín-López et al., 2019). Unlike ordinary sets, fuzzy sets enable their elements to show a partial degree of membership in the range from 0 (no membership) to 1 (full membership). In this way, fuzzy logic models are capable of

representing continuous graduations from one class to another class (Hellwig et al., 2016a; Shi et al., 2004).

A 5 m resolution Digital Elevation Model (DEM) (Ezemvelo KZN Wildlife et al., 2016) was utilized to create Digital Terrain Models (DTM) utilising ArcGIS version 10.2 and ArcSIE version 10.2.105 to represent the distribution of the topographical features across the three catchment sites. The slope, elevation, and planform curvature were calculated directly from the DEM, while the wetness index was created from the filled DEM and a multipath flow accumulation raster.

A rule-based approach was undertaken. This involved understanding the relationships between the soil and landscape and was based on knowledge of the catchments and previous soil surveys. Furthermore, the aim of this study was to group the identified soil types into hydropedological groups based on the behaviour of the soils in relation to the flow dynamics of the catchment. The hydropedological classes were therefore classified as (i) recharge shallow soils; (ii) recharge deep soils; (iii) interflow soils; and (iv) responsive saturated soils (van Tol & Le Roux, 2019). The relationship between these hydropedology soil groups and the slope, elevation, topographical curvature, and inverse wetness index was identified.

A number of rules were applied to the inference engine within the ArcSIE tool. These rules were based on the outcome of the DTMs as well as knowledge of the catchments, with various parameters overlapping with each other due to the fuzzy logic nature of the rules applied. The following parameters were set for each of the DTMs within CP-III, CP-VI, and CP-IX (Table 10.1). Table 10.1 represents the information used to produce the optimal curves that describe quantitatively the relationships between soil type and a particular DTM (de Menezes et al., 2014a, b; Zhu et al., 1997). Furthermore, the wetness index was compared against the results of the NDVI analysis and mask polygons created where wetlands are known to occur. These mask polygons formed part of the input rules for the model.

Table 10.1 Environmental control variables of the hydropedological soil groups in CP-III, CP-VI, and CP-IX

Catchment	Hydropedological Soil Group	Wetness Index	Elevation (m)	Slope (%)	Planform Curvature
CP-III	Recharge shallow	<1	1900–2280	>30	<−5
	Recharge deep	1–9	1848–2200	22–30	−5 – −0.6
	Interflow	8–15	1848–2100	18–30	-0.6–2
	Responsive saturated	15–21	1848–1956	<18	2–3.6
CP-IV	Recharge shallow	< 2	1860–2040	>80	<−2.3
	Recharge deep	3–5	1830–2070	25–79	−2.3–0.4
	Interflow	–7	1830–2040	15–	0.4–3.6
	Responsive saturated	>8	1830–2000	<15	>3.6
CP-IX	Recharge shallow	<4	1838–1985	>29	>0
	Recharge deep	3–8	1820–1985	1–28	−0.5–3.6
	Interflow	7–10	1820–1930	14–28	−3.5–0.4
	Responsive saturated	9–13	1820–1911	<15	−6.9–0.5

After identifying the environmental control variables for each of the hydrological soil groups in each of the catchments, the continuous function curves set by ArcSIE were utilized to precisely define each parameter. The continuous function is applicable to environmental features with interval or ratio values (e.g. elevation, and slope gradient) and these were utilized for each of the parameters defined in this study. ArcSIE provides three basic function curves, which are used to further fine-tune the curve shape. These are the bell-shape curve, s-shape curve, and z-shape curve. These are described by Shi (2013) as follows.

The bell-shape curve optimality value decreases as the difference between the environmental feature and the central value increases (e.g. in CP-VI, the bell-shape curve defines that for the interflow hydropedological soil group a 15–25% slope is optimal, i.e. receiving the highest membership and the membership value decreases as the slope increases from 25% or decreases from 15%). The s-shape curve defines the optimality of the environmental variable will always get the maximum value if the environmental feature values are greater than a defined value (e.g. in CP-III, the s-shape curve defines that for the recharge shallow hydropedological group, a slope steeper than 30% is always optimal and thus receiving the highest membership). The z-shape curve defines that the optimality will always receive the maximum value if the environmental feature values are less than a defined value (e.g. in CP-VI, the z-shape curve defines that for the responsive saturated hydropedological group, a slope gentler than 21% are always optimal, and thus receiving the highest membership). Examples of these function curves are provided in Fig. 10.2.

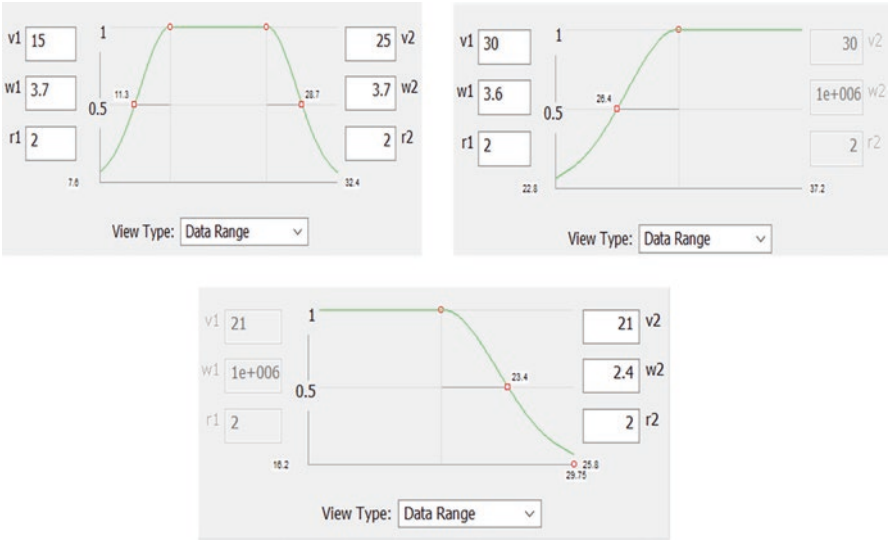

Fig. 10.2 Examples of the bell-shape, S-shape, and Z-shape optimality curves utilized in the ArcSIE inference interface

10.3 Ground Truthing and Validation

The ArcSIE interface allows for the input of case-based features with the aim of adjusting the predictive models created within the rule-based phase, to better reflect the knowledge about a particular landscape. Cases are spatial features (points, lines, polygons, or raster cells) pinpointed, delineated, or derived by the soil scientist to express the knowledge of local soils (Shi, 2019). Existing soil maps and soil information gathered at specific points within the catchments were added as individual cases to the ArcSIE interface and this information is utilized to refine the mapping rules. Forty-nine validation points were utilized for CP-III, 47 for CP-VI, and 27 for CP-IX. Soil sampling points were chosen to cover the range in altitude, planform curvature, slope, and topographical wetness of the individual catchment areas. The soils were classified as per the South African soil classification system (Soil Working Group, 2018) and their locations are displayed in Fig. 10.3.

The weighted average function was furthermore utilized in the validation process. Under the weighted-average method, ArcSIE calculates a linear weighted average of the optimality values of individual environmental features to get the overall optimality value for the instance. It therefore assigns different weights to different environmental features utilising the Analytical Hierarchy Process, which uses a structured process to assign weights consistently (Shi, 2013, 2019). An example of this is given in CP-III where slope is specified to be more important than elevation. The ArcSIE interface then quantifies this specification by assigning the score of slope against elevation.

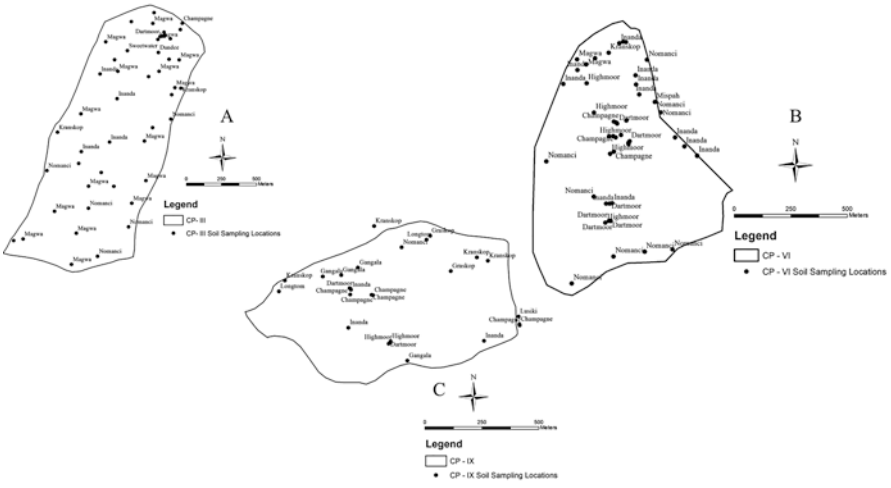

Fig. 10.3 Location of the soil sampling points as well as the classification of the soils in (**a**) CP-III, (**b**) CP-VI, and (**c**) CP-IX

10.3.1 Statistical Validation

The performance of the ArcSIE interface to create the combined hydropedological maps for each of the catchments was analysed using the Kappa coefficient of agreement. This was used to measure the accuracy of the classifications utilized in the maps.

This was first undertaken using the classification of the pixel values versus the ground-truthed results that were obtained during previous soil surveys. Following the identification of the accuracies presented for each hydropedological soil group in each catchment, the Kappa coefficient equation (Cohen, 1960) was calculated. For computational purposes, the following formula is presented:

$$K = \frac{P_o - P_e}{1 - P_e}$$

Where

P_o = sum of each hydropedological group accuracy/total number of variables
P_e = (sum of probability of a random raster pixel being in the correct hydropedological group) – (sum of probability of a random raster pixel being in the incorrect hydropedological group)

10.4 Results and Discussion

The results section follows the same sub-headings as set out in the methodology section. These sub-sections identify the hydropedological classification of the soils delineated within the three catchments, the results of the NDVI analysis, the ArcSIE rule-based and validation inputs, as well as the statistical analysis of the results obtained. A discussion of the results then highlights the effectiveness of utilising ArcSIE for the mapping of the hydropedological soil groups.

10.4.1 Hydropedological Classification of Soils

Soil surveys to map the soils were undertaken within the three catchment areas. These soils were classified as per the South African soil classification system (Soil Working Group, 2018). The soils were then reclassified according to their hydropedological character, based on the classifications from van Tol and Le Roux (2019). The hydropedological soil groups are defined for this study as per Table 10.2.

Table 10.2 Hydropedological Soil Groups mapped in the catchments

Hydropedological Soil Group	Soil forms (Soil Working Group, 2018)	Characteristics of soils
Recharge shallow soils	Nomanci, Mispah, Graskop	These are soils that are freely drained and do not show any indication of saturation. They are typically shallow in nature (<500 mm). The freely drained B horizon merges with fractured rock or a lithic horizon. These soils typically occur on steeper convex slopes in the higher lying or steeper parts of the catchments.
Recharge deep soils	Kranskop, Magwa, Inanda, Longtom, Sweetwater, Gangala	These are soils that are freely drained and do not show any indication of saturation. They are typically deeper than the Recharge Shallow Soils (>500 mm). The freely drained B horizon merges into fractured rock or a lithic horizon. These soils were identified throughout the catchments on gentler convex and concave slopes and away from wetlands and watercourses
Interflow soils	Dartmoor, Highmoor	These soils have a freely drained upper solum which overlies relatively impermeable bedrock. Hydromorphic properties are identified at this interface and signify periodic saturation associated with a water table. They typically occur on gentler concave slopes in areas delineated as wetlands, as well as adjacent to watercourses
Responsive saturated soils	Champagne, Katspruit	These soils display morphological indications of long-term saturation. They characteristically respond quickly to rainfall events and generate overland flow as they are typically close to saturation during the wet season, and therefore any additional precipitation will flow overland due to saturation excess. These soils were identified in the valley bottom positions of the catchments, in permanently saturated wetlands. They typically occur on gentle concave slopes

10.4.2 NDVI Analysis

The results of the NDVI analysis are given in Fig. 10.4. The NDVI values vary from 0 to 0.79 for all catchments with lower values indicating bare soil and higher values vegetation. The higher the value, the denser the vegetation. The CP-III NDVI values ranged from 0.05 to 0.79, CP-VI results ranged from 0.06 to 0.55 and CP-IX results varied from 0 to 0.64. Firebreaks, which had been burned around the boundary of each of the catchments are clearly visible, with these areas displaying low values (<0.2) due to the exposure of bare soil as a result of the fire. Based on knowledge of the catchments, areas which are known to be wetlands and watercourses displayed values in the mid to high value ranges and are displayed in Fig. 10.3 as areas with values higher than 0.4 (blue colouring). As CP-IX consists of denser vegetation as a result of the dominance of the woody scrub, *Leucasidea serica*, wetlands and watercourses were classified as areas with a higher NDVI value, 0.5, compared to CP-III

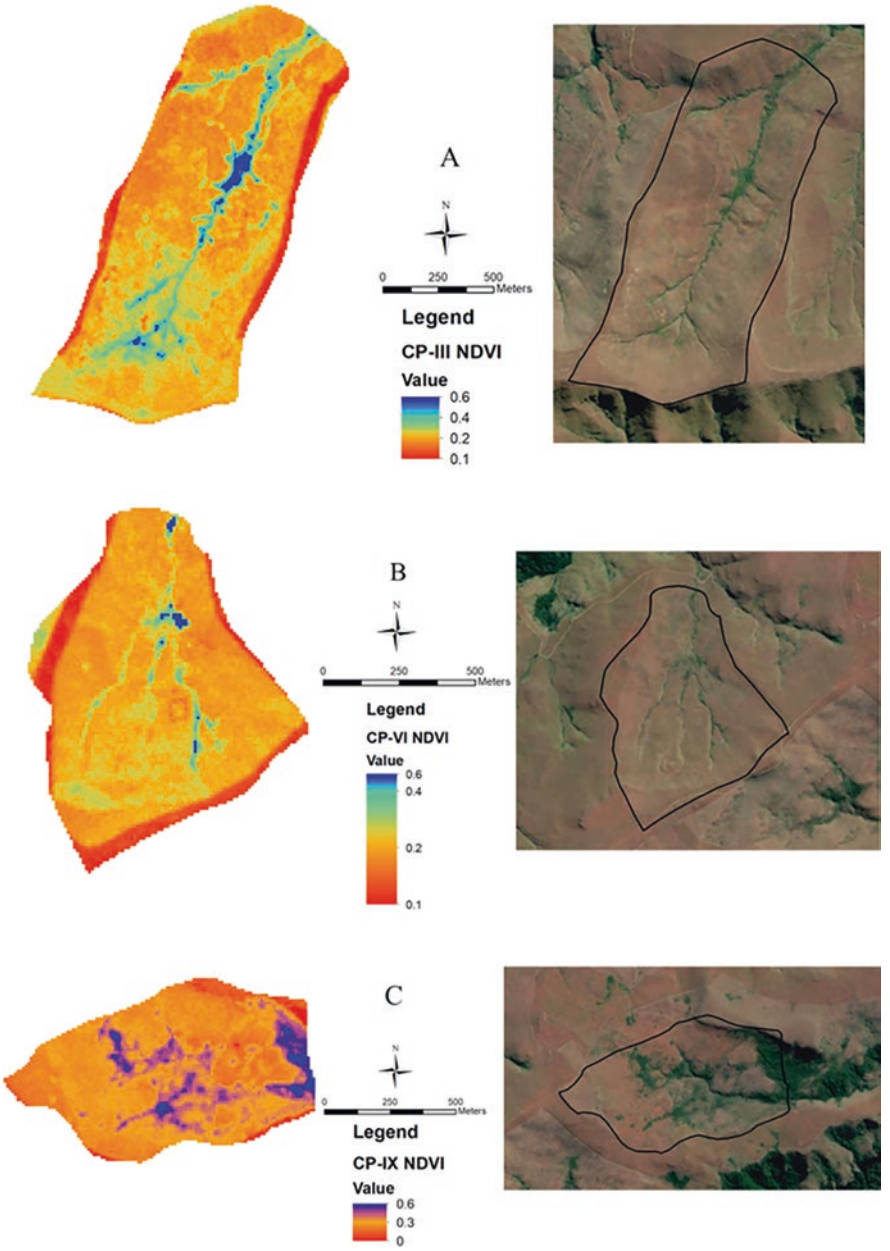

Fig. 10.4 NDVI analysis results for the three catchments: (**a**) CP-III, (**b**) CP-VI, and (**c**) CP-IX

and CP-IV. As the satellite imagery was taken in June (dry season), no areas of open water were identified.

The use of the NDVI analysis to form a basis for the location of wetlands and watercourses relied on the knowledge of the catchments and the use of previous soil survey work. Watercourses and wetland zones were defined in all three catchments in the NDVI analysis as areas with denser vegetation. Prior knowledge of these areas as well as the use of the topographical wetness index as part of the rule-based processing of the maps confirmed their classification as watercourses and wetland systems. It is therefore difficult to delineate watercourses and wetlands with the use of NDVI analysis alone. This is corroborated in various studies in which it was concluded that rule-based classifiers provide more accurate results if supported by ancillary data such as Digital Elevation Models (Lidzhegu et al., 2019; Ozesmi & Bauer, 2002; Quinn & Epshtein, 2014). The NDVI analysis results combined with the topographical wetness index and knowledge of the catchments, however, provided useful data in the creation of polygon masks which were input into the ArcSIE interface to aid in the correct prediction of areas as wetlands and watercourses.

10.4.3 Rule-Based Digital Soil Mapping

Figure 10.5 shows an example of the fuzzy membership maps produced for the four hydropedological classes in CP-III. These were created according to the instances for each of these classes (Table 10.1) and the input of polygon masks where wetlands and watercourses are known to occur. Similar fuzzy membership maps were created for CP-VI and CP-IX. These maps are the first product generated by the inference engine and are used as the basis for the final map. Every pixel in each of the fuzzy membership maps is assigned a value ranging from 0 to 100 depending on the similarity of that pixel location to the hydropedology classes being mapped.

These maps reveal more details about the hydropedology classes than conventional polygon maps because they are made at pixel size spatial resolution (de Menezes et al., 2014a, b). The ArcSIE interface then allows for the creation of a combined map in which the individual fuzzy membership maps are integrated and a draft map of the hydropedological classes for the catchments created (Fig. 10.5).

10.4.4 Validation

Based on the specific locations of the soil points in each of the catchments, the results of the NDVI analysis, as well as the use of the linear weighted average, a finalized refined hydropedological soil group map was created. These are displayed in Fig. 10.6.

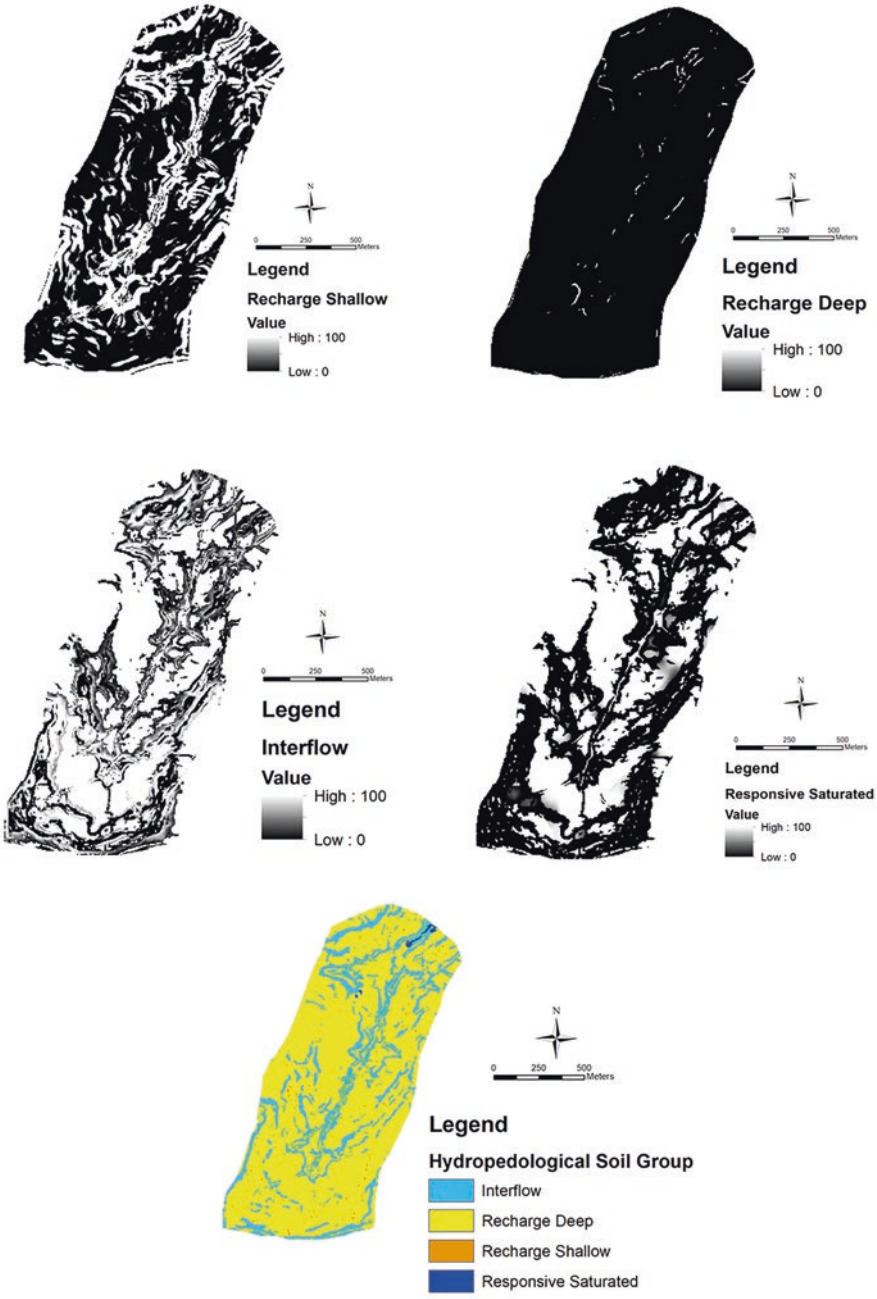

Fig. 10.5 Fuzzy membership maps for each hydropedological soil group as well as the draft combined map for CP-III

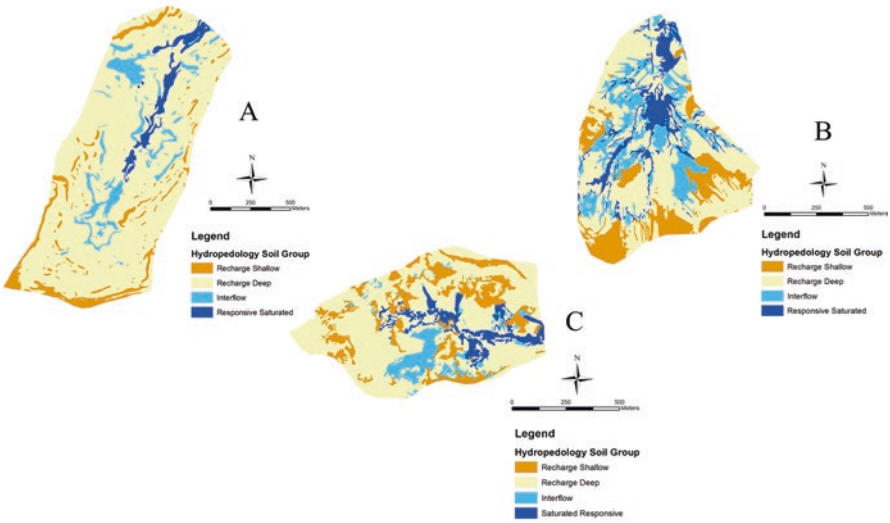

Fig. 10.6 Refined hydropedological soil group maps for the three catchments: (**a**) CP-III, (**b**) CP-VI, and (**c**) CP-IX

10.4.5 Statistical Analysis

The accuracy table displaying the classification of the pixel values versus the ground-truthed results of each catchment is presented in Table 10.3. Accuracy percentage values varied between catchments and between the different hydropedological soil groups.

The overall Kappa coefficient for CP-III is 0.57, for CP-VI is 0.59, and for CP-IX is 0.74. These values range from a weak (CP-III and CP-VI) to a moderate (CP-IX) agreement between the predicted maps and the ground-truthed points (McHugh, 2012). Various studies which utilize DSM for the prediction of both soil types and physical properties of soils within catchments have resulted in similar (weak to moderate) agreements (de Menezes et al., 2014a, b; Hellwig et al., 2016a, b; Silva et al., 2019).

The quality of the hydropedological soil group maps produced is determined by the method (rule-based versus case-based) and the environmental covariates used for the model predictions. The accuracy of the DEM utilized in the initial rule-based approach plays a large role in determining the effects of slope, elevation, planform curvature, and the wetness index on the modelled predictive maps for each hydropedological soil group. Furthermore, inaccuracies and uncertainties in the input of the value ranges in the function curves as part of the rule-based approach, as well as the use of weighted average function in the case-based approach plays a role in determining the quality of the final maps produced. These inaccuracies and uncertainties were highlighted in various studies which recommended validation procedures to improve inaccuracies in the predictive models (de Menezes et al., 2014a, b; Hellwig

Table 10.3 Accuracies for modelled hydropedological group versus ground-truthed hydropedological group in CP-III, CP-VI, and CP-IX

Catchment	Hydropedological Soil Group	Ground-truthed Recharge Shallow	Ground-truthed Recharge Deep	Ground-truthed Interflow	Ground-truthed Responsive Saturated	Total	Accuracy %
CP-III	Recharge shallow	**4**	1	0	0	5	80
	Recharge deep	4	**21**	1	2	28	75
	Interflow	1	1	**8**	0	10	80
	Responsive saturated	2	2	0	**2**	6	34
	Total	11	25	9	4	**49**	
CP-VI	Responsive saturated	**8**	0	1	4	13	62
	Recharge shallow	0	**9**	1	0	10	90
	Recharge deep	1	0	**11**	5	17	65
	Interflow	0	0	2	**4**	6	67
	Total	9	9	15	13	**46**	
CP-IX	Recharge deep	**9**	0	1	1	11	82
	Recharge shallow	2	**5**	0	0	7	71
	Interflow	0	0	**3**	0	3	100
	Responsive saturated	1	0	0	**5**	6	83
	Total	12	5	4	6	**27**	

et al., 2016b). The accuracy of the location of each individual hydropedological soil group also influences the overall accuracy of the final maps produced. This varied for each catchment and depended on the quantity of observation points made in previous soil surveys.

The determined quality of the final digital soil maps reinforces the need to combine the knowledge of soil experts with soil–landscape relationships. This increases the accuracy of prediction models of soil properties within a landscape (de Menezes et al., 2014a, b).

Readily available soil information is increasingly being sought after as the importance of soil in ecosystem management is more widely recognized. The security of soils including their capability, health, connectivity, and classification forms the basis of all spheres of land management from food and nutrition security, water security, energy security, climate change, and human health. With the use of DSM, our knowledge and understanding of future soil security can be enhanced for larger areas with the use of competitive budgets and timeframes (Searle et al., 2021; van Zijl, 2019).

10.5 Conclusion

Results indicate that while the use of ArcSIE is a powerful tool to be used to gain a general idea of the relationship between the soils and the landscape from a hydropedological stance, the knowledge of the soil–landscape relationship, as with the traditional soil mapping exercise, is still necessary to improve the accuracy of the tool. The quality of the digital soil map produced is furthermore dependant on the method employed (rule-based versus case-based) as well as the environmental covariates used for the model predictions. This is true for all inputs to the prediction model. The results of the NDVI analysis, which were utilized as another input to improve the accuracy of the prediction model, identified that it is difficult to delineate the wetlands and watercourses without prior knowledge of the catchments. Therefore, the more knowledge one has of the landscape processes under study, the more accurate the outcome of the digital soil mapping exercise will be.

However, the hydropedological soil group maps achieved an appropriate representation of the complex nature of the soil–landscape relationship, with changes between one soil group and the next being gradual and continuous. These soil group correlations are not well represented in polygon-based maps and therefore require the fuzzy membership logic utilized by the ArcSIE interface to depict these relationships. The use of the ArcSIE interface to derive the hydropedological soil group maps of the three different catchments provided adequate results with regard to understanding the overall behaviour of the soils in the catchments. Of importance is that the accuracies and inaccuracies within the fuzzy membership maps can be quantified, allowing for a confidence rating in the use of these maps. These maps can therefore be used in further applications in water and land management for the area.

Numerous studies have utilized ArcSIE to create not only soil classification maps but also more detailed studies of the properties of soils across the globe (Akumu et al., 2015; de Menezes et al., 2014a, b; Moonjun et al., 2020; Pittman et al., 2021), however the use of any DSM programme has rarely been applied in Africa and particularly in Afromontane environments, with the majority of studies coming out of South Africa and Kenya. These studies are furthermore aimed at agricultural studies, the mapping of soil organic carbon, clay percentage, and for industrial and commercial developments (Mora-Vallejo et al., 2008; van Zijl, 2019).

Afromontane environments provide several ecohydrological services to downstream locations, including the ecological and physical processes that control the partitioning and routing of precipitation into evaporation, infiltration, transpiration, recharge, and runoff (Brooks & Vivoni, 2015). The characteristics of the soils of these catchments form the basis of these services. However, the remoteness and often inaccessible terrain associated with Afromontane environments often reduce the knowledge and understanding of these areas. The use of DSM which is suited to these types of environments would allow for more integration of soil knowledge into land management policies across the continent. Further training of DSM programmes in Africa would therefore lead to an improved understanding of the basis of ecohydrological processes.

References

Akumu, C. E., Johnson, J. A., Etheridge, D., Uhlig, P., Woods, M., Pitt, D. G., & McMurray, S. (2015). GIS-fuzzy logic-based approach in modeling soil texture: Using parts of the Clay Belt and Hornepayne region in Ontario Canada as a case study. *Geoderma*, 239–240. https://doi.org/10.1016/j.geoderma.2014.09.021

Ashtekar, J. M., Owens, P. R., Brown, R. A., Winzeler, H. E., Dorantes, M., Libohova, Z., Dasilva, M., & Castro, A. (2014). Digital mapping of soil properties and associated uncertainties in the llanos Orientales, South America. In *Global soil map: Basis of the global spatial soil information system - proceedings of the 1st global soil map conference* (pp. 367–372). https://doi.org/10.1201/b16500-67

Behrens, T., Förster, H., Scholten, T., Steinrücken, U., Spies, E.-D., & Goldschmitt, M. (2005). Digital soil mapping using artificial neural networks. *Journal of Plant Nutrition and Soil Science, 168*(1), 21–33. https://doi.org/10.1002/jpln.200421414

Berberoglu, S., Yilmaz, K. T., & Ozkan, C. (2004). Mapping and monitoring of coastal wetlands of Cukurova Delta in the Eastern Mediterranean region. *Biodiversity and Conservation, 13*, 615–633.

Bouma, J. (2006). Hydropedology as a powerful tool to environmental policy research. *Geoderma, 131*, 275–286.

Brooks, P. D., & Vivoni, E. R. (2015). Editorial. Mountain ecohydrology: Quantifying the role of vegetation in the water balance of montane catchments. *Ecohydrology, 1*, 187–192. https://doi.org/10.1002/eco.27

Bushnell, T. M. (1942). Some aspects of the soil catena concept. *Soil Science Society of America, Proceedings., 7*, 466–476.

Cohen, J. (1960). A coefficient of agreement for nominal scales. *Educational and Psychological Measurement., 20*(1), 37–46.

Congedo, L. (2014). Semi-automatic classification plugin documentation. Release 5.0.0.1.

de Menezes, M. D., Silva, S. H. G., Owens, P. R., & Curi, N. (2014a). Digital soil mapping approach based on fuzzy logic and field expert knowledge. *Ciência e Agrotecnologia, 37*(4). Lavras.

de Menezes, M. D., Silva, S. H. G., Owens, P. R., & Curi, N. (2014b). Solum depth spatial prediction comparing conventional with knowledge-based digital soil mapping approaches. *Scientia Agricola, 71*(4). https://doi.org/10.1590/0103-9016-2013-0416

Diek, S., Temme, A. J. A. M., & Teuling, A. (2014). The effect of spatial soil variation on the hydrology of a semi-arid Rocky Mountains catchment. *Geoderma, 235-236*, 113–126.

Drusch, M., Del Bello, U., Carlier, S., Colin, O., Fernandez, V., Gascon, F., Hoersch, B., Isola, C., Laberinti, P., Martimort, P., Meygret, A., Spoto, F., Sy, O., Marchese, F., & Bargellini, P. (2012). Sentinel-2: ESA's optical high-resolution mission for GMES operational services. *Remote Sensing of Environment., 120*, 25–36.

European Confederation of Soil Science Societies. (2004). *Scientific basis for the management of European soil resources: Research agenda*. Guthman-Peterson.

Ezemvelo KZN Wildlife, National Lottery, University of KwaZulu-Natal, and African Conservation Trust. (2016). Maloti-Drakensberg Transfronteir aerial mapping project data.

Frohn, R. C., Reif, M., Lane, C., & Autrey, B. (2009). Satellite remote sensing of isolated wetlands using object-oriented classification of Landsat-7 data. *Wetlands, 29*(3), 931–941.

Grayson, R. B., Western, A. W., Chiew, F. H. S., & Blöschl, G. (1997). Preferred states in spatial soil moisture patterns: Local and nonlocal controls. *Water Recourses Research., 33*(12), 2897–2908.

Harrison, R. L., van Tol, J., & Toucher, M. L. (2022). Using hydropedological characteristics to improve modelling accuracy in Afromontane catchments. *Journal of Hydrology: Regional Studies, 39*. https://doi.org/10.1016/j.ejrh.2021.100986

Heath, R. C. (1980). Basic elements of groundwater hydrology with reference to conditions in North Carolina. US. Geological Survey. Water Resources Investigations. Open File Report No. 80–44. pp. 87.

Hellwig, N., Graefe, U., Tatti, D., Sartori, G., Anschlag, K., Beylich, A., Gobat, J., & Broll, G. (2016a). Upscaling the spatial distribution of enchytraeids and humus forms in a high mountain environment on the basis of GIS and fuzzy logic. *European Journal of Soil Biology., 79*, 1–13.

Hellwig, N., Anschlag, K., & Broll, G. (2016b). A fuzzy logic based method for modelling the spatial distribution of indicators of decomposition in a high mountain environment. *Arctic, Antarctic, and Alpine Research, 48*(4), 623–635. https://doi.org/10.1657/AAAR0015-073

Ismail, M., & Yacoub, R. K. (2012). Digital soil map using the capability of new technology in Sugar Beet area, Nubariya, Egypt. *The Egyptian Journal of Remote Sensing and Space Science, 15*(2), 113–124. https://doi.org/10.1016/j.ejrs.2012.08.001

Jenny, H. (1941). *Factors of soil formation*. McGraw-Hill.

Kaplan, G., & Avdan, U. (2017). Mapping and Monitoring Wetlands Using Sentinel-2 Satellite Imagery. ISPRS Annals of the Photogrammetry, Remote Sensing and Spatial Information Sciences. Vol. IV–4/W4. 4th International GeoAdvances Workshop. 14–15 October 2017, Safranbolu, Karabuk, Turkey.

Kimsey, M. J. (2020). Soil mapping, monitoring, and assessment. In R. Pouyat, D. Page-Dumroese, T. Patel-Weynand, & L. Geiser (Eds.), *Forest and rangeland soils of the United States under changing conditions*. Springer. https://doi.org/10.1007/978-3-030-45216-2_9

Klemas, V. (2005). Remote sensing: Wetlands classification. In M. L. Schwartz (Ed.), *Encyclopedia of coastal science* (pp. 804–807). Springer.

Klemas, V. (2011). Remote sensing of wetlands: Case studies comparing practical techniques. *Journal of Coastal Research., 27*(3), 418–427.

Kokaly, R. F., Despain, D. G., Clark, R. N., & Livo, K. E. (2003). Mapping vegetation in Yellowstone National Park using spectral feature analysis of AVIRIS data. *Remote Sensing of Environment., 84*, 437–456.

Lagacherie, P. (2008). Digital soil mapping: A state of the art. In A. E. Hartemink, A. McBratney, & M. Mendonça-Santos (Eds.), *Digital soil mapping with limited data*. Springer. https://doi.org/10.1007/978-1-4020-8592-5_1

Lidzhegu, Z., Ellery, W. N., Mantel, S. K., & Hughes, S. K. (2019). Delineating wetland areas from the cut-and-fill method using a Digital Elevation Model (DEM). *South African Geographical Journal*. https://doi.org/10.1080/03736245.2019.1638825

Lin, Y., & Liquan, Z. (2006). Identification of the spectral characteristics of submerged plant Vallisneria spiralis. *Acta Ecologica Sinica., 26*, 1005–1011.

Lin, H., Bouma, J., Pachepsky, Y., Western, A., Thompson, J., van Genuchten, R., Vogel, H., & Lilly, A. (2006). Hydropedology: Synergistic integration of pedology and hydrology. *Water Resources Research., 42*, W05301. https://doi.org/10.1029/2005WR004085

Lindbo, D. L., & Richardson, J. L. (2000). Chapter 12: Hydric soils and wetlands in riverine systems. In J. L. Richardson & M. J. Vepraskas (Eds.), *Wetland soils: Their genesis, morphology, hydrology, landscape, and classification*. CRC Press.

Lunetta, R. S., & Balogh, M. E. (1999). Application of multi-temporal Landsat 5™ imagery for wetland identification. *Photogrammetric Engineering & Remote Sensing., 65*, 1303–1310.

Ma, Y., Minasny, B., Malone, B. P., & McBratney, A. B. (2019). Pedology and digital soil mapping (DSM). *European Journal of Soil Science., 70*, 216–235. https://doi.org/10.1111/ejss.12790

Mahmood, T. H., & Vivoni, E. R. (2011). A climate-induced threshold in hydrologic response in a semiarid ponderosa pine hillslope. *Water Recourses Research, 47*(9), W09529.

Martín-López, J. M., Da Silva, M., Valencia, J., Quintero, M., Keough, A., Casares, F. (2019). A comparative Digital Soil Mapping (DSM) study using a non-supervised clustering analysis and an expert knowledge-based model - A case study from Ahuachapán, El Salvador. Presented at: Joint Workshop for Digital Soil Mapping and Global Soil Map March 12–16 2019.

McBratney, A. B., Mendonca Santos, M. L., & Minasny, B. (2003). On digital soil mapping. *Geoderma, 117*, 3–52.

McHugh, M. L. (2012). Interrater reliability: The kappa statistic. *Biochemia Medica., 22*(3), 276–282.

Milne, G. (1936). Normal erosion as a factor in soil profile development. *Nature, 138*(3491), 548–549. https://doi.org/10.1038/138548c0

Mitsch, W. J., & Gosselink, J. G. (2015). Wetlands. Wetlands. pp. 155–204.
Moonjun, R., Shrestha, P. D., & Jetten, V. G. (2020). Fuzzy logic for fine-scale soil mapping: A case study in Thailand. *Catena, 190*, 104456. https://doi.org/10.1016/j.catena.2020.104456
Mora-Vallejo, A., Claessens, L., Stoorvogel, J., & Heuvelink, G. (2008). Small scale digital soil mapping in Southeastern Kenya. *Catena, 76*, 44–53. https://doi.org/10.1016/j.catena.2008.09.008
Mucina, L., Rutherford, M. C., & Powrie, L. W. (Eds.). (2006). *Vegetation map of South Africa, Lesotho and Swaziland* (2nd ed.). South African National Biodiversity Institute. isbn:978-1-919976-42-6.
Nanni, U. W. (1956). Forest hydrological research at the cathedral peak research station. *Journal of the South African Forestry Association, 27*(1), 2–35.
Ozesmi, S. L., & Bauer, M. E. (2002). Satellite remote sensing of wetlands. *Wetlands Ecology and Management, 10*, 381–402.
Penna, D., Borga, M., Norbiato, D., & Dalla Fontana, G. (2009). Hillslope scale soil moisture variability in a steep alpine terrain. *Journal of Hydrology, 364*(3–4), 311–327.
Phillips, R. L., Beeri, O., & DeKeyser, E. S. (2005). Remote wetland assessment for Missouri Coteau prairie glacial basins. *Wetlands, 25*, 335–349.
Pittman, R., Hu, B., & Webster, K. (2021). Improvement of soil property mapping in the Great Clay Belt of northern Ontario using multi-source remotely sensed data. *Geoderma, 381*, 114761. https://doi.org/10.1016/j.geoderma.2020.114761
Quinn, N. W. T., & Epshtein, O. (2014). Seasonally-managed wetland footprint delineation using Landsat ETMþ satellite imagery. *Environmental Modelling & Software., 54*, 9–23.
Rhoton, F. E., Bigham, J. M., & Lindbo, D. L. (2002). Properties of iron oxides in streams draining the loess uplands of Mississippi. *Applied Geochemistry, 17*, 409–419.
Searle, R., McBratney, A., Grundy, M., Kidd, D., Malone, B., Arrouays, D., Stockman, U., Zund, P., Wilson, P., Wilford, J., Van Gool, D., Triantafilis, J., Thomas, M., Stower, L., Slater, B., Robinson, N., Ringrose-Voase, A., Padarian, J., Payne, J., … Andrews, K. (2021). Digital soil mapping and assessment for Australia and beyond: A propitious future. *Geoderma Regional., 24*. https://doi.org/10.1016/j.geodrs.2021.e00359
Shi, X. (2013). ArcSIE user guide. http://www.arcsie.com/Download/htm. Accessed 8 June 2020.
Shi, X. (2019). ArcSIE tutorial with geodatabase. http://www.arcsie.com/Download/htm. Accessed 8 June 2020.
Shi, X., Zhu, A., Burt, J. E., Qi, F., & Simonson, D. (2004). A case-based reasoning approach to fuzzy soil mapping. *Soil Science Society of America Journal., 68*, 885–894.
Silva, B. P. C., Silva, M. L. N., Avalos, F. A. P., de Menezes, M. D., & Curi, N. (2019). Digital soil mapping including additional point sampling in Posses ecosystem services pilot watershed, southeastern Brazil. *Scientific Reports, 9*, 13763. https://doi.org/10.1038/s41598-019-50376-w
Smith, S., Bulmer, C., Flager, E., Frank, G., & Filatow, D. (2010). Digital Soil Mapping at multiple scales in British Columbia, Canada. In Program and Abstracts. 4th Global Workshop on Digital Soil Mapping, 24–26 May 2010, Rome. p. 17.
Soil Classification Working Group. (2018). *Soil classification: A natural and anthropogenic system for South Africa*. ARC-Institute for Soil, Climate and Water.
Teuling, A. J., & Troch, P. A. (2005). Improved understanding of soil moisture variability dynamics. *Geophysical Research Letters, 32*(5), L05404.
Thompson, J. A., Roecker, S., Grunwald, S., & Owens, P. R. (2012). Chapter 21: Digital soil mapping: Interactions with and applications for hydropedology. In H. Lin (Ed.), *Hydropedology*. https://doi.org/10.1016/B978-0-12-386941-8.00021-6
Toucher, M. L., Clulow, A., van Rensburg, S., Morris, F., Gray, B., Majozi, S., Everson, C. E., Jewitt, G. P. W., Taylor, M. A., Mfeka, S., & Lawrence, K. (2016). Establishment of a more robust observation network to improve understanding of global change in the sensitive and critical water supply area of the Drakensberg. 2236/1/16. Water Research Commission, Pretoria, South Africa.

van Tol, J. J., & Le Roux, P. A. L. (2019). Hydropedological grouping of south African soil forms. *South African Journal of Plant and Soil., 36*(3), 233–235. https://doi.org/10.1080/02571862.2018.1537012

van Tol, J. J., Lorentz, S. A., van Zijl, G. M., & Le Roux, P. A. L. (2018). The contribution of hydropedological assessments to the availability and sustainable water, for all (SDG#6). In R. Lal, R. Horn, & T. Kosaki (Eds.), *Soil and sustainable development goals* (pp. 102–117). Catena-Schweizerbart.

van Tol, J. J., van Zijl, G., & Julich, S. (2020). Importance of detailed soil information for hydrological modelling in an urbanized environment. *Hydrology., 7*(2), 34. https://doi.org/10.3390/hydrology7020034

van Zijl, G. (2019). Digital soil mapping approaches to address real world problems in southern Africa. *Geoderma, 337*, 1301–1308. https://doi.org/10.1016/j.geoderma.2018.07.052

van Zijl, G., van Tol, J. J., Tinnefeld, M., & Le Roux, P. (2019). A hillslope based digital soil mapping approach, for hydropedological assessments. *Geoderma, 354*, 113888.

Vepraskas, M. J., & Lindbo, D. J. (2012). Chapter 5: Redoximorphic features as related to soil hydrology and hydric soils. In H. Lin (Ed.), *Hydropedology* (pp. 143–172). Academic Press. https://doi.org/10.1016/B978-0-12-386941-8.00005-8

Zadeh, L. A. (1965). Fuzzy sets. *Information and Control, 8*, 338–353.

Zhao, L., Zhang, P., Ma, X., & Pan, Z. (2017). Land cover information extraction based on daily NDVI time series and multiclassifier combination. *Mathematical Problems in Engineering, 2017*, 6824051. https://doi.org/10.1155/2017/6824051

Zhu, A. X., Band, L., Vertessy, R., & Dutton, B. (1997). Derivation of soil properties using a soil land inference model (SoLIM). *Soil Science Society of American Journal., 61*, 523–533.

Zhu, A. X., Qi, F., Moore, A., & Burt, J. E. (2010). Prediction of soil properties using fuzzy membership values. *Geoderma, 158*, 199–206.

Chapter 11
Effect of Climate Variability and Change on Land Suitability for Irish Potato Production in Kigezi Highlands of Uganda

Nadhomi Daniel Luliro, Daniel Saul Ddumba, Irene Nammanda, and Yeeko Kisira

Abstract The impact of climate variability and change on land suitability for crop growing is not clearly understood. Glaring evidence exists in temperate world where rising global mean temperatures will, most likely, improve crop production. This contravenes the evidences in the tropical environments where gross crop yield decline is a clear manifestation of the rising temperatures. This lacuna jeopardizes standardization on the adoption of appropriate climate change mitigation measures. The Kigezi Highlands are highly vulnerable to climate change impacts; of which, it is quite challenging for small scale farmers to identify suitable areas for Irish potato growing. Our objective was to identify suitable areas for Irish potato production under different climatic scenarios and strengthen the small scale farmers' adaptability to climate variability and change impacts in Kigezi Highlands. Using Agricultural Production Systems Simulator (APSIM) model, we simulated historical and future time scenarios, and using Spatial Multi Criteria Evaluation (SMCE) coupled with remote sensing of a Sentinel 2 image, we generated suitable areas for Irish potato production. The results showed that 30.8% of the site was under agriculture, of which 71.5% was under Irish potato. Of this 71.5%, the most suitable area was only 1.95%, while 5.34% was completely not suitable, and the remaining areas were either moderately or marginally suitable. In the March–May (MAM) and September–November (SON) seasons, the trend of minimum and maximum temperatures was significantly ($P < 0.05$) increasing. However, rainfall was not significant ($P > 0.05$), and its trend was decreasing in the MAM and increasing in the SON seasons. The yield of Irish potato was not significant ($P > 0.05$) and its trend was decreasing in MAM and SON seasons. We concluded that climate variability and change will

N. D. Luliro (✉)
Kyambogo University, Department of Geography, Kyambogo, Uganda

D. S. Ddumba · I. Nammanda · Y. Kisira
Makerere University, Department of Geography, Geo-informatics and Climatic Science, Kampala, Uganda
e-mail: dddumba@caes.mak.ac.ug

S. Adelabu et al. (eds.), *Remote Sensing of African Mountains*,
https://doi.org/10.1007/978-3-031-04855-5_11

decrease land suitability for Irish potato; thus, appropriate soil and water conservation measures applicable to a highland environment need to be adopted.

Keywords APSIM · Climate change · Yield · Irish potato · Highland · Uganda

11.1 Introduction

Climate change and its variability is a world-wide reality whose impacts are threatening the land suitability for many agricultural activities (Worqlul et al., 2019). Global mean surface temperatures have increased by 0.8 °C over the last century (IPCC, 2018), and this has been largely blamed on unsustainable anthropogenic activities. The extreme events are expected to be more rampant and very severe in developing countries, most especially in Sub-Saharan Africa (SSA). Since agricultural enterprises in SSA are rainfed and subsistence in nature, majority of the farmers have limited adaptive capacity to cope with climate change and its impacts (Harvey et al., 2014). Due to these impacts, many communities are now facing food insecurity as a result of increasing unsuitable agrarian landscapes. The cardinal issue underlying this problem is limited farmers' ability to identify the highly suitable areas with specific requirements in resonance to different crops for increased crop production (Daccache et al., 2012). With rapid population growth rates, the demand for food has drastically increased especially in SSA. Thus, to stop gap subsistence, farmers tend to cultivate even on the most unsuitable landscapes such as the marginal and fragile mountain slopes (Bamutaze et al., 2021).

This, notwithstanding, climate change projections have shown that the mountainous and other highland environments, which are affected by heavy and erratic rains, will have a decrease in crop yield (Gatiso, 2015). This is because the topographic factor coupled with high rainfall erosivity indices can lead to very high magnitudes of top soil and nutrient losses (Bamutaze et al., 2021). Vast highland areas of SSA, most especially those in Uganda, have become victims of land unsuitability for certain essential food security crops due to soil and nutrient losses (Twagiramaria & Tolo, 2016). Thus, effort to evaluate the possible impacts of climate change on land suitability is pivotal in planning sustainable agricultural systems for adaptation to climate variability and change (Csillik & Belgiu, 2016).

Although Irish potato (*Solanum Tuberosum*) plays an important role in global food and nutritional security, its yield is highly sensitive to weather and climate variability. In Africa, where wide weather and climate uncertainties are a common phenomenon, the yield for Irish potato is as low as 535.9 t ha^{-1}, and in East Africa, it is as low as 56.5 t ha^{-1} (FAO, 2015) In Uganda, Irish potato production is still poor. This country is ranked the third largest producer of the crop after Rwanda and Kenya (FAO, 2015). In general terms, this crop is mainly grown in the mountains of southwestern, and of the eastern parts of the country. These are areas which tend to receive heavy and generally reliable rains, with fertile soils deriving from igneous volcanic materials (Bonabana-Wabbi et al., 2013). Available historical climate data

show that the rainfall received in this country is more erratic, in and out of season and tending to be shorter in duration and in most cases extreme. Even within the traditionally recognizable seasons, unusual events such as heavier rains, long dry spells, and high temperature fluctuations are rampant (Hepworth & Goulden, 2008). This casts a gloomy situation in Uganda in the sense that the uptake for sustainable agricultural systems to cope with climate variability and change is still low.

While the mountainous and highland areas in Uganda are suitable for Irish potato growing, its distribution across this landscape is not evenly distributed due to land suitability differences (Akinci et al., 2013; Mwaura & Okoboi, 2014). Little work has been done on land suitability for Irish potato on a slope profile. Yet evaluating the potential land resources is crucial for sustainable agricultural activities in the face of climate change (Dawit et al., 2020). Land Suitability Analysis is a GIS-based approach used to define the suitability of a particular area for planned use by relating the suitability of an area with its characteristics (Jafari & Zaredar, 2010). Plenty of literature is available on land suitability with respect to different crops using the GIS approach (Kamau et al., 2015), but scanty information exists specifically on Irish potato.

By and large, a pragmatic analysis of land suitability for a specific crop under different climate scenarios is one of the essential ingredients for enhancing the resilience of smallholder farmers to climate variability and change (Hood et al., 2006). It is not possible to influence rainfall and temperature trends of any region as a means of dealing with climate variability and change impacts (Nimusiima et al., 2018). However, one of the most viable approaches can be equipping the smallholder farmers with knowledge and skills on land suitability for improved crop production if certain climatic trends are well understood. We assumed crop yield to be a key indicator of land suitability. Therefore, our objective was to identify suitable areas for Irish potato production under different climatic scenarios and strengthen the small scale farmers' adaptability to climate variability and change impacts in Kigezi Highlands.

11.2 Materials and Methods

11.2.1 Study Location

This study was conducted in two administrative districts, namely, Kabale and Rubanda, covering the entire area of Kigezi highlands. This site is bordered by Uganda's districts of Kisoro to the west, Kanungu and Rukungiri to the north, Ntungamo to the east, and the Republic of Rwanda to the south. As shown in Fig. 11.1, the Kigezi Highlands are located between Latitudes 1°00′ and 1°29′ south of the Equator and Longitudes 29°45′ and 30°15′ east of the Greenwich.

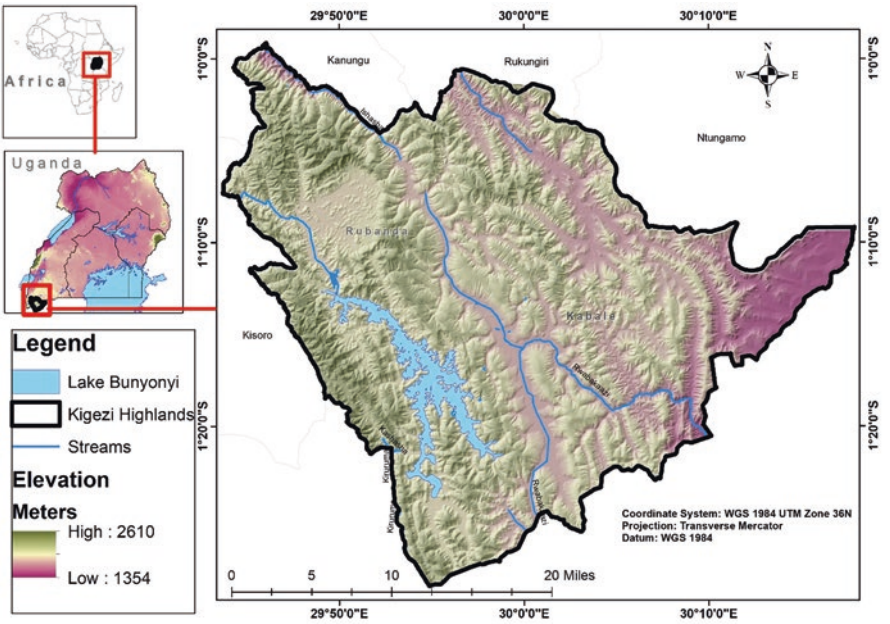

Fig. 11.1 Uganda showing the location of Kigezi Highlands

11.2.2 Site Description

11.2.2.1 Geomorphology

The Kigezi Highlands are associated with the African Surface, which was formed during the Jurassic (180–135 million years B.P) and Cretaceous (135–65 million years B.P). Moveover, this surface was believed to be generally coherent and stable. However, during the mid-Tertiary period (35 million years B.P), a greater portion of the African Surface underwent numerous denudational forces that degraded it to form a distinctive peneplain. This peneplain was further subjected to regional upliftment and dissection by erosion processes to form an accentuated topography. These highlands are characterized by distinctive advanced erosion surfaces which are represented by steeply rising slopes and flat-topped ridges that exist between 1500 and 2600 metres above sea level (NEMA, 2010).

11.2.2.2 Geology

The geology of Kigezi Highlands is generally composed of sedimentary rock system of the Pre-Cambrian Era (Ollier, 1969). This area has isolated cases of volcanic rock system which underlay the volcanic mountains in the extreme southwest of Uganda. Besides there are metamorphosed rock products such as schists, gneisses,

and granites (NEMA, 2010). These rocks belong to the Karagwe-Ankolean system, which is dominated by phyllite, shale, and quartzites. Occasional metamorphism also takes place in the site, a condition which has led to formation of strong schists along crested ridges of the Kigezi Highlands. The ridges are characterized by steep middle slopes and gentle pediments ending in flat valley bottoms. The phyllites and shales dominate the middle slopes; while on summits, the sediments are more arenaceous and are overlain by thick sandstones and sandy micaceous shales (Bagoora, 1989). Sandy alluvium and clay occupy valleys of these highlands. Coarse sand and fine sand occur in the down warped valleys which are underlain by gneisses and granites, while shales and phyllites dominate clay deposits in these valleys (NEMA, 2010).

11.2.2.3 Soil

According to FAO (1990), the major soil of the Kigezi Highlands can be classified as Andosols (young soils formed from volcanic deposits), Histosols (soils which are highly composed of organic materials), Luvisols (soils with subsurface accumulation of high activity clays and high base saturation), Acric Ferralsols (deep, strongly weathered soil with a chemically poor, but physically stable subsoil), and Dystric Regosols (soil with very limited soil development potential). While a greater portion of the Kigezi Highlands soil are generally deep, they are highly susceptible to climate change impacts such as erosion due to runoff (Bagoora, 1993).This situation has rendered a huge percentage of the Kigezi Highlands unsuitable for crop farming. Thus, there is need to harness local-scale adaptive measures to cope with weather and climate uncertainties for improved livelihoods within and outside the local community.

11.2.2.4 Climate

This area receives an annual rainfall between 1000 and 1500 mm. This rainfall is bimodal, occurring generally between August and December, and also between March and May. It also has two dry seasons, that is, in January and between June and July. The mean temperature is 18 °C with maximum of 24.4 °C and minimum of 10.9 °C. The relative humidity ranges between 90% and 100% in the mornings and decreases to 42–75% in the afternoons throughout the year.

11.2.2.5 Vegetation

Due to high population, a serious modification of the indigenous vegetation cover has taken place. However, this site was predominantly having a montane type of vegetation. This vegetation was associated with numerous tree species, such as Acacia and Albizia spp., and grasses, such as Imperata, Cymbopogon, Hyparrhenia,

and Beckeropsis. The current situation is that altitudinal variation is one of the key factors influencing vegetation distribution in Kigezi Highlands (Katende et al., 1995). In light of this, a systematic analysis of the dominant trees and shrubs for this site can be presented as in Table 11.1.

Table 11.1 Variation of vegetation with altitude on Kigezi Highlands

Altitude (m a.s.l)	Tree species/shrub/ grass	Indigenous name	Characteristics	Uses
2700–3000	Mountain Bamboo (*Arundinaria alpina*) and grasses	*Migano*	(i) These are tree-like grasses (ii) Found in moist areas (iii) But can also grow in low area with water	(i) Timber (ii) Charcoal and firewood (iii) Construction
2000–2700	*Bersama abyssinica*	*Mukaka*	(i) Occur in highlands and low lands (ii) Woody species, well foliaged, and stand at 7–15 m	(i) Timber (ii) Firewood (iii) Bee hives (iv) Ornaments (v) Mulches
1400–2000	*Catha edulis*	*Munyaga*	(i) Evergreen shrub or tree (ii) Stands at about 18 m (iii) Has a compact crown	(i) Firewood and charcoal (ii) Medicine especially fresh leaves (iii) Stimulant (iv) Mulches
1300–1400	*Celtis africana*	*Nyabinunka*	(i) Wide spread from generally dry, rocky areas to moist evergreen especially near water bodies (ii) Deciduous tree standing at about 12 m with spreading crown	(i) Browsed by animals including cattle (ii) Leaves and fruits are essential diet of black-and-white colobus monkeys (iii) Mulches
1200–1300	*Cordia africana* and woody shrubs called *Cyphomandra betacea*	*Mujugangoma Ekitunda*	(i) Large-leaved tree (ii) Deciduous with round crown standing at 4–15 m (iii) Umbrella-like shrubs with shiny stems when young and rounded leaf scars when old	(i) Mulching (ii) Making drums, bee hives and furniture (iii) Firewood and charcoal (iv) Jam, fruits, vegetables

Source: Data were adapted from Katende et al. (1995)

11.2.3 Data Analytical Tools and Techniques

We employed the Agricultural Production Systems Simulator (APSIM) model and simulated historical and future time climate scenarios. Spatial Multi Criteria Evaluation (SMCE) basing on Weighted Linear Combination (WLC) coupled with GIS and remote sensing were used to generate maps showing suitable areas for Irish potato production in the Kigezi Highlands. Furthermore, we examined the climate trends against yields of Irish potato using Regression and Sen's slope analysis.

11.2.3.1 Data Sources

Land Mapping Units and Soil Data

The land mapping units (LUMs) and soil data were obtained from the soil map of Uganda which was found at http://www.fao.org/soils-portal/soil-survey/soil-maps-and-databases/harmonized-world-soil-database-v12/en. The soil data included soil pH, soil texture, cation exchange capacity, soil drainage, organic matter, and total phosphorus. Table 11.2 shows a summary of the LUMs and mean values of soil data with spatial resolution of 30 by 30 m obtained for the study site.

Climate Data

The historical climate data for use in this study included mean temperature and mean rainfall over the baseline period of 1950–2000. These data were obtained from WorldClim found at https://www.worldclim.org/.

Table 11.2 Land mapping units (LMUs) and soil data

	Soil properties								
LMUs	Soil pH	% organic matter	Meq/100 g CEC	Soil drainage	% Base saturation	% Total phosphorus	% Sand	% Clay	Texture
Skeletic andosols	5.4	20.5	36.8	Well drained	39.1	11	83	6	Loamy Sand
Histosols	7	4	18	Poor drained	44	25	0	67	Clay
Luvisols	5.5	11.9	44.6	Well drained	86.3	11	51	37	Sand clay
Acric Ferralsols	5	23.9	41.3	Well drained	28	15	74	6	Sandy loam
Dystric Regosols	4	1.76	8.79	Well drained	1	17	77	18	Sandy loam

Slope Data

The slope data were obtained from a Shuttle Radar Topography Mission (SRTM) Digital Elevation Model (DEM) with spatial resolution of (90/90) metres. This DEM was downloaded from the following web site https://earthexplorer.usgs.gov/.

Remote Sensing Data

With a spatial resolution of (10/10) metres, an image from Sentinel 2 platform was obtained from Copernicus European Union website for March to July of 2017, to target the first Irish potato growing season in Kigezi Highlands. Sentinel 2 was used because it is a multi-spectral image which was developed by the European Space Agency for agricultural applications, such as crop monitoring and management, and for other uses (Nthuni et al., 2017).

11.2.4 Identification of Irish Potato Production Areas

The Irish potato production areas were identified by using GIS and remote-sensing techniques. Using a supervised classification method in Arc GIS 10.2, appropriate bands were selected with definition of signature for training samples. The polygons of non-agricultural land were drawn out and merged as one polygon so as to minimize the interference of non-agricultural with the agricultural land. The non-agricultural land included the built-up areas, bare land, wetlands, water bodies, and forests. Field visits intended for ground truthing with the help of a Global Positioning System (GPS) were done. The Irish potato fields were selected at random and the GPS coordinates (X and Y) were taken at particular points in the Irish potato fields. The collected GPS coordinates were overlaid onto the Sentinel image which was classified in Arc GIS 10.2 using supervised classification method. This image was later on-screen digitized in ArcGIS 10.2 to create a shape file from which the Irish potato map was generated. Suitability maps were overlaid with the Irish potato distribution map and the total production area covered by the suitable and unsuitable soils of Kigezi Highlands was determined.

11.2.5 Accuracy Assessment

During image classification, it is prudent to establish whether the classification result derived from the remote-sensing image has sufficient quality for operational application (Stehman & Czaplewski, 1998). Therefore, an accuracy assessment was undertaken on a Sentinel 2 image for this purpose. While there are several methods for accuracy assessment, namely, population-based statistical framework,

multiple-objective assessment, geographically weighted accuracy measures, and stratified random sample for National Land Cover Database (Stehman & Wickham, 2011), for this site we used a confusion matrix. This matrix is more robust and was carried out to determine accuracy assessment and the error of commission, error of omission, overall classification accuracy, and kappa coefficient were obtained. A confusion matrix contains information about actual and predicted classifications done by a classification system. Performance of such systems is commonly evaluated using the data in the matrix. The accuracy (AC) is the proportion of the total number of predictions that were correct. It was determined using Eq. 11.1:

$$\mathrm{AC} = \frac{a+d}{a+b+c+d} \tag{11.1}$$

where

a is the number of correct predictions that an instance is negative
b is the number of incorrect predictions that an instance is positive
c is the number of incorrect of predictions that an instance negative
d is the number of correct predictions that an instance is positive

11.2.6 Suitability Rating

While there are several methods for land evaluation (Bodaghabadi et al., 2015), the land suitability rating for Irish potato production in Kigezi Highlands was based on the FAO standard rating structure (FAO, 1976). This structure seeks to match the land utilization types with the land use requirements across the land units, and it also requires a description of land in terms of its characteristics in order to understand its intended use. This method differentiates the degree of suitability into four classes, namely, highly suitable (S1), moderately suitable (S2), marginally suitable (S3), and not suitable (N). Table 11.3 shows a summary of Irish potato soil conditions as derived from reviewed literature.

11.2.7 Spatial Multi-Criteria Evaluation (SMCE) and Weighted Linear Combination (WLC)

Using GIS, the soil map of the study site was clipped from that of Uganda and the data layers which included soil pH, soil texture, cation exchange capacity, soil drainage, organic matter, and total phosphorus were extracted. The layers were then converted into raster format. The raster layers were then reclassified according to the four suitability classes previously identified in Table 11.2. The topography of the area was obtained in raster format from the SRTM Digital Elevation Model (DEM)

Table 11.3 Factor rating of land-use requirements for Irish potato

Land use requirements			Factor rating				References
Land quality	**Diagnostic factor**	**Units**	>80	40–80	20–40	<20	FAO (1988)
			S1	S2	S3	N	
Nutrient availability	Soil pH	Reaction	6.0–5.0	6.0–7.0 5.0–4.0	7.0–8.0 4.0–3.5	>8.0 < 3.5	Kamau et al. (2015)
	Organic matter	%	>1.2	0.8–1.2	<0.8	–	Smith et al. (1997)
	Base saturation	%	65–50	50–35	<35	–	Das (2015)
	Total phosphorus	%	>15	–	–	–	Smith et al. (1997)
Nutrient retention capacity	Cation exchange capacity	Meq/100 g	>16	16–5	<5	–	Das (2015)
Oxygen availability	Soil drainage	Class	Well/ moderate	Imperfect	Poor	Very poor	Kamau et al., (2015)
Moisture availability	Mean rainfall	mm	≥1000	1000–800	800–600	<600	Kamau et al. (2015)
	Mean temperature		≤18	18–20	20–22	>220	Kamau et al. (2015)
Erosion hazard	Slope	%	≤6	6–13	13–25	> 25	Kamau et al. (2015)
	Soil texture	Class	Sand clay <15%	Loam clay 15–35%	Clay >35%	–	Smith et al. (1997)

of the area, which was mosaicked to form a continuous layer. The percentage slope of the study area was later calculated. This slope was also then reclassified into four suitability classes, as in Table 11.2, for Irish potato growing.

Furthermore, climate data were downloaded as raster with 1 arc-second (30/30) metre resolution from WorldClim (http://www.worldclim.org/). Twelve tiles for each of mean precipitation, and of mean temperature with interpolations of observed data, as well as representative data of 1950–2000 were extracted for the study site. The temperature and rainfall raster files were then also reclassified into four suitability classes of Table 11.2 for Irish potato growing. After reclassifying the SMCE maps, those areas that belonged to the same land quality were added using the Arithmetic Function which is embedded in ArcGIS (Wayne & Olympia, 2003). They were then standardized by the score range procedure, as in Eq. (11.2), which was developed by Malczewski (1999).

$$x'_{ij} = \frac{x_{ij-x_{jmin}}}{x_{jmax-x_{jmin}}} \tag{11.2}$$

Table 11.4 Assigned weights by the Ratio Estimation Procedure

Criterion	Ratio scale	Original weight	Normalized weight
Nutrient availability	100	1	0.2
Nutrient retention capacity	100	1	0.2
Oxygen availability	100	1	0.2
Moisture availability	100	1	0.2
Erosion hazard	100	1	0.2
	Total	5	1

where

x'_{ij} = standardized score for the *i*th object and the *j*th attribute
x_{jmin} = raw score
x_{jmax} = maximum score for the *jth* attribute
x_{jmin} = minimum score for the *jth* attribute
$x_{jmax} - x_{jmin}$ = range of a given criterion

Each of the standardized SMCE maps were then assigned equal weights. These weights were obtained using the ratios estimation procedure, whereby a score of 100 was assigned to each of the land qualities. Ratios were calculated basing on the score assigned to the attributes. The weights were normalized by dividing each weight by the total (Malczewski, 1999) as indicated in Table 11.4.

The SMCE maps were combined by applying the normalized weight to each criterion followed by summation of the results using the Raster Calculator Function which is embedded in ArcGIS. The procedure used the Eq. (11.3) by Mahini and Gholamalifard (2006).

$$S = \sum w_i x_i \tag{11.3}$$

where

S = Suitability
w_i= Weight of factor *i*
x_i= criterion score of factor *i*

The weighted criterion maps were normalized and then overlaid together with extracted Irish potato production area map from a Sentinel 2 image; in order to generate a Suitability Map for Irish potato in the Kigezi Highlands.

11.2.8 Climate Change Modeling and Irish Potato Production

We explored the Agricultural Production Systems Simulator (APSIM) to model historical climate change trends and Irish potato production in Kigezi Highlands. According to McCown et al., 1996, APSIM model is described as a software tool

that permits sub-models or modules to be linked to simulate agricultural systems. Several modules are assembled and characterized as plant, management, and environment. APSIM simulates the physical development of crops, soil processes, and variety of management practices while taking into account the cropping systems (Zeng et al., 2016). APSIM operates using input data namely, soil data, crop management data, and long-term daily climate data. Climate data required are daily rainfall (mm), daily temperatures (both minimum and maximum °C units) and solar radiation (MJ m^{-2}). The important soil parameters for consideration are nitrogen and organic carbon. For the model to predict correctly, there is need to input accurate data. Crop management data include crop type and variety, sowing dates, weeding dates and fertilizer management with respect to type, amount, date of application (Holzwoth et al., 2014).

The APSIM-potato model is a comprehensive daily time step, deterministic potato crop model build in the APSIM Plant.Net Framework which integrates with the APSIM soil, management, and user interface components to provide a robust and user-friendly potato crop model. Predictions of yield are made daily based on the production of total dry matter (DM) and its partitioning and reallocation to plant organs. Equation (11.4) represents how total daily DM production can be calculated.

$$\Delta DM = \left(\text{Radn} * \frac{I}{I_o} * \text{RUE} * fw * ft * fCO_2 \right) \tag{11.4}$$

where **Radn** is the daily solar radiation level (MJ m^{-2}), $\frac{\boldsymbol{I}}{\boldsymbol{I_o}}$ is the fraction of radiation that the crop intercepts each day. This is calculated from crop cover, the proportion of the ground that the crops canopy is covering which is calculating using an extinction coefficient of 0.8.

RUE is the potential radiation use efficiency of the crop which is a constant value of 1.44 g/MJ and RUE is multiplied by adjustment factors to account for the effects of water ***(fw)*** and temperature ***(ft)*** stresses and atmospheric carbon dioxide concentration **(fCO_2)** (Brown et al. 2011).

11.2.9 Climate Data Preparation

Meteorological (met) files were arranged in Microsoft Excel according to the APSIM model format requirements. These met files included daily values for solar radiation (MJ/m^2), minimum and maximum temperatures (°C), and rainfall (mm). The Constants Average Ambient (Tav) and Average Amplitude (Amp) temperatures were calculated and inserted into the met files using the Tav Amp software.

11.2.10 Model Calibration

The model was calibrated using control experiment observed data collected by (Lemaga et al., 2001). Experiments were conducted for three seasons, during 1998 (A) spanning from May to August; 1998 (B) from October to January; and 1999 (A) from March to July. In the calibration process, the parameterized model was run for a chosen single year; then the simulated outputs were compared with observed values from the experiment. In case of any inconsistences, parameters were re-adjusted within tolerable limits, and the process would be repeated until an acceptable model performance was achieved.

11.2.11 Sensitivity Analysis

In order to perform this function, the 'Manager' module and 'Climate control' module embedded in APSIM model were used to determine the most sensitive parameters influencing Irish potato yield. A sensitivity analysis was done on the climatic parameters, namely, temperature and rainfall. These two climatic parameters were the most critical elements that affect Irish potato growth (Hijimans, 2003). One parameter was adjusted at a time from the base year period. The maximum and minimum temperatures were simultaneously increased by 1 °C increments up to a total of 3 °C, while rainfall was increased and decreased by 5% up to 15%. Atmospheric CO_2 concentration was kept fixed at 350 ppm. From these parameter adjustments in the Kigezi Highlands, Table 11.5 represents the results of APSIM model sensitivity analysis.

The interpretation of results in Table 11.3 is that an increase in minimum and maximum temperature of up to 3 °C led to a decrease in yield of 6.25%. Besides this, a gradual increase in rainfall from 5%, 10%, and 15% resulted into a gradual increase in yield of 1.17%, 2.03%, and 2.21%, respectively. While a gradual decrease in rainfall from 5%, 10%, and 15% resulted into a decrease in yield of 2.73%, 5.88%, and 10.60%, respectively.

11.2.12 Model Evaluation and Validation

The performance and efficiency of the APSIM model in simulating Irish potato yield was compared with the observed experimental data of 1998 (A), 1998 (B), and 1999 (A) using the root mean square error (RMSE) as in Eq. (11.5), modelling efficiency (EF) as in Eq. (11.6), standard deviation, and coefficient of determination (r^2). The standard deviation and coefficient of determination (r^2) were computed using Microsoft Excel, whereas for RMSE and EF the formulae as stated in Eqs. (11.5) and (11.6), respectively.

Table 11.5 Sensitivity of Irish potato yield to temperature and rainfall

Parameter	Climate scenarios	Yield (Kg ha^{-1})	Yield change (%)
Minimum and maximum temperature (°C)	Base scenario 0 °C	9781.81	
	Increase base by 1 °C	9501.52	−2.87
	Increase base by 2 °C	9309.92	−4.82
	Increase base by 3 °C	9170.18	−6.25
Rainfall (mm)	Base scenario 0%	9781.81	
	Increase base by 5%	9896.62	1.17
	Increase base by 10%	9980.76	2.03
	Increase base by 15%	9998.11	2.21
	Decrease base by 5%	9514.85	−2.73
	Decrease base by 10%	9206.18	−5.88
	Decrease base by 15%	8744.60	−10.60

$$\text{RMSE} = \sqrt{\sum\left(\text{yield simulated} - \text{yield observed}\right)^2 / n} \tag{11.5}$$

$$EF = 1 - \frac{\sum_{i=1}^{n}\left(O_i - S_i\right)}{\sum_{i=1}^{n}\left(O_i - \overline{O_i}\right)} \tag{11.6}$$

where

n is the number of years in which data have collected from an experiment
O_i is the observed yield
S_i is the simulated yield
$\overline{O_i}$ is the average observed yield

The interpretation of results in Eqs. (11.5) and (11.6) is that for both r^2 and EF, a value of 0.65 is considered 'satisfactory', 0.8 as 'good', and 0.9 as 'very good'. For agricultural models if RMSE between simulated and observed values is around the same value or slightly smaller than the standard deviation within the observed values, then this shows that the model is capable of simulating the observed behaviour (Wang et al., 2019). The APSIM-potato model adapted was robust in simulating Irish potato yield in the Kigezi Highlands since a RMSE of 5621 Kg ha^{-1} with a standard deviation of 6609 Kg ha^{-1} were realized in model evaluation and validation exercise. Furthermore, the results of the coefficient of determination (r^2) and the EF are good and satisfactory, respectively; thus proving its worthiness in simulating

Table 11.6 Evaluation of model performance in reproducing the observed data

Year and growing season	Observed yield (Kg ha^{-1})	Predicted yield (Kg ha^{-1})
1998 (A) (May to August)	3300	3814
1998 (B) (October to January)	9300	8014
1999 (A) (March to July)	16,500	7537
R^2	**0.94**	
RMSE (Kg/ha)	**5621**	
Standard deviation (Kg/ha)	**6609**	
EF	**0.99**	

Irish potato yield in Kigezi Highlands. Table 11.6 represents a summary of the APSIM-potato model evaluation and validation results.

11.2.13 Seasonal Climate Trend Analysis and Irish Potato Production

The Mann–Kendall test with 95% confidence limit was used to assess the seasonal trends for temperature, rainfall, and Irish potato yield. With Mann–Kendall test, two hypotheses were tested the null hypothesis, H0: there is no trend in the time series; and the alternative hypothesis, Ha: there is a significant trend in the series, for a given α significance level in this case ($\alpha = 5\%$). Probability (P) in percent was calculated to determine the level of confidence in the hypothesis. If the computed p-value is greater than the significance level ($\alpha = 0.05$, one cannot reject the null hypothesis H0 and if the computed p-value is lower than the significance level ($\alpha = 0.05$), one should reject the null hypothesis H0 and accept the alternative hypothesis Ha (Gavrilov et al., 2016). In addition, the magnitude of the trend was quantified using Sen's slope method (Sen, 1968). The Sen's slope is an index used to quantify the trend using the non-parametric analytical procedures. To achieve this, the XLSTAT software, which is embedded in Microsoft Excel, was used in establishing and computing this trend.

11.3 Results and Discussion

11.3.1 Land Cover Classification

A Sentinel 2 image of the study area was classified into six land cover classes: forest, water bodies, built-up area, wetland, bare land, and agricultural area. Values of the results are in Table 11.7 which showed that 7.6% of the study area is under water bodies, 23.5% is under forest, 3.2% is under built up, 24.1% is under wetland, 10.8% is under bare land, and 30.8% is under agricultural land. Table 11.8 shows

Table 11.7 Area under different land cover

Land cover	Area (hectare)	Percent area coverage (%)
Water bodies	13,161	7.6
Forest	40,731	23.5
Built-up area	5523	3.2
Bare land	18,801	10.8
Wetland	41,775	24.1
Agriculture	53,482	30.8

Table 11.8 Satellite image classification accuracy assessment

Overall accuracy	0.73
Kappa coefficient	0.68

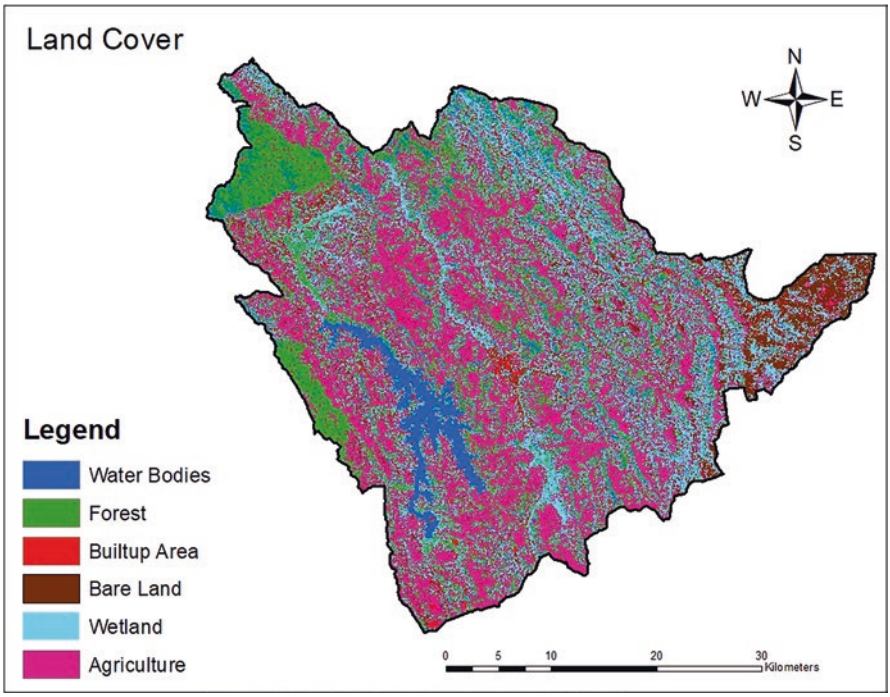

Fig. 11.2 Land cover of Kigezi Highlands

the image classification accuracy assessment results. However, the spatial distribution of these different land covers is shown in Fig. 11.2.

11.3.2 The Extent and Suitability of Irish Potato Production Area

After merging the non-agricultural area and digitizing Irish potato cultivation areas from the entire agricultural land, it was established that Irish potato cultivation covers 71.50% of the agricultural area (Fig. 11.3a and Table 11.9). Out of this area, 5.3% is not suitable, 25.9% is marginally suitable, 66.8% is moderately suitable, and 1.9% is highly suitable as shown in Fig. 11.3b and Table 11.10.

Irish potato production area covers about three quarters of the total area under agriculture. Irish potato is mostly cultivated in areas around Lake Bunyonyi and in the wetland areas probably due to the huge concentrations of alluvia deposits. These deposits are usually rich in exchange bases, SOM, and other nutrients for plant growth. Strikingly, however, is the fact that not all the Irish potato production area is suitable for its cultivation. Figure 11.3b indicates that the moderately suitable (S2) class has the highest percentage (66.79%) as opposed to the highly suitable (S1) class which covers the smallest percentage (1.95%). The moderately suitable (S2) class covers more than half (1/2) of the Irish potato production area and is located in areas with high suitability with respect to moisture, nutrient and oxygen availability, nutrient retention capacity, and other diagnostic factors. Further research is needed to investigate more on the potential impact of these factors on land suitability for different crops in different ecological zones.

The areas under marginally suitable (S3) and not suitable (N) classes are generally poor in Irish potato production because of deficits in soil moisture available for plant growth. Moisture stresses due to increasing temperatures in the Kigezi Highlands can reduce total dry matter production, which in turn affects the proportion of the matter that can be partitioned into tubers. Thus, strategies for improving soil moisture can potentially increase Irish potato yields in Kigezi Highlands.

11.3.3 Temperature Trends and Irish Potato Production

The Man–Kendall test was used to determine the significance of the trend, and it was quantified using Sen's slope. The results for this test are presented in the subsequent sections.

11.3.4 Temperature Trend in March to May Season

The results showed that in the March to May (MAM) season, minimum and maximum temperature had significant increasing trend ($P < 0.05$), the Sen's Slope value indicates an increase of 0.033 °C and 0.039 °C, respectively (Fig. 11.4).

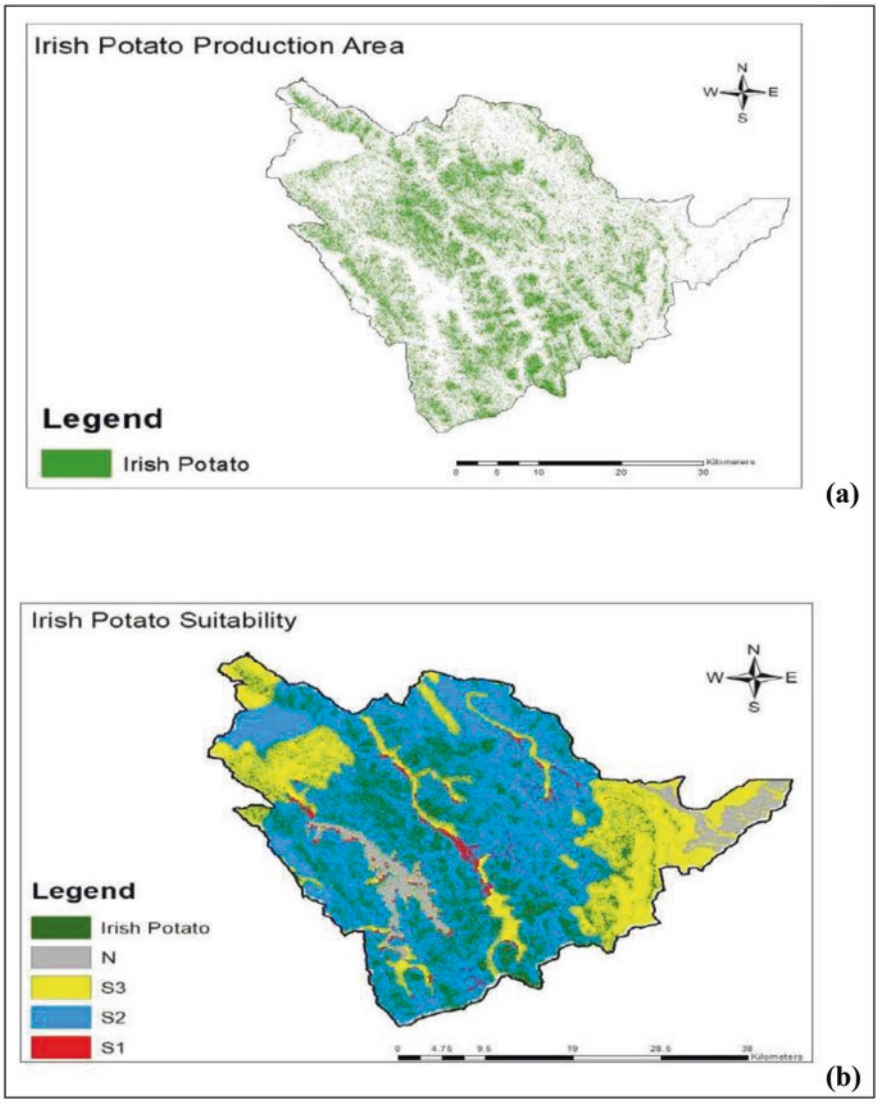

Fig. 11.3 Spatial extent and suitability classes for Irish potato in Kigezi Highlands

Table 11.9 The total production area of Irish potato

Land cover	Area (hectare)	Percent area coverage (%)
Agricultural area	53,482	
Irish potato cultivation area	38,237	71.50%

Table 11.10 The area of Irish potatoes under different suitability classes

Suitability class and code	Area (hectare)	Percent area coverage (%)
Not suitable (N)	2040	5.34
Marginally suitable (S3)	9914	25.93
Moderately suitable (S2)	25,539	66.79
Highly suitable (S1)	744	1.95

11.3.5 Temperature Trend in September to November Season

The temperature trend results for September to November (SON) showed a significant ($P < 0.05$) increase in minimum and maximum temperature by 0.042 °C and 0.035 °C, respectively (Fig. 11.5). In the two seasons, MAM and SON, temperature showed an increasing trend, which was recognized to affect land suitability for Irish potato production.

11.3.6 Rainfall Trends

While there was a significant increasing trend in temperature, the results for rainfall indicated an insignificant decreasing ($P > 0.05$) trend in the MAM season with Sen's slope value of −0.382 mm. Moreover in the SON season, rainfall had an insignificant increasing ($P > 0.05$) trend with Sen's slope value of 0.165 mm (Fig. 11.6).

11.3.7 Irish Potato Yield Trends

In the MAM season, the yield trend was decreasing but it had not changed significantly over time ($P > 0.05$) with Sen's slope magnitude of −5.87 Kg ha^{-1}. Furthermore, in the SON season, the yield was insignificant ($P > 0.05$) and decreased over time by −38.16 Kg ha^{-1} (Fig. 11.7).

11.3.8 Climate–Irish Potato Relationship

To test whether there is a functional relationship between Irish potato yield and the different climate variables (rainfall, minimum temperature, and maximum temperature), a regression analysis for both seasons (MAM and SON) was performed.

(a) Minimum temperature trend

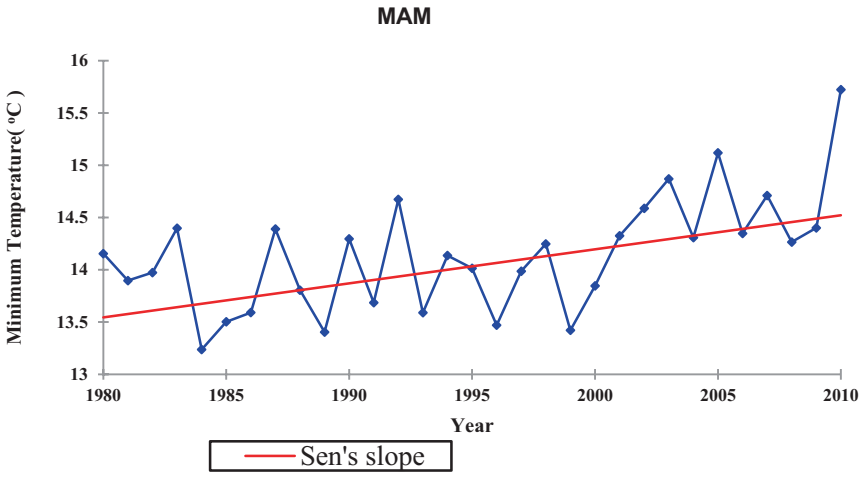

(b) Maximum temperature trend

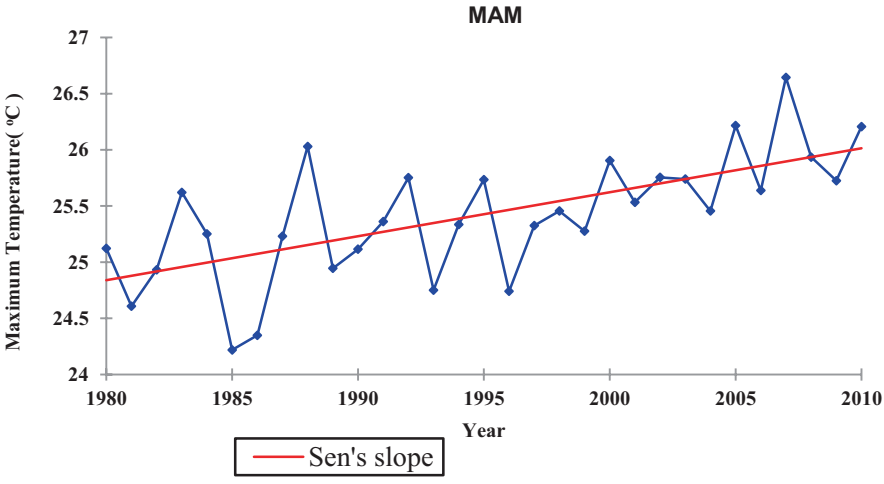

Fig. 11.4 (**a**) Mean minimum temperature trend in Kigezi Highlands (1980–2010), (**b**) Mean maximum temperature trend in Kigezi Highlands (1980–2010)

11.3.9 Climate–Irish Potato Relationship in March to May Seasons (1980–2010)

Results of the linear regression analysis revealed that all climatic variables contributed significantly ($P < 0.05$) to the variations in Irish potato yield in MAM season.

(a) Minimum temperature trend

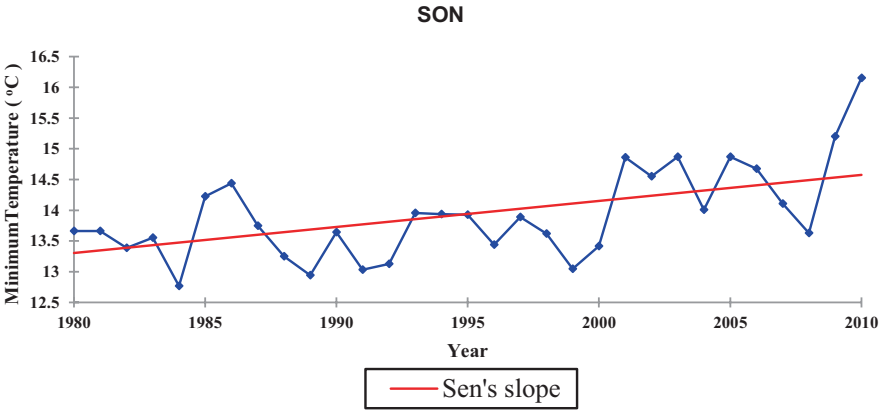

(b) Maximum temperature trend

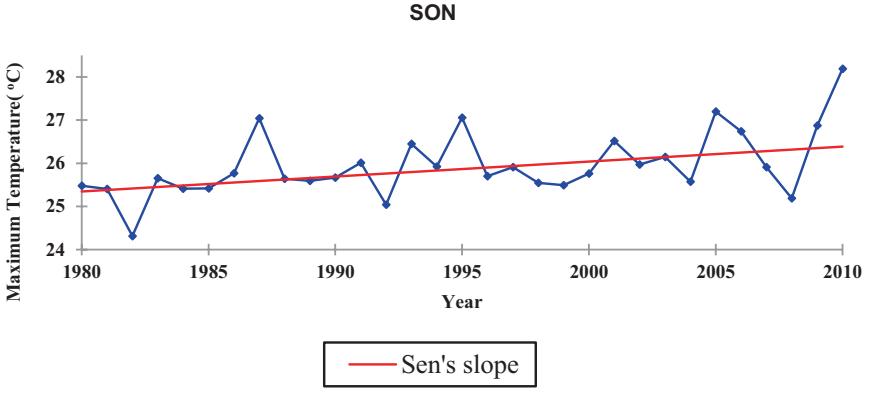

Fig. 11.5 (**a**) Mean minimum temperature trend in Kigezi Highlands (1980–2010). (**b**) Mean maximum temperature trend in Kigezi Highlands (1980–2010)

Minimum temperature and maximum temperature contributed to 16.08% and 13.38% of the variations in Irish potato yield, respectively. It was also established that both minimum and maximum temperature had a negative impact on Irish potato yield. For instance, an increase by 1 °C of the minimum temperature reduced the average Irish potato yield by 937.56 Kg ha^{-1} and an increase by 1 °C of the maximum temperature reduced this yield by 849.56 Kg ha^{-1}, respectively (Fig. 11.8a).

On the other hand, in the MAM, rainfall accounted for 63.59% of the variation in Irish potato yield (Fig. 11.8b). Rainfall had a positive impact on yield. For instance, an increase by 1 mm of rainfall increased the average Irish potato yield by 51.558 Kg ha^{-1}. By and large, this is generally realistic as it is in line with literature on rainfall–crop productivity relationship.

(a) Mean rainfall trend in March to May season

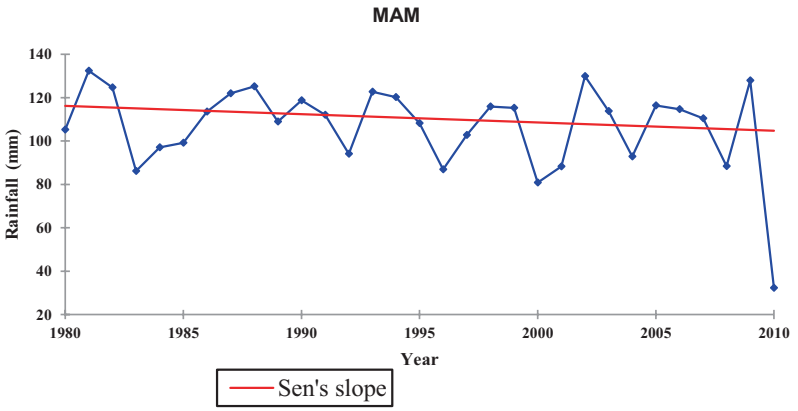

(b) Mean rainfall trend in September to November season

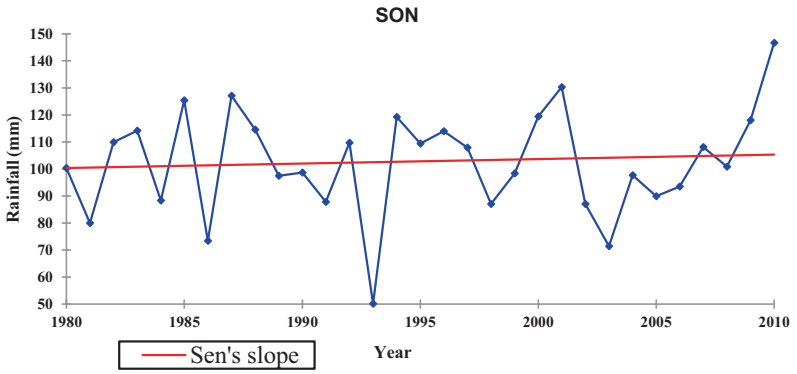

Fig. 11.6 (**a**) Mean rainfall trend in Kigezi Highlands (1980–2010), (**b**) Mean rainfall trend in Kigezi Highlands (1980–2010)

11.3.10 Climate–Irish Potato Relationship in September to November Seasons (1980–2010)

In the SON season, the linear regression analysis results revealed that minimum temperature and maximum temperature contributed to 9.96% and 5.35% of the variations in Irish potato yield, respectively (Fig. 11.9a). While these variations were not significant ($P > 0.05$), both minimum temperature and maximum temperature had a negative impact on land suitability for Irish potato production. For instance, as according to available results, an increase by 1 °C of the minimum temperature reduced the average Irish potato yield by 554.4 Kg ha^{-1}. However, an increase by 1 °C of the maximum temperature reduced the average Irish potato yield by 402.41 Kg ha^{-1}.

(a) Irish Potato yield trend in March to May season

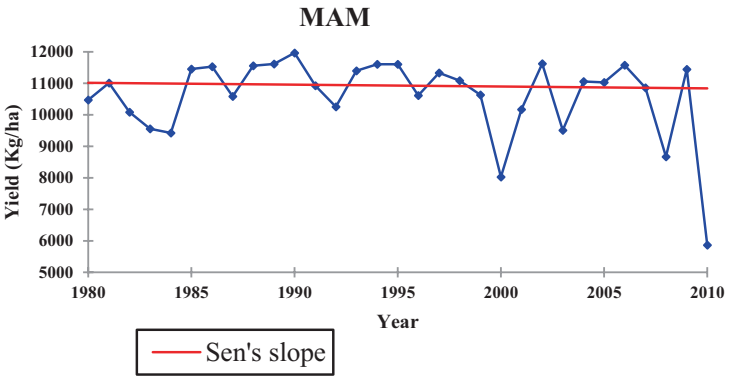

(b) Irish Potato yield trend in September to November season

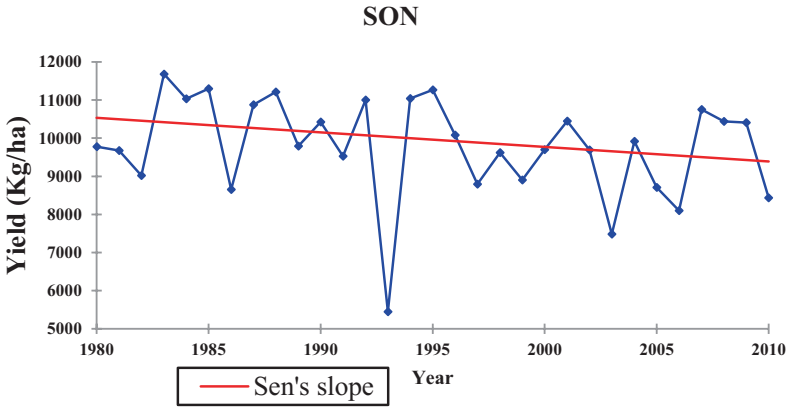

Fig. 11.7 (**a**) Yield trend for Irish potato in MAM seasons (1980–2010) (**b**) Yield trend for Irish potato in the SON seasons (1980–2010)

Much as temperature was not substantially important in this season, rainfall was a very critical factor ($P < 0.05$) that induced the variations in Irish potato yield. Rainfall accounted for 34.68% of the variation in Irish potato yield (Fig. 11.9b). Rainfall had a positive impact on Irish potato yield. For instance, results have shown that an increase by 1 mm of rainfall increased the average Irish potato yield by 39.577 Kg ha^{-1}.

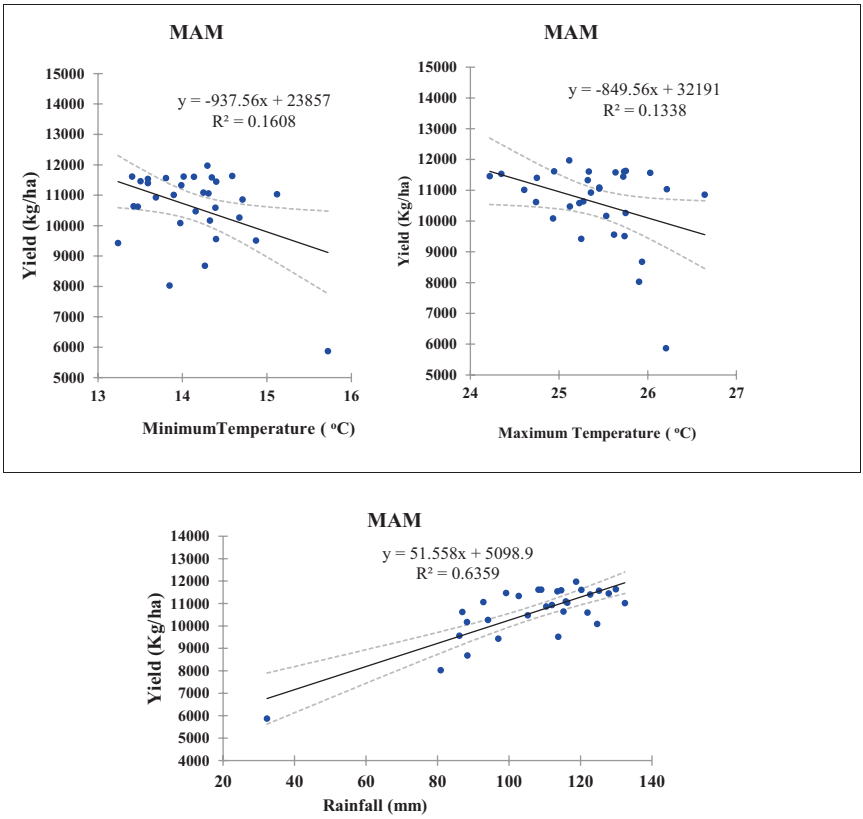

Fig. 11.8 (**a**) Irish potato yield in response to minimum and maximum temperature (**b**) Irish potato yield in response to rainfall

11.4 Conclusions

11.4.1 Conclusions Drawn for the Study

The different soils of Kigezi Highlands are still suitable for Irish potato production with a moderate rate and can be enriched through adoption of appropriate soil and water conservation technologies. The Irish potato production area covers about three-fourths of the total agriculture area of Kigezi Highlands. Not all the Irish potato production area is suitable for its cultivation; S2 (Moderately suitable) has the highest area percentage as opposed to S1 (Highly suitable) with the smallest area percentage; and seasonal variations greatly affected Irish potato yields. Thus, yield increase to sustain livelihoods amongst small-scale holder farmer communities can be anchored on proper soil fertility management.

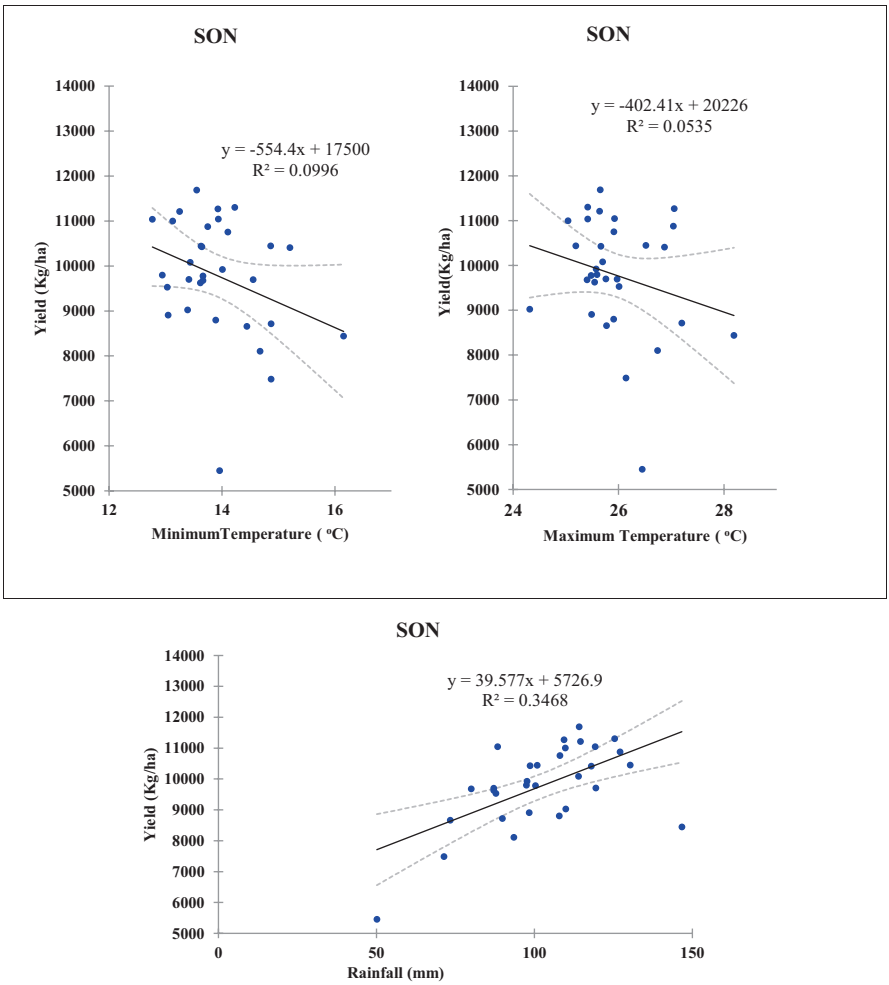

Fig. 11.9 (**a**) Irish potato yield in response to minimum and maximum temperature (**b**) Irish potato yield in response to rainfall

11.5 Recommendations

We recommend the following:

(a) Farmers can use the readily available organic residues from homesteads for soil organic amendments.
(b) Given the rolling terrain, farmers should plant hedge rows, use alternative drainage diversion methods, construct runoff ditches and water storages to reduce runoff losses, and increase soil available water.
(c) Farmers can adjust the timing of farm operations depending on the seasonal variability of rainfall in Kigezi Highlands.

Acknowledgement We wish to thank the peer reviewers for the constructive comments which significantly helped us to improve the quality of this work; Sida Sarec Research Project 377 under Makerere University (2016–2022) for financial support to undertake this work; Kyambogo University for granting us ample time and a good academic working environment to produce this book chapter; and Research assistants, field assistants, and local farmers, most especially the Kagyenza family, for providing land for primary soil data.

Conflict of Interest All authors have no conflict of interest.

References

Akinci, H., Özalp, A. Y., & Turgut, B. (2013). Agricultural land use suitability analysis using GIS and AHP technique. *Computers and Electronics in Agriculture, 97*, 71–82. https://doi.org/10.1016/j.compag.2013.07.006

Bagoora, F. D. K. (1989). A preliminary investigation into the consequences of inadequate conservation policies on steep slopes of the Rukiga Highlands, Southwestern Uganda. In D. B. Thomas, E. K. Biamah, & A. M. Kilewe (Eds.), *Soil conservation in Kenya*. University of Nairobi.

Bagoora, F. D. K. (1993). An assessment of some causes and effects of soil erosion hazard in Kabale Highland, Southwestern Uganda, and people's attitude towards conservation. In Abdellatif (Ed.), *Resource use and conservation* (*Mountain Research and Development*) (Vol. 8). Faculty of Social Sciences, Mohammed V. University.

Bamutaze, Y., Mukwaya, P., Oyama, C., Nadhomi, D. L., & Nsemire, P. (2021). Intersecting RUSLE modeled and farmers perceived soil erosion risk in the conservation domain on mountain Elgon in Uganda. *Applied Geography, 126*, 102366. https://doi.org/10.1016/j.apgeog.2020.102366

Bodaghabadi, M. B., Casasnovas, J. A. M., Khakili, P., Masihabadi, M. H., & Gandomkar, A. (2015). Assessment of the FAO traditional land evaluation methods, a case study: Iranian Land Classification method. *Soil Use and Management., 31*, 384–396. https://doi.org/10.1111/sum.12191

Bonabana-Wabbi, J., Ayo, S., Mugonola, B., Taylor, D. B., Kirinya, J., & Tenywa, M. (2013). The performance of potato markets in Southwestern Uganda. *Journal of Development and Agricultural Economics., 5*(6), 225–235. https://doi.org/10.5897/JDAE12.124. https://www.academicjournals.org/JDAE.

Brown, H. E., Huth, N., & Holzworth, D. (2011). A potato model built using the APSIM Plant. NET Framework. In *19th International Congress on Modelling and Simulation* (pp. 12–216).

Csillik, O., & Belgiu, M. (2016). Cropland mapping from Sentinel-2 time series data using object-based image analysis, 2016.

Daccache, A., Kegye, C., Jones, R. A., Weatherhead, E. K., Stalham, M. A., & Knox, J. W. (2012). Climate change and land suitability for potato production in England and Wales: Impacts and adaptation. *The Journal of Agricultural Science., 150*(2), 161–177. https://doi.org/10.1017/s00218596/10000839

Das, S. (2015). Geo-analyst, ISSN 2249-2909 2015, 10–18.

Dawit, M., Megarsa, O., Olkeba, L. T., & Fiseha, M. B. (2020). Impact of climate change on land suitability for the optimization of irrigation system in the Anger River Basin, Ethiopia. *Climate, 8*, 97. https://doi.org/10.3390/cli8090097

FAO. (1976). A framework for land evaluation. UN FAO. Soils Bulletin 32, Rome.

FAO, I. (1988). Revised legend of the FAO-UNESCO soil map of the world. ISRIC Report, 1.

FAO. (2015). Strengthening linkages between small actors and buyers in the Roots and Tubers sector in Africa: Rwanda Work Plan, 1–16. Retrieved from http://www.fao.org/3/a-bc578e.pdf

FAO/UNESCO/ISRIC. (1990). Revised legend of the soil map of the world. World Soil Resources Report, FAO, Rome, Italy.

Gatiso, T. G. (2015). Effectiveness of climate change adaptation strategies: House-level evidence from Ethiopia. *Economics and Sustainable Development, 6*(19), 99–110. Retrieved from https://www.iiste.org.

Gavrilov, M. B., Tosic, I., Markovic, S. B., Unkasevic, M., & Petrovic, P. (2016). Analysis of annual and seasonal temperature trends using the Mann-Kendall test in Vojvodina, Serbia. *Quarterly Journal of the Hungarian Meteorological Service, 120*(2), 183–198. https://www.researchgate.net/publication/304102479.

Harvey, C. A., Rakotobe, Z. L., Rao, N. S., Dave, R., Razafimahatratra, H., Rabarijohn, R. H., & Mackinnon, J. L. (2014). Extreme vulnerability of smallholder farmers to agricultural risks and climate change in Madagascar. *Philosophical Transactions of the Royal Society B: Biological Sciences, 369*(1639), 20130089–20130089. https://doi.org/10.1098/rstb.2013.0089

Hepworth, N., & Goulden M. (2008). Climate change in Uganda: Understanding the implications and appraising the response. *LTS International, Edinburgh*. Retrieved from www.Itsi.co.uk

Hijimans, R. J. (2003). The effect of climate change on global potato production. *American Journal of Potato Research., 80*, 271–279.

Holzwoth, D. P., Huth, N. I., de Voil, P. G., Zurcher, E. J., Herrmann, N. I., McLean, G., Chenu, K., Oosterom, E. K., Snow, V., Murphy, C., Moore, A. D., Brown, H., Whish, J. P. M., Verrall, S., Fainges, J., Bell, L. W., Peake, A. S., Poulton, P. L., & Keating, B. A. (2014). APSIM-evolution towards a new generation of agricultural systems simulation. *Environmental Modelling and Software., 62*, 327–350. https://doi.org/10.1016/j.envsoft.2014.07.009

Hood, A., Cechet, B., Hossain, H., & Sheffield, K. (2006). Options for Victorian agriculture in a 'new' climate: Pilot study linking climate change and land suitability modelling. *Environmental Modelling and Software., 21*(9), 1280–1289. https://doi.org/10.1016/j.envsoft.2005.04.022

Intergovernmental Panel on Climate Change (IPCC). (2018). *Report on Impact of global warming. Switzerland*. Retrieved from (https://www.ipcc.ch).

Jafari, S., & Zaredar, N. (2010). Land suitability analysis using multi attribute decision making approach. *International Journal of Environmental Science and Development, 1*(5), 441–445.

Kamau, S. W., Kuria, D., & Gachari, M. K. (2015). Crop-land suitability analysis using GIS and remote sensing in Nyandarua County, Kenya. *Journal of Environment and Earth Science, 5*(6), 121–132.

Katende A. B., Birnie A., & Tengnas, B. (1995). Useful Trees and Shrubs for Uganda: Indentification, Propagation and Management for Agricultural and Pastoral Communities. Technical Hand Book No. 10, RELMA/Sida, ICRAF House, Gigiri, Nairobi, Kenya.

Lemaga, B., Kanzikwera, R., Kakuhenzire, R., Hakiza, J. J., & Manzi, G. (2001). The effect of crop rotation on bacterial wilt incidence and potato tuber yield. *African Crop Science Journal, 9*(1), 257–266.

Mahini, A. S., & Gholamalifard, M. (2006). Siting MSW landfills with a weighted linear combination methodology in a GIS environment. *International Journal of Environmental Science and Technology, 3*(4), 435–445. https://doi.org/10.1007/BF03325953

Malczewski, J. (1999). GIS and multicriteria decision analysis. *Journal of Operational Research Society., 51*(2), 247. https://doi.org/10.2307/254268

McCown, R. L., Hammer, G. L., Hargreaves, J. N. G., Holzworth, D. P., & Freebairn, D. M. (1996). APSIM: A novel software system for model development, model testing and simulation in agricultural systems research. *Agricultural Systems, 50*, 225–271. Yale-NUIST Center on Atmospheric Environment.

Mwaura, F. M., & Okoboi, G. (2014). Climate variability and crop production in Uganda. *Journal of Sustainable Development., 7*(2), 159–172. https://doi.org/10.5539/jsd.v7n2p159

National Environment Management Authority (NEMA). (2010). National state of the environment report for Uganda for 2009/2010. Kampala, Uganda.

Nimusiima, A., Basalirwa, C. P. K., Majaliwa, J. G. M., Kirya, D., & Twinomuhangi, R. (2018). Predicting the impacts of climate change scenarios on maize yield in the cattle corridor of Central Uganda. *Journal of Environment and Agricultural Science, 14*, 63–78. ISSN: 2313-8629.

Nthuni, S., Karanja, F., Pellikka, P., & Siljander, M. (2017). Testing the potential application of simulated multispectral data in discriminating tree species in Taita Hills*, 5*(5), 243–250. https://doi.org/10.12691/jgg-5-5-3

Ollier, C. D. (1969). Terrain classification and data storage. In *Uganda land system* (MEXE Report no. 959). University of Oxford Press, UK.

Sen, P. K. (1968). Estimates of the regression coefficient based on Kendall's. *Journal of American Statistical Association., 63*, 1379–1389.

Smith, J. U., Powlson, D. S., McGill, W. B., Arah, J. R. M., Chertov, O. G., Coleman, K., Franko, U., Frolking, S., Jenkinson, D. S., & Jensen, L. S. (1997). A comparison of the performance of nine soil organic matter models using datasets from seven long-term experiments. *Geoderma, 81*(1–2), 153–225.

Stehman, S. V., & Czaplewski, R. L. (1998). Design and analysis of thematic map accuracy assessment: Fundamental principles. *Remote Sensing and Environment, 64*, 331–344. https://doi.org/10.1016/S00034-4257(98)00010-8

Stehman, S. V., & Wickham, D. J. (2011). Pixels, blocks of pixels, and polygons: Choosing a spatial unit for thematic accuracy assessment. *Remote Sensing and Environment, 115*, 3044–3055. https://doi.org/10.1016/j.rse.2011.06.007

Twagiramaria, F., & Tolo, C. U. (2016). Climate variability and soil nutrient status along altitudinal gradient in Kigezi highlands, southwestern Uganda. *Scientific Research Publishing, 7*, 1–22. https://doi.org/10.4236/nr.2016.71001

Wang, B., Liu, L. D., Evans, J. P., Ji, F., Waters, C., Macadam, I., Feng, P., & Beyer, K. (2019). Modelling and evaluating the impacts of climate change on three major crops in Southeastern Australia using regional climate models simulations. *Theoretical and Applied Climatology., 138*, 509–526. https://doi.org/10.1007/s00704-019-02843-7

Wayne, B. C., & Olympia, E. (2003). Suitability analysis with raster data, *2* (June).

Worqlul, A. W., Dile, T. Y., Jeong, J., Adimassu, Z., Lefore, N., Gerik, T., Srinivasan, R., & Clarke, N. (2019). Effects of climate change on land suitability for surface irrigation potential of the shallow ground water in Ghana. *Computers and Electronics in Agriculture., 157*, 110–125. https://doi.org/10.1016/j.compag.2018.12.040

Zeng, W., Wu, J., Hoffmann, M. P., Xu, C., Ma, T., & Huang, J. (2016). Testing the APSIM sunflower model on saline soils of Inner Mongolia, China. *Field Crops Research, 192*, 42–54. https://doi.org/10.1016/j.fcr.2016.04.013

Index

S. Adelabu et al. (eds.), *Remote Sensing of African Mountains*,
https://doi.org/10.1007/978-3-031-04855-5